

High Frequency Flow / Structural Interaction in Dense Subsonic Fluids

B.-L. Liu and J.M. O'Farrell

(NASA-CR-4652) HIGH FREQUENCY
FLOW-STRUCTURAL INTERACTION IN
DENSE SUBSONIC FLUIDS (Rockwell
International corp.) 216 p

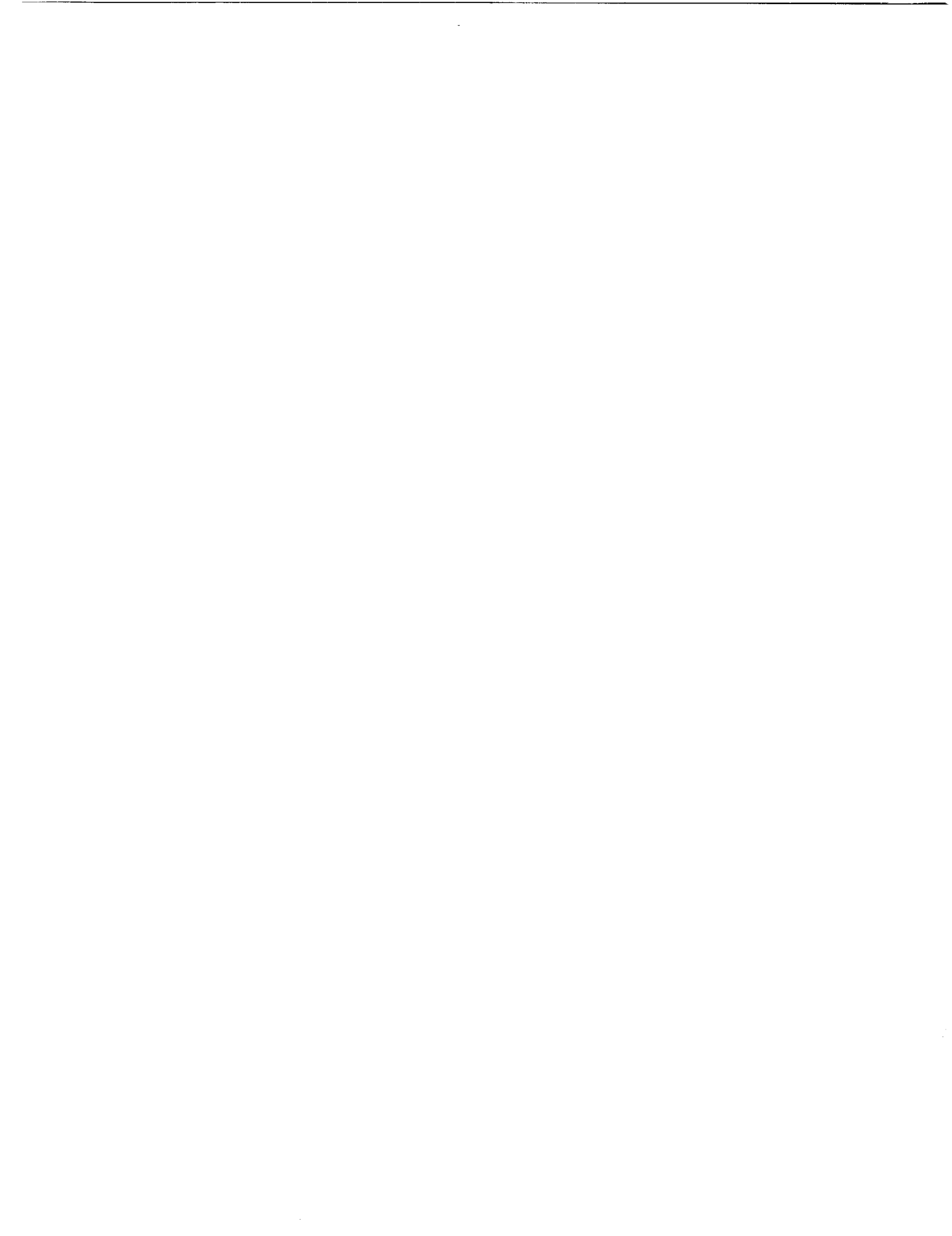
N95-24217

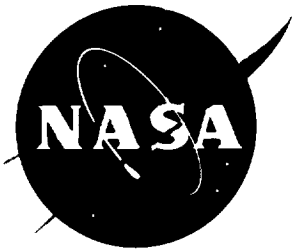
Unclas

H1/02 0044763

Contract NAS8-38187
Prepared for Marshall Space Flight Center

March 1995





High Frequency Flow / Structural Interaction in Dense Subsonic Fluids

B.-L. Liu and J.M. O'Farrell
Rockwell International • Huntsville, Alabama

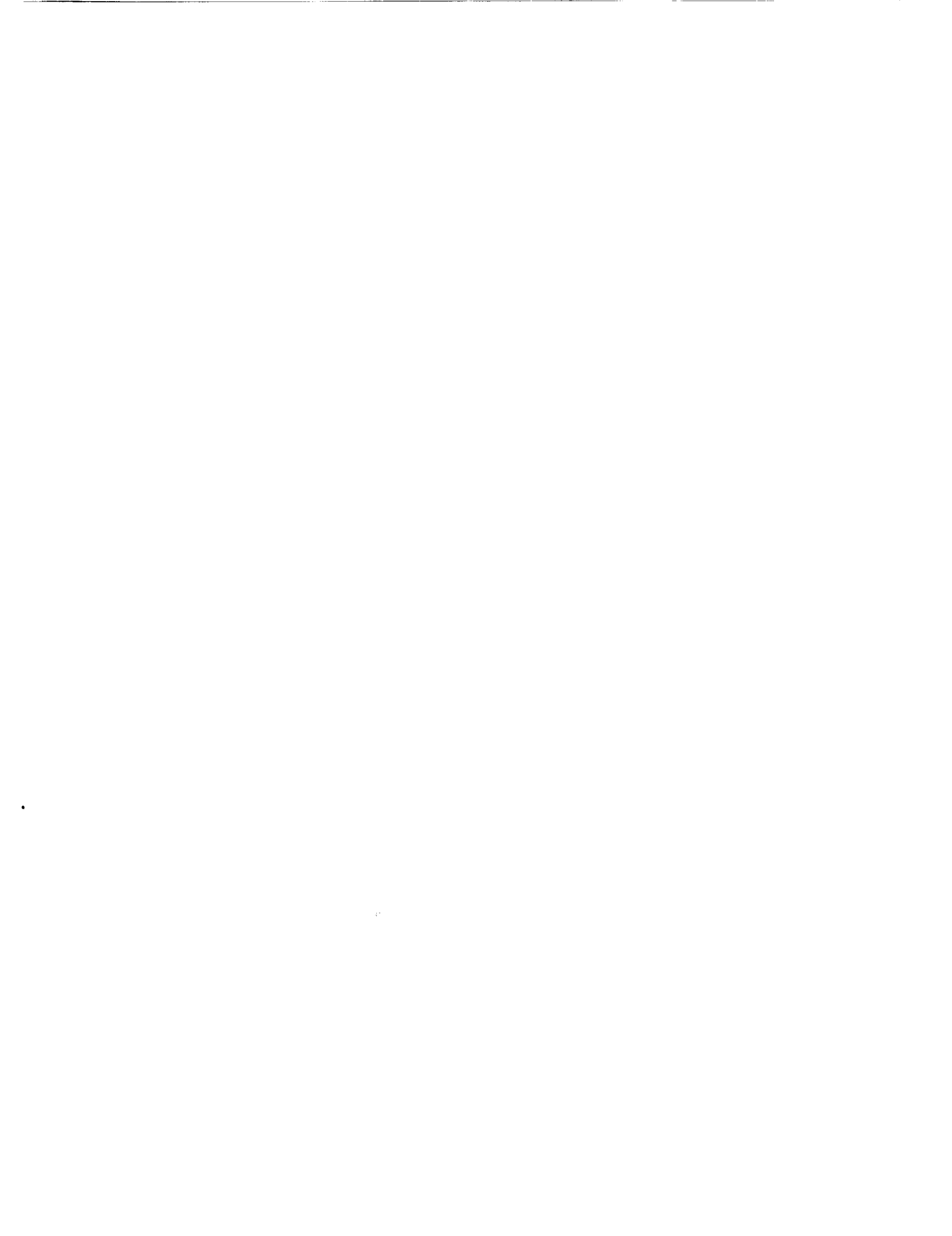


TABLE OF CONTENTS

| | |
|---|-----|
| 1. Flow/Structural Interaction (FSI) Program | 1.1 |
| 1.1 Starting the Flow/Structural Interaction Program (FSI) | 1.1 |
| 1.2 FSI Program Menu Description..... | 1.2 |
| <i>Apple, File, Edit, Structures, Fluids, Interactions, Graphics, Windows</i> | |
| 1.3 FSI Program Window Description..... | 1.3 |
| <i>Startup, About, Geometry, Material, Fluid, Flow Parameters, Structural Interaction, Flow Interaction, Display, Graphics, Reference</i> | |
| 2. Basic Principles | 2 |
| 2.1 Categories of Flow/Structural Interaction | 2.1 |
| <i>Critical Onset Flow Conditions , Resonance and Lock-in Dynamic Characteristics</i> | |
| 2.2 Geometric and Structural Parameters | 2.2 |
| <i>Characteristic Length, Reduced Velocity, Strouhal number, Reduced Amplitude, Mass Ratio, Reduced Damping, Added Mass, Strip Theory</i> | |
| 2.3 Fluid Parameters..... | 2.3 |
| <i>Mach Number, Reynolds Number, Drift Volume</i> | |
| 2.4 Extraneously Induced Excitations (EIE)..... | 2.4 |
| <i>Buffeting, Turbulence-induced Vibrations, Two-Phase Flow Induced Vibrations</i> | |
| 2.5 Instability Induced Excitations (IIE)..... | 2.5 |
| <i>Vortex Induced Vibrations, Cavitation</i> | |
| 2.6 Movement Induced Excitations (MIE)..... | 2.6 |
| <i>Galloping</i> | |
| 2.7 Extraneous Fluid Oscillators (EFO) | 2.7 |
| <i>Class I Whistles, Class II Whistles, Class III Whistles</i> | |
| 3. Geometric Analysis | 3 |
| <i>Structural Modes and Amplitudes, Added Mass, Vortex-induced Vibration and Lock-in, Galloping Responses, System Damping for Galloping, Effect of Turbulence on Galloping</i> | |
| External Flow/Structural Elements (Bluff Bodies) | |
| 3.1 Rectangular Sections, Plates, and Vanes | 3.1 |
| <i>Bending Modes, Added Mass and Structural Frequencies, Vortex Shedding Strouhal Number, Effect of Reynolds Number, Effect of Base-to-Height Ratio, Effect of Angle-of-Attack, Effect of Trailing Plate, Galloping and Turbulence, Equivalent Circular Cylinder, Aerodynamic Forces, Development of Rectangular Section Code, Vortex Shedding Frequency and Structural Response, Added Moment of Inertia and Torsional Modes, Application to Rectangular Vane, Lift, Drag and Strouhal Number, Strouhal Number Dependence on Corner Roundness, Natural Frequencies of Flat Plate</i> | |
| 3.2 Cylinders..... | 3.2 |
| <i>Circular Cylinder Geometry and Flow Phenomena, Cylinder Nomenclature, Method of Analysis, Vortex Shedding and Flow Regimes, Effective Structural Mass, Single Circular Cylinder in a Cross Flow, Single Circular Cylinder Near a Wall, Two Parallel Circular Cylinders, Crossflow Velocity and Reynolds Number, Strouhal Number and Vortex Shedding Frequency, Structural Modes and Amplitudes, Vortex Correlation Length and Joint Acceptance, System Damping, Cylinder Displacement, Reduced Velocity and General Amplitude</i> | |

TABLE OF CONTENTS

| | |
|---|------------|
| <i>Estimation, Lift Coefficient Estimation, Drag Coefficient Estimation, Wall Effect on Drag Forces, Turbulence-Induced Vibrations, Methods of Suppressing Vortex Shedding, Rotating Cylinder - No Vortex Shedding</i> | 3.3 |
| 3.3 Tube Arrays | 3.3 |
| <i>Vibration due to Whirling, Wake-Induced Vibration, Jet-Switching Vibration</i> | |
| 3.4 Other Bluff Bodies..... | 3.4 |
| <i>Trailing Edges of Vanes and Struts, H-Shaped Sections, Impinging Shear Layer Instability, Strouhal Number and Force Coefficients, Lock-in Phenomena, Torsional Vibration and Galloping, Strouhal Numbers for Several Bluff Bodies</i> | |
| External Flow/Structural Elements (Streamlined Bodies) | |
| 3.5 Airfoils and Turbomachinery Blades | 3.5 |
| <i>Airfoils, Turbomachinery</i> | |
| 3.6 Other Streamlined Bodies | 3.6 |
| <i>Instabilities and Onset Critical Flow Velocities of Vanes, Vane Parameters Needed for Estimation of Onset Flow Velocities</i> | |
| Internal Flow/Structural Elements | |
| 3.7 Internal Flow in Pipes | 3.7 |
| <i>Equations of Motion, Pipe Fixed at Both Ends, Cantilevered Pipe, Curved Pipes, Pipe Whip</i> | |
| 3.8 Fittings and Bends | 3.8 |
| <i>Fittings, Bends, Pipe Systems, Dynamic Approach, Modeling a Fluid Column and Coupled Straight Pipe, Coupling at Direction/Area Changes, Long Radius Elbows, Losses, Terminal Hydraulic Impedances</i> | |
| 3.9 Bellows and Liners..... | 3.9 |
| <i>Bellows and Flexible Hoses, Bellows Numerical Example, Liners, Mode Shapes and Frequencies</i> | |
| 3.10 Valves and Gates | 3.10 |
| <i>Jet Flow-Inertia Induced Vibrations, Turbulence Induced Vibrations, Acoustically-Induced Vibrations, Valve Whistling, Gate Vibration, Strouhal Number Data, Valve Struts</i> | |
| 3.11 Surge Tanks and Sloshing..... | 3.11 |
| <i>Surge Tanks, Fluid Container Sloshing, Compressor Surge</i> | |
| 4. Avoidance and Corrective Measures | 4 |
| 4.1 Avoidance | 4.1 |
| <i>Evidence of High Cycle Fatigue Cracking, Fatigue Reliability of Structures</i> | |
| 4.2 Corrective Measures..... | 4.2 |
| <i>Bellows Elimination - the Apollo/Saturn S-II Stage Engine Shutdown Occurrence, Addition of Flow Shields -Stiffeners to Injector LO₂ Posts, Reduce Vortex Shedding Effects- the LO₂ Inlet Tee Vanes 4 kHz Phenomenon, Eliminate Cavity Noise - the Main Oxidizer Valve (MOV) Buzz Phenomenon, Reduce the Turbulence Intensity</i> | |
| Units | U |
| Glossary | G |
| References | Ref |
| Index | Ind |

1. Flow/Structural Interaction (FSI) Program

1.1 Starting The Flow/Structural Interaction Program (FSI)

The Flow Structural Interaction Program is started by double-clicking on the Flow Structural Interaction Icon. This opens a startup window to introduce the program. Clicking on the "Continue" button in the lower right corner or pressing a key enables the main menu bar and closes the startup window.

1.2 Flow/Structural Interaction Program Menu Description

The Main menu bar for the Flow Structural Interaction program appears at program startup. In this section of the manual, first level menu options are in large type on the left. Sub menu items are indented and printed in smaller type. For example, the "About FSI" window is available under the main "Apple" menu heading. An arrowhead beside a selection indicates there are further sub menu selections available in a hierarchical menu.

Apple

These options allow interaction with the Macintosh System software through the Apple Menu Items or Desk Accessories (DA's) under the Multifinder and System 7 operating systems and offer help with the FSI program.

About FSI - This option opens a window which tells about the FSI program.

Help - This option opens a help window for information concerning operation of the FSI program. (Help is not available yet).

System DA's - This option allows operation of the Desk Accessories (DA's) available under the "Apple" menu. The DA's available vary according to user preferences for the particular machine. No DA's tested have been found dysfunctional with the FSI program.

File

Options available under this heading are the standard Macintosh file options.

New - (not functional)

Open - This option opens a standard "Open File" window in which new values from a file, containing fluid and/or structural parameters, may be read and incorporated in the appropriate parameter window(s) for subsequent analysis. For example, to read saved values for an entire case containing both fluid and structural parameters, click the cursor in the Display Window and choose the "Open" menu option, or to read a case containing only fluid parameters, click the cursor in the Fluid Window and choose the "Open" menu option.

Close - This option closes the window which is currently in use. Clicking on the close box in the upper left hand corner of the window produces the same result.

Save/Save As... - This option opens a standard "Save file" window through which current fluid and/or structural parameters from the active parameter window(s) are saved. For example, to save values for an entire case containing both fluid and structural parameters, click the cursor in the Display Window and choose the "Save As..." menu option, or to save a case containing only fluid parameters, click the cursor in the Fluid

FSI PROGRAM

Window and choose the "Save As..." menu option. The "Save " option has the same result as the "Save As..." option.

Revert to Saved - This option closes the current window and does not save any of the work done since the last save command. - (not functional)

Page Setup... - This option opens a standard "Page Setup" window .

Print... - This option opens a standard "Print" window. The printer accessed must be chosen through the "Chooser" DA available under the "Apple" menu. If the "Display" window is active, "Display" text is printed. If the "Graph" window is active, the graph is printed.

Analysis - Analyzes current fluid and structural data and displays results in the Display Window.

Export - (not functional)

Quit - This option closes all open windows and quits the FSI program.

Edit

These options are the standard Macintosh "Edit" options.

Structures

This option opens the "Geometry" and/or "Material" parameter windows and allows definition of the structural parameters.

Geometry - This option opens a window for definition of a particular geometry. The standard geometries available are listed below and are accessed in a hierarchical menu under the "Geometry" sub menu. Choosing one of these standard geometries loads parameters particular to the selected geometry. The "Geometry" window is opened to allow inspection and/or modification of the parameters.

- Airfoil**
- Backstep**
- Beam**
- Cavity**
- Cylinder**
- Frontstep**
- Generic**
- Jet**
- Jet-Edge**
- Miscellaneous**
- Nozzle**
- ORB_ET_SSME**
- Pipe**
- Plate**
- Sphere**
- SSME**
- Valve**
- Define Geometry**

Selection of the "Define Geometry" option allows operator input of parameters. Selection of the geometry "Airfoil" opens the data file "Airfoil" and loads geometric parameters. If a particular set of parameters are being used often, modifying the "Airfoil" file to reflect the often used parameters will allow that data to be loaded upon selection of "Airfoil" from the menu.

Material - This option opens the "Material" window for definition of a structural materials.

Fluids

These options open the "Fluid" and "Flow" parameter windows and allow definition of fluid parameters.

Fluid Parameters - This option opens the "Fluid" window for definition of fluid parameters.

Flow Parameters - This option opens the "Flow" window for definition of flow parameters. Common flow parameters include flow velocity, angle-of-attack, and yaw angle.

GASP - This option opens the "Gas Properties" window for computation of gas/fluid parameters to be inserted into the appropriate Fluid Parameters text selection boxes. The properties are calculated using the NASA/COSMIC "GASP" program. Ten gases under varying conditions are available through this option.

Interactions

This option opens the "Structural" and/or "Fluid Interaction" windows which allow definition of factors effecting flow/structural interaction.

Structural Factors - This option opens a window for definition of flow/structural parameters where the effect is dominated by structural characteristics. For example, Greenspon factor for added mass for partially submerged plates are referenced here.

Fluid Factors - This option opens a window for definition of particular flow/structural parameters where the effect is dominated by fluid characteristics. For example, the vortex correlation length factor is referenced here.

Graphics

This option opens the "Settings" and "Graph" windows for displaying results from calculations.

Settings - This option opens a window for definition of graphics options. Graphics options include x, y, and z ranges. 3D graphs are not functional.

Graph - This option opens the "Graphics" window for graphic display of data using options chosen under "Settings".

Windows

These options open the selected window or bring the selected window to the foreground. The following windows are included:

- Geometry Window**
- Material Window**
- Fluid Window**
- Flow Window**
- Structural Interaction Window**
- Flow Interaction Window**
- Display Window**
- Reference Window**
- Graphics Window**

1.3 Flow Structural Interaction Program Window Description

Windows are the basic input and output devices. Parameters defining a particular analysis are entered through specific windows. This section of the handbook describes each window and its expected input and output.

The "Startup" window, Figure 1-1, displays the title of the handbook and the authors. The main purpose of the "Startup" window is to inform the user that the program has started. To exit the startup window, press any key or click the continue button located in the lower right-hand corner.

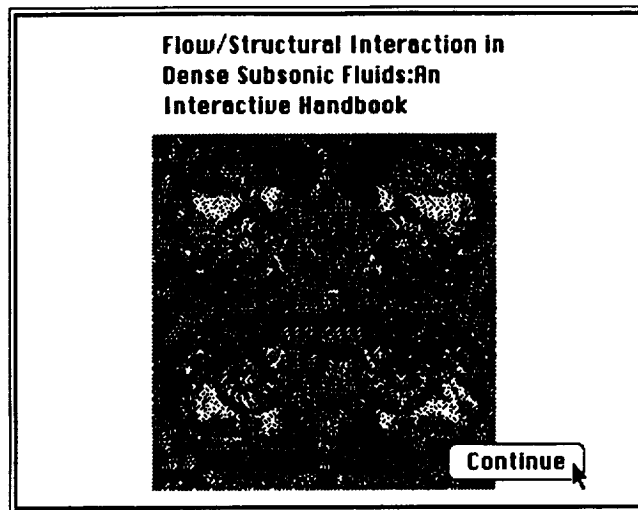


Figure 1-1 Startup Window

The names of the programmers and authors of the FSI code and where you may get in touch with them in case of difficulty are included in the "About" window, Figure 1-2.

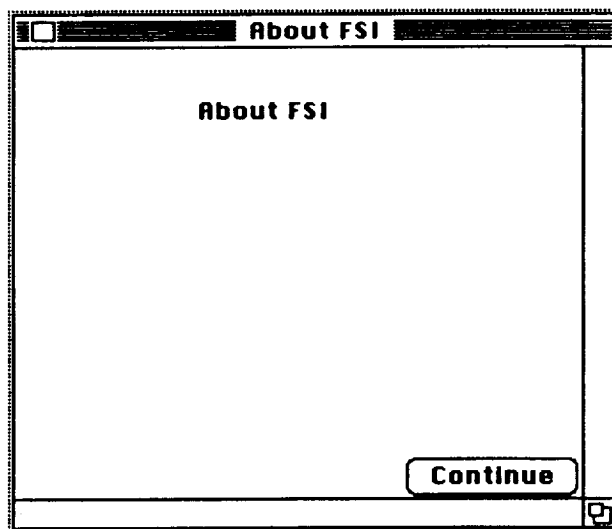


Figure 1-2 About FSI Window

The "Geometry" window, Figure 1-3, is for input and review of structural parameters. Physical dimensions, the structural damping factor ζ , and the mode shape factor for the selected structure may be modified by editing their input boxes. End constraints are selected by holding down the mouse button in the appropriate constraint input box to access available options in a pop-up menu. Predefined geometries may be read from a file by clicking the cursor in the Geometry text box choosing the "Open" menu option. Geometry parameters may be saved by clicking the cursor in this window and choosing the "Save/Save As..." menu option.

The screenshot shows a window titled "Geometry" with a close button in the top-left corner. The window contains the following fields and controls:

- Geometry:** A text box containing the word "plate".
- Dimensions:** Two radio buttons: Two_Dimensional and Three_Dimensional.
- Height (meters):** A text box containing "7.112000e-03".
- Width (meters):** A text box containing "4.064000e-03".
- Depth (meters):** A text box containing "5.689600e-02".
- Bending End Constraints:** A text box containing "Free-Free".
- Torsion End Constraints:** A text box containing "Free-Free".
- Zeta:** A text box containing "1.000000e+00".
- Shape Factor:** A text box containing "1.000000e+00".

Figure 1-3 Geometry Window

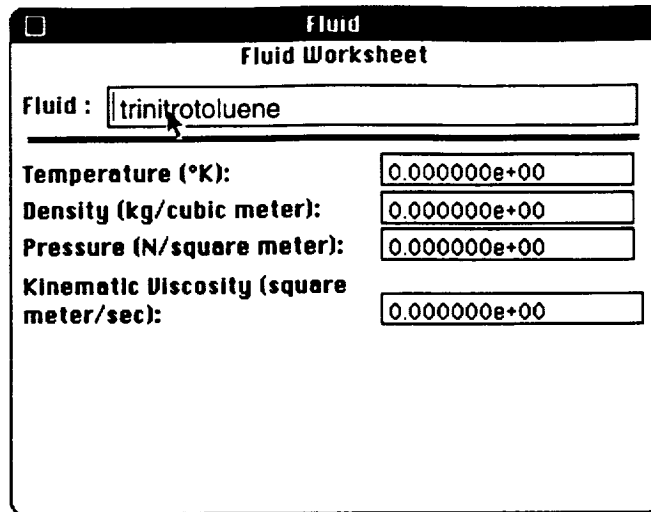
The "Material" window, Figure 1-4, is for input and review of material parameters. Density, Young's modulus, shear modulus, Poisson's ratio, and temperature for the selected material may be modified by editing their input boxes. Predefined materials may be read from or saved to a file as in other input windows.

The screenshot shows a window titled "Materials" with a close button in the top-left corner. The window contains the following fields and controls:

- Material:** A text box containing the word "glass".
- Density (kg/cubic meter):** A text box containing "0.000000e+00".
- Young's Modulus (Pascal):** A text box containing "0.000000e+00".
- Shear Modulus (Pascal):** A text box containing "0.000000e+00".
- Poisson's Ratio:** A text box containing "0.000000e+00".
- Temperature *K:** A text box containing "0.000000e+00".

Figure 1-4 Material Window

The "Fluid" window, Figure 1-5, is for input and review of fluid parameters. Temperature, density, pressure, and kinematic viscosity for the selected fluid may be modified by editing their input boxes. Predefined fluids may be read from or saved to a file as in other input windows.

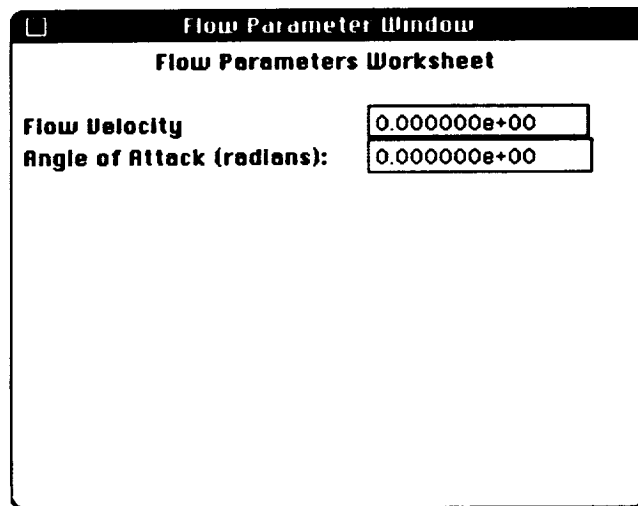


The screenshot shows a window titled "Fluid" with a subtitle "Fluid Worksheet". It contains a text box for "Fluid" with the value "trinitrotoluene". Below this are four rows of parameters, each with a label and a numerical input box:

| | |
|---|--------------|
| Temperature (°K): | 0.000000e+00 |
| Density (kg/cubic meter): | 0.000000e+00 |
| Pressure (N/square meter): | 0.000000e+00 |
| Kinematic Viscosity (square meter/sec): | 0.000000e+00 |

Figure 1-5 Fluid Window

The "Flow Parameters" window, Figure 1-6, is for input and review of flow parameters. Flow velocity and angle of attack may be modified by editing their input boxes. Predefined flow parameters may be read from or saved to a file by clicking the cursor in the Angle of Attack text box.



The screenshot shows a window titled "Flow Parameter Window" with a subtitle "Flow Parameters Worksheet". It contains two rows of parameters, each with a label and a numerical input box:

| | |
|----------------------------|--------------|
| Flow Velocity | 0.000000e+00 |
| Angle of Attack (radlans): | 0.000000e+00 |

Figure 1-6 Flow Parameter Window

The "Structural Interaction" window, Figure 1-7, is for input and review of structural interaction parameters. Greenspon factor (Greenspon, J. E., "Vibrations of Cross-stiffened and Sandwich Plates with Application to Underwater Sound Radiators," J. Acoustic Soc. Am., 33,1485-1497, 1961) may be modified by editing the input box. Predefined structural interaction parameters may be read from or saved to a file as in other input windows.

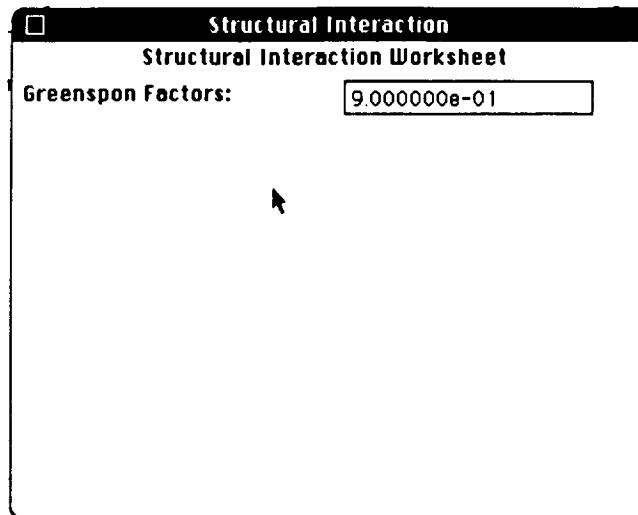


Figure 1-7 Structural Interaction Window

The "Flow Interaction" window, Figure 1-8, is for input and review of flow interaction parameters. Vortex correlation length may be modified by editing the input box. Predefined flow interaction parameters may be read from or saved to a file as in other input windows.

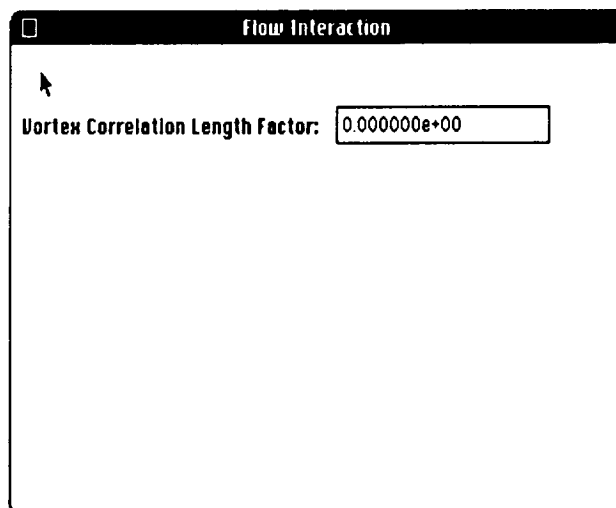


Figure 1-8 Flow Interaction Window

Analysis is presented in the "Display" window, Figure 1-9. Predefined cases, including all parameters, may be read from a file by clicking the cursor in this window and choosing the "Open" menu option. Cases may be saved by clicking the cursor in this window and choosing the "Save/Save As..." menu option.

The results shown in the "Display" window include all input parameters describing the particular case, calculated structural and flow values, and deduced results such as whether lock-in will occur for the case analyzed.

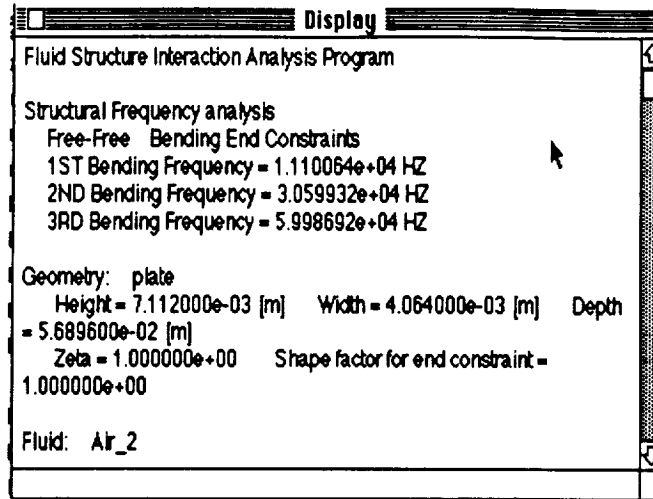


Figure 1-9 Display Window

The Graphics windows present graphic data derived from the analysis of a particular case. Options for range and type of graph are input in the "Grset" window, Figure 1-10.

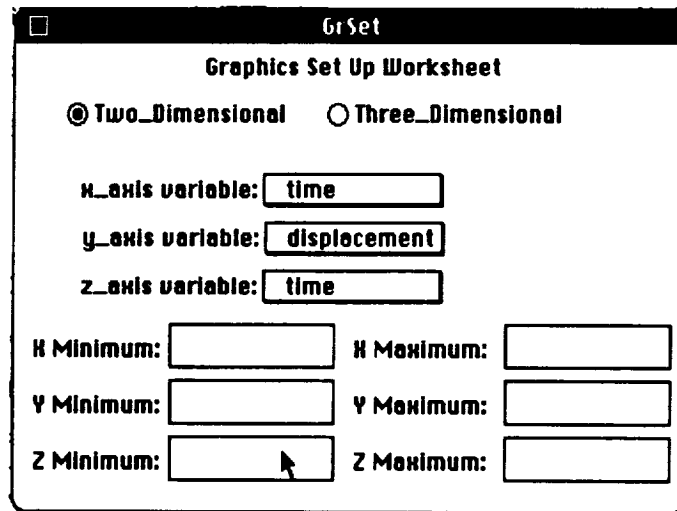


Figure 1-10 Grset Window

The "Graphics" window, Figure 1-11, displays the x-y graph set from the "Settings" window.

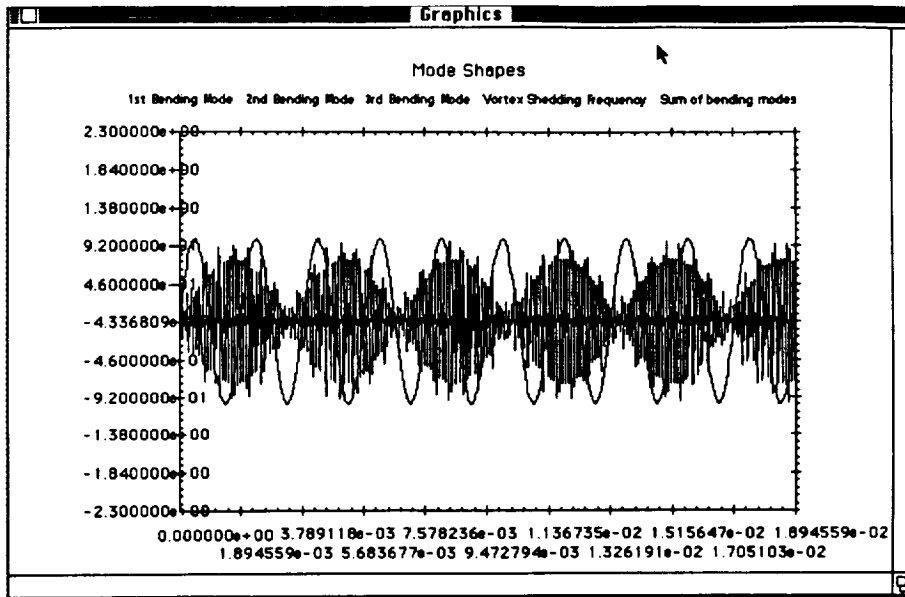


Figure 1-11 Graphics Window

The "Reference" window, Figure 1-12, provides a literature search by geometry type and keywords. The geometries available for review are listed in a pop-up menu. Up to three search strings may be entered in the "Search" input boxes. To execute the search, press <enter> on the numeric keypad while the cursor is in one of the "Search" input boxes. The title and author of the first article meeting the search criteria will be displayed in the "Author" and "Title" boxes. A synopsis of the article is displayed in the "Display" window, Figure 1-13. To continue searching with the same criteria, simply press enter again.

Figure 1-12 Reference Window

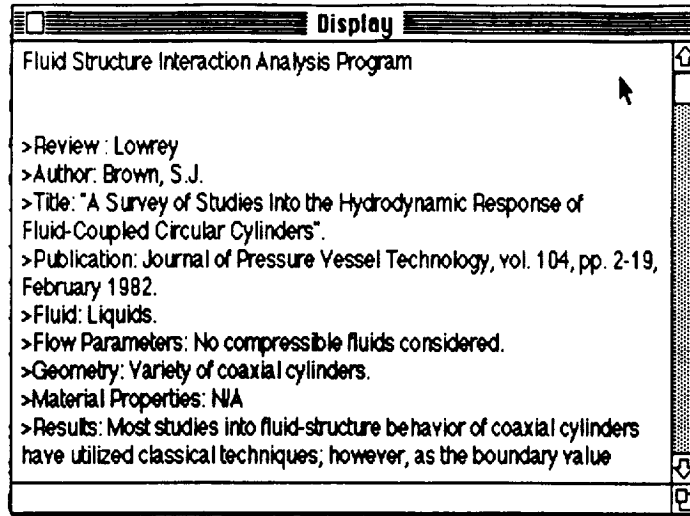


Figure 1-13 Sample Output from the Reference Search in the "Display" Window

2. Basic Principles

2.1 Categories of Flow/Structural Interaction

Structures in a fluid flow will generally induce fluctuating components. These fluctuating or flow-induced oscillations are important aspects of the flow pattern which may in turn excite natural modes of the structure. Such feedback loops in the fluid-structure system are highly nonlinear and under certain conditions may dominate the motion of the fluid-structure system. For each vibrational mode, data usually include the amplitudes of deflection, velocity and acceleration. These responses are linear and translational for bending modes and angular for torsional modes. When each vibrational mode is independent, the system may be described by studying each mode separately. In general however, systems have two or more degrees-of-freedom and the response can be analyzed only by solving a system of simultaneous differential equations.

As strongly emphasized by Naudascher¹, the engineer is advised to carry out a detailed preliminary investigation in which all sources providing hydrodynamic loading are identified and their effect assessed. Sarpkaya², Davenport and Novak³, D. Rockwell and E. Naudascher note several classes of fluctuating hydrodynamic forces. Naudascher develops a very workable scheme for distinguishing the sources of hydrodynamic loading and we use the terminology and classifications developed by Naudascher. The reader is referred to his monograph for a more detailed and illuminating treatment. There are four broad categories of fluctuating fluid forces, as shown in Figure 2-1. These categories are fluctuations from: 1) extraneously induced excitations (EIE), 2) instability induced excitations (IIE), 3) movement induced excitations (MIE), and 4) excitations due to fluid oscillators (EFO).

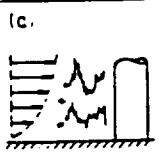
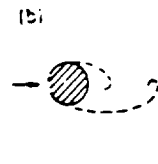
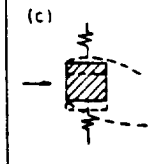
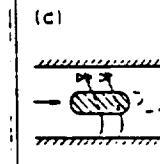
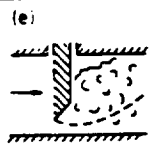
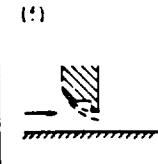
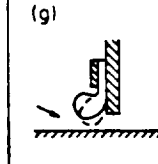
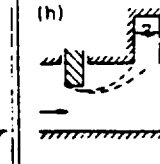
| | | Elements leading to fluctuating hydrodynamic forces | | | |
|----------|-----------------------|---|---|--|---|
| | | EXTRANEOUSLY INDUCED EXCITATION (EIE) | INSTABILITY INDUCED EXCITATION (IIE) | MOVEMENT INDUCED EXCITATION (MIE) | EXCITATION DUE TO FLUID OSCILLATORS (EFO) |
| Examples | Cylindrical structure | (c)  | (b)  | (c)  | (c)  |
| | Control gate | (e)  | (f)  | (g)  | (h)  |

Figure 2-1 Categories of Flow/Structural Interaction

¹ E. Naudascher, "Hydrodynamic Forces", IAHR Monograph, Balkema/Rotterdam/Brookfield/ 1991.

² T. Sarpkaya, "Vortex-induced Oscillations: A Selective Review" Jour. of Appl. Mech., 46, June 1979.

³ Harris, Cyril M. "Shock and Vibration Handbook" / Section: Davenport, A.G., and M. Novak, "Vibration of Structures Induced by Wind" McGraw-Hill, 1988

BASIC PRINCIPLES

EIE type fluctuations are caused by fluctuating velocities or pressures which are independent of flow instabilities originating from the structure and independent of any structural motion except for added mass effects. These EIE fluctuations are developed from motion induced into or inherent in the flow such as turbulence, buffeting from upstream structures, gravitational influence, flow impulses due to machines, two-phase or multi-phase flow, and oscillations or gusts in the flow pattern. Some examples of this type fluctuation are shown in Figure 2-2.

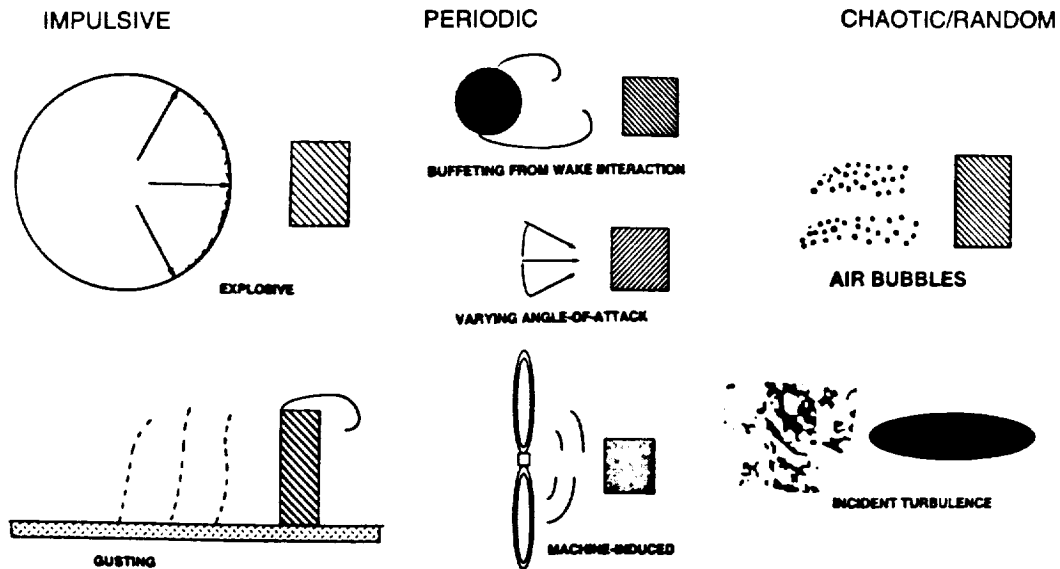


Figure 2-2 Extraneously Induced Excitations (EIE).

IIE type fluctuations are flow instabilities caused as a result of interaction of the flow with the structure. Typical IIE fluctuation generators are vortex shedding, impinging shear layers, cavitation and interface instabilities, bi-stable flow instabilities, and swirling flow instabilities. Some examples of this type fluctuation are shown in Figure 2-3.

MIE type fluctuations are a direct result of motion by the structure. A moving body in a fluid induces unsteady flow around the body and hence fluid-dynamic forces on the body are generated. These forces may be described in terms of components in-phase and out-of-phase with the body displacement, and act as added mass and damping type forces. These forces may become a source for the excitation of the structural oscillations themselves, that is these sources may become self-exciting. Naudascher develops three main categories for MIE fluctuations: 1) single mode, negligible coupling, where body movement causes a change in the hydrodynamic force such that energy is transferred from the flow to the moving body causing it to oscillate, 2) fluid coupling involving discharge variations, where there is a pulsation of the flow rate due to body oscillation, and 3) mode coupling and multi-body coupling, where excitation is induced from one mode generating fluid dynamic forces which transfer energy to the body in other modes. Flapping, galloping, flutter, rotating stall, and gap flow switching are examples of this type of fluctuation. Some examples of this type fluctuation are shown in Figures 2-4 and 2-5.

EFO type fluctuations are a result of the fluid itself being induced to oscillate. There are two main categories of fluid oscillators: 1) discrete fluid oscillators, such as the U-tube, surge tank, and the Helmholtz resonator, where a discrete mass of fluid oscillates like a solid body, and 2) distributed fluid oscillators producing the standing waves, where the oscillating fluid is treated as a continuum. Some examples of this type fluctuation are shown in Figure 2-6.

BASIC PRINCIPLES

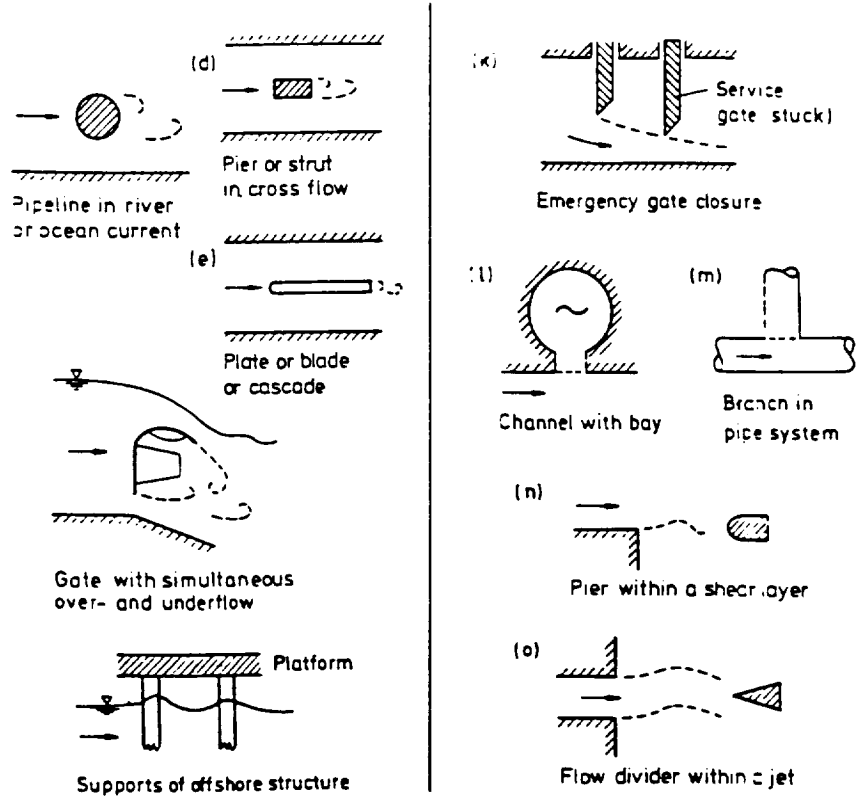


Figure 2-3 Instability Induced Excitations (IIE)

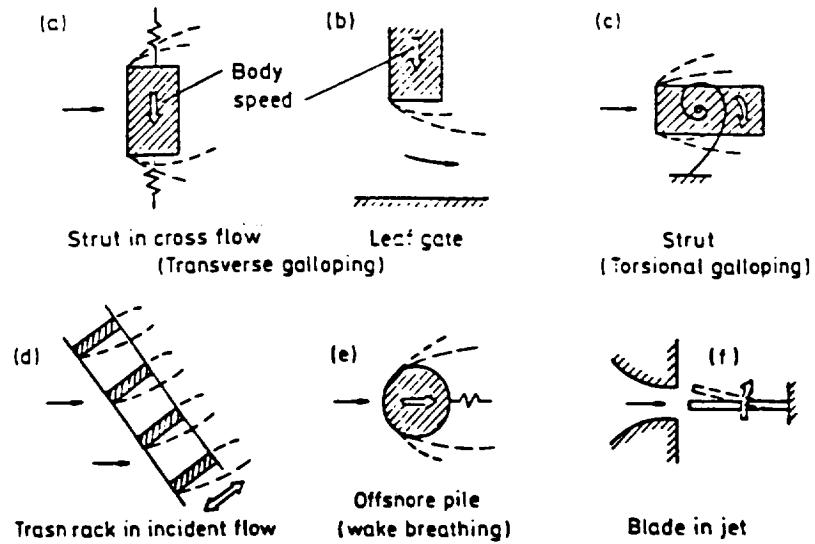


Figure 2-4 Motion Induced Excitations (MIE)

BASIC PRINCIPLES

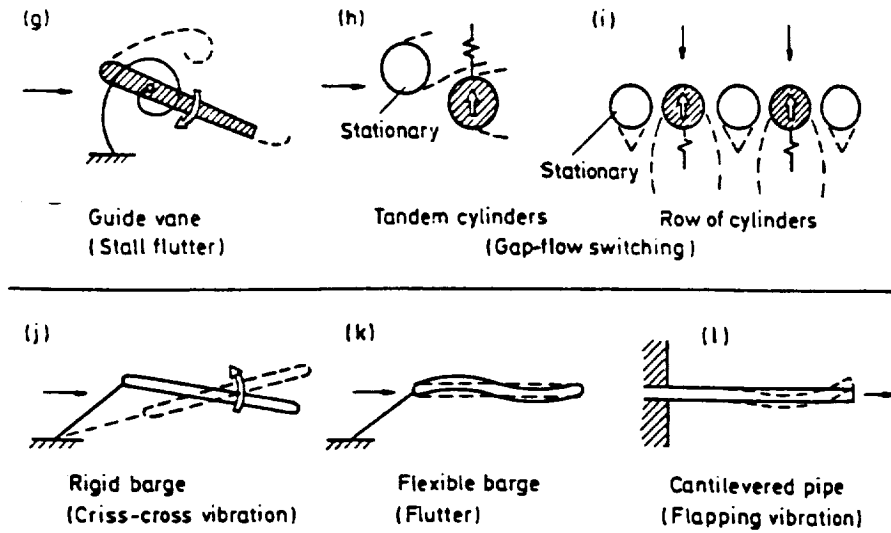


Figure 2-5 Motion Induced Excitations (MIE) (continued).

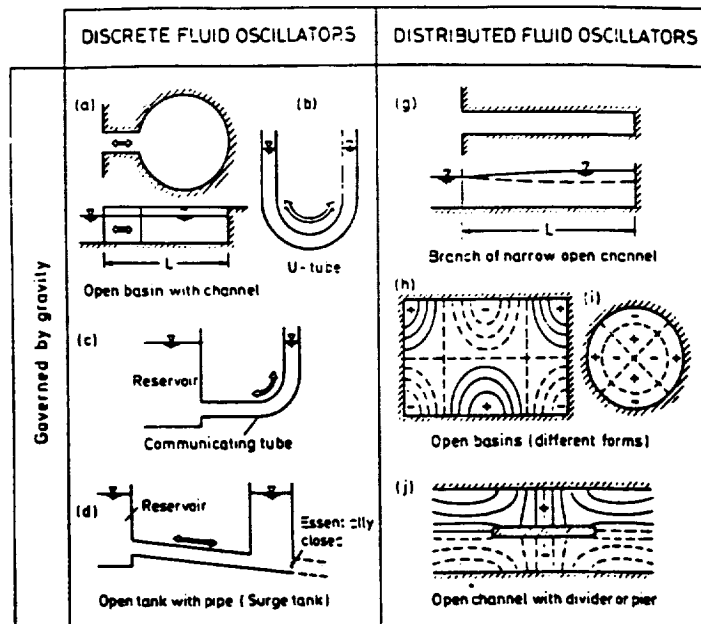


Figure 2-6 Excitations due to Fluid Oscillators (EFO)

Critical Onset Flow Conditions

Flow characteristics may change as the flow condition changes. There are several critical flow parameters. For example, in the case of laminar to turbulent transition, the critical Reynolds number in a pipe is around 2300. When a pipe flow operates above this Reynolds number, turbulent flow takes place. In the case of flow/structural interaction, critical onset flow conditions are initiated by flow instabilities. When these instabilities couple with structural vibrations, the structure becomes a system of forced vibrations. In cases where the flow induced oscillation frequencies (such as those associated with vortex shedding) match with or approach the structure's natural frequencies, unacceptable resonant flow-induced vibrations may occur. Flow separation and vortex shedding usually exist for structural elements in which the flow path is altered. For instance, bluff bodies, bellows, bends, expansions and engine parts cause flow oscillations in certain critical Reynolds number ranges.

Not all flow instabilities are due to change of flow directions. There are several types of classical instabilities, for instance those due to gravitational, inertia, and surface tension effects. When there is a high density fluid existing on top of a low density fluid, gravitational instabilities may occur. The free surface instability due to the acceleration of a liquid container and the Taylor-Goertler vortex formation in a viscous fluid between concentric rotating cylinders are examples of inertia instabilities. Surface tension may induce flow instabilities as shown by Rayleigh instability in a circular liquid jet. Benard's cells are related to surface tension nonuniformity induced by temperature difference.

From an energy point of view, a state is unstable if a small perturbation causes the release of energy from the system and is capable of doing work. For instance, a sphere on a peak in a gravitational field is unstable, because movement of the sphere may cause the release of its potential energy. The equilibrium of a high density fluid on top of a low density fluid is unstable for similar reasons. The flow between concentric rotating cylinders is unstable when the specific angular momentum in an inner fluid particle is greater than that on the outer one. In this case, a position exchange of these fluid particles would release the kinetic energy of the system which may result in the formation of ring vortices.

Resonance and Lock-in Dynamic Characteristics

Lock-in is a resonance phenomenon which is one of the most important dynamic characteristics in flow/structural interaction. When flow-induced dynamic loads match frequency with or approach natural frequency components of the structure, the structure may vibrate as a forced vibration at the resonance state. Flow/structural lock-in is a self-sustained phenomenon in which the frequency of flow-induced forces and the frequency of the vibrating structure both settle to a frequency close to the natural frequency of the structure. If the structure is adequately damped and flexible, lock-in may not cause damage to the structure.

The lock-in may cause little change in the structural properties or natural frequencies and the flow-induced loads no longer excite the structure mode. This type of lock-in is termed unsteady. If the flow-induced loads, fed back from the structural motion, do not respond in-phase with the motion of the structure, lock-in may be self-limited or self-destructive, and the motion does not increase any more or the motion diminishes.

BASIC PRINCIPLES

Vibrations maintained by an exciting force are said to be *forced vibrations*. Analogous to the flow/structural type of resonance is the resonant RLC (resistance-inductance-capacitance) electrical circuit. The differential equation for forced vibration of a mass-damper-spring system, Figure 2-7, and the similar differential equation of an RLC electrical circuit can be expressed in the following:

Forced Vibration

$$\ddot{y} + 2n\dot{y} + py = A \sin \omega t$$

where

y = displacement
 m = mass
 $n = \frac{c}{2m}$
 c = damping coefficient
 $p = \text{natural frequency of the system}$
 $= \sqrt{k/m}$
 k = spring constant
 $A = F/m = \text{forcing amplitude}$
 $F = \text{amplitude of the exciting force}$

RLC Circuit

$$\ddot{Q} + 2n\dot{Q} + pQ = A \sin \omega t$$

Q = electrical charge
 L = inductance
 $n = \frac{R}{2L}$
 R = resistance
 $p = 1/\sqrt{LC}$
 C = capacitance
 $A = E/L$
 $E = \text{amplitude of the exciting voltage}$

Here the equivalence is apparent by viewing the analogy between displacement and electrical charge in addition to the other system parameters. The complete solution of the system is in form of

$$y \text{ or } Q = e^{-nt} \left[C_1 \sin \sqrt{p^2 - n^2} t + C_2 \cos \sqrt{p^2 - n^2} t \right] + \frac{A}{\sqrt{(p^2 - \omega^2)^2 + 4n^2\omega^2}} \sin(\omega t - \phi)$$

Note that the term with e^{-nt} is a transient term which damps out with increasing time. The remaining forcing term is the steady-state term. When the forcing frequency ω is equal to the natural frequency p , the amplitude of the steady-state term is a maximum. This state of maximum amplitude is called *resonance*, which means the forcing frequency matches the natural frequency of the system, either in a mechanical or an electrical system described in the foregoing.

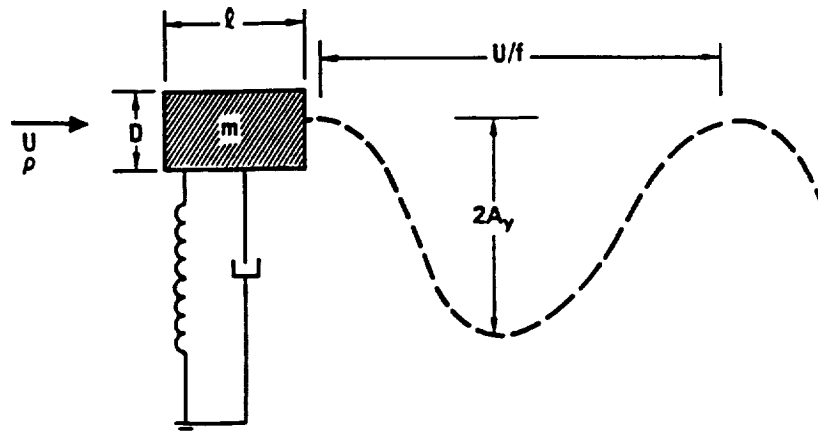


Figure 2-7 Vibration of a Spring-Supported Damped Model.

2.2 Geometric and Structural Parameters

Natural frequencies are the rate of energy exchange from the cyclic transfer between kinetic and potential energy within a structure. Only natural modes of the structure are considered in vibrational analyses in a vacuum. With the addition of a fluid to the system, energy transfer between the fluid and structure results in new characteristics. One such example is added mass. The acceleration of an immersed structure entrains fluid and the virtual mass of the structure is increased. This results in decreasing the frequency of structural vibration. The basic elements of the structural system characterized in this chapter are the structure or geometry, the non dimensional parameters related to geometry, and the fluid added mass.

Dimensionless and Reduced Variables

As noted in Blevins¹, geometry is the most important characteristic in determining the fluid forces acting on the structural model. Linear measurements are frequently normalized or reduced according to a fixed length (usually the diameter or maximum structural model width) which is characteristic of the model being analyzed. This *characteristic length* is used in other non-dimensional parameters. Frequently, as in the case of a cylinder, the diameter is used for the characteristic length and length measurements are reduced by this quantity, e.g. the width of the wake is measured in cylinder diameters. The diameter at the orifice of a jet is another example of a characteristic length used to reduce geometric measurements. Several reduced or non dimensionalized parameters of systems are listed below. Since most characteristic lengths are determined by the diameter of the model, the term, D , is employed for the characteristic length.

For a particular frequency and mode of vibration, the length of the path traveled by the structure during one cycle is U/f where U is the free stream velocity and f is the frequency of vibration. The *reduced velocity*, or dimensionless time, V_r , is this path length per cycle divided by the characteristic model length. The inverse of the reduced velocity is the non dimensional frequency, or *Strouhal number*.

$$\text{Reduced velocity} = \frac{U}{fD} \quad (2.2.1)$$

The displacement of the structure during one cycle of vibration may also be reduced by the characteristic length chosen for the model. The length of the path of the model during one cycle is $2A_y$, where A_y is the amplitude of vibration. The amplitude normalized by the characteristic length, the *reduced amplitude*, is then defined by,

$$\text{Reduced Amplitude} = \frac{A_y}{D} \quad (2.2.2)$$

The *mass ratio*, employs reduction by a characteristic area (or volume, depending on the units of density) of the model to provide a measure of the buoyancy effects and inertia of the model relative to that of the fluid. The mass ratio is the relationship of the mass of the structural model to the fluid which is displaced. As the ratio of fluid density to structural density increases the possibility for flow induced vibration also increases.

¹ Blevins, R.D., "Flow-Induced Vibration", R. Krieger Pub., Malabar, Florida, 1986, p5-8.

BASIC PRINCIPLES

$$\text{Mass Ratio} = \frac{m}{\rho_f D^2} \text{ or } = \left(\frac{m}{\rho_f D^3} \right) \text{ for volumes.} \quad (2.2.3)$$

The displacement of a lightly damped system versus time is shown in Figure 2-8. The *reduced damping*, δ_r , of the system is the product of the mass ratio with the damping factor of the system. The *damping factor*, $2\pi\zeta$, of a structure is defined as the natural logarithm of the amplitudes of any two successive cycles of a lightly damped structure in free decay. This is also equated with the ratio of the energy dissipated per cycle to 4π times the total energy of the structure.

$$\text{Reduced Damping} = \frac{4\pi m\zeta}{\rho D^2} \quad (2.2.4)$$

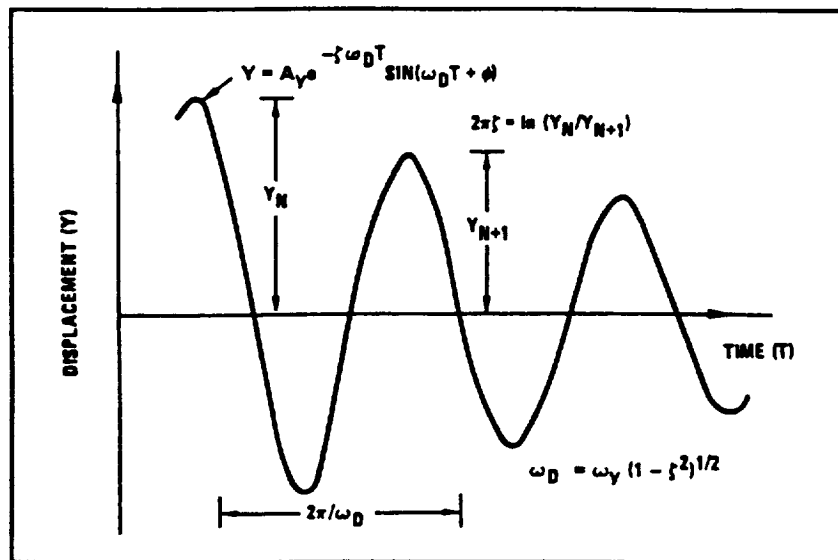


Figure 2-8. Vibration of a Lightly Damped System.

If the energy input to the structural model is greater than the energy expended in damping, then the flow-induced vibrations will increase. Thus, lower reduced damping implies greater amplitude of structural response and consequently greater range of fluid flow velocities over which lock-in occurs². For lightly damped structures in dense fluids the reduced velocity is on the order 3.0 and lock-in may persist over a $\pm 10\%$ variation above and below the velocity which causes resonance.

Structural Modes and Amplitudes

Each natural frequency of a linear structure can be associated with a mode shape that characterizes the form of free vibrations of that structure. Formulas for the mode shapes of simple structures are usually found by solving the linear equations of motion governing the system. For each degree-of-freedom of motion for a structure there is a corresponding vibrational mode. Mode shapes for natural frequencies of many simple geometries under different boundary

²Harris, C.M. "Handbook of Shock and Vibration", p29.9.

BASIC PRINCIPLES

constraints have been cataloged by Blevins³. The cataloged geometries include cross-sections, plates, shells, pipes, and three-dimensional bodies.

The geometric shape is the determining factor for analysis of structural vibrations. In this manual the mode shapes for a particular geometry are found detailed in the chapter analyzing that shape.

Added Mass

When a body immersed in a fluid moves, it induces motion in the surrounding fluid. *Added mass* (hydrodynamic mass, m_a) physically represents the mass of fluid that is accelerated due to body motion⁴ and is usually defined as the mass of fluid added to that of the structure in calculating the total kinetic energy of the structure. Alternately, added mass has been defined as fluid entrained or displaced by movement of the body. Each fluid element will be accelerated to some extent as a body moves in the fluid, with fluid elements adjacent to the body being accelerated more than distant fluid elements. The *virtual mass*, m , of a body is defined as the sum of the *structural mass*, m_s , and the fluid added mass. Also used in this manner is the effective mass or apparent mass, which refers to the portion of the mass involved in the specific mode of energy transfer under investigation, e.g. calculations involving mass using the projection of the virtual mass along an axis is the apparent mass of the system along the axis. In a vacuum, virtual mass is due entirely to the structural mass. As the density of the fluid increases, effects of the added mass may become a significant design parameter. The natural frequency of vibration of a structure will decrease with increased virtual mass. For a structure with a constant mass immersed in a fluid, observed frequencies are lower than the natural frequencies of that structure in a vacuum. This phenomenon is due to the fluid added mass.

Mechanics Approach to Added Mass

There are two basic approaches assessing added mass, one approach from mechanics, the other from fluids. The mechanics viewpoint begins from the equation of motion. Consider a structure of two-dimensional cross section oscillating in a quiescent fluid. If the structural oscillation is harmonic with amplitude X_0 and circular frequency ω , then the displacement, X , velocity, V , and acceleration, A , of the vibration can be given by,

$$\begin{aligned} X &= X_0 \sin (\omega t) \\ V &= v_0 \cos (\omega t), & v_0 &= \omega X_0 \\ A &= -a_0 \sin (\omega t), & a_0 &= \omega^2 X_0 \end{aligned}$$

The structural motion induces an oscillating fluid force, F , applied to the surface of the structure in the form of,

$$F = a \sin (\omega t) + b \cos (\omega t)$$

The first term is in phase with acceleration and the second with velocity, and one writes,

$$F = -m_a A - C_a V = -m_a A_0 \sin (\omega t) - C_a V_0 \cos (\omega t)$$

³ Blevins, R.D., "Formulas for Natural Frequency and Mode Shape", R. Kreiger Pub. Co., 1987.

⁴ Newman, J.N., "Marine Hydrodynamics", MIT Press, England, 1977, 103-155.

BASIC PRINCIPLES

where $m_a = a/A_0$ and $C_a = -b/V_0$. For a simple spring-supported symmetric structure in a still fluid, the equation of motion is

$$F = m A + C V + k X = -M_a A - C_a V \quad \text{or,} \\ (m_s + m_a) A + (C + C_a) V + k X = 0$$

This equation is equivalent to the free vibration of a body with effective mass $(m_s + m_a)$ and effective damping $(C + C_a)$. Thus, the effect of the fluid on the vibration of a symmetric structure is to increase the mass and damping.

According to Newtonian mechanics, the work done by an external force, F , in the direction of motion of the structure, produces work equal to the rate of increase of the total kinetic energy, T , and therefore

$$F_{\text{total}} = \text{mass} \times \text{acceleration} = (m_s + m_a) \frac{dU}{dt} = \frac{1}{U} \frac{dT}{dt}, \quad \text{and}$$

$$\frac{dT}{dt} = (m_s + m_a) U \frac{dU}{dt}$$

from which we derive, by integrating the time element through, the energy equation used in either the velocity or velocity potential form as in the fluids viewpoint,

$$T_f = \int_S \frac{1}{2} \rho_f U^2 dS$$

In potential flow, the added mass coefficients are dependent only on the geometry of the surface of the structure. However, with a vibrating body, when the wavelength is on the order of the diameter of the body, i.e., the non dimensional amplitude, $\frac{A_y}{D}$, is 0.1 or greater, the effects of amplitude and frequency on added mass are no longer negligible. In general, added mass decreases as frequency increases. Comparison of experimental and theoretical results suggests that potential flow predictions are within 10% of the experimentally measured added mass values, given that the Mach number of the oscillation is small, $\frac{A_y}{D} < 0.1$, and the Vibrational Reynolds number is large.

Two-Dimensional Sections

The added mass of a two-dimensional section with two perpendicular axes of symmetry is completely specified by the added masses along each of the axes and the added moment of inertia for rotation about the intersection of the axes.

In general, added mass is a tensor quantity. For asymmetric sections, the fluid force of added mass in the X-direction may induce added mass in Y-direction. In fact, there may also be a coupling effect from translation and/or rotation. The fluid force due to the added mass may be written in matrix form, as:

BASIC PRINCIPLES

$$\begin{bmatrix} F_x \\ F_y \\ F_\tau \end{bmatrix} = \begin{bmatrix} A_{xx} & A_{xy} & A_{x\tau} \\ A_{xy} & A_{yy} & A_{y\tau} \\ A_{x\tau} & A_{y\tau} & A_{\tau\tau} \end{bmatrix} \begin{bmatrix} \ddot{X} \\ \ddot{Y} \\ \ddot{T} \end{bmatrix}$$

where F_x , F_y = added fluid force per unit length acting in the x and y direction, respectively, F_τ = fluid moment per unit length of rotation about the point $x = y = 0$, $|A|$ = matrix of added masses and added moment of inertia per unit length (potential flow requires this matrix to be symmetric for vibration in a still fluid), X , Y = mutually perpendicular displacements, T = angle of rotation about the point $x = y = 0$.

The total of the inertia forces is the sum of inertia forces associated with added mass and the inertia forces associated with the general structural mass:

$$\{F\} = -([M] + [A]) \{\ddot{X}\}$$

where $\{F\}$ is the total vector inertia force, $\{\ddot{X}\}$ is the vector acceleration of the structure, and $[M]$ and $[A]$ are the mass matrix and added mass matrix, respectively.

Strip Theory

The added masses of slender bodies can be approximated using strip theory. The basic assumptions of strip theory are that (1) the flow of a narrow local section (strip) over a three-dimensional body is locally two-dimensional and (2) the interaction between adjacent strips is negligible. The added mass of a slender body can be found by summing the added masses of individual two-dimensional strips, $m_{a,i}$ multiplied by the length of the strip, such as (see Figure 2-9):

$$m_a = \sum_{i=1}^N m_{a,i} \Delta x_i$$

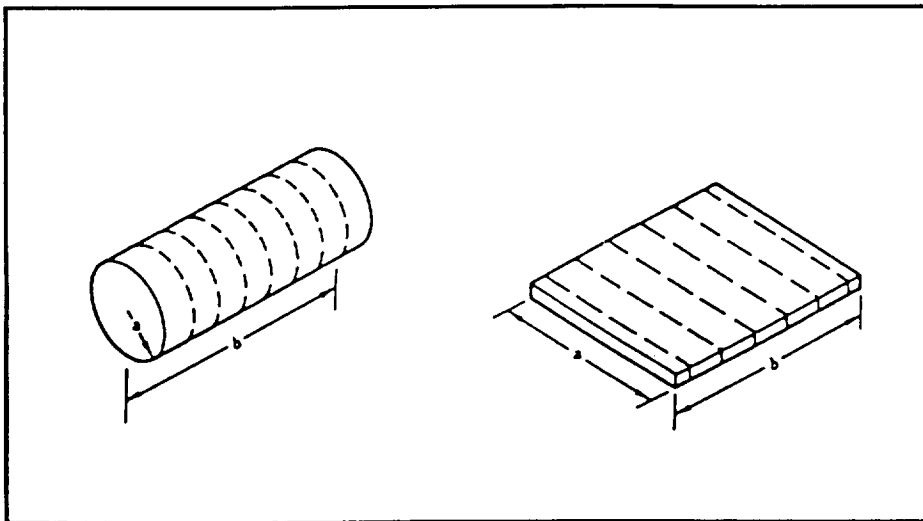


Figure 2-9. Illustration of Strip Theory Models

BASIC PRINCIPLES

Multiple Frequency Vibration

When a vibrating system has more than one vibrational mode, the values of added mass and added moment of inertia are approximately the same provided that each mode is valid by itself. Modal frequency data can be used to provide semi-empirical calculations for the added mass of the fluid. The fluid added mass is related to the structural mass and the frequencies in air and in the fluid medium by :

$$m_a = m_s \left[\left(\frac{f_{air}}{f} \right)^2 - 1 \right] + m_{air} \left(\frac{f_{air}}{f} \right)^2,$$

where m_s = structural mass of object, m_a = added mass of object due to fluid forces, m_{air} = added mass of object in air, f_{air} = frequency of object in air, f = frequency of object in fluid flow.

By measuring the structural frequencies in both air and fluid and knowing the structural mass, the added mass of the fluid can be determined from the above equation for each of the structural modes.

The added mass of many structures is comparable to the mass of fluid displaced by the structure. For many geometrically simple structures, Blevins⁵ and Chung and Chen⁶ present formulas, tables and charts as aids in determining added mass. Chen also has two computer programs available for estimating added mass: AMASS for a group of circular cylinders and AMASS-FEM for structures of irregular and complex geometries.

⁵ Op. Cit. Blevins (4), p. 31.

⁶ Chen, S.S. and H. Chung "Design Guide for Calculating Hydrodynamic Mass Part I: Circular Cylindrical Structures", Components Technology Division, Argonne National Laboratory, Argonne, Illinois, June 1976, Document No. ANL-CT-76-45.

BASIC PRINCIPLES

2.3 Fluid Parameters

A structure moving in a fluid encounters forces not experienced by the same structure moving in a vacuum. A boundary layer develops at the structural surface, wakes form and interact with the motion of the structure, and the structure experiences resistance to motion from viscous effects of the fluid. Parameters useful in characterizing fluid response and flow are listed below.

Dimensionless and Reduced Variables

The *Mach number* of a flow is the ratio of the fluid velocity to the speed of sound in the fluid. Mach number is a measure of the tendency of a fluid to compress as it nears a structure.

$$\text{Mach number} = \frac{U}{c}$$

The ratio of inertial forces to viscous forces in a fluid is called the *Reynolds number*. The inertial force is determined by the product of the characteristic length of the structure, D , with the fluid velocity, U , and the fluid inertial force is defined by the kinematic viscosity of the fluid, ν . This dimensionless ratio is employed as a measure of boundary layer thickness, transition from laminar to turbulent flow and flow separation from bluff bodies.

$$\text{Reynolds number} = \text{Re} = \frac{U D}{\nu}$$

When heat transfer becomes important, additional nondimensional parameters need be considered for heat and mass transfer effects including

$$\text{Prandtl number} = \text{Pr} = \frac{\nu}{a} = \frac{\mu c_p}{k}$$

$$\text{Grashof number} = \text{G} = \frac{g \beta (\Delta T)_0 L^3}{\nu^2}$$

$$\text{Eckert number} = \text{E} = \frac{U_\infty^2}{c_p (\Delta T)_0}$$

$$\text{Nusselt number} = \text{Nu} = \frac{h L}{k}$$

In dense subsonic fluid-structural interaction analysis, Reynolds number is a particularly important nondimensional flow parameters.

Added Mass

Fluid Dynamic Approach to Added Mass

The term hydrodynamic mass originates from the fluids viewpoint which begins with the equations for the hydrodynamic mass of a structure vibrating in a fluid as derived from kinetic energy equations of the fluid surrounding the structure. For a structure of volume, V_s , and mass per unit thickness, ρ_s , fluid of volume, V_f , and mass density, ρ_f , and fluid velocity U , the total kinetic energy of the fluid and the structure is given by the simplified equation

BASIC PRINCIPLES

$$\text{Total Kinetic Energy} = T = \frac{1}{2} (V_s \rho_s + V_f \rho_f) U^2$$

The effect of the added mass and moment of inertia of the fluid was addressed in depth by Milne-Thompson¹. He assumes a potential function for the fluid of the following form, $\phi = \mathbf{u} \cdot \boldsymbol{\varphi} + \boldsymbol{\omega} \cdot \boldsymbol{\chi}$, specifying the angular velocity of the body, $\boldsymbol{\omega}$, as well as the linear velocity of the body, \mathbf{u} . For a point \mathbf{r} , the velocity is given by $\mathbf{u} + \boldsymbol{\omega} \otimes \mathbf{r}$. Boundary conditions at the surface of the body must be satisfied, and therefore if \mathbf{n} is a unit outward normal at \mathbf{r} , the following condition must be satisfied,

$$-\frac{\partial \phi}{\partial n} = \mathbf{n} \cdot (\mathbf{u} + \boldsymbol{\omega} \otimes \mathbf{r}).$$

where $\boldsymbol{\varphi}$ and $\boldsymbol{\chi}$ are vectors whose components along the Cartesian axes are solutions of Laplace's Equation whose gradient tends to zero at infinity and which satisfy the boundary conditions,

$$-\frac{\partial \boldsymbol{\varphi}}{\partial n} = \mathbf{n} \quad \text{and} \quad -\frac{\partial \boldsymbol{\chi}}{\partial n} = \mathbf{r} \otimes \mathbf{n}.$$

The total kinetic energy of the fluid is then obtained from,

$$T_f = \int_S \frac{1}{2} \rho_f \phi \frac{\partial \phi}{\partial n} dS = \int_S \frac{1}{2} \rho_f (\mathbf{u} \cdot \boldsymbol{\varphi} + \boldsymbol{\omega} \cdot \boldsymbol{\chi}) (\mathbf{n} \cdot (\mathbf{u} + \boldsymbol{\omega} \otimes \mathbf{r})) dS,$$

where S refers to the surface of the structure. Noting that T_f is a homogeneous quadratic function of the vectors \mathbf{u} and $\boldsymbol{\omega}$, the following relation holds,

$$\mathbf{u} \frac{\partial T_f}{\partial \mathbf{u}} + \boldsymbol{\omega} \frac{\partial T_f}{\partial \boldsymbol{\omega}} = 2 T_f. \quad \text{Then}$$

$$\frac{\partial T_f}{\partial \mathbf{u}} = \int_S \rho_f \mathbf{n} \cdot \boldsymbol{\varphi} dS \quad \text{and similarly} \quad \frac{\partial T_f}{\partial \boldsymbol{\omega}} = \int_S \rho_f (\mathbf{r} \otimes \mathbf{n}) \cdot \boldsymbol{\chi} dS.$$

The action of the liquid pressures resulting from the motion of the structure is then represented by the force, \mathbf{F}_f , and couple, \mathbf{L}_f , as

$$\mathbf{F}_f = \frac{d}{dt} \left(\frac{\partial T_f}{\partial \mathbf{u}} \right) - \boldsymbol{\omega} \frac{\partial T_f}{\partial \boldsymbol{\omega}}$$

$$\mathbf{L}_f = \frac{d}{dt} \left(\frac{\partial T_f}{\partial \boldsymbol{\omega}} \right) - \left(\boldsymbol{\omega} \otimes \frac{\partial T_f}{\partial \boldsymbol{\omega}} \right) - \left(\mathbf{u} \otimes \frac{\partial T_f}{\partial \mathbf{u}} \right)$$

The flow potential may be expressed in coordinates fixed relative to the structure, as

¹ Milne-Thompson, L.M., "Theoretical Hydrodynamics (5th Edition)", Macmillan Co., 1968, p.545-554.

BASIC PRINCIPLES

$$\phi = U(t) \Phi(x', y', z'),$$

where $U(t)$ is the flow velocity relative to the body, x' , y' , and z' are the coordinates that are fixed to the body. In this way, an added mass tensor, $m_{k,i}$, may be defined for each component in the above equations,

$$m_{k,i} = \int_S \rho_f \Phi_i \frac{\partial \Phi_k}{\partial n} dS$$

This allows expression of the equations in component form depending only on the body velocity and acceleration components, such as;

$$F_j = -\dot{U}_i m_{j,i} - \epsilon_{j,k,l} \omega_k m_{l,i} \quad \text{and,}$$

$$L_j = -\dot{U}_i m_{j,i} - \epsilon_{j,k,l} U_i \omega_k m_{l,i} - \epsilon_{j,k,l} U_i U_k m_{l,i}.$$

where $\epsilon_{j,k,l}$ is the alternating tensor for cross products, i.e. $\epsilon_{j,k,l} = 1$ if the indices are in cyclic order and $\epsilon_{j,k,l} = -1$ if the indices are acyclic, and the indices k and l range over the entire six degrees of freedom in translation and rotation. When the body is not symmetric, there is coupling between motions in the three coordinate directions. For example, if a body is not symmetric about the X-axis, acceleration in the X-direction generally induces added mass force in the Y direction and a moment as well.

If the motion is steady and the structure does not rotate, the action of the structure on the fluid reduces to zero net force and a remaining couple term $-\left(\mathbf{u} \otimes \frac{\partial \mathbf{T}_f}{\partial \mathbf{u}}\right)$ which would tend to rotate the structure, the D'Alembert paradox,. This couple term will vanish only if the vector product vanishes, i.e. the vectors \mathbf{u} and $\frac{\partial \mathbf{T}_f}{\partial \mathbf{u}}$ are parallel. The directions satisfying this relation for a body are called the *directions of permanent translation*. A body without rotation, set in motion along one of these directions will continue to move in that direction without rotation.

Relation of Drift Volume to Added Mass

Darwin² investigated the trajectories of an infinitely thin plane of particles, orthogonal to the direction of motion of a body. As a body moves through a fluid, it induces motion in nearby particles of the fluid. The *drift*, ξ , of a particle in the fluid, as illustrated in Figure 2-10, is defined as the total displacement of the fluid particle in the direction of movement of the body.

$$\xi = \int_S \left(\frac{dx}{dt} + U \right) dt$$

Assuming that the body moves along the x-axis, drift is the total displacement along the x-axis.

² C. Darwin, Proc. Camb. Phil. Soc., 49, (1953), p.342-354.

BASIC PRINCIPLES

The *drift volume*, D , is defined as the volume enclosed between the initial and final position of the infinitely thin plane. Darwin equates this drift volume to the volume corresponding to the added mass in the case of a body moving in an unbounded fluid.

$$\rho_f D = \int_{-\infty}^{+\infty} \rho_f \xi d\eta$$

where the integrator η represents the set of streamlines of the flow about the body.

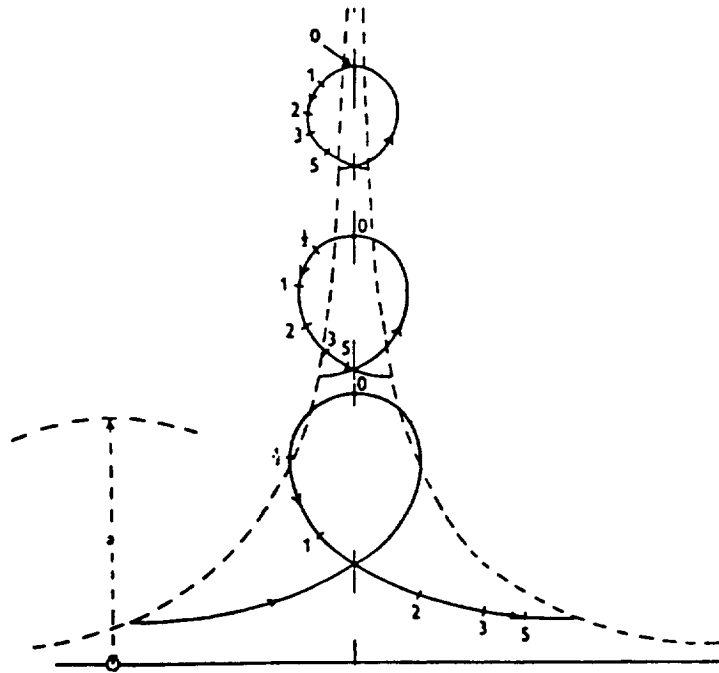


Figure 2.-10. Broken line on left is upper half of wall of dye before passage of cylinder, that on right after passage; 'a' is cylinder's radius. Firm lines show three trajectories. Numbers mark times of passage to these points in units in which cylinder moves distance a.

2.4 Extraneously Induced Excitations (EIE)

These types of instabilities are caused by fluctuating velocities or pressures which are independent of any flow instabilities originating from the structure or structural motion. These fluctuations also include any source of fluctuations which has been introduced into the flow before introduction into the control volume being investigated. Categories include buffeting and oscillating flow, turbulence induced oscillations, and two-phase flows instabilities. Cavitation may be included as caused by a two-phase (fluid-gas) fluctuation for certain flow regimes; however, cavitation is a result of the interaction of a sudden depressurization in the flow and in that context is mainly covered in the section on IIE fluctuations.

Buffeting

Excitation due to buffeting is the most common cause of fluctuation in fluid-structural systems. Buffeting is commonly considered as the motion of a structure due to unsteady fluid loading; however, buffeting may also be viewed as the fluid loading on the structure causing the structural motion. It is in this respect that we view buffeting in this report. As such, we consider buffeting as a process which may occur in the absence of structural motion. Buffeting may be impulsive, periodic, chaotic or random in nature. Impulsive buffeting may also be characterized by excitations which involve a single, well-defined wavelength and uniformity of amplitude and phase such as the effects of randomly gusting flow, two-phase interactions such as large pockets of gas bubbling across a body through a liquid. Periodic buffeting is characterized by multiple, well-defined wavelengths and uniformity of amplitude and phase. Such excitation may be the result of: wake interactions on the downstream body, such as vortex shedding which is highly periodic; induced periodic flow on the body, such as created by mechanical means, or flow disturbances induced by a variable angle-of-attack, such as flow from one body impinging on another only at certain angles-of-attack. Turbulence buffeting is characterized by multiple, random wavelengths and a nonuniformity of amplitude and phase. Buffeting which is chaotic or random in nature is usually referred to as turbulence buffeting.

Turbulence Induced Vibrations

In flow separation, free shear layers are formed between the main flow and zones of separation, Figure 2-11. The free shear layers are inherently unstable and they tend to roll up and form turbulent eddies which merge and finally dissipate. The degree of intermixing of these turbulent eddies gives the turbulent flow its random character. These turbulent eddies are characterized by a reduction in mean pressure and intense pressure fluctuations. In a turbulent flow, energy is transmitted to the structure from the fluctuating pressures due to the turbulent eddies impinging on or passing near the surface of the structure. Even though the fluctuating hydrodynamic forces due to turbulence induced vibrations are essentially random, the response of the structure to these forces is usually periodic and all zones which come into contact with free shear layers and the turbulence caused by separation should be examined.

Schlichting¹, describes the origin and growth of a turbulent boundary layer on a flat plate, Figure 2-12. Such turbulence generation goes through the following stages: (1) Stable laminar flow following the leading edge, (2) Unstable, laminar flow with two-dimensional Tollmien-Schlichting waves, (3) Development of unstable, laminar, three-dimensional waves and vortex formation, (4) Bursts of turbulence in places of very high local vorticity, (5) Formation of turbulent

¹Schlichting, H., "Boundary Layer Theory", McGraw-Hill Book Co., 1979.

BASIC PRINCIPLES

spots in places when the turbulent velocity fluctuations are large, and (6) Coalescence of turbulent spots into a fully developed turbulent boundary layer.

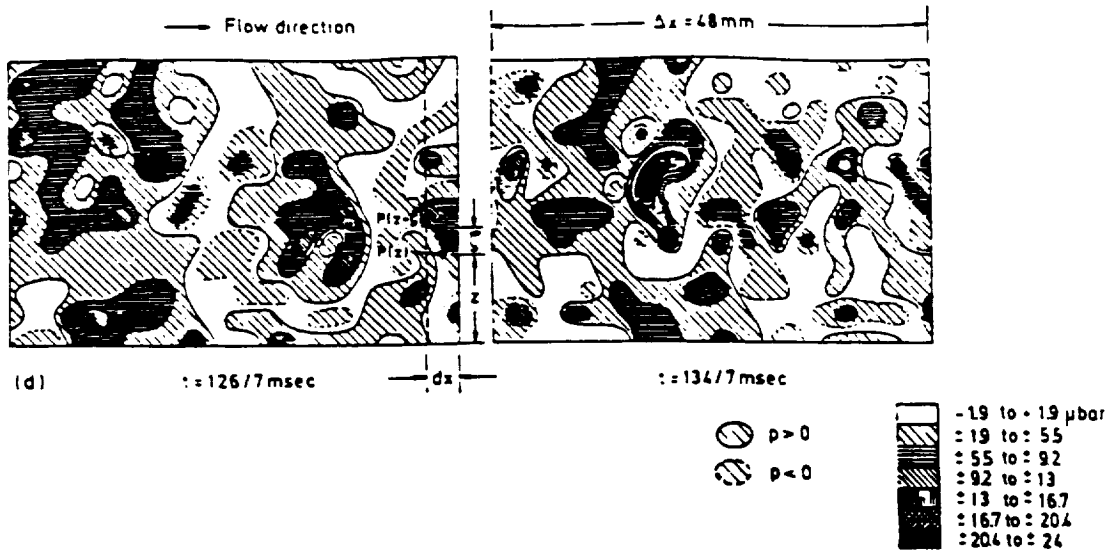


Figure 2.-11. Separation Regions in a Shear Layer.

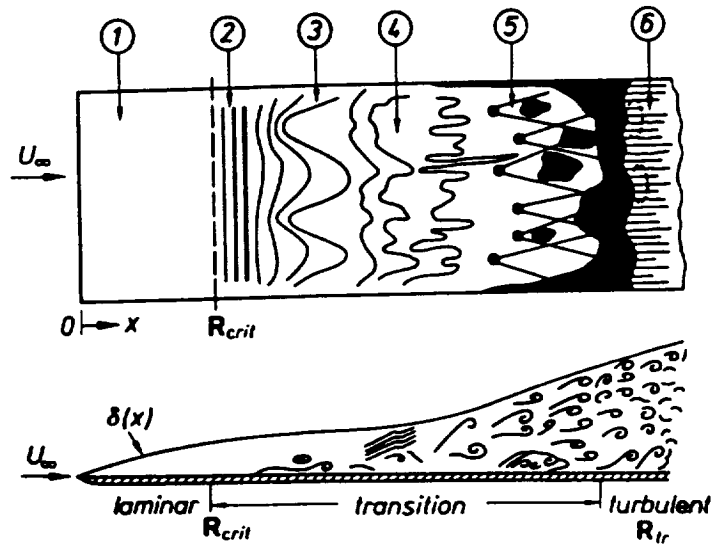


Figure 2-12 Turbulent Boundary Layer at a Wall

Effect of Surface Roughness on Turbulence

The height of a protuberance which causes transition in a laminar boundary layer is called the critical height or critical roughness². In the case of a turbulent boundary layer roughness has no effect on the flow if all protuberances are contained within the laminar sublayer. Roughness

² Op. Cit. Schlichting (14).

BASIC PRINCIPLES

affects the resistance offered by the wall, moving the transition point upstream toward the protuberance and possibly affecting the drag on the body. The critical value of roughness, k_{crit} , is given by the dimensionless roughness Reynolds number

$$\frac{k_{crit}v_*}{\nu} = Re_{Rough}$$

where $v_* = \sqrt{\frac{\tau_0}{\rho}}$ = frictional velocity, τ_0 is the shearing stress at the wall in the laminar boundary layer, and ν is the kinematic viscosity.

The effect of surface roughness on flow-induced vibrations was investigated by Sarpkaya (Reference 2). Sand roughened circular cylinders were forced to oscillate in the transverse direction in the uniform flow with amplitude ratios from 0.25 up to 1.0 and reduced velocities in the range 3 to 8. The Reynolds number ranged from about 20,000 to 50,000, and the roughness Reynolds number from about 200 to 512. Vortex lock-in was observed in the neighborhood of the Strouhal frequency.

Substantial differences were noted between the out-of-phase component of the force for a rough cylinder and that of a smooth cylinder. The difference was largest at perfect synchronization and increased with increasing roughness Reynolds number, Re_k . The in-phase component of the force for a rough cylinder was nearly identical with that for a smooth cylinder. At perfect synchronization, the in-phase component was nearly equal to unity and the out-of-phase component at $Re_k = 200$ was about 20% larger than that of a smooth cylinder; at $Re_k = 400$ was about 35% larger; and at $Re_k = 512$ was about 50 % larger. Here $Re_k = U k_s / \nu$ and k_s = mean roughness height.

Two-Phase Flow Induced Vibrations

In this type of fluctuation, the fluctuating load on the structure is induced by regions of differing density (gas/liquid, liquid/liquid, solid/liquid, solid/gas), separated by a phase transition boundary, which are carried along in the flow. In case of air bubbles in a water flow, the intermittent trapping and release of air with the fluid flow is termed blow-out and against the flow is termed blow-back. Naudascher³ included an example of air-water interface accelerated toward a conduit gate. The interface produced a water-hammer type of pressure peak of up to twice the static pressure level. The blow-out process is inherent to pressurized conduits of two-phase flow, and the release of the gas before it reaches the control structure would alleviate the impact force.

³E. Naudascher, "Hydrodynamic Forces", IAHR Monograph, Balkema/Rotterdam/Brookfield/ 1991.

2.5 Instability Induced Excitations (IIE)

Vortex Induced Vibrations

As a fluid particle flows toward the leading edge of a bluff body, the fluid pressure rises from the free stream value toward the stagnation pressure. This high fluid pressure impels the developing boundary layers along both sides of the bluff body. Unless the fluid is at very low Reynolds number conditions, the pressure force is not sufficient to force the boundary layer around the back side of the bluff body. Near the widest section of the body, the boundary layers separate from each side of the body surface and form two free shear layers that trail aft and bound the wake flow. Since the inner portion of the shear layers moves more slowly than the outer portion, the layers tend to roll up into discrete vortices. Any structure with a sufficiently bluff trailing edge sheds vortices. In subsonic flow, periodic forces on the structure are generated as the vortices are alternately shed from each side of the trailing edge. This class of induced motion is termed vortex-induced vibration. Naudascher and Wang¹ summarized three types of vortex shedding mechanisms, namely, i) leading-edge vortex shedding, ii) impinging leading-edge vortices, and iii) trailing-edge vortex shedding for rectangular sections as shown in Figure 2-13. In practical applications, regions of possible transverse vibration and galloping as indicated in the reference figure should be avoided.

Cavitation

When a subcooled fluid is not far from its saturated state or the pressure fluctuation in the flow is adequately strong, the liquid changes phase and becomes vapor, cavitates, at locations of low pressure. This cavitation usually takes place at a solid surface where the flow is separated. Due to pressure fluctuation, the vapor phase often collapses back to liquid and subsequently evaporates again in a frequency comparable to that of the pressure fluctuation. Cavitation often occurs in dense fluids subjected to high frequencies and affects the flow/structural interaction through the density fluctuations inherent in the phase change.

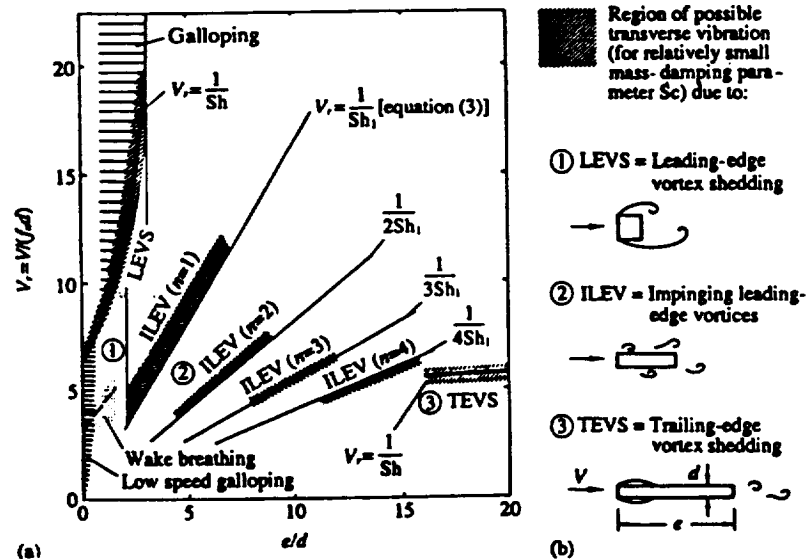


Figure 2-13. (a) Flow Map of Reduced Velocity Versus Aspect Ratio of Rectangular Section, (b) Modes of Vortex Formation.

¹Naudascher, E. and Wang, Y., "Flow-Induced Vibrations of Prismatic Bodies and Grids of Prisms," Journal of Fluids and Structures, Vol. 7, 341-373, 1993

2.6 Movement Induced Excitations (MIE)

Galloping

Galloping is a flow-induced vibration on bluff structures. The classical example of galloping is the vibration of ice-coated power lines. Moderate wind velocities can cause power lines of low structural damping to witness large amplitude oscillations. In a galloping vibration, the aerodynamic force is usually small compared with the weight of the massive structure, and the change in the natural frequency of the structure is usually small.

The fundamental assumption of galloping analysis is that the fluid force is quasi-steady, i.e., the fluid force on the structure is determined solely by the instantaneous relative velocity and the angle-of-attack of the flow to the structure.

Condition for Transverse Galloping

The typical equation of motion for a transverse deflection of a structure can be written as

$$\ddot{y} + 2\zeta \omega \dot{y} + \omega^2 y = \frac{\rho U^2 D}{2m} C_y \quad (2.6.1)$$

where the transverse force coefficient, C_y is a function of angle-of-attack, $\alpha \approx \frac{\dot{y}}{U}$:

$$C_y = C_{y0} + \frac{\partial C_y}{\partial \alpha} \dot{y} \quad (2.6.2)$$

The equation of motion is therefore after combining terms for \dot{y} :

$$\ddot{y} + 2 \left(\zeta - \frac{\rho U D \partial C_y}{4 m \omega \partial \alpha} \right) \omega \dot{y} + \omega^2 y = \frac{\rho U^2 D}{2m} C_{y0} \quad (2.6.3)$$

The system damping can be a negative number when

$$\zeta' = \zeta - \frac{\rho U D \partial C_y}{4 m \omega \partial \alpha} \leq 0 \quad (2.6.4)$$

This is possible for a structure has a positive angular rate of transverse force coefficient:

$$\frac{\partial C_y}{\partial \alpha} > 0 \quad (2.6.5)$$

and when the incident velocity U is greater than a threshold/critical onset velocity:

$$U_{cr} = \frac{4 m \omega \zeta}{\rho U D \frac{\partial C_y}{\partial \alpha}} \quad (2.6.6)$$

When this occurs the total damping force would be in phase with the structure velocity rather than retard against the motion. Typical transverse force coefficients versus angle-of-attack for several

BASIC PRINCIPLES

cross-sections are shown in Figure 2-14 [Figure 4-4 of Blevins¹]. The 'long' rectangle and square which have positive angular rates of transverse force coefficient would gallop while the 'tall' rectangle and the semi-circle with flat face forward would not gallop according to the foregoing equation of motion.

When galloping occurs the nondimensional amplitude increases as flow velocity increases further from the critical onset velocity as shown in Figure 2-15 [Figure 4-6 of Blevins].

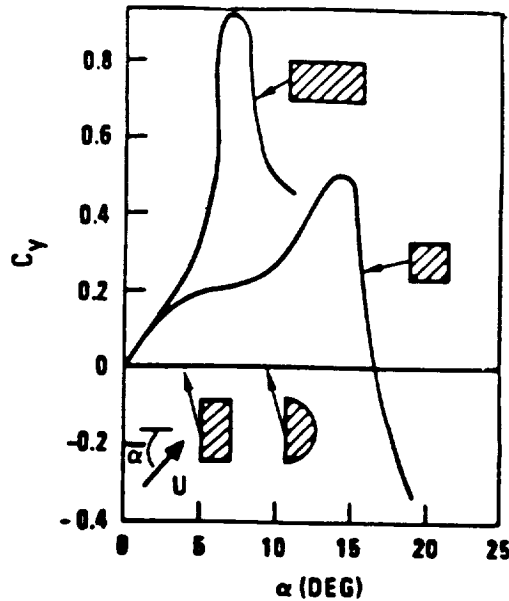


Figure 2-14. Aerodynamic Force Coefficients $Re = 33,000$ to $66,000$.

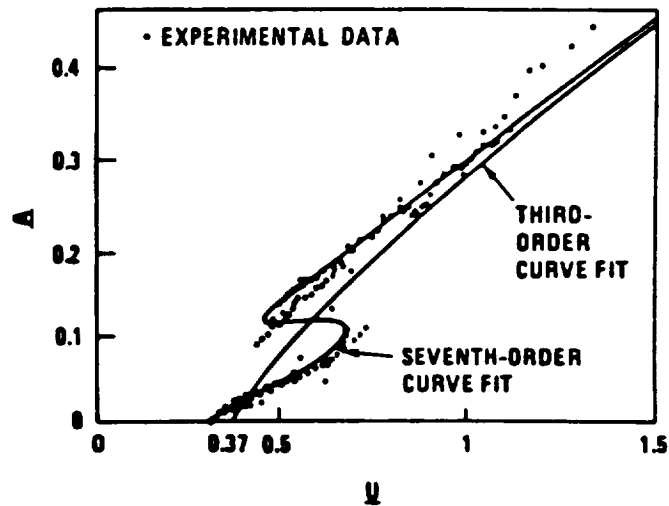


Figure 2-15. Experimental Data and Response of a Square Section for $Re = 4,000$ to $20,000$.

¹Blevins, R. D., Flow-Induced Vibration, second edition, Van Nostrand Reinhold, 1990.

EFO FLUCTUATIONS

2.7 Extraneous Fluid Oscillators (EFO)

Fluid oscillators which are self-sustained by feedback processes generated by instability in the fluid flow are known as aerodynamic whistles. The frequency of oscillations of these whistles is governed by the periodicity of the feedback cycle. Chanaud¹, in an article written for Scientific American magazine, categorized aerodynamic whistles into three classes. Class I whistles are those whose feedback consists primarily of hydrodynamic oscillations. Examples of these whistles are the aeolian tone generators, such as aeolian harps, telephone wires, and circular cylinders in a flow. Sound from these particular whistles is generated from the instability created by vortices formed and released into a flow. Class II whistles exhibit feedback from acoustic waves generated by the whistle and fed directly back to the region of instability. Examples of this type of whistle are the edge-tone, hole-tone, and ring-tone, where sound is generated from flow interaction with an edge and fed back upstream destabilizing the jet. Class III whistles have acoustic feedback which is reflected back to the region of instability by some ancillary structure. These whistles generate sound by resonance effects from a structure. The organ pipe tones are the best known examples of this phenomena. These whistles exhibit the ability to jump from one well-defined frequency to another well-defined frequency with a hysteretic effect occurring at the frequency jumps. This is usually due to a change either between flow impingement and separation distance or a change in flow velocity² as shown in Figure 2-16.

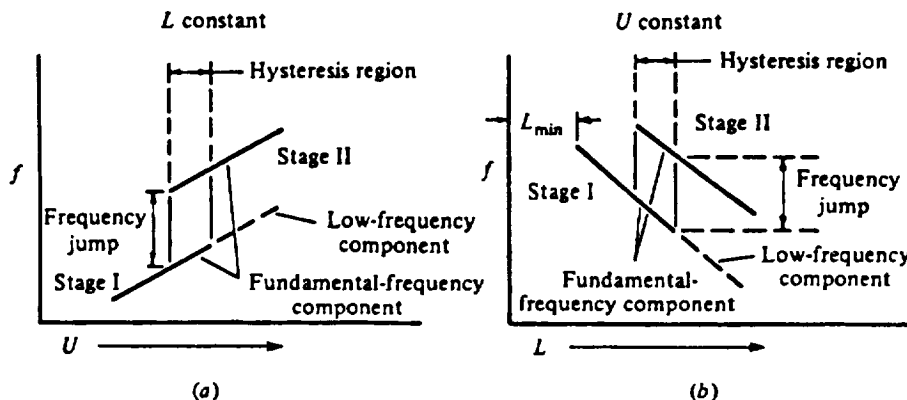


Figure 2-16. Frequency Jumps with a) Varying Free-Stream Velocity and b) Varying Impingement Length

Class I Whistles

Aeolian tone generators are essentially long thin objects in a fluid flow. At certain velocities, unsteady fluid flow around the object creates a pattern of alternate vortex shedding from opposing sides of the object, with each vortex influencing the formation and growth of the succeeding vortex. The vortices formed in this manner develop a wake flow pattern downstream of the object known as the Karman Vortex Street. The oscillations produced in the wake by these vortices generate a sound pressure field with a maximum amplitude at right angles to the vortex street. The frequencies developed by the aeolian tone generators are directly related to the speed of the fluid and the characteristic length, usually the diameter, of the object. The relationship between object characteristic length, L , fluid velocity, U , and frequency, f , may be described for this class

¹ Chanaud, R. C., "Aerodynamic Whistles," Scientific American, pp. 40-46, June 1970.

²Knisely, C. and D. Rockwell, "Self-Sustained Low-Frequency Components in an Impinging Shear Layer," Journal of Fluid Mechanics 116, pp. 157-186, 1982.

EFO FLUCTUATIONS

of whistle by the Strouhal number, S , associated with the oscillations such as shown in Figure 2-17.

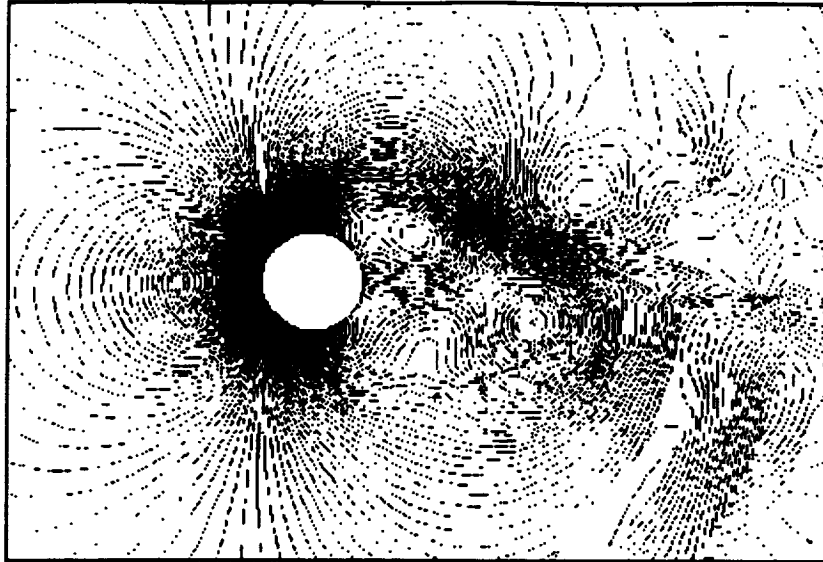


Figure 2-17. Class I Whistle: Normalized Pressure Contours of a Cylinder in a Crossflow

Class II Whistles

Class II whistles are typified by the edge-tone and cavity acoustic generator phenomena. The acoustic feedback plays an important role in sustaining synchronous hydrodynamic shear layer oscillations causing these tones.

Edge-tones

The typical edge-tone configuration is a jet issuing from a slit and impinging against a sharp edge. The hydrodynamic/acoustic feedback mechanism operating in this whistle is illustrated in Figure 2-18, from Ziada³. The jet velocity, U , the orifice width, d , the distance from the orifice to the wedge, h , and the wedge angle, α , are the defining parameters of this system. At the jet orifice, a shear layer defining the jet is developed. From the instability of this shear layer at the corners of the jet orifice, vortices are generated and released to be convected downstream. With certain edge-tone configurations, depending on the flow velocity and wedge distance from the orifice, the developed jet instability causes alternate vortex shedding at the corners of the jet orifice. Vortex formation may also develop in the shear layer of the jet away from the orifice at higher frequency stages. Downstream, the alternating impingement of the vortices on the wedge creates a flow/structural system acting as an acoustic dipole. This acoustic energy propagates back upstream to organize and enhance flow instability at the jet orifice, further strengthening the alternate vortex shedding pattern developing at the orifice. As the vortex shedding frequency matches phase with the acoustic frequency of the wedge dipole, an audible edge-tone develops. This vortex-acoustic interaction is the basic mechanism of the edge-tone phenomenon. The closed-loop feedback cycle of regular vortex shedding and jet disturbances generated by acoustic

³ Ziada, S., and E.T. Buhlmann, "Flow Impingement as an Excitation Source in Control Valves," *Journal of Fluids and Structures* 3, pp. 529-549, 1989.

EFO FLUCTUATIONS

feedback controls the edge-tone phenomenon. A formula developed by G.B. Brown⁴ for edge-tone frequencies for flow through a 1.0 mm jet orifice, and developing several stages, k , using the jet velocity U (cm/sec) and the distance of the wedge to the jet orifice, h (cm), is given by:

$$f_k = 0.466k \left(U - 40.0 \right) \left(\frac{1}{h} - 0.07 \right) \quad (2.7.1)$$

with stages $k=1, 2.3, 3.8, 5.4$

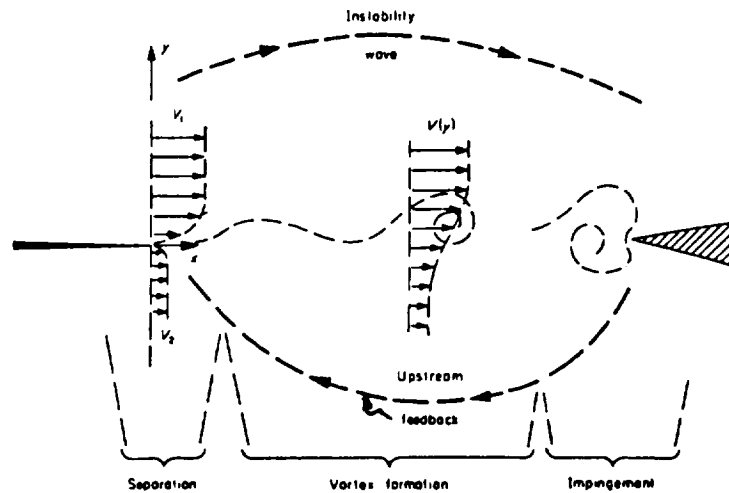


Figure 2-18. Class II Whistle: The Edge-tone Phenomena

These jet flow oscillations occur at predictable frequencies for a particular range of jet velocities and edge distances from the jet orifice. The frequency is limited by the acoustic and vortex transport (convection) times and the process of vortex formation. Results of a numerical analysis⁵ given in Figure 2-19 confirmed Brown's experimental data. Interference and disruption of the in-phase vortex-acoustic interaction can very effectively eliminate edge-tones.

Cavities

Unsteady flow over an open cavity for which the aspect ratio is such that the separated shear layer reattaches on the cavity back wall, will usually produce large, unsteady fluctuations of the pressures located in and near the cavity. Consequently, structures near the cavity are affected by these oscillations. The determining factor for these oscillations is the length-to-depth ratio (L/D ratio) for the cavity and the mean flow speed across the cavity opening.

In shallow cavities, where the L/D ratio is much greater than 1.0, flow over the front and rear cavity walls are essentially independent of one another and each may be studied separately. The fluid flow separates from the leading edge of the cavity and reattaches at some point along the cavity opening. In this separated region the developed pressure is somewhat lower than the free-stream pressure, due primarily to an increase in the speed of the fluid as it enters the cavity. As

⁴Brown, G.B., "The Vortex Motion Causing Edge Tones", Proc. Physical Society(London), vol.49,pp.493-507, 1937.

⁵ Dougherty, N. S., Liu, B. L. and O'Farrell, J. M., "Numerical Simulation of the Edge Tone Phenomenon," NASA Contract Report 4581, February 1994.

EFO FLUCTUATIONS

the fluid reaches the rear wall of the cavity, the flow is retarded and an increase in local pressure occurs until the boundary layer again separates forming a high pressure region just ahead of the rear wall. The boundary layer then reattaches downstream of the cavity. As the length-to-depth ratio of the cavity is decreased, the attachment and separation points at the leading edge and trailing edge move closer together until reverse flow develops between the high pressure separation ahead of the rear wall and the low pressure region behind the front wall, a large captive eddy then forms within the cavity.

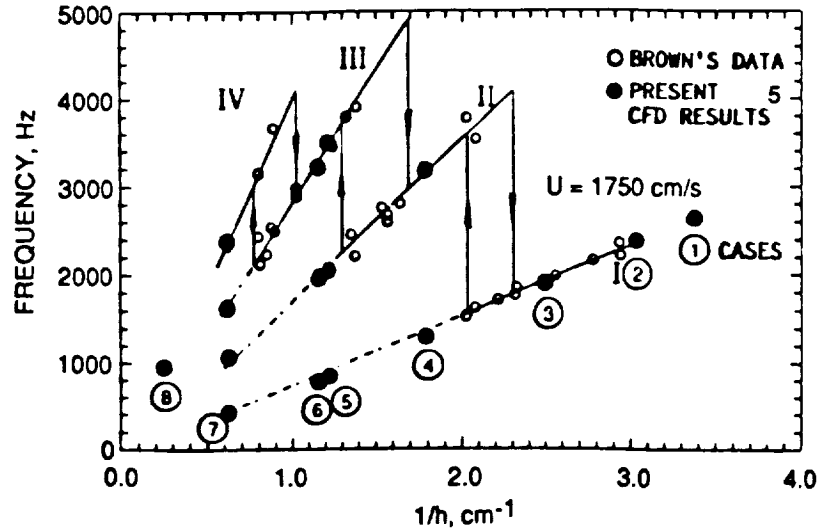


Figure 2-19. Frequency Variation in Edge-tone Phenomena

Cavity flow oscillations are attributable to fluctuations in the cavity shear layer generated by upstream propagation of acoustic disturbances occurring at the downstream cavity edge, thus the cavity source is of the same type as a Class II aerodynamic whistle. The observed oscillatory pressure is dependent upon Mach number and Reynolds number based upon the cavity length. The oscillations generated by the cavity are illustrated in Figures 2-20 and 2-21. The pressure oscillation frequency of the cavity, due to the vortex shedding generated by unsteady flow, may be approximated by using an equation developed by Rossiter⁶:

$$f_n = \frac{U(n-\zeta)c}{L\left(\frac{1}{K} + M\right)} \quad n=1,2,3,4,5,\dots \quad (2.7.2)$$

where f_n is the observed frequency, n is the mode of cavity oscillations, U is the freestream velocity, L is the length of the cavity, M is the Mach number, K is the fraction of freestream velocity obtained by vortices (disturbances) in the cavity, and ζ is a phase constant relating the acoustic and vortex generated oscillations from the cavity. For most cases, values of K fall in the range of 0.57 to 0.61 and values for ζ fall in the range of 0.21 to 0.25. The mode of cavity oscillations, also called the wavenumber, is determined by the number of vortices simultaneously observed in the shear layer formed between the cavity and the freestream flow during one vortex shedding cycle. The vortex shedding cycle is determined by the process requiring a single vortex to progress from the point of flow separation at the leading edge of the cavity to the point of impingement on the trailing edge of the cavity.

⁶Rossiter, J. E., "Wind Tunnel Experiments on the Flow over Rectangular Cavities at Subsonic and Transonic Speeds", Royal Aircraft Establishment Technical Report No. 64037, October 1964.

EFO FLUCTUATIONS

Class III Whistles

Class III whistles require a resonant or reflecting structure to perpetuate the acoustic feedback. The frequency of the tone is governed principally by the resonant modes of the reflecting geometry and not the speed of the flow. The flow speed can be varied over a wide range without affecting the pitch of the whistle. When the speed of the flow increases to a point where the first resonance of the reflecting structure is no longer amplifying the oscillations, the frequency jumps from the first frequency stage to a second stage.

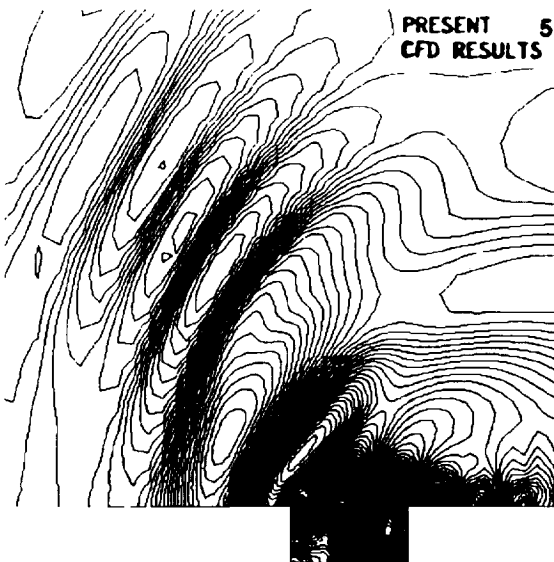


Figure 2.7.5 Acoustic Field Generated by Flow Over a Cavity at Mach 0.6

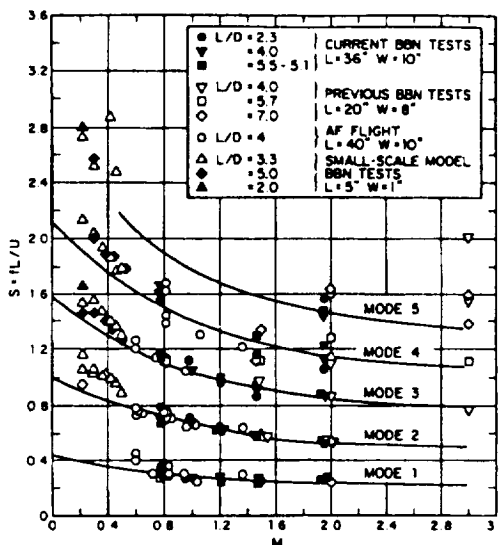


Figure 2.7.6 Strouhal frequencies of Cavity Modes Approach Constant Values at High Mach Numbers

Helmholtz Resonators

The Helmholtz resonator (side-branch resonator, volume resonator) is typified by the structure in Figure 2.7.7. The resonance frequencies are determined by the dimensions of the opening shown leading into the resonator, the cross sectional area and the length of the duct, and the inner volume of the resonator.

The equation for the resonant frequency of the Helmholtz resonator is given in the following formula⁷:

$$f = \frac{c}{2\pi} \sqrt{\frac{A}{Vl}} \quad (2.7.3)$$

where A is the cross sectional area of the duct leading to the resonator, l is an adjusted length of the duct leading to the inner volume of the resonator, V is the volume of the resonator, and c is the speed of sound.

The adjusted length of the duct, l , is approximated by:

$$l = l + 0.8\sqrt{A} \quad (2.7.4)$$

EFO FLUCTUATIONS

$$l = l + 0.8\sqrt{A} \quad (2.7.4)$$

where A is the cross sectional area of the duct and l is the length of the duct. If there are several branches of the duct leading into the resonator volume, the area A in equation 2.7.4 should reflect the number of branches as in:

$$l = l + 0.8\sqrt{\frac{A}{n}} \quad (2.7.5)$$

where n is the number of branches of the duct leading into the resonator.

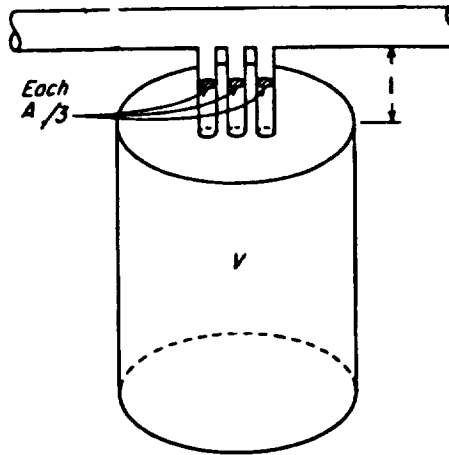


Figure 2-22. Schematic of Helmholtz Resonator

"Open-Open" (Closed-Closed) Organ Pipe Resonators

Organ pipe resonators are the most common acoustic resonators. Longitudinal organ pipe modes play a role in amplifying the acoustic pressure oscillations in the ducts. The organ pipe is a simple example of sound being generated by a vibrating fluid in a chamber or pipe where the axial wave motion of these vibrations creates a resonant condition. When both ends of a pipe are open or closed, standing waves form in the pipe and the fluid resonates at the natural frequencies based on a wavelength corresponding to twice the length of the pipe, i.e. the length of travel of a pressure wave from one end of the pipe to the other and back.

The standing wave frequencies observed from the "open-open" organ pipe acoustic source are given by:

$$f_n = \frac{n c}{2 l} \quad n=1,2,3,4,5,\dots \quad \text{"Open-Open or Closed-Closed" Organ Pipe (2.7.6)}$$

where f is the observed frequency, n is the mode, c is the speed of sound for the fluid, and l is the length of the pipe.

EFO FLUCTUATIONS

"Open-Closed" Organ Pipe Resonators

In an open-open pipe, Figure 2-23, the first longitudinal mode or fundamental frequency has antinodes at each end with a displacement node in the center or half the length of the pipe. The fundamental acoustic frequency of the open-closed pipe is one-half that of the open-open pipe for equal pipe lengths and harmonics increase in frequency at a rate half that of the open-open system as illustrated in Figure 2-24.

The basic formula for the open-closed "organ pipe" acoustic frequencies are given by:

$$f_n = \frac{2(n-1)c}{4l} \quad n=1,2,3,4,5,\dots$$

"Open-Closed"
Organ Pipe (2.7.7)

where f is the observed frequency, n is the mode, c is the speed of sound for the fluid, and l is the length of the pipe.

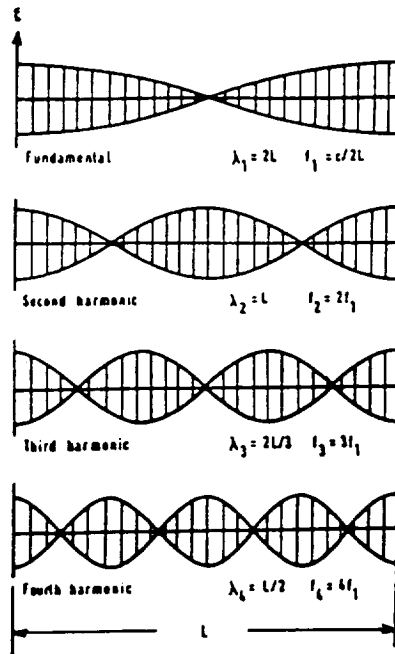


Figure 2-23. "Open-Open" Organ Pipe Resonance

EFO FLUCTUATIONS

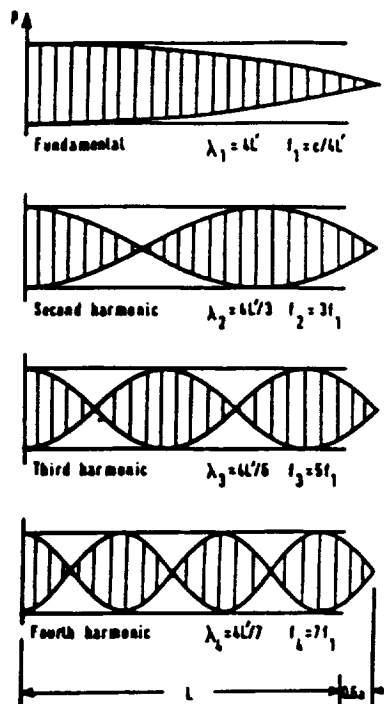


Figure 2-24. "Open-Closed" Organ Pipe Resonance

Side-Branch Resonance in Pipes

Complex piping systems with multiple side-branches are prone to flow-induced acoustic resonances. Resonances of deep cavities and side branches are self-sustaining oscillations due to the coupling between the resonant acoustic field and the oscillations of the unstable shear layer spanning the mouth of the cavity. Resonances occur at frequencies corresponding to acoustic modes in the piping systems and can be estimated from the equation⁸

$$f_n = \frac{(2n - 1) c}{4 \left[L + \frac{l}{2} \right]} \quad n = 1, 2, 3, \dots \quad (2.7.8)$$

where L is the branch length, l is the distance between branches, and c is the speed of sound in the media. Typical side-branches in piping systems which illustrate lengths used in Equation 2.7.8 are shown in Figure 2-25.

⁸Ziada, S., and E.T. Buhlmann, "Multiple Side-Branches as Tone Generators," International Conference on Flow-Induced Vibrations, Brighton, U.K. May 1991. (Submitted: J. Fluids and Structures)

EFO FLUCTUATIONS

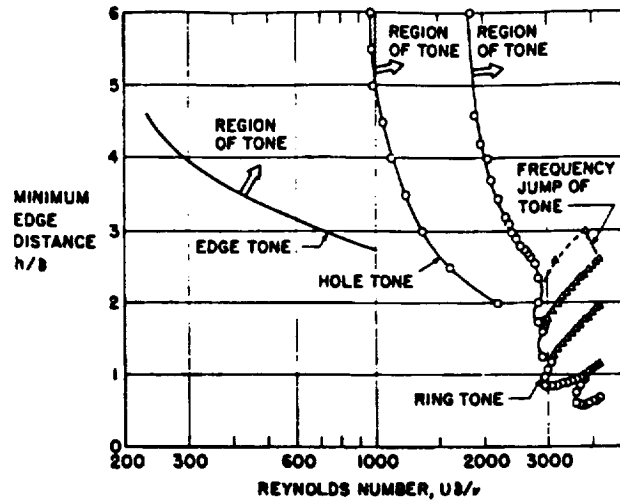


Figure 2-27. Comparison of Minimum Edge Distance For Generation of Edge-Tones, Hole-Tones and Ring-Tones

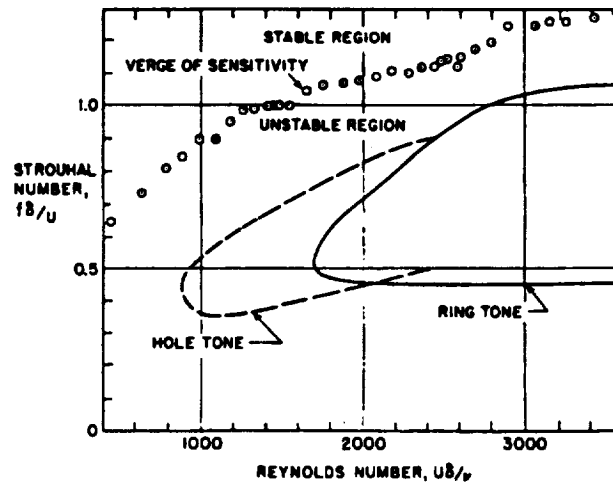


Figure 2-28. Hole-Tones and Ring-Tones Operate in the Jet Instability Region.

GEOMETRIC ANALYSIS

3. Geometric Analysis

Geometric analysis and flow characterization are performed together in making an assessment of potentials for flow-structural interaction. Unsteady fluid loads are either motion-independent or motion-induced as broken down in Figure 3-1. Motion-independent loads may be periodic or random, whereas motion-induced loads are primarily periodic. Periodic fluid forces include those resulting from vortex shedding. Random fluid oscillations include turbulence and acoustics.

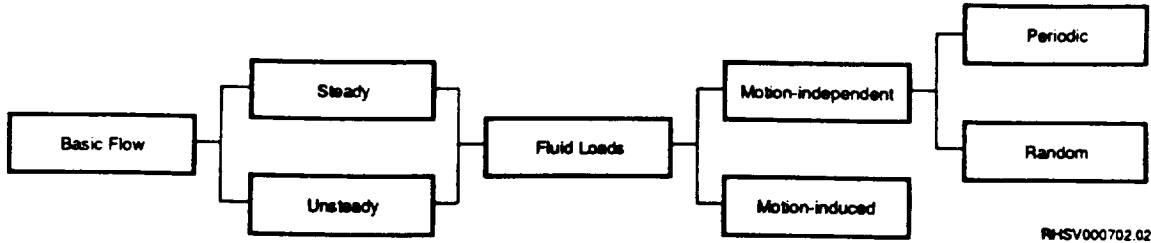


Figure 3-1. Characteristics of the Flow and its Interaction with Structure.

In some cases, the fluid forces are altered by the structural response, and motion-dependent fluid loads must be considered. These are cases of flow/structural interaction. Motion-induced unsteady fluid loads occur in the closed-loop feedback response of an elastic structure, Figure 3-2.

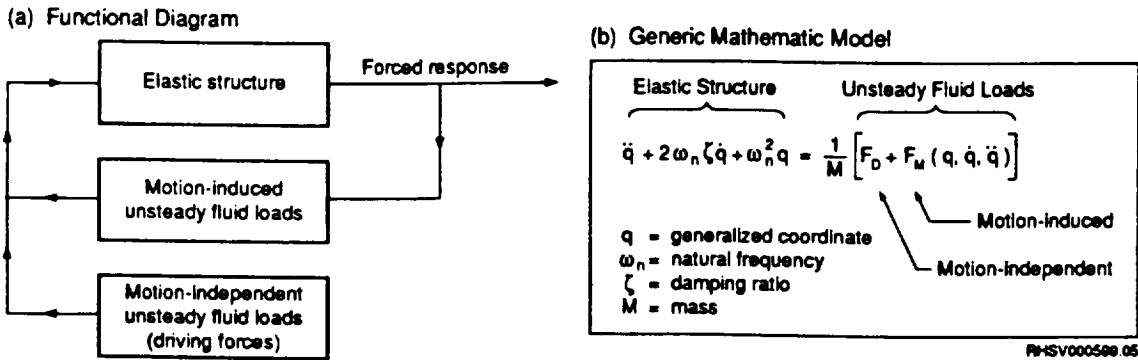


Figure 3-2. A Hydroelastic Forced Oscillation Model for Fluid/Structural Interaction.

Flow-structural interaction problems occur in specific regimes of reduced velocity. Quick estimates of Strouhal numbers at critical Reynolds numbers are made possible by handbook reference to basic geometry classifications and to fluid added mass as outlined in Figure 3-3. In many cases it is possible to quickly categorize the actual geometry in some design problem or some problem of high cycle fatigue in an operating system as being close to one of these basic fundamental geometries and thereby obtain the needed estimates.

These key words are used in organizing the material that has been collected and included in this handbook and in searching the vast literature available on flow/structural interaction at subsonic speeds where fluid density may be sufficiently high to drive significant structural responses and hence be a concern in fluid systems design.

GEOMETRIC ANALYSIS

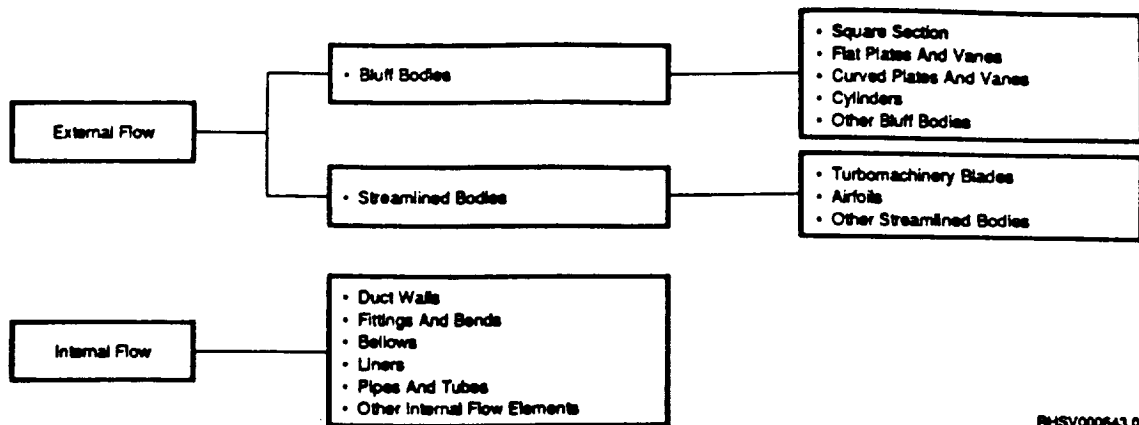


Figure 3-3. Key Words Based on Geometry Categorize Problem Types and Bring Out the Important Physics.

Structures in a fluid flow generally induce fluctuations in the flow field. These fluctuations or flow-induced oscillations may in turn excite natural modes of the structure. Such feedback loops in the fluid-structure system are sometimes nonlinear and under certain conditions may dominate the motion of the fluid-structure system. For each vibration mode, data required include the amplitudes of deflection, velocity and acceleration. These responses are translational for bending modes and angular for torsional modes. When each vibration mode is independent, the system may be described by studying each mode separately. In general however, systems have two or more degrees-of-freedom and the response can be analyzed only by solving a system of simultaneous differential equations.

Naudascher¹ provided an outline to identify hydrodynamic loads. Fluctuating hydrodynamic forces fall into this categories. These categories are fluctuations from: 1) extraneously induced excitations (EIE), 2) instability induced excitations (IIE), 3) movement induced excitations (MIE), and 4) excitations due to fluid oscillators (EFO). A variety of flow-structural elements^{2,3,4} such as vanes and struts at certain flow velocities are prone to flow-induced transverse, in-line, and torsional vibrations which are due to trailing-edge vortex shedding as well as leading-edge vortex shedding. A variety of internal flow elements are excited to vibrate from within the flow.

Dimensionless and reduced variables are first introduced. These include reduced velocity, Strouhal number, reduced amplitude, mass ratio, and reduced damping. If the energy input to the structural model is greater than the energy expended in damping, then the flow-induced vibrations will increase. Thus, lower reduced damping implies greater amplitude of structural response and consequently larger range of fluid flow velocities over which lock-in occurs. For lightly damped structures in dense fluids the reduced velocity is on the order of 5 and lock-in may persist over a 20% variation above and below the velocity which causes resonance.

¹E. Naudascher, "Hydrodynamic Forces", IAHR Monograph, Balkema/Rotterdam/Brookfield/ 1991.

²Sarpkaya, T., "Vortex-induced Oscillations: A Selective Review" Jour. of Appl. Mech., 46, June 1979.

³Davenport.A.G., and M. Novak, "Vibration of Structures Induced by Wind" in Harris, Cyril M. Shock and Vibration Handbook, McGraw-Hill, 1988.

⁴Rockwell, D. and Naudascher, E., "Review - Self-Sustaining Oscillations of Flow Past Cavity," J. Fluid Engineering, Transactions of ASME, vol. 100, pp. 152-165, June 1978.

Structural Modes and Amplitudes

Each natural mode of a linear structure is associated with a mode shape and natural frequency that characterize the form of free vibrations of that structure. The mode shapes of simple structures can be found by solving the linear equations of motion governing the system. For each degree-of-freedom of motion for a structure there is a corresponding vibration mode. Mode shapes for various simple geometries under different boundary constraints have been cataloged by Blevins⁵. The cataloged geometries include cross-sections, plates, shells, pipes, and various three-dimensional bodies.

Added Mass

Since each fluid element will be accelerated to some extent as a body moves in the fluid, fluid elements adjacent to the body are accelerated more than distant fluid elements. The effective mass of a body is defined as the sum of the structural mass and the fluid added mass. It refers to the portion of the mass involved in the specific mode of energy transfer along the direction of motion. For a structure with a constant mass immersed in a fluid, observed frequencies are lower than the natural frequencies of that structure in a vacuum. As the density of the fluid increases, effects of the added mass become significant.

The added mass of a structure is comparable to the mass of fluid displaced by the structure. For many geometrically simple structures, Blevins⁶ and Chen and Chung⁷ present formulas, tables and charts as aids in determining added mass. Chen and Chung also have two computer programs available for estimating added mass: AMASS for a group of circular cylinders and AMASS-FEM for structures of irregular and complex geometries. Relevant material on added mass including equations of motion, added mass tensor, simplified strip theory, and the effect on frequency reduction are also assembled in the handbook.

Vortex-Induced Vibration and Lock-In

Washizu et al⁸ investigated transverse vibrations of rectangular sections with wind-tunnel measurements. There were two types of aeroelastic instabilities which are vortex-induced vibration and transverse galloping. The base-to-height aspect ratio, c/d , is the key parameter which determines the type of instability. For rectangular sections with $c/d > 3$, transverse galloping motions would not occur and the heaving is due to the vortex shedding only. For rectangular sections with $c/d < 2.5$, both vibration modes can happen.

Based on their data of vibrating rectangular sections, they found two ranges of vortex shedding frequencies. In the case of $c/d = 2$, the Strouhal number ranges are $0.066 < S < 0.091$ and $0.143 < S < 0.294$. These rather wide ranges of Strouhal numbers are probably due to the range of vibration amplitudes and the range of system damping in the experiments. Their reduced damping had a range from 3 to 60.

When vortex shedding frequency falls in a range ($\pm 10\%$) containing a structural vibration mode, the structural vibration and vortex shedding would synchronize at a frequency and the nondimensional structural vibration amplitude, A_y , may go as high as in a range of 0.1 or greater. This synchronization is referred as the flow-structure lock-in phenomenon. Although lock-in is usually self-limited due to phase shifting between the displacement and lift coefficient, amplitudes

⁵Blevins, R.D., *Formulas for Natural Frequency and Mode Shape*, R. Kreiger Pub. Co., 1987.

⁶Blevins, R. D., *Flow-Induced Vibration*, second edition, Van Nostrand Reinhold, 1990.

⁷Chen, S.S. and Chung, H. "Design Guide for Calculating Hydrodynamic Mass Part I: Circular Cylindrical Structures", Components Technology Division, Argonne National Laboratory, Argonne, Illinois, June 1976, Document No. ANL-CT-76-45.

⁸Washizu, K. et al., "Aeroelastic Instability of Rectangular Cylinders in a Heaving Mode," J. Sound and Vibration, 59, 195-210, 1978.

GEOMETRIC ANALYSIS

on the order of 0.1 can be unacceptably high vibrations. Corless⁹ and Berger and Plaschko¹⁰ treated vortex-induced and galloping responses using the method of multiple time scales with considerable success in predicting amplitudes of transverse displacement and lift coefficient as well as the phase angle of experimental data.

In the case of $c/d = 4$, the two ranges of Strouhal numbers are $0.095 < S < 0.147$ and $0.2 < S < 0.294$. Thus, the aspect ratio c/d indeed affects the flow pattern. In terms of reduced velocity, the above Strouhal number ranges correspond to $15 > Vr > 11$ and $7 > Vr > 3.4$ for $c/d = 2$; and $10.5 > Vr > 7$ and $5 > Vr > 3.4$ for $c/d = 4$.

The vibration amplitudes (normalized by height) for vortex induced vibration are generally less than 0.1. From the above reduced velocities, the vortex-induced lock-in phenomenon would not occur at high flow velocities, because the reduced velocities for vortex-induced vibrations are generally under ~ 15 . Also, the amplitudes are limited (usually less than ~ 0.1) for the experimental range of the system damping used by Washizu et al⁸.

Galloping Responses

Galloping arises when the rate of change in an aerodynamic force coefficient produces a negative damping which exceeds the dissipative damping. When galloping occurs, the total damping force would more or less in-phase with the structure velocity, and unacceptable high vibration amplitudes are usually the result. According to data of Washizu et al, the transverse galloping response was found having amplitudes greater than 0.1 and tends to be unbound. In the range of system damping considered, the transverse galloping took place at high flow velocities, $Vr > 15$. The higher the system damping, the higher the onset critical galloping velocity necessary to trigger the galloping response. As aforementioned, transverse galloping would occur for $c/d = 2$, but not for $c/d = 4$.

For rectangular sections with $c/d = 2$ and flow velocity around $Vr = 15$, the flow vibration continues from vortex-induced vibration ($Vr < 15$) to transverse galloping ($Vr > 15$) in the case of low damping. Vortex shedding may initiate galloping; however, the flow velocity must be greater than the onset velocity to sustain the galloping. From their data, the vortex-induced vibration can probably be alleviated with high system damping, however, high system damping can only delay the galloping response to a higher onset flow velocity. Whether there can be galloping or not is basically geometry-dependent as indicated in the above cases for rectangular sections.

System Damping for Galloping Estimation

Flow-induced vibrations due to vortex shedding and turbulence do not always lead to galloping as long as the total damping does not become negative. In fact, for certain structure geometries such as circular cylinders, galloping will not occur. In order to predict the structural dynamic response, one needs the knowledge of system mass, system damping, structure natural frequencies, external excitation forces, and cross-sectional geometry.

Bearman et al¹¹ investigated experimentally flow-induced vibration of square sections for Reynolds number range of 10^4 to 3×10^4 and three levels of turbulence of 0.0%, 6.5% and 10.5%. In a square section, since the derivative of transverse force coefficient with respect to angle-of-attack, $A_1 = \partial C_y / \partial \alpha$, is positive; galloping response is possible and the estimate of the onset critical flow velocity is the primary objective. According to their data, the parameter A_1 has values of 5.4, 3.9 and 3.4, respectively, for the turbulence levels given above. Based on the reference formulation, the critical galloping velocity can be written as

⁹Corless, R. M. and Parkinson, G. V., "Mathematical Modeling of the Combined Effects of Vortex-Induced Vibration and Galloping. Part II", J. Fluids and Structures, 7, 825-848, 1993.

¹⁰Berger, E. and Plaschko, P., "Hopf Bifurcations and Hysteresis in Flow-Induced Vibrations of Cylinders," J. Fluids and Structures, 7, 849-866, 1993.

¹¹Bearman, P. W., Gartshore, I. S., Maull, D. J., and Parkinson, G. V., "Experiments on Flow-Induced Vibration of a Square-Section Cylinder," J. of Fluids and Structures, 1, 19-34, 1987.

GEOMETRIC ANALYSIS

$$U_o = \frac{2\beta}{n A_1} \quad (3.0.1)$$

where

$$U_o = \frac{V_o}{\omega_n h} = \text{critical reduced velocity of galloping}$$

$$n = \frac{\rho h^2}{2m} = \text{mass parameter}$$

ω_n = circular frequency of the nth bending mode

β = system damping ratio

h = size of the square section

m = mass per unit length including fluid added mass

V_o = critical galloping velocity

System damping is due to structure-related and fluid-related damping contributions. In the reference experimental range, system damping is between 9×10^{-4} to 6×10^{-3} . In most beam and plate cases, system damping can be written as the sum of structural material damping, end-constraint damping, fluid viscous damping and acoustic damping

$$\beta = \frac{\beta_s}{\sqrt{m/m_s}} + \beta_{ec} + \frac{C_D \rho D^2 V}{4 m \omega_n D} + \beta_{ac} \quad (3.0.2)$$

where the structural material damping can be estimated as a Zener damping constant¹²

$$\beta_s = \frac{\omega/\omega_R}{1 + (\omega/\omega_R)^2} \quad (3.0.3)$$

and the Zener relaxation frequency is given by

$$\omega_R = \frac{k \pi^2}{\rho_s c_p h^2} \quad (3.0.4)$$

and k, ρ_s , c_p = thermal conductivity, density and specific heat of the material when the fluid and the structure may not be in thermal equilibrium.

End-constraint damping is estimated as follows. Heat-exchanger tubing in air which is a typical clamped structure element, has a damping factor in the range of 0.002 to 0.008 as compiled by Blevins⁶. This includes material damping (~0.001) and clamping damping. For steel-like, clamped structures, an end-constraint damping of 0.001 is deemed a good conservative estimate.

¹²Crawley, E. F. and Van Schoor, M. C., "Material Damping in Aluminum and Metal Matrix Composites," MIT Industry Liaison Program Report, June 5, 1987.

GEOMETRIC ANALYSIS

The acoustic radiation damping can be a major item for flat plates, high frequencies, or dense fluids. As given by Blevins⁶, the acoustic damping for a rectangular section where the thickness to acoustic wave length ratio is small (ie., $a/\lambda < 0.2$) is given by

$$\beta_{ac} = \frac{\pi \rho (a^2 + b^2)}{16 \rho_s h \lambda} \quad (3.0.5)$$

where a, b, and h are the width, base and thickness of the rectangular element. The wave length relates to the speed of sound by

$$\lambda = \frac{2 \pi c}{\omega_n} \quad (3.0.6)$$

Effect of Turbulence on Galloping

Lindner¹³ presented a concise article on the effect of turbulence on the galloping of a rectangular section. Galloping oscillations are self-excited aeroelastic oscillations which occur perpendicular to the direction of the incident flow. They are, for example, observed on ice-coated cables, masts and pylons. Analytical solutions to this phenomenon have been known for some time. Since in nature, wind is subjected to turbulence, the influence on galloping oscillation is rather important. The y-component of the equation of motion for laminar flow is given by

$$m \ddot{y} + d \dot{y} + c y = F \frac{\rho}{2} u_{\infty}^2 b l c_y \quad (3.0.7)$$

where m, d, c are system mass, damping and spring constant; and b, and l are height and length of the section. The transverse force coefficient c_y as a function of incident angle was given in the reference. The coefficient increases with the incident angle up to 12°, then decreases linearly between 12° and 16°. The turbulent flow velocity vector is then presented in the form of

$$\mathbf{u} = \begin{bmatrix} u_{\infty} + \bar{u}' \\ 0 + \bar{v}' \end{bmatrix} \quad (3.0.8)$$

where the \bar{u}' and \bar{v}' represent the rms turbulent fluctuations of the flow velocity. Consequently the equation of motion for turbulent flow is written as

$$m \ddot{y} + d \dot{y} + c y = \frac{\rho}{2} (u_{\infty} + \bar{u}')^2 b l c_y(\phi^*) \quad (3.0.9)$$

where the instantaneous incidence angle is given by

$$\phi^* = \tan^{-1} \frac{\dot{y} + \bar{v}'}{u_{\infty} + \bar{u}'} \quad (3.0.10)$$

External Flow/Structural Elements (Bluff Bodies)

Idealized external flow exists for a body or structural element in an infinite fluid medium. An aircraft in free flight is an example. A body immersed in an internal flow passage sees wall constraint effects that change the local velocity and pressure about the body depending upon its

¹³Lindner, H., "Influence of Turbulence on Galloping Oscillations of a Rectangular Cylinder," ZAMM · Z. angew. Math. Mech. 70 (1990) 4, pp. 74-77, 1990.

GEOMETRIC ANALYSIS

cross-sectional area relative to that of the flow passage. In a wind tunnel at subsonic flow speeds or in a water tunnel when the body is very much smaller than the wind tunnel test section, the external flow conditions about the body nearly simulate those in free flight. Added mass and added moment of inertia effects are characterized for idealized external flow. They are provided in Table 3-1 for six of the basic geometries treated in this handbook.

Added mass and added moment of inertia can be estimated from these simple formulas for these body shapes. They increase linearly with increases fluid density. One fluid of particular interest for example, is LO₂ because of its high density and operation often under high pressure giving potentially high dynamic loads in rocket engine flow passages. Hydrogen-rich turbine gases in the 4,500 psi operating range also possess sufficient energy to drive structural elements to fracture or fatigue. Water, liquid nitrogen, and steam as well as any number of high-density or high-pressure fluids found in chemical processing industries possess sufficient energy to be of concern for hydrodynamic flow-structural interactions. Frequencies of structural response in a vacuum or even in air shift dramatically downward due to added mass and added moment of inertia effects in dense subsonic fluids.

Table 3-1. Formulas for Added Mass and Moment of Inertia

| GEOMETRY | ADDED MASS | ADDED MOMENT OF INERTIA |
|--|----------------------------|---------------------------------------|
| 1. Circular cylinder of radius a .  | $\rho \pi a^2 b$ | 0 |
| 2. Square section of side a .  | $1.51 \rho \pi a^2 b$ | $0.234 \rho \pi a^4 b$ |
| 3. Elliptical section with major radius a .  | $\rho \pi a^2 b$ | $\rho \frac{\pi}{12} (a^2 - c^2)^2 b$ |
| 4. Flat plate of height $2a$.  | $\rho \pi a^2 b$ | $\rho \frac{\pi}{12} a^4 b$ |
| 5. Sphere of radius a .  | $\frac{2}{3} \rho \pi a^3$ | 0 |
| 6. Cube of side a .  | $0.7 \rho a^3$ | — |

Note: b is the body length dimension for 1 through 4.

PH-SV000644.04



GEOMETRIC ANALYSIS

External Flow/ Structural Elements (Bluff Bodies)

RECTANGULAR SECTIONS

3.1 Rectangular Sections, Plates and Vanes

A rectangular section is a beam with a rectangular cross-section of base width, w and height, h . A square section is a rectangular section with equal base and height, $w = h$. A flat plate is a rectangular section with height-to-base ratio, h/w , of ~ 0.2 or smaller. A flat vane is a flat plate usually with a rounded leading edge and/or a shaped trailing edge. Since a square section is a special case of a rectangular section, we shall discuss square sections with rectangular sections in the following. Flow/structural interaction problems concerning these geometries are discussed in this section.

Bearman and Luo¹ experimentally investigated the aerodynamic instability of a square-section under forced vibration. The data base included a) lift and drag coefficients as functions of the reduced velocity; b) critical reduced velocities as functions of vibration amplitude for both minimum lift and onset of asymptotical lift; c) phase angle versus reduced velocity at various amplitudes; d) power spectral densities of lift fluctuations for different reduced velocities; and e) a flow map for flow regimes of multiple lock-in range, fluctuating lift recovery range and small-incidence-quasi-steady range. The range of applicability is for Reynolds numbers (based on the side length of the square) between 10,000 and 80,000.

Bending Modes, Added Mass and Structural Frequencies

Added mass can be calculated for slender bodies using a potential flow approximation by strip theory. In this theory, the body is considered as a union of two-dimensional cross-sections in its axial direction. For instance, the added mass for a circular cross-section of radius, r , is the fluid mass displaced by the cross-section. When summed over the length, L , of the cylinder, the added mass is $\rho \pi r^2 L$. In the case of a thin slender beam of height, h , side width, w , and axial length, L , the added mass in the beam normal direction is

$$M_a = \alpha \rho (\pi w^2/4) L \quad (3.1.1)$$

where the hydrodynamic mass coefficient, α , is 1 under strip theory (valid for $h \ll w \ll L$). In practice when the aspect ratio, L/w , is on the order of one, three-dimensional end effects become significant, this coefficient would deviate from unity. And, the plate may vibrate in modes higher than the first mode so that parts of the plate move upward while other parts move downward, the retarding effect of the surrounding fluid on the plate is hence reduced and $\alpha < 1$.

Cited by Blevins², Greenspon has proposed correlations for rectangular plates with one side exposed to fluid and presented results for all-side clamped (CCCC), all-side simply supported (SSSS) and two-side clamped two-side simply supported (CSCS) cases. For the SSSS case, the factor even greater than 1 (when $L/w = 1$) indicates some 'focusing' effect due to the 'hinged' end constraints. When there are clamped edges the α factor is lower than the all-edge simply supported case by a factor of ~ 2.7 . In these cases with one-sided fluid (for instance a flat wall of a water tank), the effect of the aspect ratio, L/w , on the added mass is the opposite to those for two-side submerged plates. Since structural frequencies can be substantially reduced by added mass, accurate estimate of structural frequencies relies on the proper selection of the added

¹Bearman, P. W. and Luo, S. C., "Investigation of the Aerodynamic Instability of a Square-Section Cylinder By Forced Oscillation", J. Fluids and Structures, 2, 161-176, 1988.

²Blevins, R. D., Formulas for Natural Frequency and Mode Shape, Van Nostrand Reinhold, New York, 1987.

RECTANGULAR SECTIONS

mass correlations. We may call this coefficient an added mass factor to indicate the deviation from strip theory result. This factor can be considered to be a product of several multipliers:

$$\alpha = w_h L_w M_d \quad (3.1.2)$$

The first multiplier, w_h , is due to width-to-height ratio, w/h , the second multiplier, L_w , is due to aspect ratio, L/w , and the third multiplier, M_d , is due to end constraints or mode shapes. The multiplier w_h was deduced from data of Wendel (1950) cited by Blevins².

| | | | | | | | | | |
|-------|-------|------|------|------|------|------|------|-------|--------|
| w/h | 0.10, | 0.20 | 0.50 | 1.00 | 2.00 | 5.00 | 10.0 | 100.0 | 1000.0 |
| w_h | 2.23 | 1.98 | 1.70 | 1.51 | 1.36 | 1.21 | 1.14 | 1.07 | 1.00 |

Meyerhoff³ and Chung and Chen⁴ obtained added mass for a thin plate from potential flow theory. The multiplier L_w , which approaches to unity when $L \gg w$, can be written as

$$L_w = \frac{L/w}{\sqrt{1+(L/w)^2}} \left[1 - 0.425 \frac{L/w}{1+(L/w)^2} \right] \quad (3.1.3)$$

Lindholm et al⁵ obtained added mass expressions for cantilevered plates for several modes. Let (i) be the mode index along the plate, and (j) be the mode index transverse the plate. One may deduce from their results the mode shape multipliers, M_d . For the translational modes (i=1, j=1), (i=2, j=1) and (i=3, j=1), the multipliers are unity; for the rotational modes (i=1, j=2) and (i=2, j=2), the multipliers are 0.375; while for the warping mode (i=1, j=3), the multiplier is 0.3212.

A general closed-form solution does not exist for vibration of a rectangular plate with various elementary boundary conditions on each of the four edges. However, it has been found that each of the mode shapes can be well approximated by the product of two beam modes in the separable form of the variables. Consequently, the mode shape multiplier can be obtained either exactly or with a numerical integration method.

$$M_d = \frac{\left(\int_A x_i z_j dA \right)^2}{w L \int_A x_i^2 z_j^2 dA} \quad (3.1.4)$$

This equation for thin plates may not be valid for rectangular beams. For instance, if one of the beam modes has both free ends, this multiplier is zero which may not be valid for a beam. For the first bending mode of a rectangular beam $M_d = 1$ is recommended. Consequently, the added mass per unit length is $m_a = M_a/L$, the structure mass is $m_s = \rho_s h w$ and the effective mass for transverse vibration is $m = m_a + m_s$. The area moment of inertia of a rectangular section for transverse vibration is given by $I = w h^3/12$. With these parameters known, the bending mode frequencies are calculated by an equation for uniform beams. For non-uniform beams, averaged E , I and m along the beam length need be obtained so to estimate the bending

³Meyerhoff, W. K., "Added Mass of Thin Rectangular Plates Calculated from Potential Theory," J. Ship Res. 14, 100-111 (1970).

⁴Chung, H. and Chen, S. S., "Hydrodynamic Mass," Argonne National Laboratory.

⁵Lindholm, U. S., Kana, D. D. and Abramson, H. N., "Elastic Vibration of Cantilever Plate in Water," J. Ship Res., 9, 11-22 (1965).

RECTANGULAR SECTIONS

frequencies with Equation 3.1.5. The deviation in structural frequency which results from using an added mass based on strip theory without a correction factor can be estimated with the following equation:

$$\frac{f}{f_{st}} = \sqrt{\frac{1 + \frac{m_a}{m_s}}{1 + \alpha \frac{m_a}{m_s}}} \quad (3.1.5)$$

where m_a and f_{st} are fluid added mass and estimated frequency based on strip theory, m_s is the structure mass and f is the more realistic structural frequency. The frequency ratio can reach a factor of the square root of 2 if the strip theory added mass is as much as the structure mass while the realistic added mass coefficient is zero ($\alpha = 0$) rather than 1. We conclude this discussion by citing a set of experimentally determined frequencies by Reed et al⁶ to show how the added mass reduces structure frequencies. The measured straight vane first bending frequency in air (low added mass) is 1085 Hz while in water (high added mass) is 369 Hz. These indicate nearly a three times influence. The present methodology and computer code have confirmed these measured data in both bending and torsion for Reed's experiment.

Vortex Shedding Strouhal Number

Knisely⁷ investigated vibration characteristics for rectangular and square sections. The primary conclusion of this experimental study is that the Strouhal number of the vortex shedding frequency changes rapidly when angle of attack increases from 0 to about 15 degrees and level off between 15 to 75 degrees, then decreases from 75 to 90 degrees. Effects of other key parameters (namely, corner roundness, side ratio, turbulence intensity, fluid density and Reynolds number) were evaluated.

Okajima, Mizota, and Tanida⁸ investigated flow around rectangular cylinders. The primary summary of the paper is given in the following:

- a) Flow oscillation around a rectangular section with height H and base B was studied.
- b) Strouhal number, S , versus Reynolds number, Re , in the range of $-100 < Re < -4.2 \times 10^4$ and $1.5 < H/B < 6.0$ was measured.
- c) Jumps in S were found in the above flow region.
- d) The jumps are attributable to flow reattachment.

Typical data are summarized as follows:

w/h = 1.5

| | | | | | | | | | | |
|-----------|------|------|------|------|------|------|------|-----|------|------|
| Re | 200 | 300 | 400 | 500 | 550 | 600 | 650 | 700 | 3000 | 6000 |
| S | .161 | .175 | .173 | .160 | .103 | .117 | .108 | .06 | .052 | .055 |

⁶Reed, D., Nesman, T. and Howard, P., "Vortex Shedding Experiment with Flat and Curved Bluff Plates in Water," ASME Symposium, Chicago, Illinois, December 1989.

⁷Knisely, C. W., "Strouhal Numbers of Rectangular Cylinders at Incidence: A Review and New Data," J. Fluids and Structures, 4, 371-393, 1990.

⁸Okajima, A., Mizota, T. and Tanida, Y., "Observation of Flow Around Rectangular Cylinders," pp. 381-386 in Yang, W. J. (editor), Proceedings of the Third International Symposium on Flow Visualization, September 6-9, 1983, Hemisphere Publishing Corporation.

RECTANGULAR SECTIONS

There are jumps between $500 < Re < 650$ as indicated in the table. At higher Reynolds number range ($700 < Re < 6000$), the Strouhal number can be approximated by 0.11.

w/h = 2.0

| | | | | | |
|----|------|-----|-----|------|-------|
| Re | 40 | 400 | 500 | 2000 | 95000 |
| S | .161 | .15 | .09 | .1 | .08 |

There are jumps between $400 < Re < 600$ as indicated in the table. At higher Reynolds number range ($700 < Re < 95000$), the Strouhal number can be approximated by 0.09.

w/h = 3.0

| | | | | | | |
|----|------|------|------|------|------|--------|
| Re | 70. | 450 | 650 | 4000 | 6000 | 100000 |
| S | .110 | .175 | .160 | .150 | .060 | .058 |

There are jumps between $650 < Re < 4000$ as indicated in the table. At higher Reynolds number range ($4000 < Re < 100000$), the Strouhal number can be approximated by 0.15.

In the Reynolds number range of $-6000 < Re < -42000$, S changes with w/h as follows:

| | | | | | |
|-----|------|------|------|------|------|
| w/h | .01 | 2.6 | 3.0 | 6.0 | 9.0 |
| S | .144 | .060 | .151 | .085 | .156 |

There are jumps near $w/h = 2.6$ and 6.0 .

Effect of Reynolds number

Additional data and comparison are summarized in the following. The effect of Reynolds number is given for the typical rectangular plate with base-to-height ratio of 3.0:

| | | | | | | |
|----|-------|-------|-------|-------|-------|--------|
| Re | 70. | 450 | 650 | 4000 | 6000 | 100000 |
| S | 0.110 | 0.175 | 0.160 | 0.155 | 0.151 | 0.150 |

There are jumps between $650 < Re < 4000$. There the Strouhal number may drop as low as 0.058. One may refer to Okajima et al⁸ for more details.

Effect of Base-to-Height Ratio

The effect of base-to-height ratio, w/h, is given for typical Reynolds number range of (0.6×10^4 to 4.2×10^4) as follows by Okajima et al⁸:

| | | | | | | |
|------------|------|------|------|------|------|------|
| w/h = 0.01 | 1.00 | 2.60 | 3.00 | 6.00 | 6.10 | 10.0 |
| S = 0.14 | 0.12 | 0.06 | 0.15 | 0.08 | 0.13 | 0.16 |

and Kinsely (1990).

| | | | | | | | |
|------------|-------|-------|-------|-------|-------|-------|-------|
| w/h = 0.04 | 0.25 | 0.50 | 0.80 | 1.25 | 2.00 | 4.00 | 5.00 |
| S = 0.147 | 0.153 | 0.140 | 0.136 | 0.113 | 0.120 | 0.070 | 0.124 |

RECTANGULAR SECTIONS

The jumps at $w/h = 2.60$ and at 4.00 are different between these data. However, their general agreement is good, that is, the Strouhal number is in a range of 0.1 to 0.15 for most cases of rectangular sections.

Effect of Angle-of-Attack

The effect of the angle-of-attack, β , for $Re = 18000$ to 47000 and $w/h = 3.2$ to 17.0 is given in Knisely⁷. Typical values are

| | | | | | |
|-----------|-------|-------|-------|-------|-------|
| $\beta =$ | 0.00 | 6.50 | 13.0 | 30.0 | 45.0 |
| $S =$ | 0.124 | 0.140 | 0.180 | 0.172 | 0.170 |

Effect of Trailing Plate

Arai and Tani⁹ investigated the effect of trailing plate to a square section. The experimental apparatus is shown in Figure 3-4 where the H_b is the base dimension of the square, D is the gap distance between the square and the trailing plate, and H_s is the length of the trailing plate. The vortex shedding frequency of the square without the trailing plate is termed as f_j . The frequency ratio of the frequencies with and without the trailing plate is therefore, f/f_j . Apparently, the frequency ratio is a function of Reynolds number, and the geometrical ratios, D/H_b and H_s/H_b . Typical data are summarized in Figure 3-5. The trailing plate may reduce the frequency of lift coefficient by as much as -80% as implied by the figure.

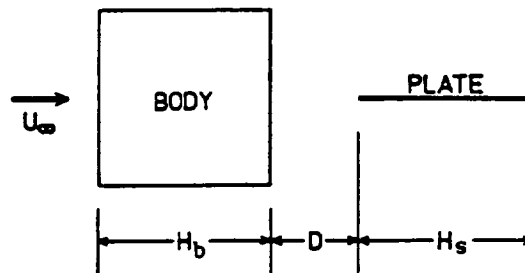


Figure 3-4. Cross-Section of the Trailing Plate

Galloping and Turbulence

The vortex-induced oscillation and hydrodynamic galloping response of rectangular rigid sections ($h/w = 2$), mounted elastically and restricting oscillations only to a plane normal to the incident water flow, was studied both experimentally and analytically by Bokian and Geoola¹⁰. Wake observations of stationary sections indicated that in the range of Reynolds number tested, the Strouhal number was roughly constant and insensitive to turbulence characteristics. The Strouhal number was estimated to be 0.137 for a sharp-edged section; and 0.169 and 0.183 for round-edged sections with $r/h = 0.141$ and 0.187 , respectively. The still water added mass of sharp-edged sections was found to be considerably higher than the value predicted through the application of the potential flow theory.

⁹Arai, N. and Tani, T., "Active Control of Vortex Shedding Frequency by a Splitter Plate," International Congress on Recent Developments in Air- and Structure-Borne Sound and Vibration, Auburn University, USA, March 6-8, 1990.

¹⁰Bokian, A. R. and Geoola, F., "Hydroelastic Instabilities of Square Cylinders," J. Sound and Vibration, 92(1), 117-141, 1984.

RECTANGULAR SECTIONS

As opposed to vortex resonance, turbulence was found to have profound effects on galloping vibrations. The variation of the lateral force coefficient with the angle of flow attack, as well as the dynamic tests, revealed that the tendency for galloping instability increased with an increase in turbulence intensity.

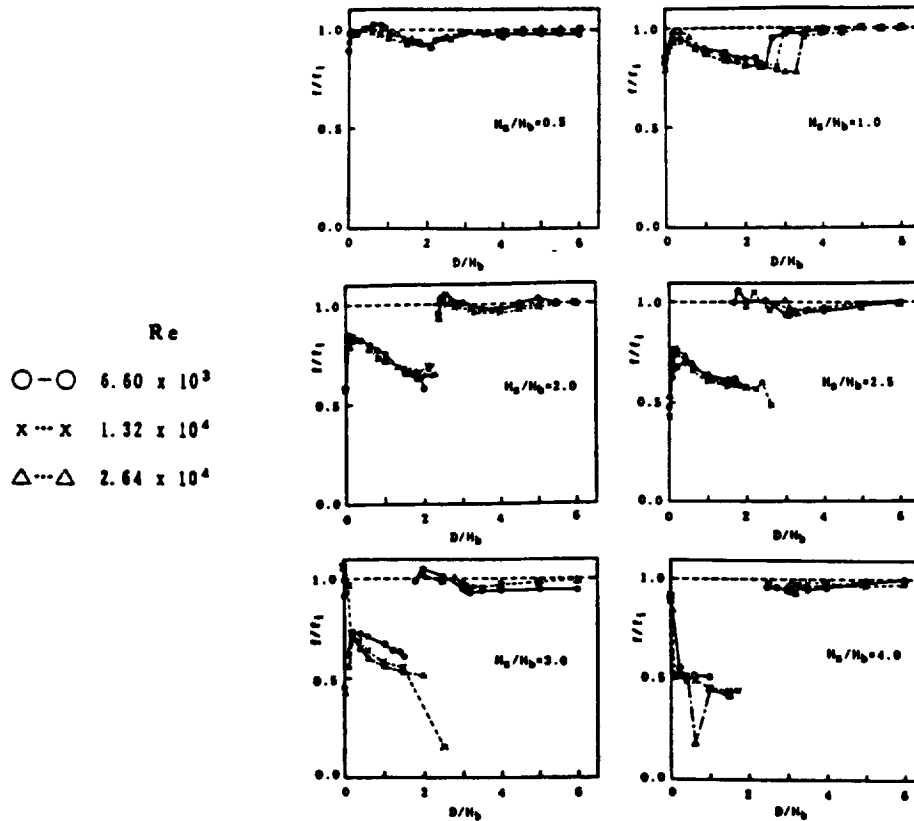


Figure 3-5. Effects of gap width on vortex shedding frequency

Equivalent Circular Cylinder

In certain ranges of Reynolds numbers if the data for a rectangular section are lacking and the data for circular cylinders are available, one may use data for circular cylinders to estimate the vibrational parameters for the rectangular section by using the concept of hydraulic diameter

$$D_h = 4 A/P = 4(\text{flow area})/\text{wetted perimeter}$$

That is, the rectangular section is treated as an equivalent circular cylinder of diameter D_h .

Aerodynamic Forces on a Flat Plate Gliding on a Freestream

Theoretical aerodynamic load coefficients are available only for simple geometries and idealized flow conditions. One set of cases is given in the following for a flat plate gliding on a freestream (free-free end conditions, unclamped). With the aid of numerical methods, the theoretical formulation becomes more tractable. A Runge-Kutta code was developed to calculate

RECTANGULAR SECTIONS

a three-degree-of-freedom motion of a two-dimensional flat plate section that is gliding on an air stream at standard density as an example. The motion state of the plate includes the falling distance, transverse displacement, and rotation angle. Added mass effects for dense fluids and end constraint effects may be estimated using the methods described above.

Force coefficients for flat plate are further addressed herein based on a theoretical formulation. Milne-Thomson (1968) gives a derivation of the Rayleigh's formula for the thrust force, T , on a thin plate exerted by the flow:

$$T = \rho U^2 h \frac{\pi \sin \beta}{4 + \pi \sin \beta} \quad (3.1.6)$$

where

- ρ = fluid density
- U = freestream flow velocity
- h = plate height
- β = angle-of-attack (AOA)

The lift, L , and drag, D , on the plate are components of the thrust force and given by

$$\begin{aligned} L &= T \cos \beta \\ D &= T \sin \beta \end{aligned} \quad (3.1.7a,b)$$

The flow configuration is shown in Figure 3-6. Equation (3.1.6) and Equation (3.1.7a) yield the relation of lift versus attack angle:

$$L = \frac{\rho U^2 h}{2} \frac{\pi \sin 2\beta}{4 + \pi \sin \beta} \quad (3.1.8)$$

The lift coefficient is therefore

$$C_L = \frac{\pi \sin 2\beta}{4 + \pi \sin \beta} \quad (3.1.9)$$

In terms of the angle-of-attack, the relation is shown in Figure 3-7 that the lift has a maximum at an angle approximately equal to 50° . The rate of change of the lift coefficient with respect to the angle-of-attack is also shown in the figure. The drag and drag coefficient can be obtain similarly

$$D = \rho U^2 h \frac{\pi \sin^2 \beta}{4 + \pi \sin \beta} \quad (3.1.10)$$

$$C_D = \frac{2 \pi \sin^2 \beta}{4 + \pi \sin \beta} \quad (3.1.11)$$

The evaluation of the moment coefficient is made in the following. The derivative of the velocity potential on the wind-side surface of the plate can be expressed as

RECTANGULAR SECTIONS

$$\frac{dw}{dz} = \frac{2hU(\zeta + a)}{(4 + \pi \sin \beta) \frac{dz}{d\zeta}} \quad (3.1.12)$$

where

$$\frac{dz}{d\zeta} = \frac{2h[1 + a\zeta + \sqrt{(1-a^2)(1-\zeta^2)}]}{4 + \pi \sin \beta} \quad (3.1.13)$$

Here $z = x + iy$ and ζ is a transformed coordinate defined by Equation (3.1.13). The equations (3.1.12) and (3.1.13) are reduced forms and only valid for the surface of the plate. On the plate, the range of ζ is from -1 to 1. The frontal pressure in excess to the back pressure which is the freestream pressure for the gliding plate is given by

$$p - p_{\infty} = \frac{1}{2} \rho U^2 \left[1 - \frac{\left(\frac{dw}{dz}\right)^2}{U^2} \right] \quad (3.1.14)$$

Thus the pressure coefficient is

$$C_p = \frac{p - p_{\infty}}{\frac{1}{2} \rho U^2} = \left[1 - \frac{\left(\frac{dw}{dz}\right)^2}{U^2} \right] \quad (3.1.15)$$

The moment coefficient is then evaluated as

$$C_M = \frac{M}{\frac{1}{2} \rho U^2 h^2} = \int_{-1}^1 \frac{z}{h} \left[1 - \frac{\left(\frac{dw}{dz}\right)^2}{U^2} \right] \frac{dz}{h d\zeta} d\zeta \quad (3.1.16)$$

The pressure coefficient along the plate is given in Figure 3-8 for several attack-angles. The lift, drag and moment coefficients are given in Figure 3-9 as functions of the attack-angle, β . Since the lift, drag and moment change as β does, the motion status of the plate would change as the plate gliding in the freestream.

RECTANGULAR SECTIONS

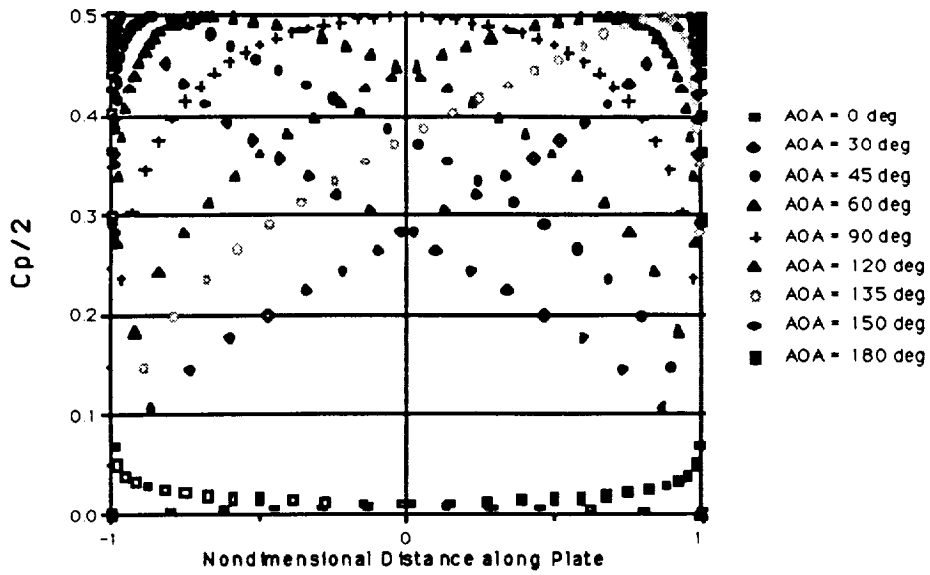


Figure 3-8. Pressure Coefficient Versus Chord Distance Along Plate.

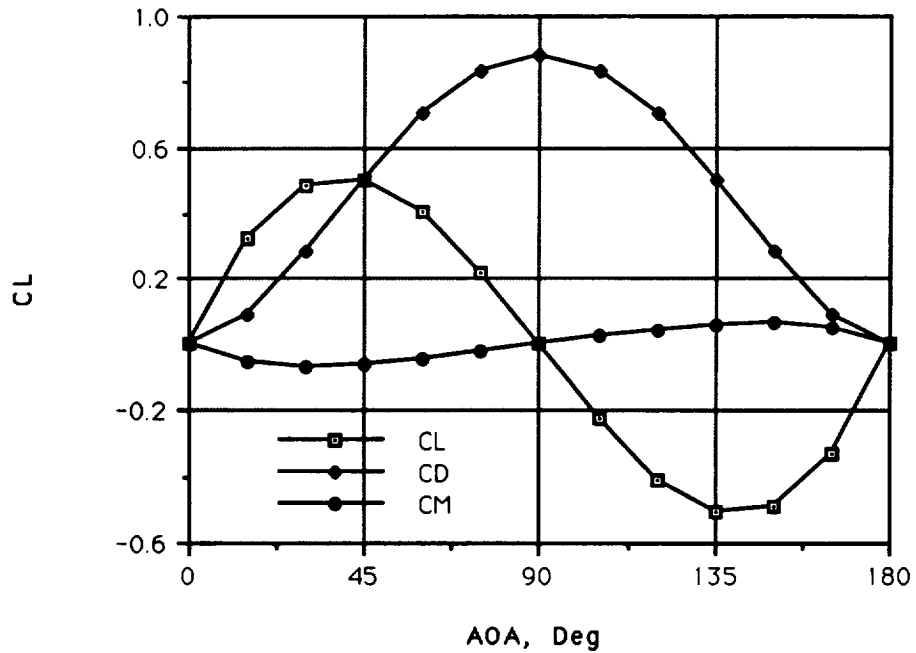


Figure 3-9. Lift, Drag and Moment Coefficients as Functions of Angle-of-Attack for Two-Dimensional Flat Plate Section.

RECTANGULAR SECTIONS

Development of Rectangular Section Code

In more general cases, the theoretical approach described in the foregoing may not be applicable, a Fortran program called RECTANGLE has been developed to provide an analysis. The program calculates the first three mode bending frequencies and estimates the fundamental mode vibration amplitudes of displacement, velocity and acceleration for a rectangle beam or vane in a fluid flow. It also calculates the first three mode torsional frequencies.

Inputs required by the code and sample values for the acrylic straight vane used by Reed et al⁶ are given as follows: a) Height $h = 0.005588$ m, b) Width $w = 0.06096$ m, c) Length $L = 0.1016$ m, d) Fluid density $\rho = 997.4$ kg/m³ for water, e) Structure density $\rho_s = 1190.2$ kg/m³ for acrylic, f) Young's modulus $E = 4.8 \times 10^9$ Pa for acrylic, g) Flow velocity = 8 m/s as a typical case, h) Flow kinematic viscosity = 9.83×10^{-7} m²/s. Flow is in x-direction, transverse is y- and span-wise is z-direction. Height is the dimension in y-direction, width is in x- and length is in z-direction.

Vortex Shedding Frequency and Structural Response

Vortex shedding Strouhal number is a function of Reynolds number. Reed et al⁶ found that the Strouhal number in the test condition is approximately 0.20. For a wider range of flow conditions including cases with non-zero yaw angle, we suggest the following equivalent cylinder method to determine the vortex shedding Strouhal number for the beam or plate: a) Find cross-flow velocity $V_n = V \sin \alpha$ as in the cylinder case. At a yaw angle, α_0 , the frontal dimension of a plate is $D_f = w \sin \alpha_0 + h \cos \alpha_0$; b) Find the Reynolds number, $Re = V_n D_f / \nu$; c) Find the Strouhal number based on circular cylinder correlations with the above Re and D_f . Flow-structural lock-in is assumed whenever the vortex shedding frequency is within $\pm 20\%$ of a structure frequency.

Using above S , equivalent diameter, reduced mass and reduced damping; the transverse vibration amplitude can be estimated with the equations given by Blevins¹¹, p. 71, for the proper end constraint. In addition, Blevins¹¹, p. 118, discusses the onset condition for galloping motion of a square section. Parameters used are $U = V_r / (2 \delta_r)$, $a_1 = 2.7$, $a_3 = -31$. and $A' = 1 - U a_1$. If $A' > 0$, galloping would not happen, otherwise the vibration amplitude is given by

$$A_y/D = \Delta \delta_r / \pi \quad (3.1.17)$$

where $\Delta = ((1 - U a_1) / 4 U / a_3)^{1/2}$. Washizu et al¹² indicated that galloping occurs in rectangular sections with $w/h < 3$. When $w/h > 3$, galloping would not occur. Therefore, the flat vane in the present study would not have galloping motion.

¹¹Blevins, R. D., Flow-Induced Vibration, p. 56, second edition, Van Nostrand Reinhold, 1990.

¹²Washizu, K. et al., "Aeroelastic Instability of Rectangular Cylinders in a Heaving Mode," J. Sound and Vibration, 59, 195-210, 1978.

RECTANGULAR SECTIONS

Added Moment of Inertia and Torsional Modes

The added moment of inertia of a plate can be written as $I_a = \rho \pi w^4 M_{dm} w_{hm}/128$, where the multiplier w_{hm} (a function of width to height ratio, w/h) can be deduced from Wendel (1950) as cited by Blevins⁶.

| | | | | | | | | | |
|----------|-------|------|-----|------|-----|-----|------|------|------|
| w/h | 0.10 | 0.20 | 0.5 | 1.0 | 2.0 | 5.0 | 10. | 100 | 1000 |
| w_{hm} | 11760 | 750 | 9.2 | 1.87 | 1.2 | 1.2 | 1.09 | 1.05 | 1.00 |

with the present w/h the added moment of inertia multiplier $w_{hm} = 1.09$. Lindholm et al⁵ obtained added mass expressions for cantilevered plates for several modes. One may deduce from their results that the mode shape multipliers, M_{dm} , for the rotational modes ($i=1, j=2$) and ($i=2, j=2$), the multiplier are 0.375. For torsional mode of a rectangular beam we recommend using this value. Parameters needed in torsional vibration analysis include shear modulus, G , and torsional constant, T_c , of the cross-section. Torsional constant for rectangle is given by Roark and Young¹³

$$T_c = (1/3 - 0.21023 (h/w - (h/w)^5/12)) w h^3 \quad (3.1.18)$$

The polar area moment of inertia is the sum of that of the structure and added moment of inertia

$$I_p = h w (w^2 + h^2)/12 + I_a/\rho_s \quad (3.1.19)$$

A length factor, L_f , is used. For full beam (or shaft) length, its value is 1. For half beam length, its value is 0.5. For first torsional mode frequency, a fixed-fixed full length beam is the same as a fixed-free beam of half length. Torsional mode eigenvalues are given: a) either free-free or fixed-fixed, $\lambda_n = n \pi$; b) fixed-free, $\lambda_n = (2n - 1)\pi/2$; c) slack-free, $\lambda_n = [(2 - S_c)n + (S_c - 1)(2n - 1)/2]\pi$. Here a slack boundary condition is a condition between a fixed condition and a free condition with a slackness coefficient, S_c , of value between 1 and 2. The torsional mode frequency is given by

$$f_r = \lambda_n (T_c G/\rho_s I_p)^{1/2} / (2 \pi L L_f) \quad (3.1.20)$$

where n is the modal index from 1, 2 and on.

Application to Rectangular Vane

An option of the RECTANGLE code is developed to deduce the amplitude of the lift coefficient from experimental data of rms acceleration, Grms. In the reference data Grms is a function of reduced velocity, V_r . By assuming that the first bending mode is the dominant vibration mode and the transverse vibration is induced by the oscillatory lift force, the maximum lift coefficient (at the mid span of the vane) amplitude is deduced and plotted in Figure 3-10. Another option is also implemented which utilizes the above experimentally deduced C_{L_e} amplitude to predict the rms acceleration. As expected a good agreement is achieved. Since the

¹³Roark, R. J. and Young, W. C., Formulas for Stress and Strain (5th ed.), p. 290, McGraw-Hill, New York, 1975.

RECTANGULAR SECTIONS

C_{Le} curve is based on a slightly modified Grms (V_r from 5.6 to 6.0) data, the prediction curve (dash line) does not follow exactly as the experimental data shown. However, this modified C_{Le} curve offers slightly larger and more conservative prediction in the lock-in regime and therefore is deemed appropriate.

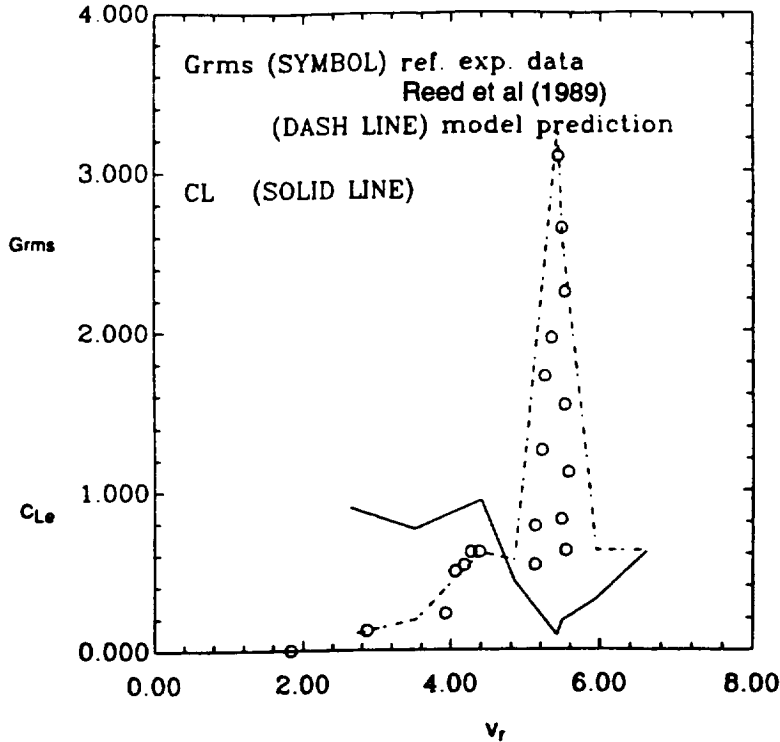


Figure 3-10. Model Prediction of Grms and CL Amplitude for Rectangular Vane.

In frequency simulation the following procedure is used: a) Determine a value of Young's modulus so that the bending frequency in air is 1085 Hz. The determined value of 4.565×10^9 Pa is indeed in the range for a lucite-acrylic material; b) Since air is very low density in comparison to acrylic, the added mass and added moment of inertia are negligible. The slackness factor is determined to have a good prediction in the torsional frequency, 1619 Hz, in air; c) Calculation for water flow is then made. Without a mode shape factor, the predicted bending frequency in water is around 360 Hz. By the input of the factor $M_{dm} = 0.9$, better prediction is obtained as shown in Table 3-2; d) The predicted torsional frequency in water is 826 Hz which is only 2% lower than the experimental data by using the same slackness factor of 1.459 and the mode shape factor of 0.9 as in the air flow prediction.

Table 3-2. Model Prediction of Reference Experimental Data

| MODE | MEDIUM | EXP. FREQ, Hz (Reed et al) | Calculated Freq., Hz (Present Method) |
|-------------|--------|-------------------------------|--|
| 1st Bending | air | 1085 | 1085 |
| | water | 380 | 377 |
| 1st Torsion | air | 1619 | 1619 |
| | water | 840 | 826 |

RECTANGULAR SECTIONS

Application to a Discharge Pipeline Rectangular Flowmeter

A typical example in the study of flow/structural interaction and to understand better liquid rocket engine flow conditions follows. An analysis on a LO₂ turbopump discharge rectangular flowmeter proposed for the Space Shuttle Main Engine (SSME) is presented herein. The way the proposed flowmeter works is that a strain gage measures the vortex shedding frequency, and a calibration of velocity based on the measured frequency gives the volumetric flowrate.

Assumptions

1. Structural modes for the vortex shedding vane transverse vibrations are considered. However, other structure modes such as shell and pipe modes are not included in the present study.
2. Parameters and methods used in the analysis lead to the conclusion. The conclusion may not be applicable to cases when the parametric values are much different from what being used herein.
3. Possibility of cavitation and its effect are not considered.

Sample Parameters

The sample dimensions are shown in Figure 3-11 with length, $L = 2.24''$, height, $h = 0.28''$ and base width, $w = 0.16''$. The fluid is liquid oxygen with average flow parameters assumed: flow velocity, $U_{\max} = 92$ ft/s, temperature, $T = 196$ °R, fluid density, $\rho_f = 70.15$ lbm/ft³, and dynamic viscosity, $\mu = 0.45$ lbm/hr/ft. The material of the flowmeter is the A26 steel, for which the following properties are assumed: Young's modulus, $E = 30.5 \times 10^6$ psi, structure density, $\rho_s = 0.287$ lbm/in³, and Poisson's ratio, $\nu = 0.29$.

Calculations

The Reynolds number based on height is obtained: $Re = \rho_f U_{\max} h / \mu = 1.2047 \times 10^6$. Liu et al (1992) summarized several correlations for the estimate of fluid added mass due to rectangular structures. The width-to-height ratio is obtained: $w/h = 0.57143$. Therefore, the width-to-height-ratio multiplier, w_h , described in the reference can be calculated as 1.6729. The length-to-width ratio is obtained: $L/w = 14$, therefore the length-to-width-ratio multiplier, L_w , is calculated to be 0.96733 from the reference. The mode shape multiplier for the both ends fixed is also given in the same reference:

$$M_d = \left(\frac{2\sigma_n [1 - (-1)^n]}{\lambda_n} \right)^2 = \begin{cases} 0.69034, & n = 1 \\ 0, & n = 2 \\ 0.13232, & n = 3 \end{cases} \quad (3.1-21)$$

where σ_n and λ_n are eigenvalues associated to the end constraints. Consequently, the added mass factor is calculated as

RECTANGULAR SECTIONS

$$\alpha = w_h L_w M_d = \begin{cases} 1.1171, n = 1 \\ 0, n = 2 \\ 0.21413, n = 3 \end{cases} \quad (3.1-22)$$

The structure mass, fluid added mass and effective mass for the first three bending modes are given in the following:

$$m_s = \rho_s w h = 0.15429 \text{ lbr/ft} \quad (3.1-23)$$

$$m_a = \alpha \rho_f \frac{\pi W^2}{4} = \begin{cases} 0.010942 \\ 0.0 \\ 0.0020974 \end{cases} \text{ lbr/ft} \quad (3.1-24)$$

$$m = m_s + m_a = \begin{cases} 5.1356e-3 \\ 4.7955e-3 \\ 4.8607e-3 \end{cases} \text{ slug/ft} \quad (3.1-25)$$

As effective mass is obtained, the transverse bending frequencies can be calculated as follows. One needs also the area moment of inertia:

$$I = \frac{w h^3}{12} = 2.9269e-4 \text{ in}^4 \quad (3.1-26)$$

$$f_n = \frac{\lambda_n^2}{2 \pi L^2} \sqrt{\frac{EI}{m}} = \begin{cases} 11227., n = 1 \\ 32028., n = 2 \\ 62370., n = 3 \end{cases} \text{ Hz} \quad (3.1-27)$$

If a Strouhal number of 0.13 is used, the vortex shedding frequency is 512.57 Hz. Since this frequency is very much smaller than the above structure bending frequencies, flow-structure lock-in would not occur and the design should be adequate for the intended purpose.

Galloping

By using a galloping analysis for a square section cited by Blevins(1990), a preliminary estimate of galloping is made in the following for the first bending mode. First the nondimensional parameters are given:

Reduced velocity, $V_r = U/f_y D = 0.35119$ for $n = 1$ (the first bending mode)

Reduced mass, $m_r = m/\rho D^2 = 4.3263$ for $n = 1$

$$U_b = \frac{U}{f_y D} \frac{\rho D^2}{4 m (2 \pi \zeta_y)} = \frac{V_r}{8 m_r \pi \zeta_y} = 0.2178, \text{ if } \zeta_y = 0.01483 \quad (3.1-28)$$

Since $U_b < 0.37$, no galloping is possible at 92 ft/sec; and the onset flow velocity would be 156 ft/sec. When velocity exceeds the onset flow velocity the nondimensional vibration amplitude can be calculated by

$$A_b = \sqrt{\left[4(1 - U_b a_1) \frac{U_b}{3 a_3} \right]} \quad (3.1-29)$$

RECTANGULAR SECTIONS

where $a_1 = 2.7$ and $a_3 = -31.0$ for typical square sections and improved values should be used if available. The diameter, D is identified with h , the flow velocity, $U = U_{max}$, the transverse frequency, $f_y = f_1$, and fluid density, $\rho = \rho_f$. Since

$$A_b = \frac{A_y \rho D^2}{D 4 m \zeta_y} \quad (3.1-30)$$

one may calculate the nondimensional transverse amplitude as

$$\frac{A_y}{D} = \frac{4 m \zeta_y A_b}{\rho D^2} \quad (3.1-31)$$

Lift, Drag and Strouhal Number

The range of values of drag and lift coefficients and Strouhal number for rectangular sections including square sections can be found in the literature. Some of the relevant data are collected in Table 3-3. Schewe's¹⁴ Reynolds number range for the square section is one of the highest in the table.

Strouhal Number Dependency on Corner Roundness

Strouhal number dependency on corner roundness can be found in the literature. Some of the relevant data are given in Table 3-4. From the table, the larger the corner roundness the higher the Strouhal number. At a roundness ratio of $r/w = 0.5$, the square section becomes a circular cylinder.

Table 3-3. C_D , C_L and Strouhal Number for Rectangular and Square Sections

| Reference | w/h | Re | C_{Drms} | C_{Lrms} | S |
|------------------------------------|-------|---------------------------------------|------------|----------------|-------------|
| Knisely ⁷ | 0.5 | 5000-3x10 ⁵ | 2.4 | 0.65-1.0 | 0.135-0.14 |
| Obasaju ¹⁵ | 1.0 | 10 ⁴ -1.25x10 ⁵ | 2.17 | -- | 0.121-0.127 |
| Bearman-Trueman ¹⁶ | 0.571 | 2x10 ⁴ -7x10 ⁴ | 2.75 | -- | 0.13 |
| Courchesne-Laneville ¹⁷ | 0.571 | 2x10 ⁴ -10 ⁵ | 2.42 | -- | -- |
| | | ⊙10% turbulence | | | |
| Bearman-Luo ¹ | 1.0 | 9x10 ⁴ | -- | 1.35 | -- |
| Schewe ¹⁴ | 1.0 | 10 ⁵ -4x10 ⁶ | 2.05-2.2 | 0.4 C_{Drms} | 0.121 |

¹⁴Schewe, G., "Force Measurements in Aerodynamics Using Piezo-Electric Multicomponent Force Transducers," In Proceedings of 11th International Congress on Instrumentation in Aerospace Simulation Facilities, Stanford University, pp.263-268, Aug. 26-28, 1985.

¹⁵Obasaju, E. D., "An Investigation of the Effects of Incidence on the Flow Around a Square Section Cylinder," Dept. of Aeronautics, Imperial College, London.

¹⁶Bearman, P. W. and Trueman, D. M., "An Investigation of the Flow Around Rectangular Cylinders," Aeronautic Quarterly, Vol. 23, 229-237, 1972.

¹⁷Courchesne, J. and Laneville, A., "An Experimental Evaluation of Drag Coefficient for Rectangular Cylinders Exposed to Grid Turbulence," J. Fluids Engineering, Vol. 104, 523-528, 1982.

RECTANGULAR SECTIONS

Table 3-4. Strouhal Number Dependency on Corner Roundness

| Reference | Re | w/h | r/w= | 0.0 | 0.164 | 0.20 | 0.318 | 0.34 | 0.5 |
|--|------------------------|-----|------|-------|-------|-------|-------|------|------|
| Bokaian-Geoola ¹⁰ (1984) | 1000~2x10 ⁴ | 1.0 | S= | 0.125 | 0.14 | -- | 0.156 | -- | 0.21 |
| Knisely ⁷ | 5000~3x10 ⁵ | 0.5 | S= | 0.138 | -- | 0.192 | -- | -- | -- |
| | | 1.0 | S= | 0.132 | -- | 0.142 | -- | 0.16 | 0.21 |

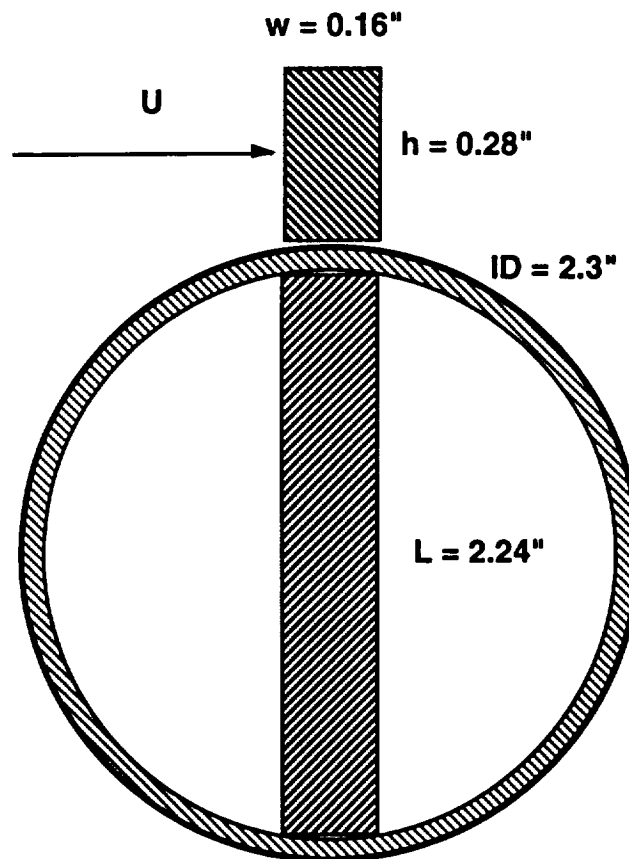


Figure 3-11. Pump Discharge Line Flowmeter Dimensions Used In the Example.

Natural Frequencies of Flat Plate

Leissa¹⁸ presented exact solution of natural frequencies of rectangular plates. Three basic boundary conditions considered are Free (F), Simply-supported (S), and Clamped (C). Numerical

¹⁸Leissa, A. W., "The Free Vibration of Rectangular Plates," J. Sound Vibration, 31, 257-293, 1973.

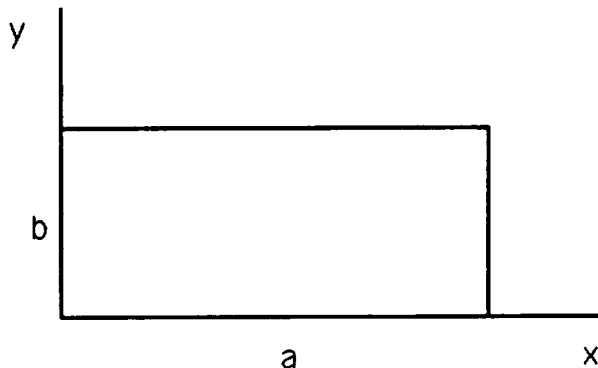
RECTANGULAR SECTIONS

data of the first six modes for all 21 combinations of these three basic boundary conditions on the four edges of the plates were presented for the eigenvalues, λ_{ij}^2 in the frequency formula:

$$f_{ij} = \frac{\lambda_{ij}^2}{2\pi a^2} \left[\frac{E h^3}{12 \gamma (1 - \nu^2)} \right]^{1/2} \quad (3.1-32)$$

$$i = 1, 2, 3 \dots, j = 1, 2, 3 \dots$$

where f_{ij} = natural frequencies,
 a, b = plate dimensions as shown in the sketch,



ν = Poisson's ratio,
 γ = mass per unit area,
 E = Young's modulus,
 h = plate thickness, and
 λ_{ij}^2 = eigenvalues which are functions of plate aspect ratio, a/b , and edge constraints.

For additional modes, the natural frequencies can be estimated with Rayleigh's energy technique. The natural frequencies of isotropic, thin, rectangular plates can be approximated with the formula as given by Dickinson¹⁹:

$$f_{ij} = \frac{\pi}{2} \left[\frac{G_1^4}{a^4} + \frac{G_2^4}{b^4} + \frac{2 J_1 J_2 + 2\nu (H_1 H_2 - J_1 J_2)}{a^2 b^2} \right]^{1/2} \left[\frac{E h^3}{12 \gamma (1 - \nu^2)} \right]^{1/2} \quad (3.1-33)$$

$$i = 1, 2, 3 \dots, j = 1, 2, 3 \dots$$

where $G_1, G_2, H_1, H_2, J_1, J_2$ = mode parameters, functions of plate constraints.

¹⁹Dickinson, S. M., "The Buckling and Frequency of Flexural Vibration of Rectangular, Isotropic and Orthotropic Plates Using Rayleigh's Method," J. Sound Vibration, 61, 1-8, 1978.

RECTANGULAR SECTIONS

By comparison the above formulas, the approximate method is to use the following expression to evaluate the eigenvalues:

$$\lambda_{ij}^2 = (\pi a)^2 \left[\frac{G_1^4}{a^4} + \frac{G_2^4}{b^4} + \frac{2 J_1 J_2 + 2 \nu (H_1 H_2 - J_1 J_2)}{a^2 b^2} \right]^{1/2} \quad (3.1-34)$$

A FORTRAN code (isotrop) is prepared to calculate the natural frequencies, Equation (3.1-33). The first of the input data as given is Poisson's ratio. One may then enter as many sets of boundary condition, mode, and aspect ratio as desired. For instance, the set of {3, 1, 1, 1, 3, 1} indicates that the x direction boundary condition is Clamped-Free = 3, the mode index = 1 and the aspect ratio $a/b = 1$, the y direction boundary condition is Free-Free = 1, and the mode index = 3. The last number, 1, should always be entered as 1. The code then calculates for each set of input the natural frequencies. As expected the approximate method generally agrees well with the exact solution of partial differential equation.

Experimental Data Reference

Grinsted²⁰ obtained considerable experimental data on a cantilevered rectangular plate. Frequencies and mode patterns of the mild steel plate having length $a = 5.12$ inches, width $b = 2.76$ inches, and thickness $h = 0.053$ inches are shown here in Figure 3-12. The modal frequencies were compared with the computer code prediction. The material properties used in the present calculation are given in Table 3-5.

Table 3-5. Properties for the Cantilevered Steel Plate

| | |
|------------------------------|--|
| Length, $L = a$ | 5.12 inches |
| Width, b | 2.76 inches |
| Thickness, h | 0.053 inches |
| Young's modulus, E | 27×10^6 psi |
| Density, ρ | 0.287 lb/in ³ |
| Poisson's ratio, ν | 0.3 |
| Mass per unit area, γ | 4.7277×10^{-4} slug/in ² |
| Length-to-width ratio, a/b | 1.86 |

The model of a marine propeller blade investigated by Grinsted²⁰ is also considered here to show that an equivalent rectangular plate method can be used to estimate the natural frequencies of a nearly rectangular plate. Grinsted experimentally determined the frequencies and mode shapes of a mild steel, flat, oval-shaped, cantilevered plate designed to simulate a marine propeller blade. The dimensions of the model propeller is cited by Leissa¹⁸ as shown here in Figure 3-13. The properties and dimensions used in the present study is given in Table 3-6.

²⁰Grinsted, B., "Nodal Pattern Analysis," Proc. Inst. Mech. Eng., ser. A, vol. 166, pp. 309-326, 1952.

RECTANGULAR SECTIONS

Table 3-6. Properties for the Model Propeller Plate

| | |
|------------------------------|--|
| Length, L = a | 5.17 inches |
| Maximum Width, b | 3.38 inches |
| Thickness, h | 0.0535 inches |
| Young's modulus, E | 27×10^6 psi for mild steel |
| Density, ρ | 0.287 lb/in ³ |
| Poisson's ratio, ν | 0.3 |
| Mass per unit area, γ | 4.7723×10^{-4} slug/in ² |
| Area, $A = \pi a b/4$ | 13.725 sq. in. |
| Equivalent width, $w = A/a$ | 2.65 in. |
| Length-to-width ratio, a/b | 1.9505 |

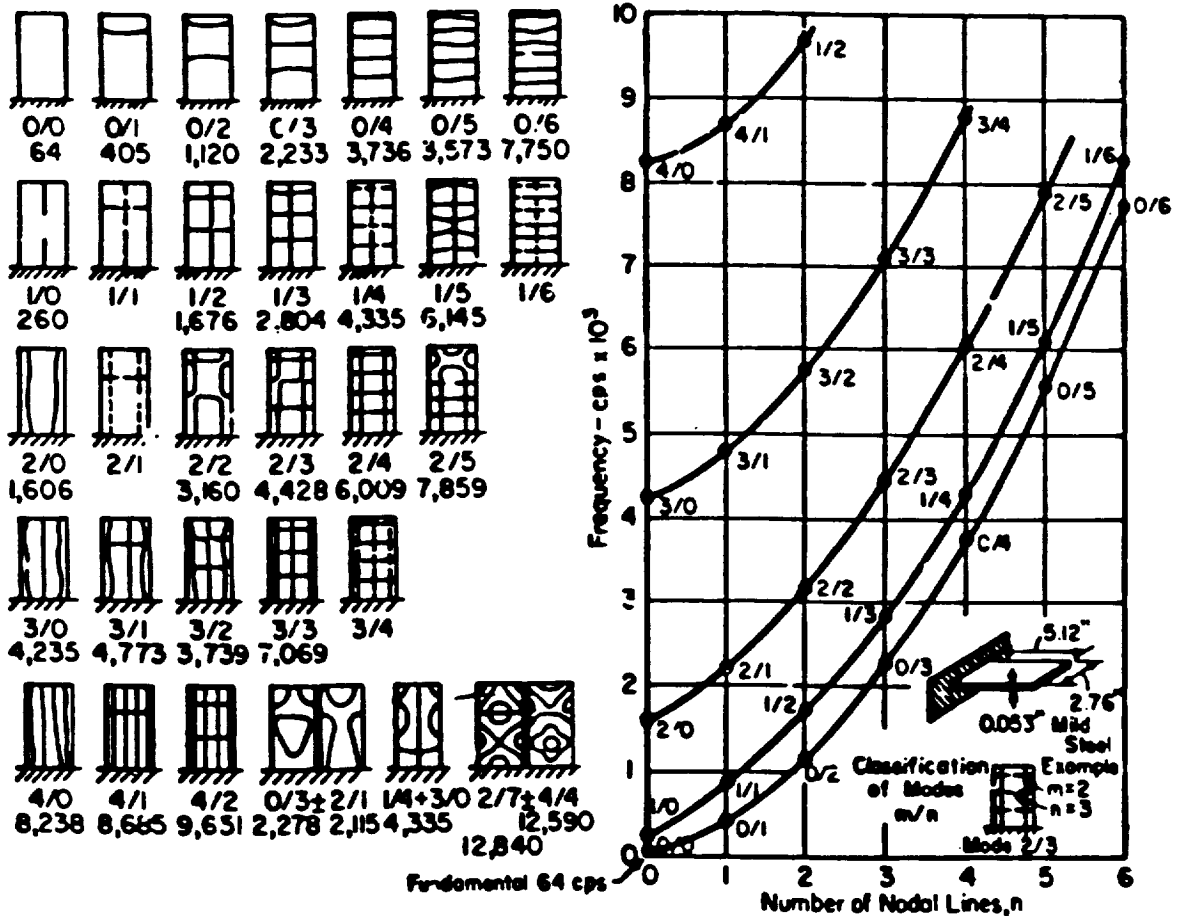


Figure 3-12. Rectangular Plate Data of Reference Experiment

RECTANGULAR SECTIONS

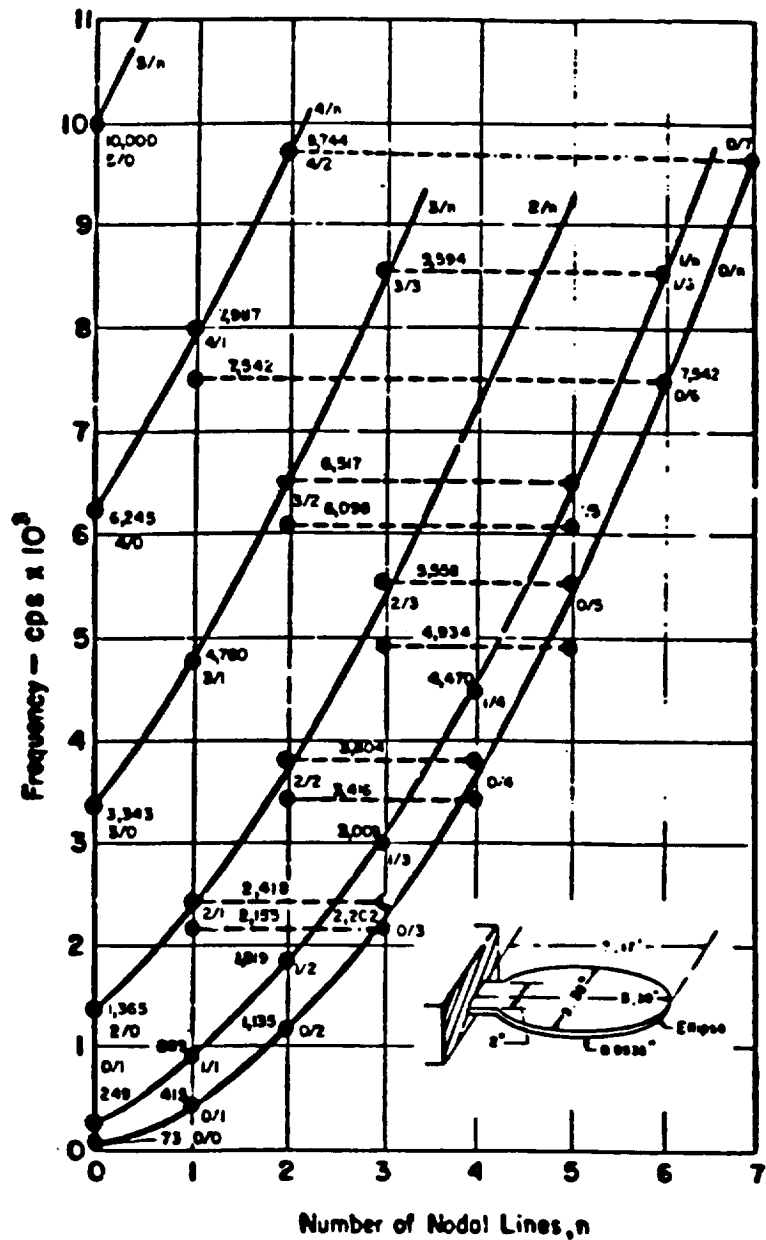


Figure 3-13 Reference Model Propeller Data.

The present approach for plates which are not exactly rectangular is first to find an equivalent rectangular plate of the same length and area. Then find its modal frequencies using Equation (3.1-33) to estimate the frequencies.

RECTANGULAR SECTIONS

Data Comparison

The original frequency data of Grinsted²⁰ are given in Figure 3-14. Using the plate properties given in Table 3-5, one may calculate frequencies using Equation (3.1-33) as shown in parentheses of the figure. The mode indices m/n in the figures and the mode indices i, j in the equation are related by

$$m = j - 1, n = i - 1 \quad (3.1-35)$$

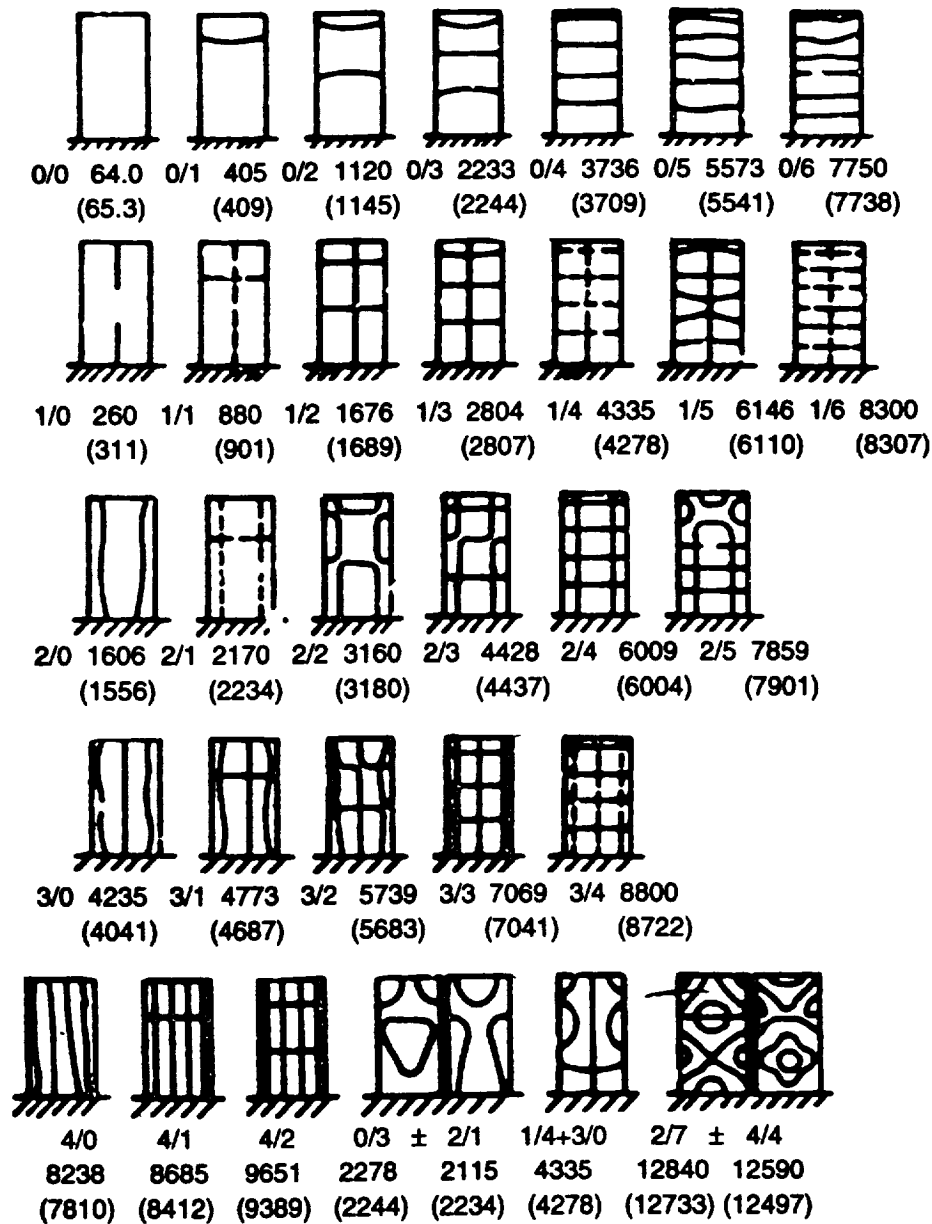


Figure 3-14. Computer Code Prediction of Reference Experimental Frequencies.

RECTANGULAR SECTIONS

Note that the order of the indices is transposed. The comparison is generally very good. However, the comparisons for the modes 1/0, 2/0, 3/0 and 4/0 are merely fair.

Using the plate properties for the model propeller given in Table 3-6, one may likewise calculate the frequencies using Equation (3.1-33). The results are given in parentheses of Figure 3-15 together with the original experimental data. The mode indices m/n in the figures and the mode indices i, j are related by equation (3.1-35). Again note that the order of the indices is transposed. The comparison is not as good as in the rectangular plate. However, the comparisons for the modes 0/1, 0/2, 0/3, 1/5, 0/6, 2/2 are relatively good.

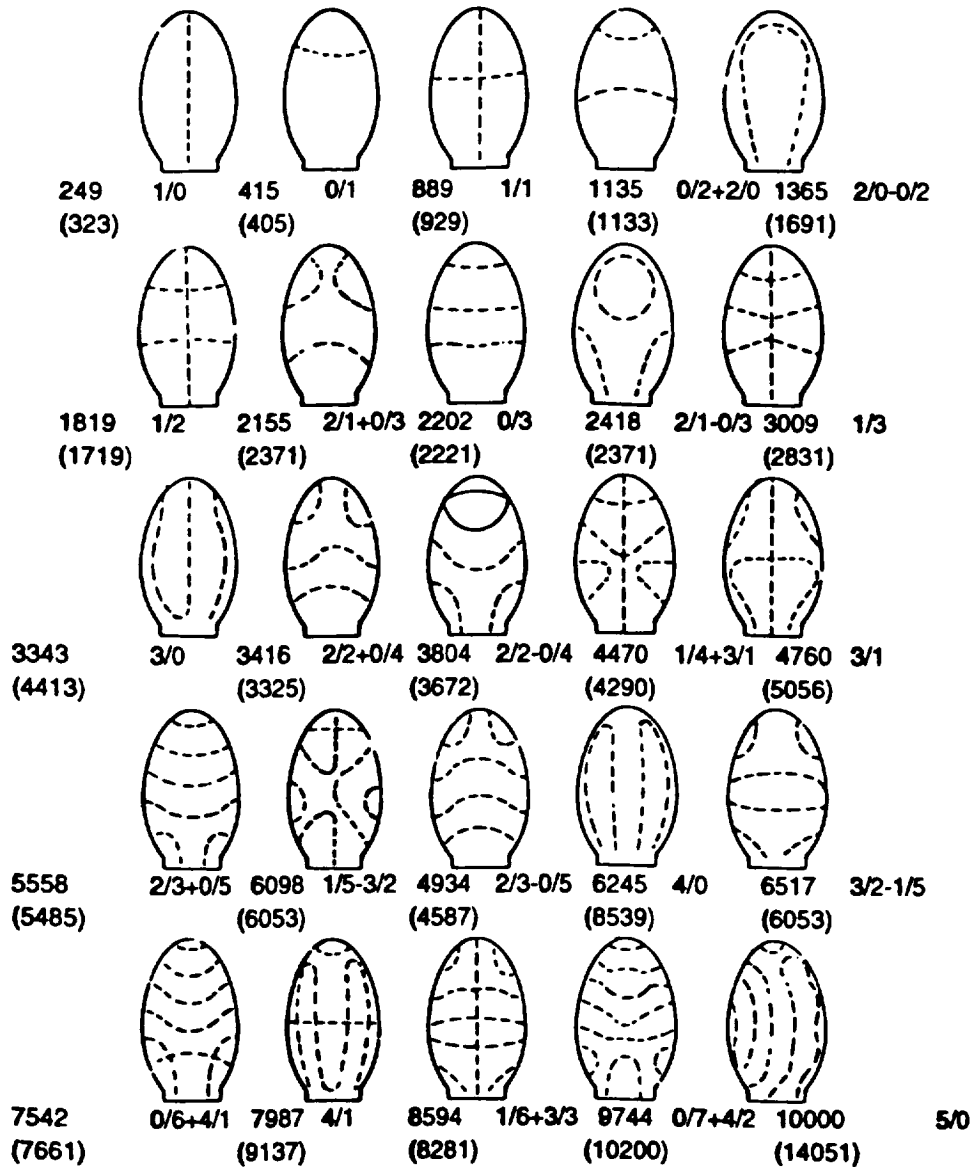


Figure 3-15. Estimated Oval Plate Frequencies Using Rectangular Plate Approximation.

3.2 Cylinders

Circular Cylinder Geometry and Flow Phenomena

Fundamental relationships of flow interaction with cylinders are discussed in this section. The basic structural modes considered for cylinders in this book are derived from formulas for a slender elastic beam. The cylinders are assumed to be uniform with rotation and translation treated as uncoupled. Each section develops formulas for a special case of cylinder geometry. The important cylinder geometric, flow and fluid parameters for analysis are illustrated in Figure 3-16.

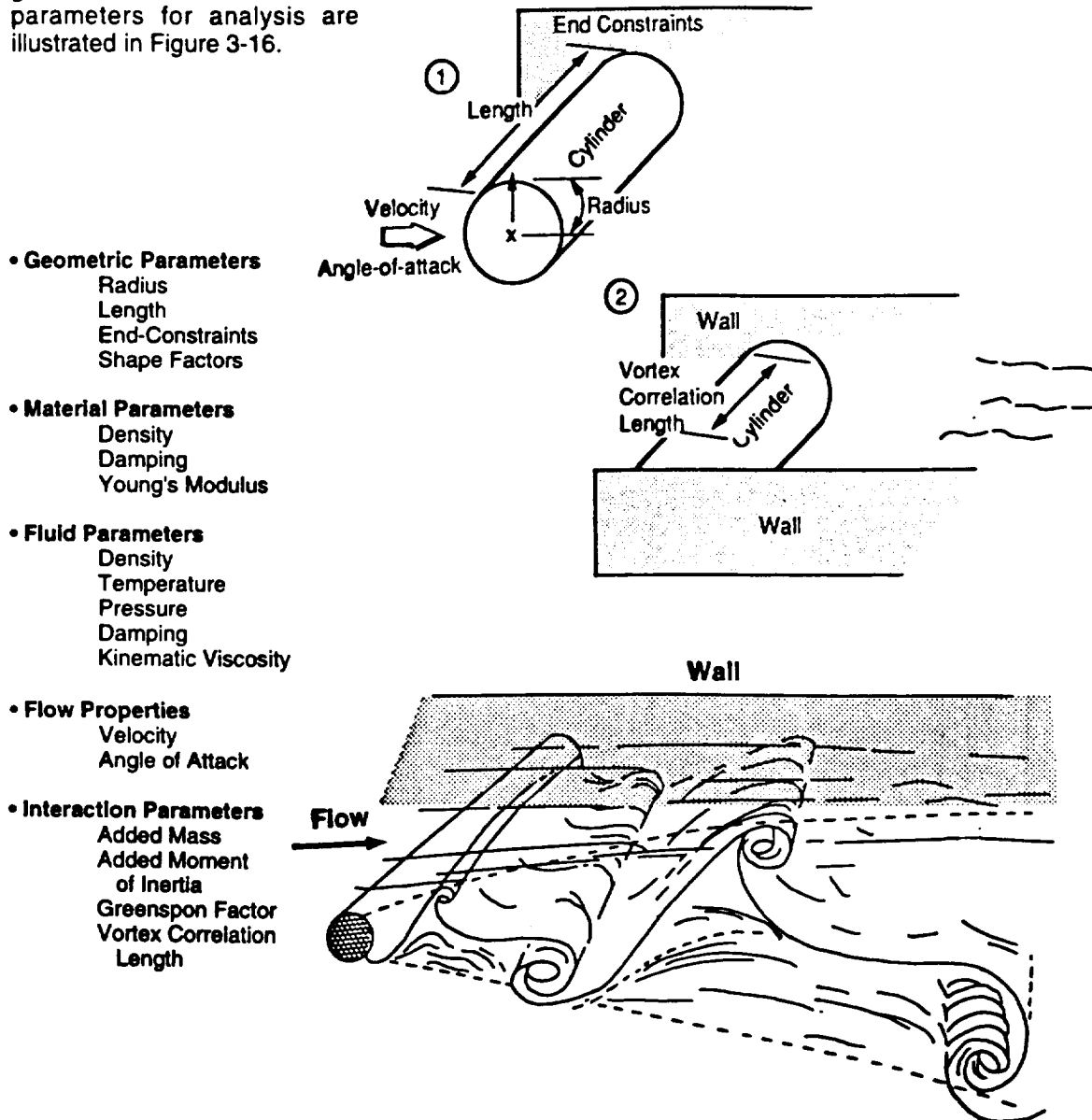


Figure 3-16 Right Circular Cylinder Geometric and Flow Parameters.

Cylinder Nomenclature

A_y = transverse deflection amplitude
 A_z = in-line deflection amplitude
 C_D = drag coefficient
 C_{D0} = drag coefficient for a stationary structure
 C_L = lift coefficient
 D = diameter
 E = Young's modulus
 f = frequency
 f_n = n-th mode natural frequency
 f_s = vortex shedding frequency
 $Im()$ = Imaginary part of a complex number
 I_a = area moment of inertia
 I_0, I_n = Modified Bessel functions of the first kind
 J = joint acceptance
 J_n = Special Bessel functions of the first kind
 K_0, K_n = Modified Bessel Functions of the second kind
 k = spring constant in a spring-mounted cylinder
 L = beam/rod length
 L_c = vortex correlation length
 m = effective mass per unit beam length
 m_a = added mass per unit length
 m_s = structural material mass per unit length
 m_{ij} = element of hydrodynamic mass matrix (per unit length)
 m^a_{ij} = element of hydrodynamic mass matrix (per unit area)
 M_d = mode shape factor
 m_r = structural reduced mass
 P = non-dimensional cycle power
 r = radius of cylinder
 $R = \log_{10}(Re)$, R = radius of cylinder
 Re = Reynolds number based on diameter
 $Rea()$ = Real part of a complex number
 S = Strouhal number = $f D/U$
 $T(t)$ = temporal part of transverse deflection
 t = time
 U = cross flow velocity
 V = flow velocity
 V_r = reduced velocity
 w_r = wake response parameter
 $X(x)$ = mode shape, i.e., spatial part of transverse deflection, $Y(x, t)$
 x = axial distance
 $Y(x, t)$ = transverse deflection
 y = transverse deflection
 z = in-line deflection
 α = angle-of-attack
 α = hydrodynamic mass coefficient
 β = fundamental frequency
 δ_r = reduced damping = $4\pi m \zeta_n / (\rho D^2)$
 ϵ = correction factor for the organ pipe
 ϕ = phase angle
 γ = shape factor
 λ_n = eigenvalues for the n-th bending mode
 μ = fluid viscosity

ν = fluid kinematic viscosity
 ρ_f = fluid density
 ρ_s = structural density
 σ_n = mode shape coefficient of the n-th beam vibration mode
 ω_n = circular frequency of the n-th beam vibration mode, rad/s
 ω_s = circular vortex shedding frequency, rad/s
 ω_y = circular frequency of beam transverse vibration, rad/s
 ζ = damping ratio
 ζ_t = total or system damping ratio
 ζ_f = fluid damping ratio
 ζ_s = structural damping (including material damping) ratio

Method of Analysis

Determination of flow structural lock-in conditions requires information concerning the structural geometry, the structural material, the fluid properties, and the ambient conditions of the fluid flow and structure. The parameters supplying this information, primary variables in this analysis, are: the cylinder radius, the cylinder length, cylinder end-constraints, cylinder shape factors, structural density, structural damping, Young's Modulus, fluid density, fluid damping, fluid kinematic viscosity, fluid velocity, and the angle-of-attack.

The method of analysis for circular cylinders, as used in the Flow Structural Interaction program developed for the Macintosh, is as follows:

- 1) Determine structural mass, added mass, effective mass, the area moment of inertia and the added moment of inertia,
- 2) Determine velocity of fluid perpendicular to cylinder longitudinal axis, the crossflow velocity, Reynolds number, Strouhal number and vortex shedding frequency,
- 3) Determine structural bending modes for the specific material and boundary conditions with added mass effects, and check for lock-in,
- 4) Determine system damping, reduced velocity, mass ratio (reduced mass)
- 5) Estimate cylinder transverse and in-line displacement using lift and drag coefficients and the reduced velocity

Vortex Shedding and Flow Regimes

The most important effect produced by cross flow on a cylinder is vortex shedding. Cross flow impinging on a circular cylinder develops boundary layers on the sides of the cylinder. These separated boundary layers form free shear layers in the fluid flowing away from the cylinder and roll up forming vortices in the cylinder wake. These vortices are formed at regular intervals and the frequency of formation and separation gives rise to lift and drag forces on the cylinder. When these flow-induced forces are coincident with, or near, the structural frequencies, lock-in conditions may occur and the amplitude of cylinder oscillation in the flow increases and may become great enough to cause structural damage. Figure 3-17, from Lienhard¹, illustrates the observed flow regimes for the circular cylinder.

The array of vortices shed from the cylinder, travel in a predictable wake pattern known as the Karman vortex street, illustrated in Figure 3-16. Dougherty et al² performed time-dependent Navier-Stokes simulations of the flow over a cylinder. Examination of these simulations yields quantitative information on the vortex shedding phenomena in the flow region near the cylinder. The vortex convection speed in the wake, Figure 3-18, which is usually approximated as 0.6 to

1 Lienhard, J.H., " *Synopsis of Lift, Drag, and Vortex Frequency Data for Rigid Circular Cylinders,*" Washington State University, College of Engineering, Research Division Bulletin 300, 1966.

2 Dougherty, N., J. Holt, B.W. Liu and J.M. O'Farrell, " *Time-Accurate Navier-Stokes Computations of Unsteady Flows: The Karman Vortex Street,*" AIAA 27th Aerospace Sciences Meeting January 9-12, Reno, Nevada, Paper No. AIAA-89-0144.

CYLINDERS

0.7 freestream speed, is more accurately defined. The stagnation point motion, Figure 3-19, and separation point motion, Figure 3-20, and development of the shedding cycle, Figure 3-21, are illustrated in this paper.

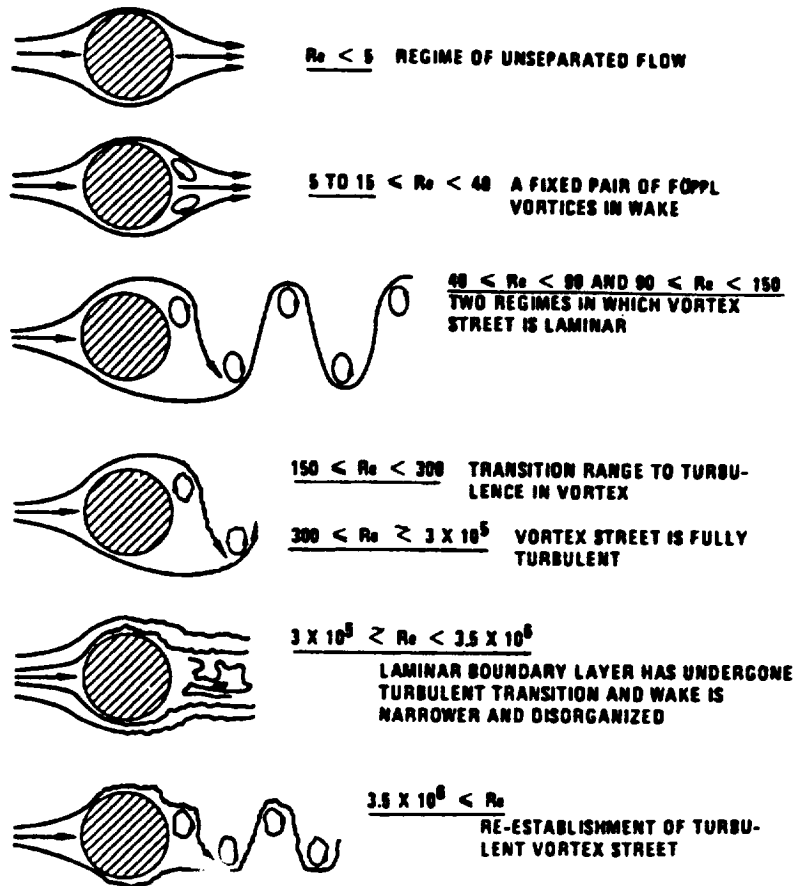


Figure 3-17. Flow Regimes for the Circular Cylinder

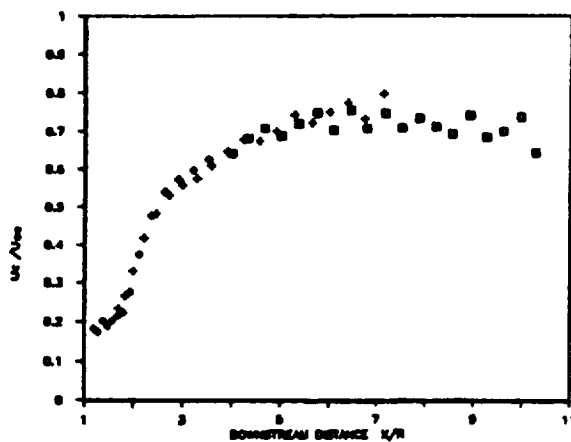


Figure 3-18. Computed Vortex Convection Speed

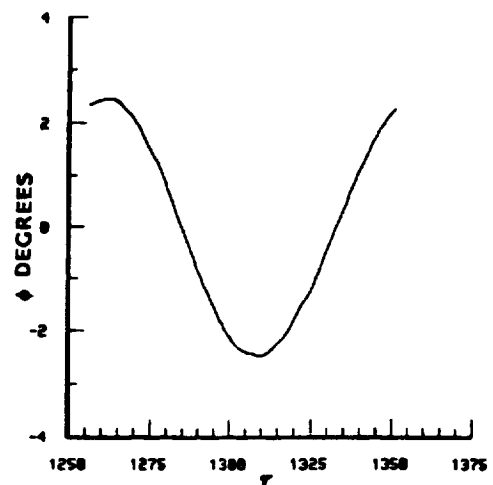


Figure 3-19. Stagnation Point Motion

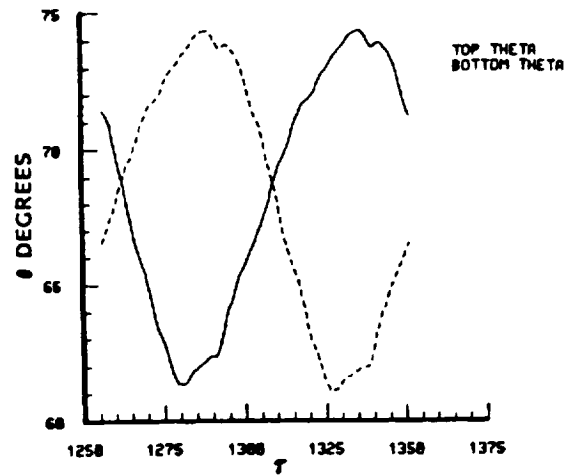


Figure 3-20. Separation Point Motion

| Streamlines | Density | Mach Number | Phase |
|-------------|---------|-------------|--|
| (a) | | | $\omega = 0$ -0.6140 1.1995 Phase C_L C_D |
| (b) | | | $\omega = \pi/4$ -0.2926 1.1596 Phase C_L C_D |
| (c) | | | $\omega = \pi/2$ 0.2059 1.0898 Phase C_L C_D |
| (d) | | | $\omega = 4\pi/5$ 0.5923 1.1395 Phase C_L C_D |
| (e) | | | $\omega = \pi$ 0.6202 1.1838 Phase C_L C_D |

Figure 3-21. Vortex Shedding Cycle Development

There are repeatable vortex/wake fundamental synchronization patterns which were studied by Williamson and Roshko.³ The relevant parameters for investigating these patterns are the Amplitude ratio, A/D , and Wavelength ratio, λ/D , where $\lambda = UT_0$ with T_0 being the period of cylinder oscillation in the transverse direction. Figures 3-22 to 3-24 illustrate the vortex shedding patterns. In these figures, S indicates a single vortex shed, P indicates a vortex pair, and P+S means a pattern where in each cycle a vortex pair and a single vortex are shed.

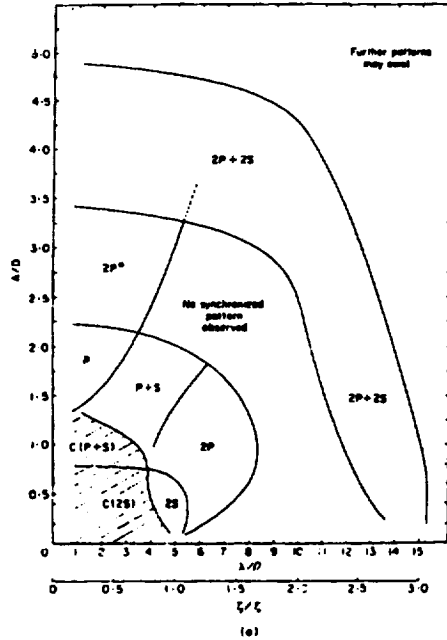


Figure 3-22. Regions of Fundamental Vortex Synchronization Patterns

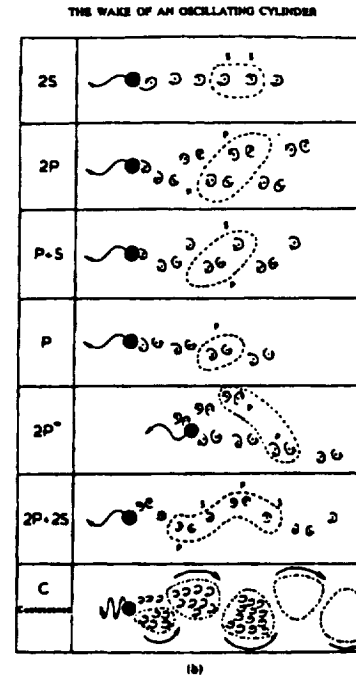


Figure 3-23. Patterns of Fundamental Vortex Synchronization

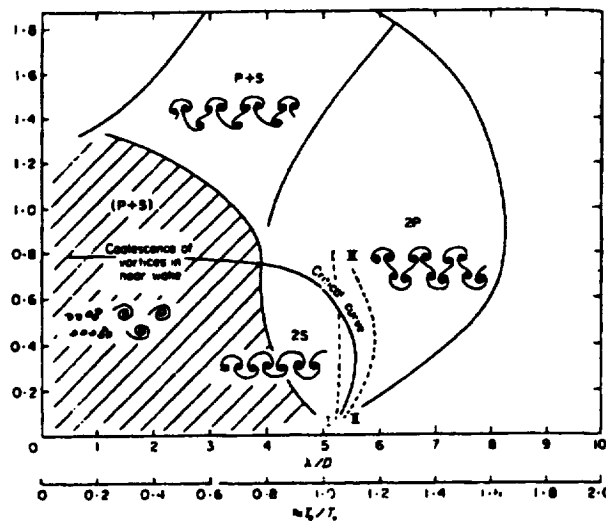


Figure 3-24. Detail of Lock-in Region for Fundamental Vortex Synchronization

³ Williamson, C.J.K., and A. Roshko, "The Wake of an Oscillating Cylinder," *Journal of Fluids and Structures*, 2, pp. 355-381, 1988.

Effective Structural Mass

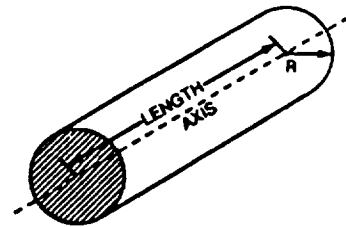
For a uniform circular cylinder composed of homogeneous material, the structural mass per unit length is the product of the cross sectional area and the density of the material. The effective mass, m , used in calculation of the structural frequencies of the cylinder in a fluid medium must include the added mass of the entrained fluid, m_a . The effective mass, is then:

$$\begin{aligned} m &= m_s + m_a \\ m &= \rho_m \pi R^2 + \rho_f \pi R^2 C_m \end{aligned} \quad (3.2.1)$$

where C_m is the hydrodynamic mass coefficient, m_s is the structural mass per unit length, m_a is the added (hydrodynamic) mass per unit length, ρ_m is the density of the cylinder material, ρ_f is the density of the fluid and R is the radius of the cylinder. The hydrodynamic mass coefficient for a single circular cylinder may be approximated as unity over a large range of Reynolds numbers. For more complicated cylinder systems more extensive calculations are necessary. Techniques presented here for calculating hydrodynamic mass for circular cylinders are those enumerated for various circular cylinder configurations from the excellent presentation by Chen and Chung⁴. In the following, formulas for Bessel functions referenced are found in the most mathematical texts. While different end conditions contribute to the added mass formulas, only the rigid body or simply supported configuration is calculated here. Chen remarks that the hydrodynamic mass is a function of the vibration amplitude and frequency, and fluid damping is a function of the first and second powers of the cylinder velocity. The added mass effects experienced from the free-free (rigid body) end condition are taken to be representative of most end conditions.

Single Circular Cylinder in a Cross Flow

The hydrodynamic mass of a single circular cylinder in an infinite fluid was computed as a function of the vibrational Reynolds number, B . From Figure 3-25, it may be seen that for values of the vibrational Reynolds number which are above 100.0, the values of C_m are near 1.0 and the normally used value for the added mass of a singular circular cylinder approaches $\rho_f \pi R^2$.

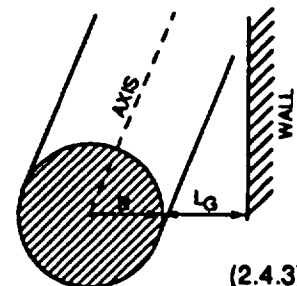


$$C_m = \text{Rea}(H) \quad (3.2.2)$$

where, $H = 1 + \frac{4K_1(\alpha)}{\alpha K_0(\alpha)}$, $\alpha = \sqrt{Bi}$, and $B = \frac{\omega R^2}{\nu}$.

Single Circular Cylinder near a Wall

Chen gives the hydrodynamic mass for a vibrating cylinder near a wall which is parallel to the axis of the cylinder in the following formula for the hydrodynamic mass coefficient:



(2.4.3)

⁴ Chen, S.S. and H. Chung "Design Guide for Calculating Hydrodynamic Mass Part I: Circular Cylindrical Structures", Components Technology Division, Argonne National Laboratory, Argonne, Illinois, June 1976, Document No. ANL-CT-76-45.

CYLINDERS

$$C_m = 1 + 4 \sinh^2(a) \sum_{k=1}^{\infty} \frac{k e^{-3ka}}{\sinh(ka)} \quad (3.2.3)$$

where $a = \ln\left(\frac{R + L_G + \sqrt{(R + L_G)^2 - R^2}}{R}\right)$, R is the radius of the cylinder, and L_G is the distance from the cylinder surface to the wall. The relationship of the hydrodynamic mass coefficient to the reduced distance from the wall, L_G/R , is shown in Figure 3-26.

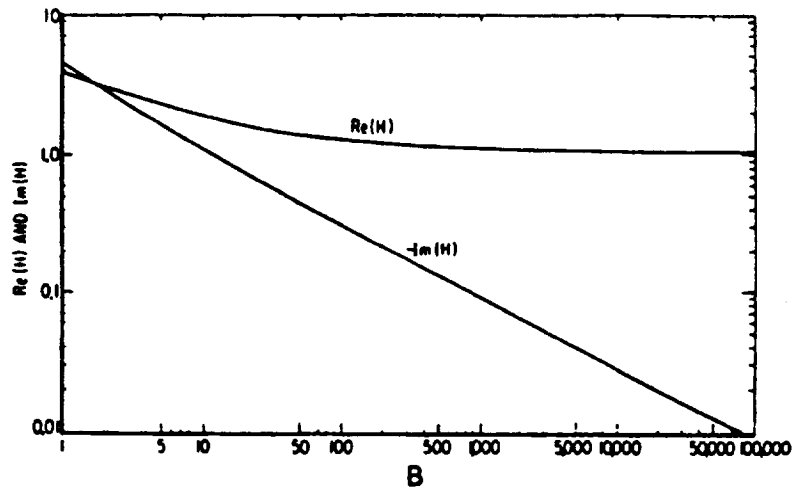


Figure 3-25. Hydrodynamic Mass Coefficient vs. Vibrational Reynolds Number

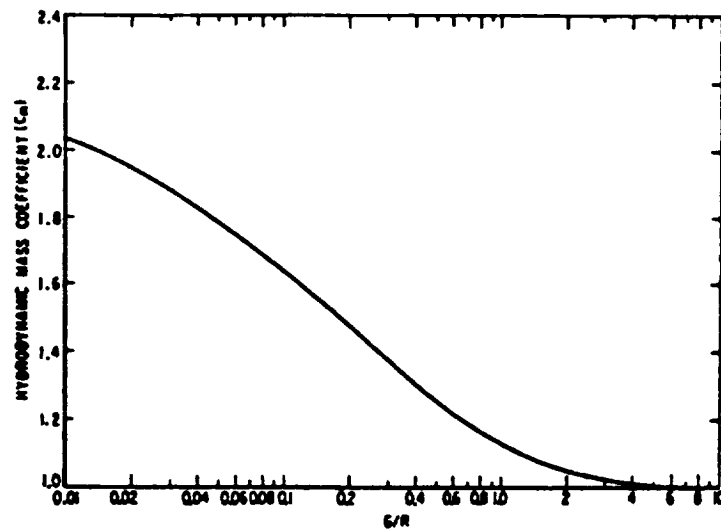
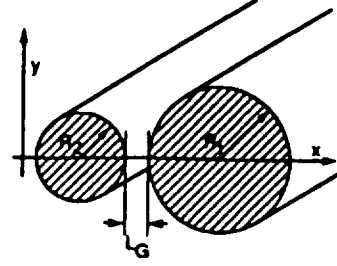


Figure 3-26. Hydrodynamic Mass Coefficient vs. Reduced Distance to Wall

Two Parallel Circular Cylinders

There are two degrees of freedom, motion in the x-direction and motion in the y-direction, for the two parallel cylinders problem. The motions in the two directions are uncoupled. The x-direction (in-plane motion) matrix is given by:



$$[m_{ij}] = \rho r \pi \begin{bmatrix} R_1^2 v_{11} & -\left(\frac{R_1 + R_2}{2}\right)^2 v_{12} \\ -\left(\frac{R_1 + R_2}{2}\right)^2 v_{12} & R_1^2 v_{22} \end{bmatrix} \quad (3.2.4)$$

and for the motion in the y-direction (out-of-plane),

$$[m_{ij}] = \rho r \pi \begin{bmatrix} R_1^2 v_{11} & \left(\frac{R_1 + R_2}{2}\right)^2 v_{12} \\ \left(\frac{R_1 + R_2}{2}\right)^2 v_{12} & R_1^2 v_{22} \end{bmatrix}.$$

The variables v_{11} , v_{12} , and v_{22} are obtained from:

$$v_{11} = 1 + \frac{p^4 - 2p^2(R_1^2 + R_2^2) + (R_2^2 - R_1^2)^2}{p^2 R_1^2} \sum_{k=1}^{\infty} k \frac{e^{-k(a+a_1)}}{\sinh(ka)}$$

$$v_{22} = 1 + \frac{p^4 - 2p^2(R_1^2 + R_2^2) + (R_2^2 - R_1^2)^2}{p^2 R_1^2} \sum_{k=1}^{\infty} k \frac{e^{-k(a+a_2)}}{\sinh(ka)},$$

$$v_{12} = \left[\frac{2R_1 R_2}{p(R_1 + R_2)} \right]^2 \left\{ 1 + \frac{p^4 - 2p^2(R_1^2 + R_2^2) + (R_2^2 - R_1^2)^2}{R_1^2 R_2^2} \sum_{k=1}^{\infty} k \coth(ka) e^{-2ka} \right\},$$

$$a = kn \left\{ \frac{p^2 - R_1^2 - R_2^2}{2R_1 R_2} + \left[\left(\frac{p^2 - R_1^2 - R_2^2}{2R_1 R_2} \right)^2 - 1 \right]^{1/2} \right\},$$

$$a_1 = 2kn \left\{ \frac{p^2 + R_1^2 - R_2^2}{2pR_1} + \left[\left(\frac{p^2 + R_1^2 - R_2^2}{2pR_1} \right)^2 - 1 \right]^{1/2} \right\},$$

$$a_2 = 2kn \left\{ \frac{p^2 - R_1^2 - R_2^2}{2pR_2} + \left[\left(\frac{p^2 - R_1^2 - R_2^2}{2pR_2} \right)^2 - 1 \right]^{1/2} \right\}, \text{ and}$$

$$p = R_1 + R_2 + L_G.$$

Values of v_{11} and v_{12} are presented in Figures 3-27 and 3-28; and v_{22} may be obtained from Figure 3-27 by exchanging subscripts 1 and 2.

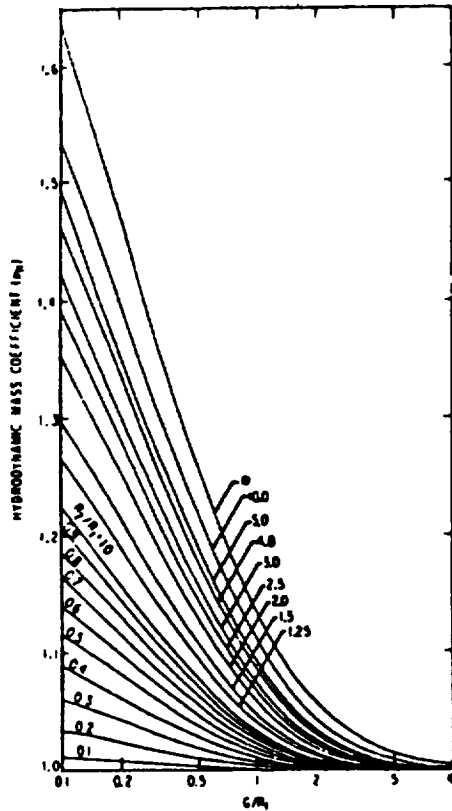


Figure 3-27. v_{11} vs. Reduced Distance

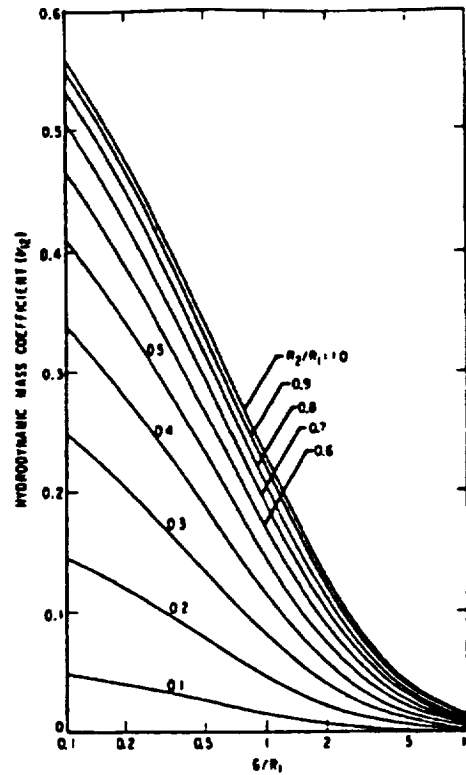


Figure 3-28. v_{12} vs. Reduced Distance

Crossflow Velocity and Reynolds Number

Many derived quantities, such as vortex shedding frequency or drag coefficient, are based directly on experimental data obtained at a particular Reynolds number. Reynolds number, Re , is calculated from the primary variables: flow velocity, kinematic viscosity, angle-of-attack, and cylinder diameter by:

$$Re = \frac{UD}{\nu} \tag{3.2.5}$$

where U is component of the flow velocity perpendicular to the cylinder axis, i.e. the crossflow velocity $U = V \cos(\alpha)$ where α is the angle-of-attack and V is the freestream flow velocity, D is the diameter of the cylinder and ν is the kinematic viscosity of the fluid.

Strouhal Number and Vortex Shedding Frequency

The frequency of vortex shedding is usually expressed in non-dimensional form, the Strouhal number, S . Figure 3-29 shows the experimentally obtained relationship between Reynolds

number and Strouhal number. From the data of Morkovin⁵ and Lienhard⁶, the Strouhal number can be evaluated using the geometric mean of an estimated upper and lower bound curve:

$$S = \sqrt{S_{up} S_{lo}} \quad (3.2.6)$$

where

$$S_{lo} = \begin{cases} -0.42021 + 0.49398 Re - 0.12605 Re^2 + 0.010189 Re^3, & \text{if } 40 < Re \leq 10^5, \\ 0.12983 + 0.008758 Re & \text{if } 10^5 < Re \leq 4.5 \times 10^7 \end{cases}$$

and,

$$S_{up} = \begin{cases} -0.51351 + 0.6201 Re - 0.16988 Re^2 + 0.014924 Re^3, & \text{if } 40 < Re \leq 10^5, \\ 257.91 - 175.84 Re + 44.536 Re^2 - 4.9621 Re^3 + 0.20533 Re^4, & \text{if } 10^5 < Re \leq 10^7, \\ 122.71 - 49.679 Re + 6.7095 Re^2 - 0.30149 Re^3, & \text{if } 10^7 < Re \leq 4.5 \times 10^7. \end{cases}$$

Experimental data bounds are curve-fit with \log_{10} of the Reynolds number, Figure 3-29. These curves have been expanded to an extremely high range of $Re = 4.5 \times 10^7$ which was based on vortex shedding data obtained from the Space Shuttle Solid Rocket Motor⁷ during reentry. The dashed region indicates where laminar/turbulent boundary layer transition occurs on the cylinder. The vortex shedding frequency, f_s , may be obtained from the Strouhal number by the following relationship:

$$f_s = \frac{SU}{D} \quad (3.2.7)$$

where S is the Strouhal number, U is the component of the flow velocity perpendicular to the cylinder axis and D the diameter of the cylinder.

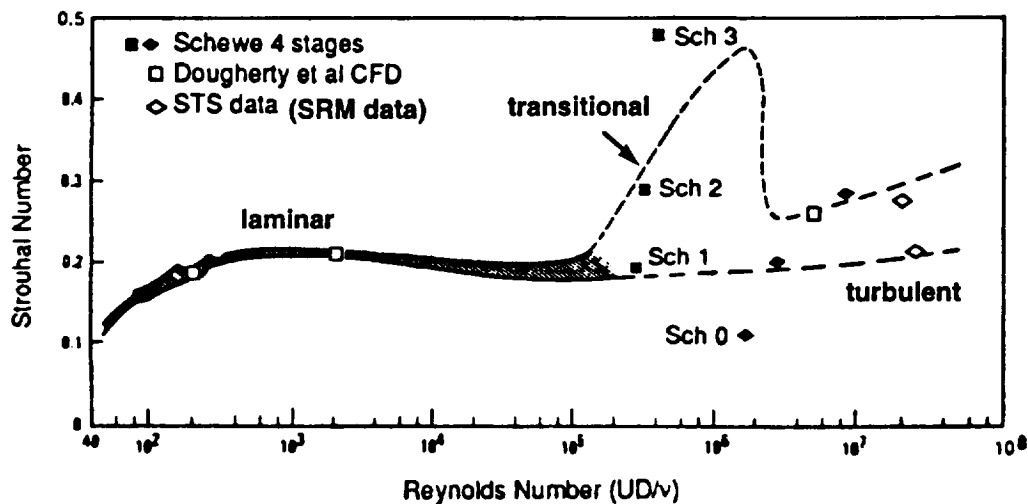


Figure 3-29. Strouhal Number vs. Reynolds number

Structural Modes and Amplitudes

Structural bending frequencies for the circular cylinder are approximated using equations for a slender beam. These bending frequencies are functions of the beam boundary conditions,

5 Morovkin, M.V. "Flow Around a Circular Cylinder," Symposium on Fully Separated Flows, ASME Proceedings, Engineering Division Conference, Philadelphia, May 1964.

6 Lienhard, J.H., op. cit. 3.2-(1).

7 RSRM data from Marshall Space Flight Center, Flight Database.

namely, 1) clamped-clamped, 2) free-free, 3) clamped-free, 4) clamped-pinned, 5) free-pinned, 6) pinned-pinned, 7) Free-Sliding, 8) Clamped-Sliding, 9) Sliding-Pinned, or 10) Sliding-Sliding. The eigenvalues and modal frequencies are given in the formulation by Chang and Craig⁸:

$$f_i = \frac{\lambda_i^2}{2\pi L^2} \left(\frac{E I_a}{m} \right)^{1/2} \quad (3.2.8)$$

where the eigenvalues, λ_i of free-free boundary conditions are 4.73, 7.8532, 10.996, 14.137, 17.279 for the first five modes and $(2i + 1)\pi/2$ for higher modes, E is Young's Modulus, and I_a is area moment of inertia for the structure. Eigenvalues and mode shapes for several beam mode conditions are given in Table 3-7. The area moment of inertia for the cylinder is:

$$I_a = \frac{\pi R^4}{4} \quad (3.2.9)$$

In Table 3-7, each end-condition listed and derived parameters is listed. For each mode n, eigenvalues λ_n , mode shape function, $\psi_n(x)$ and multiplier σ_n , and the associated mode shape factor, M_d , used in displacement magnitude calculations are presented.

For the spring mounted end-condition, λ_n and σ_n are not defined. Here k is the spring constant and m_s the mass of the structure.

Vortex Correlation Length and Joint Acceptance

As the free stream flow velocity varies over the cylinder length, spanwise coherent cells of vortex shedding develop in three-dimensional flows and the vortex shedding frequency varies discretely in ladderlike steps along the cylinder span with each step (Griffin⁹; Ramberg¹⁰; Rooney and Peltzer¹¹). The length of these spanwise coherent cells, the vortex correlation length, can be correlated with several physical parameters observed in Koopman's¹² strobe-light photography cylinder flow visualizations. Vortex filaments were noted to roll up starting from one end of the cylinder and their separation points travel to the opposing end, so that vortex filaments appear tilted by an angle, θ , from the cylinder axis, Figure 3-30. The vortex correlation length, L_c , may be estimated using:

$$L_c = \frac{bU \cot(\theta)}{2f_s} \quad (3.2.10)$$

where bU is the vortex transport velocity, a fraction of the freestream velocity perpendicular to the cylinder axis (the fraction b is usually between 0.4 to 0.8), f_s is the vortex shedding frequency and θ is the tilt angle of a filament.

The vortex correlation length is used to obtain a weighting factor for the cylinder length involving a ratio of vortex correlation length to cylinder length. This ratio, the joint acceptance, J , accounts for the effect of vortex correlation on the flow lift force and can be approximated by:

$$J = \left(\frac{L_c}{L} \right)^{1/2} \quad (3.2.11)$$

⁸ Chang and Craig, 1969.

⁹ Griffin, O.M., "Vortex Shedding from Bluff Bodies in a Shear Flow: A Review", Transactions of the ASME vol. 107, September 1985, pp. 298-306.

¹⁰ Ramberg, 1983.

¹¹ Rooney and Peltzer, 1981.

¹² Koopman, G.H., "The Vortex Wakes of Vibrating Cylinders at Low Reynolds Numbers", Journal of Fluid Mechanics (1967), vol.28, part 3, pp. 501-512.

Table 3-7. Eigenvalues and Mode Shapes for Several Beam Boundary Conditions.

| | n = 1 | 2 | 3 | 4 | 5 | n |
|----------------------------|--|----------|----------|--------------------------------------|----------|---------------|
| 1. Clamped-Clamped | | | | | | |
| $\lambda_n =$ | 4.73004 | 7.8532 | 10.9956 | 14.1372 | 17.2788 | $(2n+1)\pi/2$ |
| $\sigma_n =$ | 0.982502 | 1.00078 | 0.999966 | 1. | 1. | 1. |
| $X_n(x) =$ | $\cosh\lambda_n x/L - \cos\lambda_n x/L - \sigma_n (\sinh\lambda_n x/L - \sin\lambda_n x/L)$ | | | | | |
| $M_d =$ | $2 \sigma_n [1 - (-1)^n]/\lambda_n$ | | | | | |
| 2. Free-Free | | | | | | |
| $\lambda_n =$ | 4.73004 | 7.8532 | 10.9956 | 14.1372 | 17.2788 | $(2n+1)\pi/2$ |
| $\sigma_n =$ | 0.982502 | 1.00078 | 0.999966 | 1. | 1. | 1. |
| $X_n(x) =$ | $\cosh\lambda_n x/L + \cos\lambda_n x/L - \sigma_n (\sinh\lambda_n x/L + \sin\lambda_n x/L)$ | | | | | |
| $M_d =$ | 0. | | | | | |
| 3. Clamped-Free | | | | | | |
| $\lambda_n =$ | 1.8751 | 4.69409 | 7.85476 | 10.9955 | 14.1372 | $(2n-1)\pi/2$ |
| $\sigma_n =$ | 0.734096 | 1.01847 | 0.999224 | 1.00003 | 0.999999 | 1.0000 |
| $X_n(x) =$ | $\cosh\lambda_n x/L - \cos\lambda_n x/L - \sigma_n (\sinh\lambda_n x/L - \sin\lambda_n x/L)$ | | | | | |
| $M_d =$ | $2\sigma_n/\lambda_n$ | | | | | |
| 4. Clamped-Pinned | | | | | | |
| $\lambda_n =$ | 3.9266 | 7.06858 | 10.2102 | 13.3518 | 16.4934 | $(4n+1)\pi/4$ |
| $\sigma_n =$ | 1.00078 | 1. | 1. | 1. | 1. | 1. |
| $X_n(x) =$ | $\cosh\lambda_n x/L - \cos\lambda_n x/L - \sigma_n (\sinh\lambda_n x/L - \sin\lambda_n x/L)$ | | | | | |
| $M_d =$ | $[(-1)^{n+1} \sqrt{\sigma_n^2 + 1} - \sqrt{\sigma_n^2 - 1} + 2\sigma_n]/\lambda_n$ | | | | | |
| 5. Free-Pinned | | | | | | |
| $\lambda_n =$ | 3.9266 | 7.06858 | 10.2102 | 13.3518 | 16.4934 | $(4n+1)\pi/4$ |
| $\sigma_n =$ | 1.00078 | 1. | 1. | 1. | 1. | 1. |
| $X_n(x) =$ | $\cosh\lambda_n x/L + \cos\lambda_n x/L - \sigma_n (\sinh\lambda_n x/L + \sin\lambda_n x/L)$ | | | | | |
| $M_d =$ | $[(-1)^n \sqrt{\sigma_n^2 + 1} - \sqrt{\sigma_n^2 - 1}]/\lambda_n$ | | | | | |
| 6. Pinned-Pinned | | | | | | |
| $\lambda_n =$ | $n\pi$ | | | | | |
| $\sigma_n =$ | 0. | | | | | |
| $X_n(x) =$ | $\sin\lambda_n x/L$ | | | | | |
| $M_d =$ | $[1 - (-1)^n]/\lambda_n$ | | | | | |
| 7. Free-Sliding | | | | | | |
| $\lambda_n =$ | 2.36502 | 5.4978 | 8.63938 | 11.781 | 14.9226 | $(4n-1)\pi/4$ |
| $\sigma_n =$ | 0.982502 | 0.999966 | 1. | 1. | 1. | 1. |
| $X_n(x) =$ | $\cosh\lambda_n x/L + \cos\lambda_n x/L - \sigma_n (\sinh\lambda_n x/L + \sin\lambda_n x/L)$ | | | | | |
| $M_d =$ | $[(-1)^n \sqrt{\sigma_n^2 + 1} - \sqrt{\sigma_n^2 - 1}]/\lambda_n$ | | | | | |
| 8. Clamped-Sliding | | | | | | |
| $\lambda_n =$ | 2.36502 | 5.4978 | 8.63938 | 11.781 | 14.9226 | $(4n-1)\pi/4$ |
| $\sigma_n =$ | 0.982502 | 0.999966 | 1. | 1. | 1. | 1. |
| $X_n(x) =$ | $\cosh\lambda_n x/L - \cos\lambda_n x/L - \sigma_n (\sinh\lambda_n x/L - \sin\lambda_n x/L)$ | | | | | |
| $M_d =$ | $[(-1)^{n+1} \sqrt{\sigma_n^2 + 1} - \sqrt{\sigma_n^2 - 1} + 2\sigma_n]/\lambda_n$ | | | | | |
| 9. Sliding-Pinned | | | | | | |
| $\lambda_n =$ | $(2n-1)\pi/2$ | | | | | |
| $\sigma_n =$ | 0. | | | | | |
| $X_n(x) =$ | $\cos\lambda_n x/L$ | | | | | |
| $M_d =$ | $(-1)^{n+1}/[(2n-1)\pi/2]$ | | | | | |
| 10. Sliding-Sliding | | | | 11. Spring-mounted Rigid Beam | | |
| $\lambda_n =$ | $n\pi$ | | | $2\pi f_n = (k/M)^{1/2}$ | | |
| $\sigma_n =$ | 0. | | | | | |
| $X_n(x) =$ | $\cos\lambda_n x/L$ | | | $X_n(x) = 1.$ | | |
| $M_d =$ | 0. | | | $M_d = 1.$ | | |

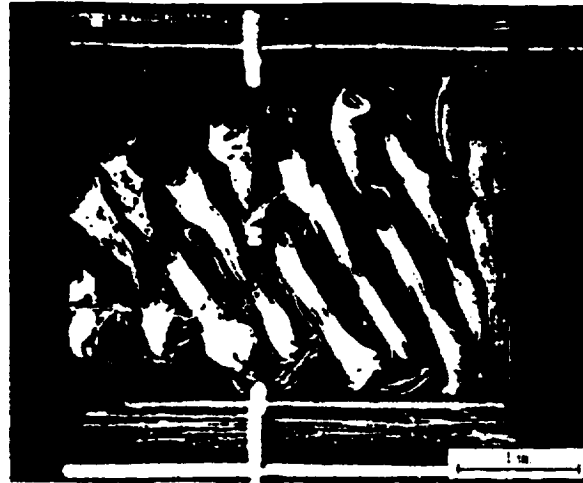
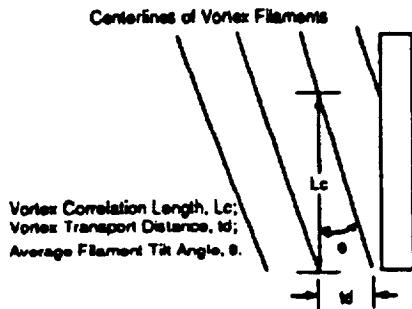


Figure 3-30. Determination of Vortex Correlation Length

System Damping

The structural viscous damping factor, ζ_s , is characterized by:

$$\zeta_s = \frac{\text{energy dissipated per cycle}}{4\pi \times \text{total energy of the structure}} \quad (3.2.12)$$

For a linear, viscously damped structure, the logarithmic decrement is a method of measuring the amount of damping of free oscillations:

$$2\pi\zeta_s = \ln\left(\frac{Y_n}{Y_{n+1}}\right) \quad (3.2.13)$$

where Y_n and Y_{n+1} are successive cycles of a lightly damped structure, as illustrated in Figure 3-31; and ζ_s may also be obtained using the resonant frequency, f_n , and f^+ and f^- , where f^+ and f^- are two frequencies on either side of the resonant frequency such that the amplitude is 0.707 times the amplitude of the resonant frequency.

$$2\zeta_s = \frac{f^+ - f^-}{f_n} \quad (3.2.14)$$

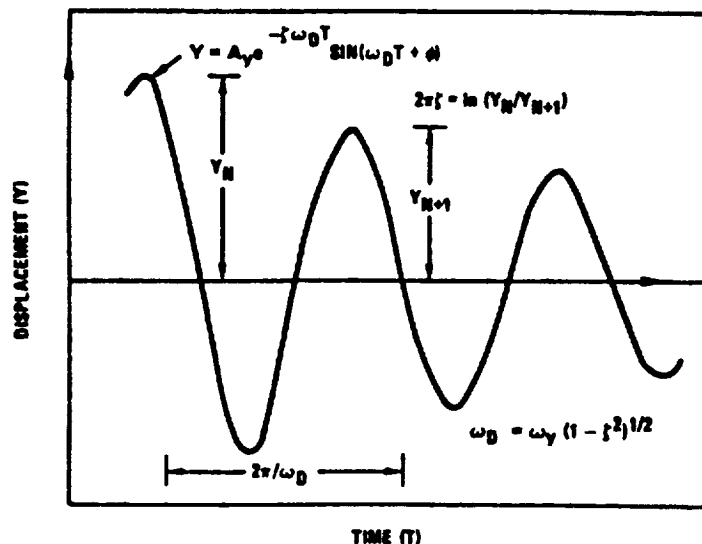


Figure 3-31. Free Decay of a One-Dimensional, Viscously Damped Structure

When the drag coefficient of a cylinder is available and the structure is assumed to vibrate in a single mode, the fluid damping ratios can be estimated as:

$$\zeta_{\text{fluid,transverse}} = \frac{C_D}{2\pi^2} \left(\frac{4\rho_f R^2}{m} \right) \left(\frac{U}{2\omega_n R} \right) \quad (3.2.15)$$

and,

$$\zeta_{\text{fluid,in-line}} = \frac{C_D}{\pi^2} \left(\frac{4\rho_f R^2}{m} \right) \left(\frac{U}{2\omega_n R} \right) \quad (3.2.16)$$

For small amplitude approximations, the total damping of a cylinder in a flow is given as the sum of structural damping and the fluid damping,

$$\zeta_t = \frac{\zeta_0}{\sqrt{m/m_s}} + \frac{C_D}{4} \left(\frac{4\rho_f R^2}{m} \right) \left(\frac{U}{2\omega_n R} \right) \quad (3.2.17)$$

where ζ_0 is the component of structural damping measured in a vacuum and ω_n is the resonant frequency.

Cylinder Displacement

Several models have been developed to estimate cylinder displacement amplitude. These models estimate a maximum displacement amplitude, A_y , which normally occurs under lock-in conditions, normalized by the diameter of the cylinder. Reduced damping, δ_r , and reduced mass, m_r , are useful non-dimensional parameters in displacement amplitude estimation of vortex shedding from bluff bodies.

Reduced mass (mass ratio), a measure of the effective mass, m , to the displaced fluid mass, is determined by:

$$m_r = \frac{m}{\rho_f D^2} \quad (3.2.18)$$

where ρ_f is the fluid density and D is the diameter of the cylinder. Figure 3-32 illustrates the effect of increasing mass ratio on cylinder displacement, using the wake oscillator model. From this model, the peak resonant cylinder amplitude may be expressed using the reduced damping parameter, δ_r . Using the reduced mass and the structural damping ratio, ζ_s , the reduced damping, is determined by:

$$\delta_r = 4 \pi m_r \zeta_s \quad (3.2.19)$$

A structural mode shape factor for displacement, γ , is employed in the following models. At a spanwise point x , along the structure, the displacement of the structure, according to the wake oscillator model, is given by:

$$y(x,t) = A_y \psi(x) \cos(\omega_s t) \quad (3.2.20)$$

where $\psi(x)$ is the mode shape, as found in Table 3-7, at a point x , and ω_s the vortex shedding frequency. The mode shape factor is determined using ψ_{max} , the maximum value of the mode shape, ψ , in the following:

$$\gamma = \psi \max\left(\frac{x}{L}\right) \left\{ \frac{\int_0^L \psi^2(x) dx}{\int_0^L \psi^4(x) dx} \right\}^{\frac{1}{2}} \quad (3.2.21)$$

Models developed for the transverse non-dimensional displacement, $\frac{A_y}{D}$, are given below, where S is the Strouhal number and γ is the structural mode shape factor.

Wake oscillator model, Blevins¹³,

$$\frac{A_y}{D} = \frac{0.07 \gamma}{(1.9 + \delta_r) S^2} \sqrt{0.3 + \frac{0.72}{(1.9 + \delta_r) S}} \quad (3.2.22)$$

Griffin and Ramberg model¹⁴,

$$\frac{A_y}{D} = \frac{1.29 \gamma}{\left[1 + 0.43(2\pi S^2 \delta_r)\right]^{3.35}} \quad (3.2.23)$$

Sarpkaya model¹⁵,

$$\frac{A_y}{D} = \frac{0.32 \gamma}{\sqrt{0.6 + (2\pi S^2 \delta_r)^2}} \quad (3.2.24)$$

Blevins and Burton Correlation (Harmonic) model¹⁶, using the lift coefficient along the cylinder span, $C_L(x)$:

$$\frac{A_y}{D} = \frac{\pi \int_0^L C_L(x) \psi(x) dx}{(2\pi S)^2 \delta_r \int_0^L \psi^2(x) dx} \quad (3.2.25)$$

Using the joint acceptance and the mode shape from Table 3-7, this model takes the simple form:

$$\frac{A_y}{D} = \frac{M_d J G_L}{4 \pi S^2 \delta_r} \quad (3.2.26)$$

13 Blevins, R.D., "Flow Induced Vibration", Van Nostrand Reinhold Company New York 1977.

14 Griffin, O.M. and S.E. Ramberg, "The Effects of Synchronized Cylinder Vibrations on Vortex Formation and Strength, Velocity Fluctuations, and Mean Flow," Paper E-3, Symposium on Flow Induced Vibrations, Karlsruhe, Germany, August, 1972.

15 Sarpkaya, T., "Vortex-Induced Oscillations", Journal of Applied Mechanics, June 1979, vol. 46, pp. 241.

16 Blevins, R.D. and T.E. Burton, "Fluid Forces Induced by Vortex Shedding," J. Fluid Eng., 95, 1976.

In the following equations derived from the Correlation model, a, b, and c are empirically determined constants. Here the vortex shedding is well correlated, i.e. the vortex correlation length is approximately equal to the beam length. These empirical constants for the Correlation model have been experimentally determined in the following cases: a = 0.35, b = 0.60 and c = -0.93.

$$\frac{A_y}{D} = \frac{4\pi S^2 \delta_r - b \sqrt{(4\pi S^2 \delta_r - b)^2 - 4ac}}{2c} \quad \text{spring-mounted rigid cylinder} \quad (3.2.27)$$

$$\frac{A_y}{D} = \frac{4\pi S^2 \delta_r - \frac{2b}{3} \sqrt{(4\pi S^2 \delta_r - \frac{2b}{3})^2 - 2ac}}{c} \quad \text{pivoted rod} \quad (3.2.28)$$

$$\frac{A_y}{D} = \frac{4\pi S^2 \delta_r - \frac{\pi b}{4} \sqrt{(4\pi S^2 \delta_r - \frac{\pi b}{4})^2 - \frac{8}{3}ac}}{\frac{4}{3}c} \quad \text{sine mode} \quad (3.2.29)$$

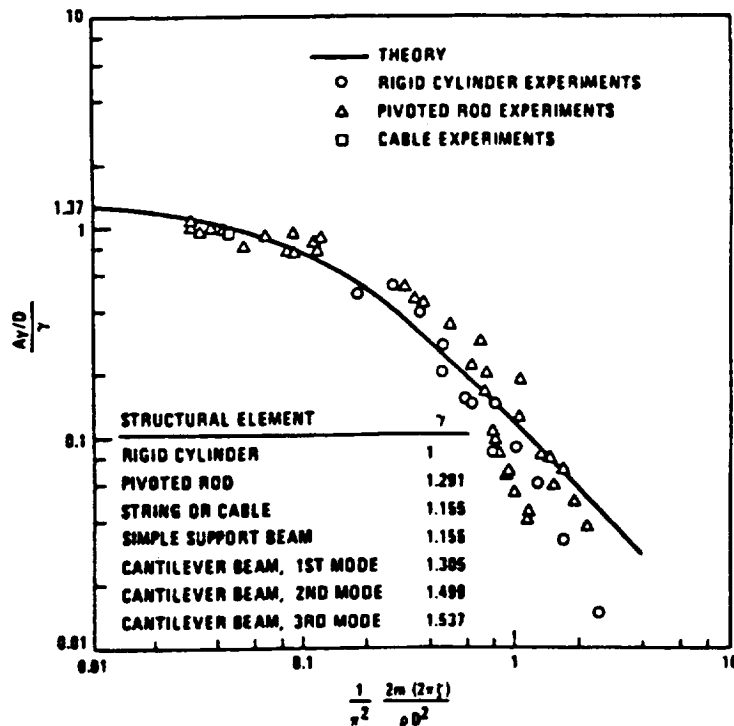


Figure 3-32. Normalized Peak Amplitude vs Reduced Damping Factor

Reduced Velocity and General Amplitude Estimation

The reduced velocity, V_r , is defined by:

$$V_r = \frac{U}{f_n D} \quad (3.2.30)$$

where U is the crossflow velocity, D is the diameter of the cylinder and f is the frequency of oscillation. As shown in Figure 3-33, the frequency of oscillation applies to the structural movement in the fluid. This same logic can be applied to oscillation of the flow with a stationary

structure, using f to be oscillation of the flow. The reduced velocity may also be applied to the structural vibration due to natural structural frequencies in steady flow. Experimental data given by Simmons and Cleary¹⁷, indicated lock-in ranges for $5.3 < V_r < 6.5$ in air and $4.2 < V_r < 7.8$ in water.

The non-dimensional transverse displacement amplitude, $\frac{A_y}{D}$, may be estimated under non-lock-in conditions, using a correlation dependent on reduced velocity. The non-dimensional correlation factor, v_r , may be derived from the Simmons and Cleary data and employed to estimate transverse displacement amplitudes out of the lock-in range.

Curve-fits for v_r from the data of Simmons and Cleary have been obtained for both air flows and water flows.

For air flows:

$$\begin{aligned} v_r &= -97.923 + 60.899 V_r - 12.608 V_r^2 + 0.87088 V_r^3 & V_r < 5.6 \\ &= -220.26 + 75.850 V_r - 6.5 V_r^2 & 5.6 < V_r \leq 5.9 \\ &= -245.85 + 82.399 V_r - 6.875 V_r^2 & 5.9 < V_r \leq 6.3 \\ &= 18.085 - 4.9707 V_r - 0.34343 V_r^2 & 6.3 < V_r \leq 7.3 \end{aligned} \quad (3.2.31)$$

and, for water flows:

$$\begin{aligned} v_r &= 29.750 - 18.862 V_r + 39.25 V_r^2 - 0.26333 V_r^3 & V_r < 5.6 \\ &= -32.088 + 14.623 V_r - 2.102 V_r^2 + 0.09733 V_r^3 & 6.3 < V_r \leq 7.3 \end{aligned} \quad (3.2.32)$$

This factor may be used to multiply with lock-in amplitudes obtained in the previous section to estimate amplitudes for non-lock-in conditions:

$$\left[\frac{A_y}{D} \right]_{\text{general}} = v_r \left[\frac{A_y}{D} \right]_{\text{lock-in}} \quad (3.2.33)$$

Lift Coefficient Estimation

The resultant force acting on a body, perpendicular to the direction of the initial velocity is referred to as lift, L . The dimensionless coefficient for lift is the lift coefficient, C_L . The lift coefficient is related to the lift by:

$$C_L = \frac{L}{\frac{1}{2} \rho_f U^2 A} \quad (3.2.34)$$

where A is a characteristic area.

Simmons and Cleary¹⁸ presented a method of obtaining the lift coefficient, C_L , based on the power, P , transmitted between fluid and structure in one vibration cycle:

$$C_L = \frac{2P}{\rho_f V_f^2 \frac{A_y}{D}} \quad (3.2.35)$$

where the non-dimensional cycle power is curve-fit from their data by:

¹⁷ Simmons and Cleary, 1979.

¹⁸ Simmons and Cleary, 1979.

$$P = 52.057 \left(\frac{V_r}{6} \right) \left(\frac{A_y}{D} \right)^{1.4909} \quad (3.2.36)$$

Figure 3-33 compiles experimental data relating the lift coefficient and Reynolds number. When the non-dimensional displacement approaches a value of 1.22, the maximum observed vibration amplitude, the lift vanishes. The lift coefficient given by Blevins¹⁹ as a function of Reynolds number is bounded by the curve-fit in the following formula where: $R = \log_{10}(Re)$, and

$$\begin{aligned} C_L &= 0.24 & 1.6 < R \leq 3.6 \\ &= -36.179 + 21.068R - 3.883R^2 + 0.22977R^3 & 3.6 < R \leq 5.7 \\ &= -245.85 + 82.399 V_r - 6.875 V_r^2 & 5.7 < R \leq 8 \end{aligned} \quad (3.2.37)$$

Blevins and Burton²⁰ presented correlations for the lift coefficient, C_L , for a cylinder in steady flow, Table 3-8, the coefficients a,b,c are as before in the previous section on displacement: $a = 0.35$, $b = 0.60$, $c = -0.93$.

Table 3-8. Lift Coefficient for Three Mode Shapes Using the Correlation Model

| Mode | $\psi(x)$ | C_L | C_L | $\frac{A_y}{D}$ | |
|----------------|------------------------------------|---|---|-----------------|-----------|
| | | $\frac{A_y}{D} \ll 1$ $L_c \ll L$ | $\frac{A_y}{D}$ $L_c \gg L$ | | |
| rigid cylinder | 1 | $a \left(\frac{L_c}{L} \right)^{\frac{1}{2}}$ | $a + b \frac{A_y}{D} + c \left(\frac{A_y}{D} \right)^2$ | 1 | (3.2.37a) |
| pivoted rod | $\frac{x}{L}$ | $a \left(\frac{4L_c}{3L} \right)^{\frac{1}{2}}$ | $a + \frac{2b}{3} \frac{A_y}{D} + \frac{c}{2} \left(\frac{A_y}{D} \right)^2$ | 1.4 | (3.2.37b) |
| sine mode | $\sin\left(\frac{\pi x}{L}\right)$ | $a \left(\frac{\pi^2 L_c}{8L} \right)^{\frac{1}{2}}$ | $a + \frac{\pi b}{4} \frac{A_y}{D} + \frac{2c}{3} \left(\frac{A_y}{D} \right)^2$ | 1.2 | (3.2.37c) |

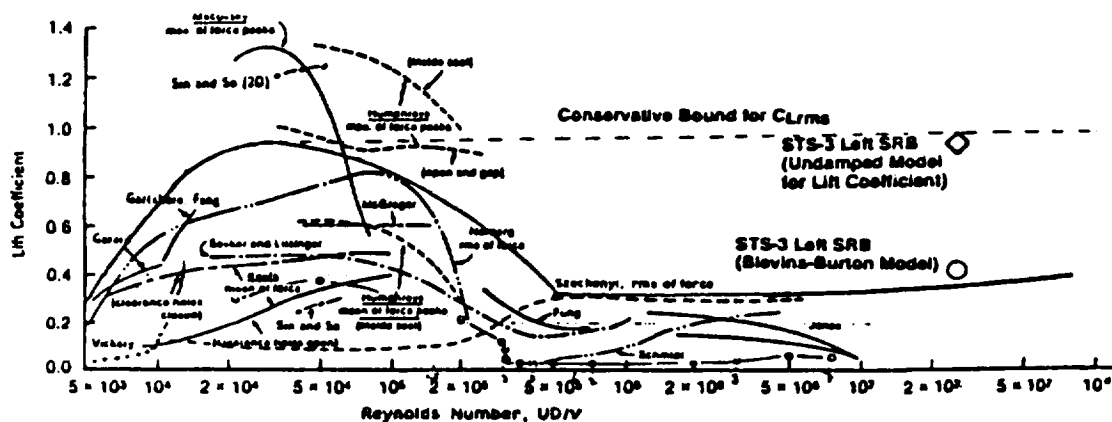


Figure 3-33. Lift Coefficient vs Reynolds Number

19 Blevins, R.D. op. cit. 3.2-(12).

20 Blevins, R.D. and T.E. Burton, op. cit. 3.2-(15).

In addition there is data relating the lift coefficient to the reduced velocity, and estimates for the lift coefficient can be made using the data from Sarpkaya²¹, Figure 3-34.

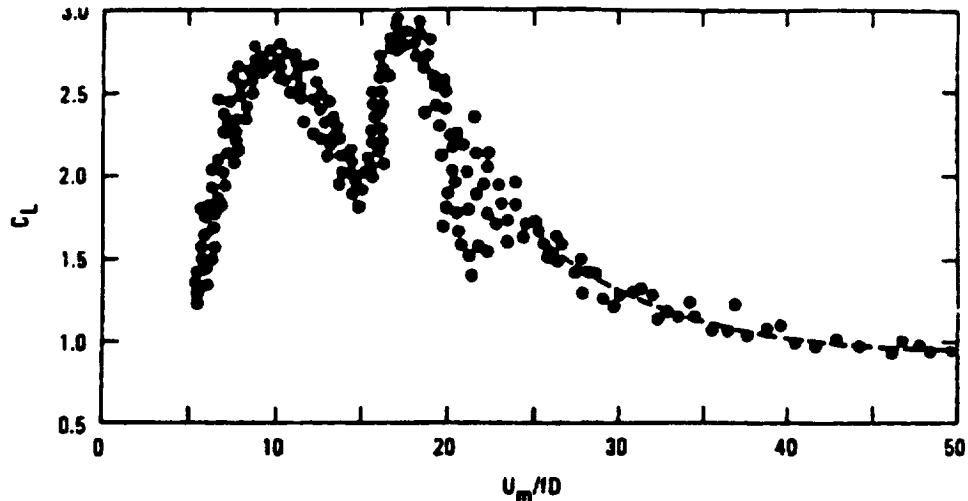


Figure 3-34. Lift Coefficient vs Reduced Velocity

Drag Coefficient Estimation

The resultant force acting on a body, parallel to the direction of the initial velocity is referred to as drag, D . The dimensionless coefficient for drag is the drag coefficient, C_D . The drag coefficient is related to the drag by:

$$C_D = \frac{D}{\frac{1}{2} \rho_f U^2 A} \quad (3.2.38)$$

where A is a characteristic area.

In-line structural bending frequencies for the circular cylinder are postulated to be the same as those for transverse bending frequencies. However, the in-line flow oscillations are twice that of the vortex shedding frequency. It takes two vortices, one from each side of the cylinder, to complete a lift cycle, however, each vortex being shed creates a fluctuation parallel to the flow direction. Dougherty et al²² have duplicated this phenomena with time-accurate CFD analysis.

Drag coefficient data cited by Schlichting²³ for the circular cylinder as function of Reynolds number, Figure 3-35, is curve-fit by the following equation where,

$$C = \log_{10}(C_D) \quad \text{and} \quad R = \log_{10}(Re)$$

| | |
|---|----------------------|
| $C = 1.0 - 0.71612R + 0.12755R^2 + 0.065666R^3$ | $-1.000 < R < 1.000$ |
| $= 0.68601 - 0.19911R - 0.0098063R^2$ | $1.000 < R < 3.000$ |
| $= 7.4712 - 6.0134R + 1.5768R^2 - 0.13415R^3$ | $0.000 < R < 4.301$ |
| $= -31.417 + 21.336R - 4.805R^2 + 0.35965R^3$ | $4.301 < R < 5.041$ |
| $= -64.033 + 24.744R - 2.3844R^2$ | $5.041 < R < 5.672$ |
| $= 708.26 - 124.94R$ | $5.672 < R < 5.673$ |
| $= -53.619 + 25.788R - 4.1964R^2 + 0.22923R^3$ | $5.673 < R < 7.073$ |

(3.2.39)

21 Sarpkaya, T., "Forces on Cylinders and Spheres in a Sinusoidally Oscillating Fluid," J. Appl. Mech., 42, 32-37 (1975).

22 Dougherty, N.S., op. cit. 3.2-(2).

23 Schlichting, H., "Boundary Layer Theory", McGraw-Hill, 1975.

Stationary cylinder data given by Rodrigues²⁴, and Dougherty et al²⁵ indicate that the oscillating portion of the drag coefficient is approximately one-tenth or smaller than that of the lift coefficient. A lower bound for the drag coefficient may be estimated by employing $C_D = 0.1 C_L$. Dahm²⁶ provides another estimate for the drag coefficient $C_D = 0.064$.

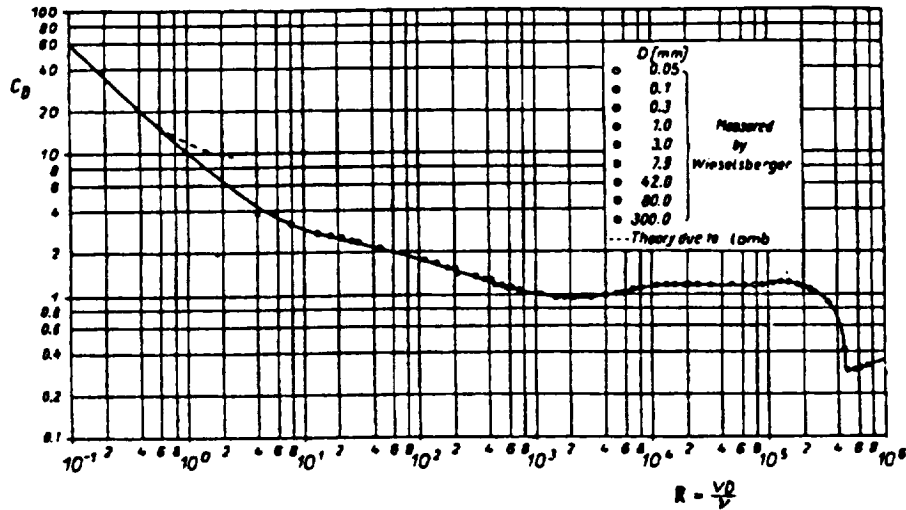


Figure 3-35. Drag Coefficient vs Reynolds Number

In addition there is data relating the drag coefficient to the reduced velocity, and estimates for the drag coefficient can be made using the data from Sarpkaya²⁷, Figure 3-36.

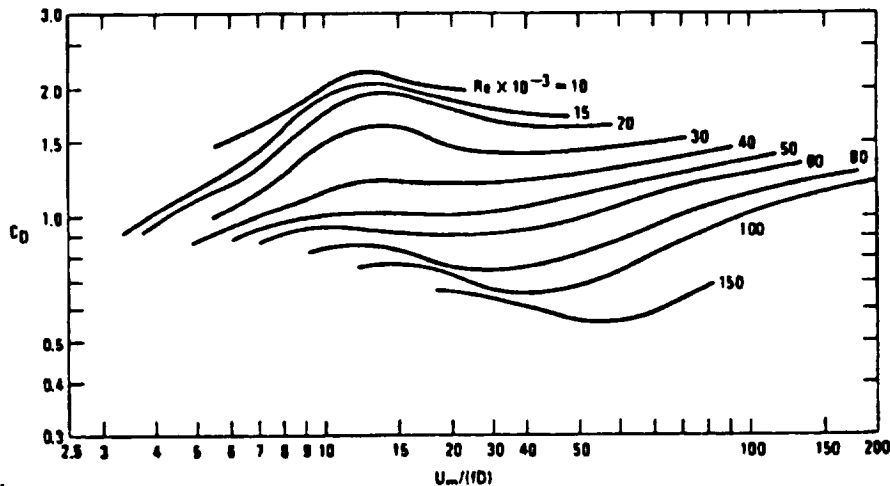


Figure 3-36. In-line Drag Coefficient vs Reduced Velocity in Oscillating Flow

Drag amplification due to vibration can be deduced from a wake response parameter presented by Skop²⁸:

²⁴ Rodrigues, 1984.

²⁵ Dougherty, N.S., op. cit. 3.2-(2).

²⁶ Dahm, W.K., "Composite Model of a Random Forcing Function for the Excitation of Long Pipes by a Crossflow", Internal NASA Communication, George C. Marshall Space Flight Center, Structures and Dynamics Laboratory, Document No. ED31-79-15, August 1979.

²⁷ Sarpkaya, op. cit. 3.2-(20).

²⁸ Skop, 1977.

$$\frac{C_D}{C_{D0}} = w_r = \frac{1 + 2 \frac{A_y}{D}}{V_r S} \quad (3.2.40)$$

At lock-in, $V_r S = 1$ and drag values calculated using the wake response parameter compare well with correlations given in Blevins²⁹. This equation is an estimate of drag amplification when there is transverse vibration.

Wall Effect on Drag Forces for Zero Mean Oscillatory Flow

The flow around a cylinder next to a wall is substantially affected. Figure 3-37 shows the drag coefficient for a cylinder in a zero mean oscillatory flow versus the reduced velocity from experiments conducted by Sarpkaya³⁰.

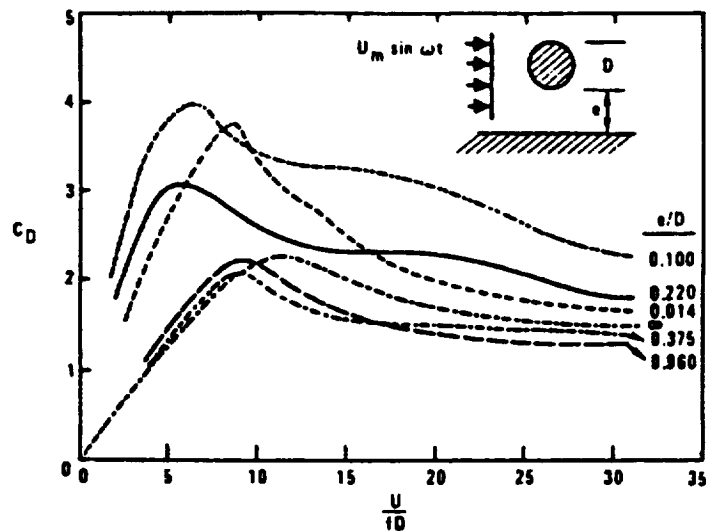


Figure 3-37. Drag Coefficient vs Reduced Velocity

Turbulence-Induced Vibrations

Structural response to turbulent flow is the induced structural vibration resulting from fluctuating surface pressures encountered in the flow. The approach taken to account for turbulence-induced vibration is based on a time-averaged mean square response of the structure.

For a sinusoidal structural mode shape:

$$\psi_j(x) = \sin\left(\frac{j\pi x}{L}\right) \quad (3.2.41)$$

the mean square resonant response, $\overline{Y_{ij}^2}$, for the j^{th} mode in the i direction, is given by:

$$\overline{Y_{ij}^2} = \frac{\pi S F_{\psi}(\omega_j) \psi_j^2(x)}{2\omega_j^3 m^2 \zeta_i} \quad (3.2.42)$$

where

²⁹ Blevins, op. cit. 3.2-(12).

³⁰ Sarpkaya, T., "Forces on Cylinders Near a Plane Boundary in a Sinusoidally Oscillating Fluid," J. Fluids Eng., 98, pp. 499-505, 1976.

$$S_{F_{ij}}(\omega_j) = \frac{S_p(\omega_j) A^2 J_{ij}^2(\omega_j)}{2 \int_0^L \psi_f^2(x) dx} \quad (3.2.43)$$

ζ_t is the total damping, $A = \pi DL$, and

$$\int_0^L \psi_f^2(x) dx = \int_0^L \sin^2\left(\frac{j\pi x}{L}\right) dx = \frac{L}{2} \quad (3.2.44)$$

The turbulence spectra $S_p(\omega)$ can be found from Figure 3-38 and the Joint Acceptance $J_j(\omega)$ can be obtained from Figures 3-39 and 3-40. The convection velocity U_c , used in Figures 3-38 to 3-40 is approximated at 70% of the freestream velocity. The correlation length L_c may also be approximated using the convection velocity divided by the frequency of the turbulence:

$$L_c \propto \frac{U_c}{\omega} \quad (3.2.45)$$

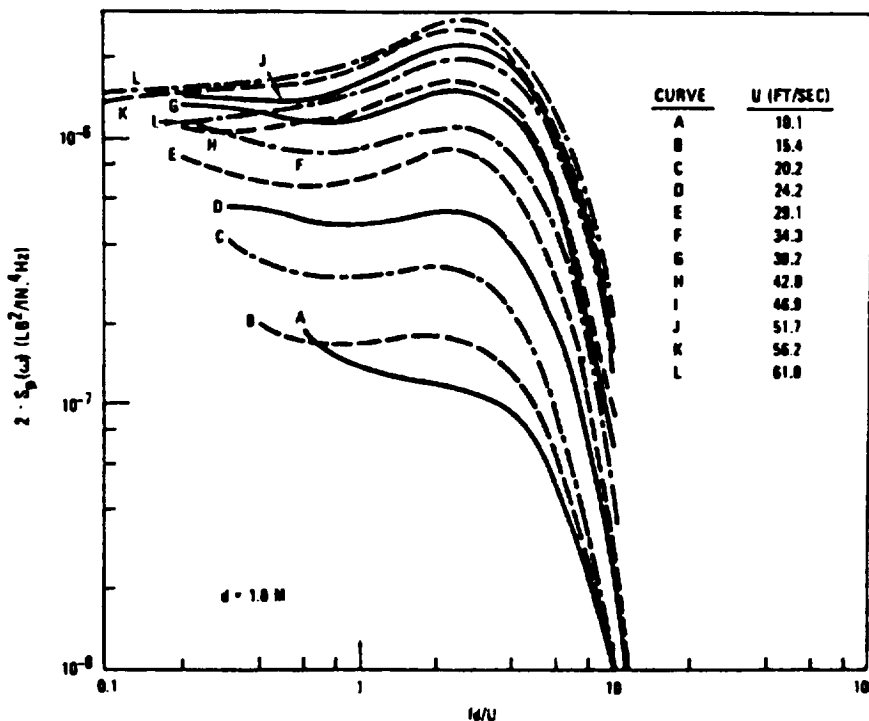


Figure 3-38. Mean-Square Spectra vs Inverse Reduced Velocity³¹

Turbulence-induced vibrations usually have smaller amplitudes (approximately one-tenth) in comparison to vortex induced vibrations at flow-structural lock-in conditions. The contribution of turbulence-induced vibration can be added to that of the vortex-induced vibration. Blevins³² summarized the turbulence induced vibration of a frontal row tube in a tube bundle. As a first order approximation, the methodology is adapted to estimate the turbulence-induced vibration on a bluff body.

$$Y_{rms}/D = (1/16/\pi^{3/2}) (1/m_r/r_{cs}^{1/2}) V_f^{3/2} J \Phi^{1/2} \quad (3.2.46)$$

³¹ Wambsganss, M.W., and S.S. Chen, "Tentative Design Guide for Calculating the Vibration Response of Flexible Cylindrical Elements in Axial Flow" Argonne National Laboratory Report ANL-ETD-71-07, 1971.

³² Blevins, op. cit. 3.2-(12).

where J = joint acceptance and the dimensionless auto spectral density of lateral force, Φ ,

$$\begin{aligned} \Phi &= 3.0 \times 10^{-6} V_r^{3.5} & 0.33 < V_r < 5.0 \\ &= 4.0 \times 10^{-4} V_r^{0.5} & 5.0 < V_r < 100.0 \end{aligned}$$

(3.2.47)

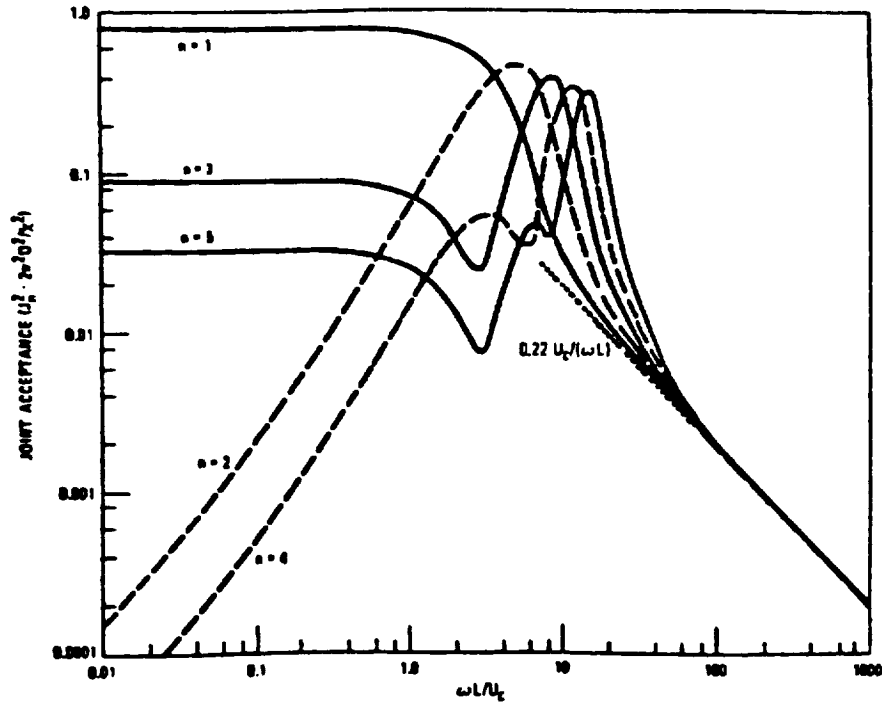


Figure 3-39. Joint Acceptance for Simply Supported Rod³³

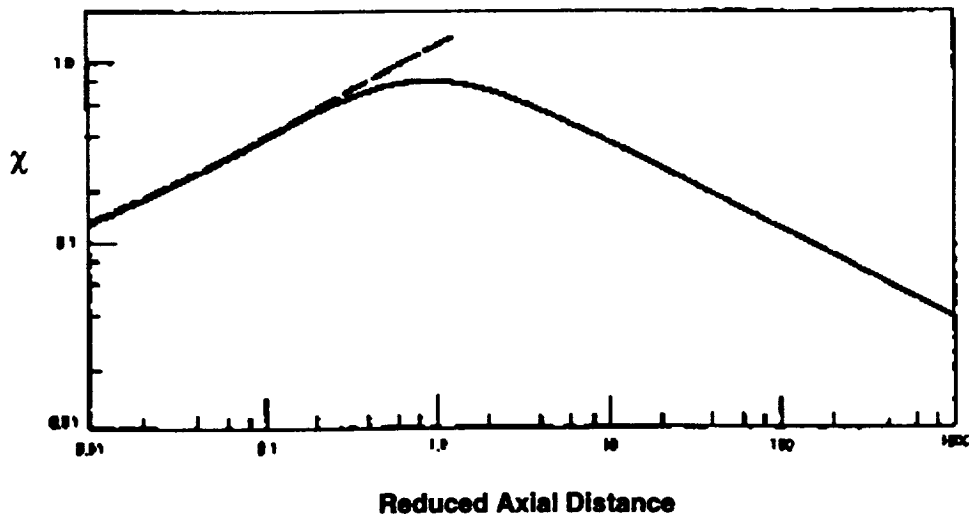


Figure 3-40. Reduced Axial Distance vs χ ³⁴

³³ Chen, S.S. and M.W. Wambsganss, "Parallel-Flow-Induced Vibration of Fuel Rods," Nucl. Eng. Design, 18, pp.253-278, 1972.

³⁴ Chen, op. cit. 3.2-(31).

Methods of Suppressing Cylinder Vortex Shedding

An excellent presentation on methods of suppressing vortex shedding over the circular cylinder is given by Zdravkovich³⁵. Zdravkovich classifies means of suppressing vortex shedding into three main categories: 1) surface protrusions, which affect separation lines and/or separated shear layers, 2) shrouds, which affect the entrainment layers, and 3) nearwake stabilizers, which prevent interaction of entrainment layers.

In the section on strakes, Zdravkovich noted that the effectiveness of strakes decreases with the intensity of turbulence of the freestream and with increasing reduced velocity for a model having the same damping.

Numerical Example

Consider a clamped-free acrylic rod of length 1.0 m with diameter 13.8 mm submerged in water and vibrating in the first bending mode under the action of oscillating lift force induced by a flow velocity of 0.19732 m/s perpendicular to the cylinder axis. Determine the cylinder displacement:

The following parameters are given:

| | | |
|------------------------------|-----------|---|
| Length of cylinder | L | = 1.0 m |
| Diameter of cylinder | D | = 2 R = 0.0138 m |
| Young's Modulus | E | = 4.8 x 10 ⁹ Pa |
| Area moment of Inertia | I | = $\pi a^4/4 = 1.7803 \times 10^{-9} \text{ m}^4$ |
| Kinetic viscosity | μ_f | = 9.8044 x 10 ⁻⁴ kg/m-s |
| Structural material density | ρ_s | = 1190.2 kg/m ³ |
| Fluid density | ρ_f | = 997.4 kg/m ³ |
| Crossflow velocity | U | = 0.19732 m/s |
| Structural damping in vacuum | ζ_0 | = 0.001 |

The rest of the parameters are calculated as:

| | | |
|---------------------------|-------------|--|
| Cylinder area | A | = $\pi R^2 = 1.4957 \times 10^{-4} \text{ m}^2$ |
| Structural mass | m_s | = 0.17802 kg/m |
| Effective Structural mass | m | = 0.3272 kg/m |
| First eigenvalue | λ_1 | = 1.8751 |
| First mode | ω_1 | = $\sqrt{\frac{EI}{m} \left(\frac{\lambda_1}{L}\right)^2} = 17.968 \text{ s}^{-1}$ |
| Reynolds number | Re | = 2770.1 |
| Strouhal Number | S | = 0.2 |

The drag and lift coefficients are obtained from the C_D and C_L vs Reynolds number curves Figures 3-33 and 3-34.

$$C_D = 0.9652 \quad C_L = 0.24$$

The total damping of a cylinder in the lift direction is given as the sum of the effective structural damping and the fluid damping. For the first mode

³⁵ Zdravkovich, M.M., "Review and Classification of Various Aerodynamic and Hydrodynamic Means for Suppressing Vortex Shedding," Journal of Wind Engineering and Industrial Aerodynamics, 7, pp. 145-189, 1989.

$$\zeta_t = \frac{\zeta_0}{\sqrt{m/m_s}} + \frac{C_D}{4} \left(\frac{4\rho_f R^2}{m} \right) \left(\frac{U}{2\omega_n R} \right)$$

$$= 0.00073761 + 0.31858(0.58052)(0.79577) = 0.14791$$

The reduced damping, mode shape factor, joint acceptance, and non-dimensional vibration amplitude are then:

$$\delta_r = 4 \pi m_f \zeta_s = 3.2018$$

$$M_d = 2 \sigma_1 / \lambda_1 = 0.78299 \quad \text{from Table 3-7 and}$$

$$J = (L_c/L)^{1/2} = (4 D/L)^{1/2} = 0.23495$$

$$\frac{A_y}{D} = \frac{M_d J C_L}{4 \rho S^2 \delta_r} = \frac{0.78299 \times 0.23495 \times 0.24}{4 \pi 0.2^2 \times 3.2018} = 0.027433$$

The maximum deflection amplitude at the free end of the clamped-free beam may be obtained by determining the maximum deflection point for the particular mode shape and multiplying the quantity A_y by this deflection value. For the clamped-free beam the maximum deflection is at the free end of the beam where the nondimensional deflection amplitude for the first mode is about 1.446. The expected maximum displacement for the cylinder is then 0.03967 m.

Rotating Cylinder - No Vortex Shedding

Tokumar and Dimotakis³⁶ investigated the mean lift coefficient of a circular cylinder executing rotary motions in a uniform flow. The rotary motions included steady rotation and rotary oscillations with a net rotation rate. A rotating cylinder moving in a uniform stream experiences a transverse force known as the Magnus force. Badr et al³⁷ observed that there was no periodic vortex shedding from a circular cylinder that was rotating with a surface velocity greater than two or three times the freestream velocity. The mean lift coefficient can be written as

$$C_L = \frac{L a}{\rho U^2} = \frac{\Gamma a}{U} \quad (3.2.48)$$

where ρ = fluid density, L = lift per unit span, U = freestream velocity, a = radius, and Γ = mean circulation. Their experimental study was performed in a 20" x 20" free surface water tunnel. A 1" D Plexiglas cylinder with 18.7" length was supported 10" above the bottom of the water channel, between 0.5" thick fairings placed flush to the sidewalls of the channel. Power was transmitted from a DC motor to the cylinder with timing belts. The angular motion of the cylinder was given non-dimensionally,

$$\Omega = \Omega_0 + \Omega_1 \sin(2\pi f t) \quad (3.2.49)$$

where $\Omega = \dot{\theta} a / U$ and $\dot{\theta}$ = angular velocity, f = forcing frequency, Ω_0 and Ω_1 are amplitudes of the steady and harmonic components of the cylinder motion. The normalized forcing frequency is the forcing Strouhal Number

$$S = \frac{2 a f}{U} \quad (3.2.50)$$

³⁶Tokumar, P. T. and Dimotakis, P. E., "The Lift of a Cylinder Executing Rotary Motions in a Uniform Flow," J. Fluid Mech., vol. 255, pp. 1-10, 1993.

³⁷Badr, H. M., Coutanceau, M., Dennis, S. C. R. and Menard, C., "Unsteady Flow Past a Rotating Circular Cylinder at Reynolds numbers 10^3 and 10^4 ," J. Fluid Mech., vol. 220, pp. 459-484, 1990.

CYLINDERS

They used the virtual vortex method to estimate lift coefficient. Instead of an infinite domain, the channel flow was considered as an infinite series of spatially periodic image vortices located above and below the cylinder (see Figure 3-41). Therefore, the transverse velocity along x-axis is given by

$$v(x, y = 0) = \frac{\Gamma}{2h} \operatorname{csch}\left(\pi \frac{x - x_0}{h}\right) \quad (3.2.51)$$

where h = channel height and x_0 = streamwise position of the virtual vortex. In terms of C_L , one has

$$\frac{v(x, y = 0)}{U} = \frac{a}{2h} C_L \operatorname{csch}\left(\pi \frac{x - x_0}{h}\right) \quad (3.2.52)$$

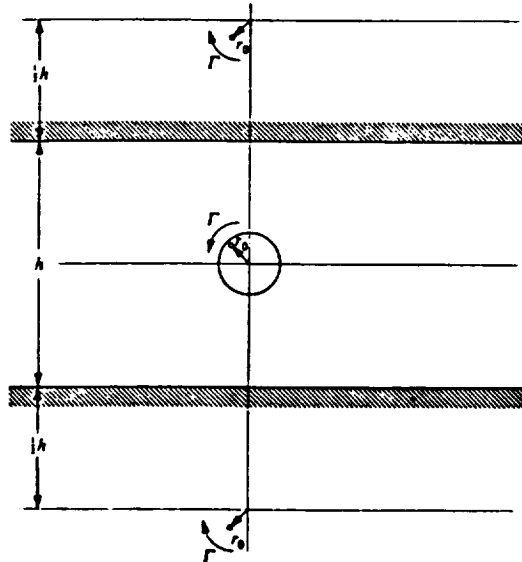


Figure 3-41. Diagram of Periodic Image Vortices. Only the Image Vortices Immediately Above and Below Are Pictured

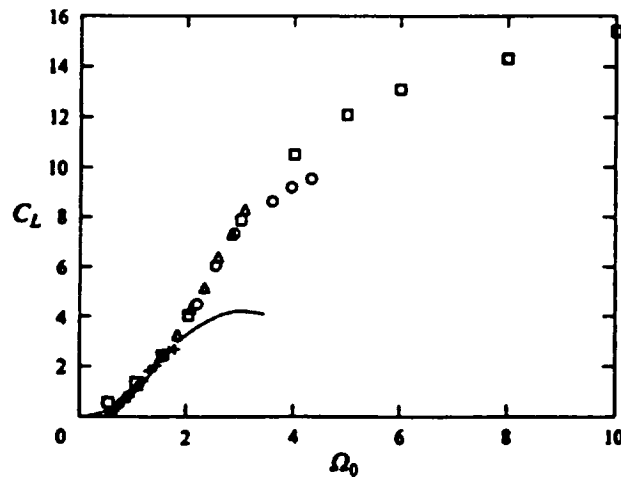


Figure 3-42. C_L Based on Data Fit and Data of Reid (1924) and Prandtl (1925)

For large x distances, one may approximate $x - x_0 \sim x$. For steady rotation, $\Omega_1 = 0$, they tested in the range of $0.5 < \Omega_0 < 10$ at $Re = 3800$. The deduced lift coefficient is given in Figure 3-42 in comparison to data of Reid (1924) and data of Prandtl (1925). They addressed the cylinder end effect from the data comparison that the higher the aspect ratio the higher the C_L . They argued that due to unsteady effect the lift coefficient can exceed the 4π limit of the maximum C_L proposed by Prandtl. They also addressed the Reynolds number effect at low values and that their C_L values remained positive even when $\Omega_0 < 0.5$.

They then investigated the forced oscillations with the forcing Strouhal Number of $S = 0.7$ and $Re = 6800$. They found that under forced oscillations, C_L values were higher for $0.0 < \Omega_0 < 2.5$ and lower for $2.5 < \Omega_0 < 4.5$ in comparison to the corresponding steady rotations. The results further indicated that for $\Omega_0 > 4.5$, the effect of forced oscillation diminished as shown in the reference Figure 3-43. Their flow visualization revealed that for $\Omega_0 < 2.5$, forced oscillation help close the wake, creating a flow that was closer to potential flow and better span-wise correlated. In contrast, for $2.5 < \Omega_0 < 4.5$, where the wake would normally close with steady rotation alone, oscillations tended to 'diverge' the wake flow.

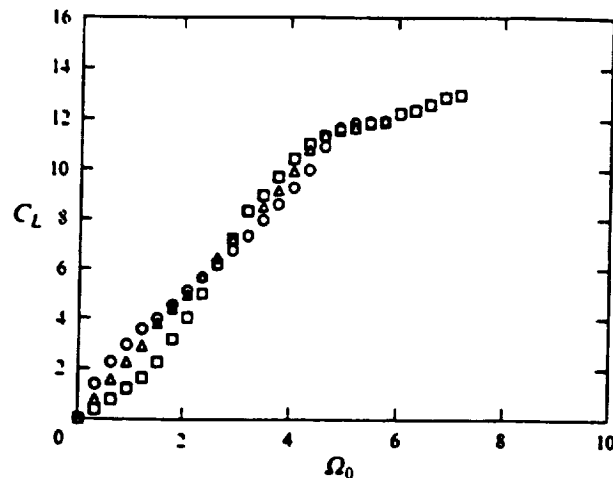


Figure 3-43. Comparison of C_L vs. Ω_0 Data for $S = 0.7$ at $Re = 6.8 \times 10^3$

3.3 Tube Arrays

Consider a pipe, one among several in an array of tubes or pipes, exposed to a fluid cross flow. A fluid force, brought about by the asymmetry of the flow field, might be exerted on the pipe with sufficient magnitude to displace the pipe from its equilibrium position. If the ratio of fluid force to pipe support damping is sufficiently large, then the pipe may vibrate with a large amplitude.

Flow-induced vibration introduces a displacement mechanism distinctly different from that for vortex-induced vibration because no inherent, unsteady component of the flow is required for vibration. The force on the pipe is generated by the interaction of the flow field on the rest of the array, resulting in vibrations that are either whirling (pipes vibrating in oval orbits), jet switching (vibration due to coupling and uncoupling of fluid jets behind the array), or vibration from the interaction of a pipe with the wake of another pipe upstream. In closely spaced pipe arrays, the vortex shedding frequency degenerates into broad-band turbulence which buffets the pipes. Whirling instability ordinarily arises at flow velocities beyond vortex-induced resonance. Jet switching produces an instability at high, reduced velocities.

Vibration due to Whirling

Consider the two-dimensional structural model for the pipe array illustrated in Figure 3-44. The terms, x_j and y_j , represent the displacement components of the j^{th} pipe from its equilibrium position in the row. The terms, k_x^j and k_y^j , are the stiffnesses of the spring supports parallel and normal to the free stream flow. The terms, ζ_x^j and ζ_y^j are the coefficients of viscous damping of each pipe parallel and normal to the free stream due to structural and fluid mechanisms.

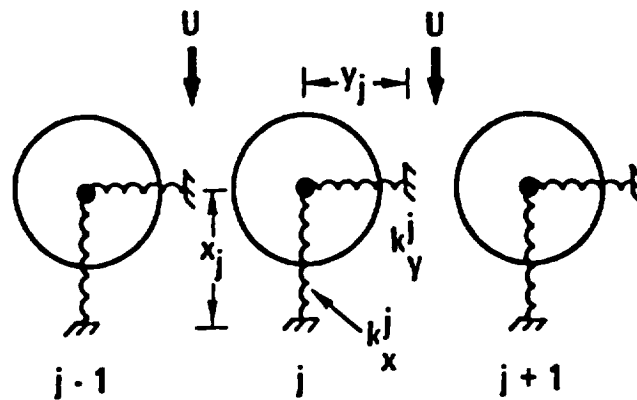


Figure 3-44. Structural Model for Array of Pipes¹

¹ Blevins, R.D., "Flow-Induced Vibration," Kreiger Publishing Co., pp. 88-117, 1977.

TUBE ARRAYS

Oscillatory fluid forces on the pipes can arise due to several reasons. First of all, fluid forces can arise from periodic vortex shedding. However, such vortex shedding generally does not produce large amplitude pipe vibrations in pipe arrays where the pipe-to-pipe spacing is 1.5 pipe diameters or less. This is because the proximity of the pipes cause the regular vortex shedding to degenerate into broad band turbulence. Another example is fluid forces caused by jet switching of a wake.

Jets issuing from sufficiently close-spaced pipes can couple. Changes in pipe position can cause the jet pairs to switch and produce pipe oscillation. Jet switching has been observed for reduced velocities, U/D , of order 100, where U is the free stream velocity between the pipes, f is the natural frequency of the pipes, and D is the outside tube diameter. The jet switch mechanism may not be operative for $U/D < 75$ owing to the time required for the switch².

Fluid forces can also be caused by asymmetry of the flow pattern as one pipe is displaced from its equilibrium position. If a pipe is slightly displaced in a regular pipe array, then the steady fluid force on the pipe will change since the flow pattern changes. Since the flow pattern through a pipe array is a function of the positions of the pipes relative to each other, it is reasonable to assume that the change in fluid force on one displaced pipe is a function of its displacement relative to the displacements of the other pipes. Furthermore, if the pipe displacements are small it is reasonable to assume that the pipe in a regular pipe array will primarily interact with its two nearest neighboring pipes. Thus, the change in steady fluid force per unit length on a pipe, say the j^{th} pipe, in the x and y directions ($F_{x,y}^j$), can be written as a function of j pipe displacements (x_j, y_j) relative to the displacements of the neighboring $j+1$ and $j-1$ pipes, i.e.

$$F_{x,y}^j = \rho U^2 g_{x,y}(x_{j+1} - x_j, x_j - x_{j-1}, y_{j+1} - y_j, y_j - y_{j-1})/4 \quad (3.3.1)$$

where ρ is the fluid density, and U is the free stream velocity at the minimum cross section between the pipes. The symmetry of the pipe geometry requires that the fluid force have certain symmetries for small displacements about the equilibrium position of $(x,y)=(0,0)$. Therefore,

$$\frac{\partial g_{x,y}}{\partial (x_j - x_{j-1})_{x=y=0}} = - (m) \frac{\partial g_{x,y}}{\partial (x_{j+1} - x_j)_{x=y=0}} = K_{x,y} \quad (3.3.2)$$

$$\frac{\partial g_{x,y}}{\partial (y_j - y_{j-1})_{x=y=0}} = \pm \frac{\partial g_{x,y}}{\partial (y_{j+1} - y_j)_{x=y=0}} = K_{x,y} \quad (3.3.3)$$

The plus and minus signs are used for the y and x components, respectively, in Equation 3.3.2, and for the x and y components, respectively, in Equation 3.3.3.

There are also fluid forces which depend on pipe velocity and acceleration. Such forces can be considered to be the sum of added mass and inertial coupling. The added mass effect can be easily incorporated in the analysis by increasing the pipe mass by the added mass of entrained fluid. The coupling between pipes arises from the fluid forces generated by the relative acceleration between vibrating pipes. The importance of inertial coupling increases with the ratio of the mass of fluid displaced by a pipe to the mass of the pipe.

² Roberts, B.W., "Low Frequency, Aeroelastic Vibrations in a Cascade of Circular Cylinders," Mechanical Engineering Science Monograph No. 4, September 1966.

TUBE ARRAYS

If there is sufficient smoothness in the variation of fluid force with pipe displacement, then only the linear terms in Equations 3.3.2 and 3.3.3 are required in the stability analysis. The linearized equations of motion for one pipe in an infinite pipe row are developed by expanding the fluid force on the j^{th} tube, Equation 3.3.1, in a Taylor series about the equilibrium position using Equations 3.3.2 and 3.3.3,

$$F_x^j = \rho U^2 (K_x(x_j - x_{j-1}) - K_x(x_{j+1} - x_j) + C_x(y_j - y_{j-1}) + C_x(y_{j+1} - y_j)) / 4 \quad (3.3.4)$$

$$F_y^j = \rho U^2 (K_y(x_j - x_{j-1}) + K_y(x_{j+1} - x_j) + C_y(y_j - y_{j-1}) - C_y(y_{j+1} - y_j)) / 4 \quad (3.3.5)$$

and applying these forces to elastically mounted pipes. The linear equation describing the pipe motion parallel to the free stream is,

$$m\ddot{x}_j + 2m\zeta_x^j \omega_x^j \dot{x}_j + k_x^j x_j = \rho U^2 (K_x(-x_{j+1} - x_{j-1} + 2x_j) + C_x(y_{j+1} - y_{j-1})) / 4 \quad (3.3.6)$$

The linear equation describing the pipe motion normal to the free stream is,

$$m\ddot{y}_j + 2m\zeta_y^j \omega_y^j \dot{y}_j + k_y^j y_j = \rho U^2 (C_y(-y_{j+1} - y_{j-1} + 2y_j) + K_y(x_{j+1} - x_{j-1})) / 4 \quad (3.3.7)$$

where ω_x^j and ω_y^j are the circular natural frequencies, ζ_x and ζ_y are the sum of the structural and fluid damping factors, and m is the mass per unit length of the tube including the entrained mass of the fluid. Note that

$$m = m_0 + C_I \pi \frac{D^2}{4} \quad (3.3.8)$$

where m_0 is the mass per unit length of the pipe and C_I is the inertia coefficient of the pipe bundle.

Equations 3.3.6 and 3.3.7, which describe a single pipe in a row, cannot be solved independent of the motion of neighboring pipes. The fluid force couples the motion of the neighboring pipes and induces vibration in the x and y coordinates. Although these equations of motion are developed for a pipe row, they apply to a pipe array if (a) the pipe arrays are regular and symmetric, as is ordinarily the case with in-line and staggered pipe arrays, and (b) each pipe interacts principally with only two of the nearest pipes.

Wake-Induced Vibration

This mechanism for generating vibration is caused by velocity gradients in the wake of an upstream pipe which imposes sufficient force on a downstream pipe to induce vibration. Consider an elastically mounted pipe in the wake of another pipe as illustrated in Figure 3-45. Lift and drag forces, F_y and F_x respectively, on the elastically mounted pipe arise from mean flow plus velocity and pressure gradients in the wake, i.e.

$$F_x = \frac{1}{2} \rho U^2 C_x \quad (3.3.9)$$

TUBE ARRAYS

$$F_y = \frac{1}{2} \rho U^2 C_f \quad (3.3.10)$$

and the coefficients of fluid force in the x and y direction are defined as

$$C_x = (C_D \cos \alpha - C_L \sin \alpha) \frac{U_{rel}^2}{U^2} \quad (3.3.11)$$

$$C_y = (C_L \cos \alpha + C_D \sin \alpha) \frac{U_{rel}^2}{U^2} \quad (3.3.12)$$

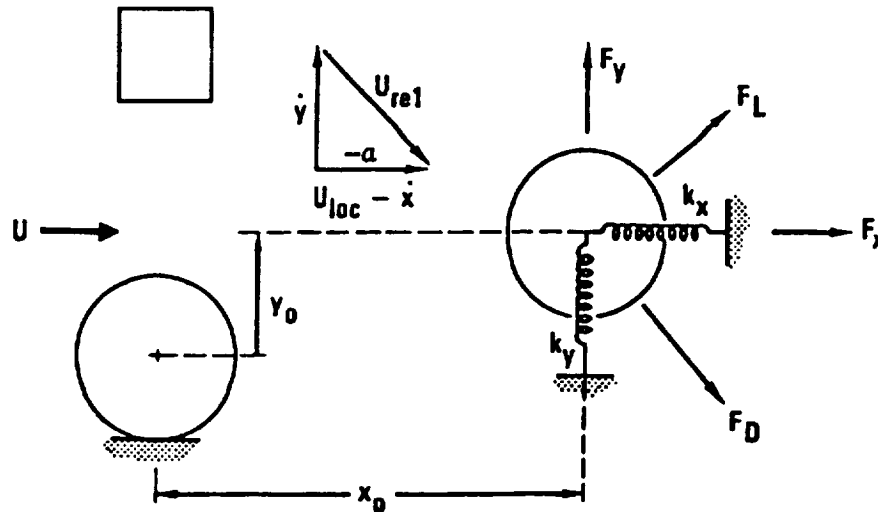


Figure 3-45. Wake Interaction Structural Model³

where C_L and C_D are the lift and drag coefficients. The angle of attack of the flow to the pipe is,

$$\alpha = -\tan^{-1} \left(\frac{\dot{y}}{U_{loc} - \dot{x}} \right) \quad (3.3.13)$$

and the relative velocity is,

$$U_{rel}^2 = \dot{y}^2 + (U - \dot{x})^2 \quad (3.3.14)$$

where U_{loc} is the local fluid velocity in the wake. The lift and drag coefficients are functions of the position of the elastically mounted pipe relative to the wake of the upstream pipe.

For small disturbances, Equations 3.3.11 through 3.3.14 can be expanded in terms of small displacements of the pipe, x and y , from its nominal position, x_0 and y_0 ,

$$X = x_0 + x \quad (3.3.15)$$

³ Blevins, R.D., op. cit.(2).

TUBE ARRAYS

$$Y = y_0 + y \quad (3.3.16)$$

Therefore, one obtains

$$C_y = C_L + \alpha C_D + O(\alpha^2) \quad (3.3.17)$$

$$C_x = C_D - \alpha C_L + O(\alpha^2) \quad (3.3.18)$$

$$C_D = C_D(x_0, y_0) + \frac{\partial C_D}{\partial x} x + \frac{\partial C_D}{\partial y} y + O(x^2, y^2) \quad (3.3.19)$$

$$C_L = C_L(x_0, y_0) + \frac{\partial C_L}{\partial x} x + \frac{\partial C_L}{\partial y} y + O(x^2, y^2) \quad (3.3.20)$$

$$\alpha = \frac{-\dot{y}}{U_{loc}} + O(\dot{x}\dot{y}) \quad (3.3.21)$$

$$U_{rel}^2 = U^2 - 2U\dot{x} + O(\dot{y}^2) \quad (3.3.22)$$

For stability analysis, only linear terms are retained. The equations of motion are obtained by substituting Equations 3.3.17 through 3.3.22 into the force equations, Equations 3.3.9 and 3.3.10, and applying these forces to the elastically mounted pipe:

$$m\ddot{x} + 2m\zeta_x \omega_x \dot{x} + k_x x = \frac{1}{2} \rho U^2 D \left(\left(\frac{\partial C_D}{\partial x} \right) x + \left(\frac{\partial C_D}{\partial y} \right) y + \frac{\dot{y} C_L}{U_{loc}} - \frac{2\dot{x} C_D}{U_{loc}} \right) \quad (3.3.23)$$

$$m\ddot{y} + 2m\zeta_y \omega_y \dot{y} + k_y y = \frac{1}{2} \rho U^2 D \left(\left(\frac{\partial C_L}{\partial x} \right) x + \left(\frac{\partial C_L}{\partial y} \right) y - \frac{\dot{y} C_D}{U_{loc}} - \frac{2\dot{x} C_L}{U_{loc}} \right) \quad (3.3.24)$$

A free stream inclined with respect to the pipe axis would introduce additional terms⁴. Fluid forces couple the x and y motions of the pipe through displacement and velocity. The coupling produces an elliptical orbit when the flow velocity exceeds the critical velocity. It is possible to obtain some limited solutions if all velocity-type terms in $\delta x/\delta t$ and $\delta y/\delta t$ are neglected⁵. However, solutions of the following form can be generally assumed,

$$x = \underline{x} (\exp \lambda t) \quad (3.3.25)$$

$$y = \underline{y} (\exp \lambda t) \quad (3.3.26)$$

where \underline{x} , \underline{y} and λ are constants. These equations are substituted into Equations 3.3.23 and 3.3.24, and conditions are sought such that λ has only negative real roots and all perturbations diminish in time. This generally requires numerical solution of the roots of a fourth-order stability polynomial for λ .

⁴ Simpson, A., "Determination of the Natural Frequencies of Multi-Conductor Overhead Transmission Lines," J. Sound and Vibration 20, pp. 417-449, 1972.

⁵ Simpson, A., "On the Flutter of a Smooth Cylinder in a Wake," Aeronautical Quarterly 22, pp. 25-41, 1971.

TUBE ARRAYS

Since C_L and C_D are functions of the location of the pipe in the wake, it is possible to map out regions in the wake where the pipe in the wake cannot be unstable. For example, if the pipe in the wake is located directly behind the forward pipe ($y_0=0$), then the symmetry of the flow implies that

$$C_L = \delta C_L / \delta y = \delta C_D / \delta y = \delta C_L / \delta x = 0 \quad (3.3.27)$$

and no instability is possible. If the pipe is located outside the wake of the forward pipe, then

$$C_L = \delta C_L / \delta x = \delta C_L / \delta y = \delta C_D / \delta x = \delta C_D / \delta y = 0 \quad (3.3.28)$$

and no instability due to wake interaction is possible. For flows with high Reynolds numbers, the lateral width of the wake is proportional to $\sqrt{x_0}$ ⁶

Jet-Switching Vibration

Consider the pipe array illustrated in Figure 3-46. The fluid jets shown form in the wake of a closely spaced pipe row or array. If the pipe-to-pipe spacing is less than about $T/D=2.2$, then the jets pair up. By sufficiently displacing pipes upstream and downstream, the jet pairs could be switched. Since the drag force on a pipe can significantly change as the jets switch, jet switching can input energy into the pipe. Jet switching is not expected to affect pipe arrays or pipe arrays with very irregular exits.

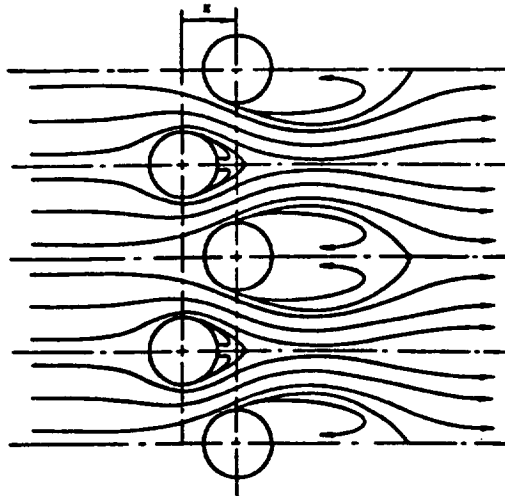


Figure 3-46. Illustration of Jet-Switching Vibration⁷

⁶ Timoshenko, S., and D.H. Young, " Vibration Problems in Engineering," D. Van Nostrand, New York, pp. 425, 1954.

⁷ Roberts, B.W., op. cit.(3).

Tube Bundle Experimental Data

Data review and compilation for onset critical flow velocities also include those for tube arrays. Andjelic et al⁸ presented flow-induced lock-in data in a triangular tube array. Their measurements were carried out on one or several flexibly mounted tubes in an otherwise fixed tube bundle. A closed-circuit wind tunnel with a 1.5 m diameter by 2.1 m test section was used for the tests. The tube bundle was comprised of eighteen 80 mm by 800 mm aluminum cylinders in the multi-row normal triangular array having a pitch-to-diameter ratio of 1.25. The transverse tube spacing, t is 100 mm. The mass-damping parameter can be varied over a range of $10 < \delta_r < 80$. Where $\delta_r = \mu \delta / \rho d^2$, μ = tube mass per unit length = 2.75 kg/m, δ = logarithmic decrement measured at no flow condition, and ρ = fluid density. The tube mid-point motions for two test conditions: a) the reduced gap velocity, V_r , is 13 and $\delta_r = 9.96$, and b) $V_r = 13.75$ and $\delta_r = 13.53$ were given. The transverse displacement had an amplitude of 5 mm and the in-line displacement amplitude was 0.4 mm in the latter and approximately one-fifths in the former condition. The lift-induced deflections are greater than the drag-induced deflections by a factor of 5 to 10 times. The reduced gap velocity is defined by $V_r = U / (f_1 d)$, where U is the mean gap velocity = $\frac{P}{d} U_\infty \left(\frac{P}{d} - 1 \right)$, P is the pitch of the tube bundle, d is the diameter of each tube, f_1 is the first natural tube vibration frequency at no flow condition = 9.85 ± 0.1 Hz, and U_∞ is the undisturbed upstream velocity. Average reduced amplitude as a function of V_r for the one iso-viscoelastically mounted tube case was considered for $\delta_r = 10.14$. The flow-structural lock-in phenomenon took place in the range of of $\sim 10 < V_r < 17$. Hysteresis effect was found. By plotting V_{rcrit} versus δ_r , the instability flow map was given. According to their results, the instability region had a critical reduced gap velocity from 12 to 24 when reduced damping was less than 14.

They measured the tube mid-point motions of nine linear iso-viscoelastically mounted tubes at two flow conditions: a) $V_r = 17.25$ and $\delta_r = 29$, and b) $V_r = 20.65$ and $\delta_r = 43$. Only six of the eighteen vibration loops have greater lift-induced deflections, therefore the drag-induced deflections in tube arrays can be on the same order of magnitude. Also, the damping can be used as a means to reduce the vibration amplitude. For this tube bundle test they recommended the use of $A = 35$, $B = 0.375$, and $\beta = 1.7$ in the empirical curve:

$$V_r = A \left(\frac{P}{d} - 1 \right)^\beta \left\{ 1 + \sqrt{1 + B \delta_r} \right\} \quad (3.3.29)$$

In addition they used a least-squares analysis to find the the curve-fit:

$$V_r = 3.43 \delta_r^{0.44} \quad (3.3.30)$$

which fits a set of 38 experimental data very well.

⁸Andjelic, M., Austermann, R. and Popp, K., "Multiple Stability Boundaries of Tubes in a Normal Triangular Cylinder Array," Institute of Mechanics, University of Hannover, Germany, 1988.

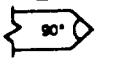
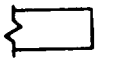
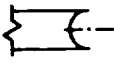
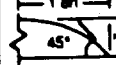
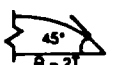
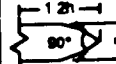
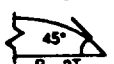
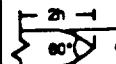
OTHER BLUFF BODIES

3.4 Other Bluff Bodies

Trailing Edges of Vanes and Struts

Vanes and struts immersed in a freestream flow, flat rectangular or curved, elliptic or approximating an airfoil shape may be designed with bluff trailing edges for ease of manufacture or added structural strength. A disadvantage can result in the installation under flow conditions conducive to vortex shedding due to the particular trailing edge design instead. Some data on vortex shedding amplitude collected by Donaldson, Heskestad and Olberts, and Ippen (cited by O'Connor and Jones¹) given in Table 3-9 show that 60° symmetric trailing edge beveling increases vortex shedding amplitude by as much as 360 percent over a straight rectangular trailing edge. The reference is a rectangular edge being 100 percent. As seen in the table, reductions in bevel angle down to 30° and asymmetric bevel cuts can reduce vortex shedding amplitude as much as two orders of magnitude. For example, a cylindrical trailing edge (reference unmodified geometry) can be improved, if the thin trailing edge section is allowable, by an asymmetric 30° bevel for example (reference geometry selected).

Table 3-9. Effect of Vane or Strut Trailing Edge Shape on Vortex Shedding Amplitude

| Donaldson | | Heskestad & Olberts | | Ippen | |
|---|---------|---|---------|--|---------|
| Geometry | Rel Amp | Geometry | Rel Amp | Geometry | Rel Amp |
|  | 360% |  | 360% |  | 320% |
|  | 280 | Unmodified Geometry | |  | 230 |
|  | 230 |  | 190 | | |
|  | 100 |  | 100 |  | 100 |
|  | 48 |  | 43 | | |
|  | 22 |  | 31 |  | 80 |
|  | 20 |  | 38 |  | 70 |
|  | > 1 |  | 3 |  | 60 |
|  | > 1 |  | < 1 | | |
|  | > 1 |  | < 1 | Geometry Selected | |
| | |  | < 1 | | |

¹O'Connor, G. M. and Jones, J. H., "Flow-Induced Vibrations of the SSME LOX Inlet Tee Vanes," AIAA-88-3132, AIAA/ASME/SAE/ASEE 24th Joint Propulsion Conference, Boston, Mass., July 11-13, 1988.

H-Shaped Sections

One of the well-studied bluff body shapes is the H-shaped section. Since the spectacular crash of the original Tacoma bridge in 1940, the aerodynamic and aeroelastic behavior of an H-shaped section has attracted many engineering analyses, including high frequency flow/structural interaction studies. It is of particular interest here because of coupled motions. In the case of flow past a rigid bluff body, the shedding of Karman vortices is usually referred as the low-frequency mode, while the shear layer instability yields the high-frequency mode. There is another instability due to the impingement of the separated shear layer (from the leading edge) on the trailing edge of a bluff body which may generate sub- and super-harmonics of the vortex shedding frequency. The H-shaped sections are also prone to this "impinging shear layer instability".

A Reference Test

Shewe² conducted an experimental study on an H-section which has the same width-to-height ratio as that of the original Tacoma bridge. The geometrical details of the H-shaped cross-section of the wind tunnel model and the coordinate system used were given in the reference Figure 3-47. The definitions of the aerodynamic drag, F_x , lift, F_z , and moment, M , in relation to the coordinate system and angle-of-attack, α , are denoted in the figure. The section has a width of $B = 0.055$ m, a height of $H = 0.11$ m and thus a ratio of $B/H = 5$ corresponding to the original Tacoma bridge. The model's length $L = 0.6$ m yielding an aspect ratio of $L/B = 10.9$. The thickness of the test model is $d = 0.003$ m. The ends of the test model were clamped to a multicomponent piezo-balance of high stiffness and sensitivity. The natural frequency and damping of the first bending mode were found to be $f_B = 103$ Hz and $\delta_B = 0.0018$. The natural frequency and damping of the first torsion mode were found to be $f_T = 401$ Hz and $\delta_T = 0.0005$.

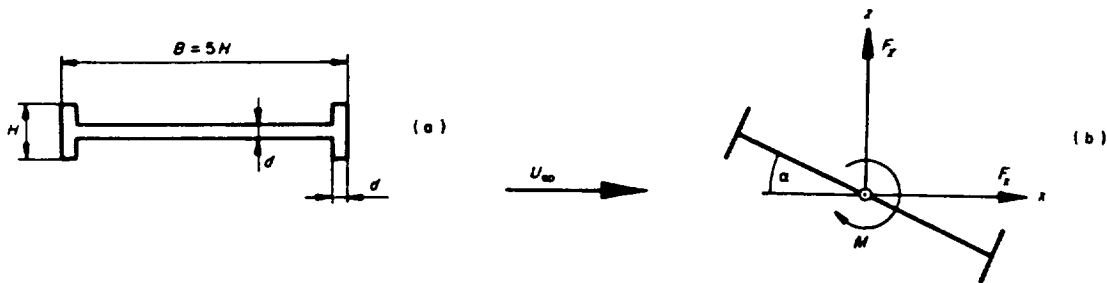


Figure 3-47. (a) Dimension of the H-shaped section; (b) definition of the coordinate system (F_x : drag; F_z : lift; M : moment).

The technical data from the wind tunnel test are as follows:

| | |
|---------------------------------|---------------------------------|
| Maximum flow speed | $u_\infty = 38$ m/s |
| Size of the square test section | 0.6×0.6 m ² |
| Pressure range | $1 < p < 100$ bar |
| Reynolds number range | $10^4 < Re < 10^7$ |
| Contraction ratio | $\kappa = 5.6$ |
| Electrical power | $N = 470$ kW |

²Shewe, G., "Nonlinear Flow-Induced Resonances of an H-Shaped Section," J. of Fluids and Structure, 3, 327-348, 1989.

OTHER BLUFF BODIES

The Reynolds number is based on a length of 0.06 m which is one-tenth of the side of the test section. The turbulence intensity of the freestream increases slightly with increasing Reynolds number but is less than 0.4%.

Impinging Shear Layer Instability

Schewe³ substantiated the impinging shear layer instability by introducing the force measurements in the flow around a square section at a -10° angle-of-attack as shown in Figure 3-48. The power spectra of the lift and drag fluctuations reveal the existence of the sub- and superharmonics including peaks at $1/2$ and $3/2$ times the vortex shedding frequency.

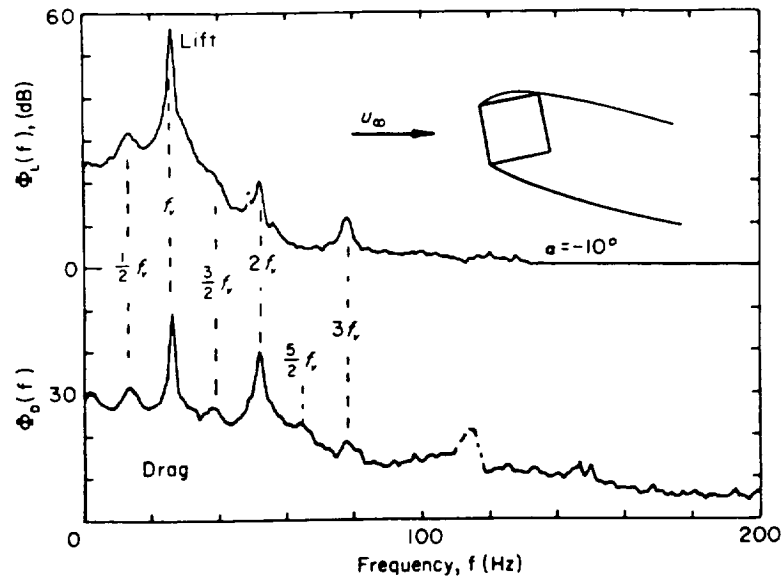


Figure 3-48. Example for the occurrence of sub- and super-harmonics in the flow around a square cylinder at angle of incidence $\alpha = -10^\circ$

Reference Test Results - Strouhal Number and Force Coefficients

Nakamura and Nakashima⁴ measured the Strouhal number of both frequency modes for wide range of width-to-height ratios ($2 < B/H < 8$). They found that for the high-frequency mode, the Strouhal number based on width B ($S_B = f B/u_\infty$) is nearly a constant with a value of 0.6 approximately. For small values of B/H there are two frequency modes, and after a transition at about $B/H = 4$, the two modes collapse to one frequency. In other words, for $B/H > 4$ including the Tacoma profile, both the Karman vortex shedding mechanism and the vortical motion in the shear layers are probably synchronized and oscillate with the same frequency. Consequently, these coupled fluid oscillators produce many secondary peaks in addition to the fundamental frequency.

Shewe (1989) measured the Strouhal number S for the H-shaped section ($B/H = 5$), which is a weak function of Reynolds number. That is, $S = 0.113$ at $Re = 2 \times 10^5$ and $S = 0.11$ at $Re = 2 \times 10^6$. There is a 3% decrease in a ten-fold increase of Reynolds number. Here the Strouhal number is based on height. Likewise, the lift and drag coefficients are also weak functions of Reynolds number. Therefore, as an approximation one may consider that they are mainly functions of angle-of-attack. The Strouhal number based on width would be from 0.565 to 0.55

³Schewe, G., "Die auf Stumpfe Profile bei Grotsen Reynolds-Zahlen Wirken," DFVLR-Mitt. 84-19, Untersuchung der Aerodynamischen Kräfte, Göttingen, 1984.

⁴Nakamura, J. and Nakashima, M., "Vortex Excitation of Prisms with Elongated Rectangular, H and T Cross-Sections," J. of Fluid Mechanics, **163**, 149-169, 1986.

OTHER BLUFF BODIES

which agrees to the finding of Nakamura and Nakashima (1986). The steady moment, lift and drag coefficients as functions of angle-of-attack are given in the reference Figure 3-49 for $Re = 8 \times 10^5$. For numerical purpose of galloping analysis, the curve-fits are provided herein, where α is the angle of attack (AOA):

$$\begin{aligned} C_M &= 1.0048e-4 - 8.5408e-3 \alpha + 2.1425e-3 \alpha^2 + 4.8097e-4 \alpha^3 + 2.2083e-5 \alpha^4 & \text{if } \alpha < 0 \\ &= -1.0048e-4 - 8.5408e-3 \alpha - 2.1425e-3 \alpha^2 + 4.8097e-4 \alpha^3 - 2.2083e-5 \alpha^4 & \text{if } \alpha \geq 0 \\ C_L &= -1.0166e-3 + 0.14795 \alpha + 1.4603e-2 \alpha^2 - 1.8611e-4 \alpha^3 - 6.5505e-5 \alpha^4 & \text{if } \alpha < 0 \\ &= 1.0166e-3 + 0.14795 \alpha - 1.4603e-2 \alpha^2 - 1.8611e-4 \alpha^3 + 6.5505e-5 \alpha^4 & \text{if } \alpha \geq 0 \end{aligned}$$

$$C_D = 1.2395 - 1.3475e-2 |\alpha| + 9.9891e-3 \alpha^2 + 3.4838e-4 |\alpha|^3$$

where α in degrees. The drag coefficient is $C_D = 1.24$ at $\alpha = 0^\circ$ and increases up to 2.0 at $\alpha = 10^\circ$. The lift and moment coefficients are highly nonlinear. The slope of the lift curve is positive with a value of $\frac{\partial C_L}{\partial \alpha} \big|_{\alpha=0} = 6.9 \text{ rad}^{-1}$ indicating that the H-section is aerodynamically stable in

bending. However, the negative value $\frac{\partial C_M}{\partial \alpha} \big|_{\alpha=0} = -0.77 \text{ rad}^{-1}$ indicates that the H-section is galloping unstable in torsion.

In fact, there are two basic mechanisms which can lead to flow-induced vibration of a bluff body. The first is a vortex resonance excitation which occurs when the dominant frequency of vortex shedding coincides with a natural frequency of the structure. The second mechanism is that of the galloping instability which appears as a self-excited oscillation in a natural mode of the structure above a certain critical flow speed.

Lock-in Phenomena

The vortex shedding frequency was recorded by Schewe (1989) with varying wind-tunnel flow speed as shown in the reference Figure 3-50. The vortex shedding frequency is normalized by the first bending mode frequency of 103 Hz. In general the vortex shedding frequency is proportional to the flow velocity and leads to a Strouhal number of $S = f_v H/U = 0.115$. The figure also includes the aeroelastic response of the lift coefficient which is the rms values of the lift fluctuations based on width B . The lift coefficient at resonance is substantially greater than the "stationary" structure values as shown in the reference Figure 3-49 (b). This is because at resonance the structure vibrations induce elastic and inertia forces in addition to the aerodynamic loadings.

In addition to the fundamental resonance when the vortex shedding frequency locks in with the first bending mode of the structure, there are several superharmonic resonances at $u_\infty/u_{cB} = 0.5, 0.3$, etc. Where u_{cB} is the critical velocity at which the vortex shedding frequency is equal to the first bending mode frequency. This is due to the impinging shear layer phenomenon associated with the H-shaped section. The lock-in at the first bending mode is significant in that the vortex shedding frequency synchronizes with the first bending frequency in a range of flow velocities in the vicinity of u_{cB} ($= 9.8 \text{ m/s}$) and shows a plateau.

Torsional Vibration and Galloping

Figure 3-51 (a) shows the response curve of torsional resonances. The normalized rms values of the fluctuating moment were taken with the corresponding rms lift. The estimated critical flow speed for the first torsional mode is $u_{cT} = 40 \text{ m/s}$ which is higher than the maximum flow speed of the wind tunnel. In the testing range, several superharmonic resonances in torsion were found as shown in the figure. Among them the second (or 1/2) order superharmonic resonance happens at a flow velocity of $\sim 25 \text{ m/s}$.

OTHER BLUFF BODIES

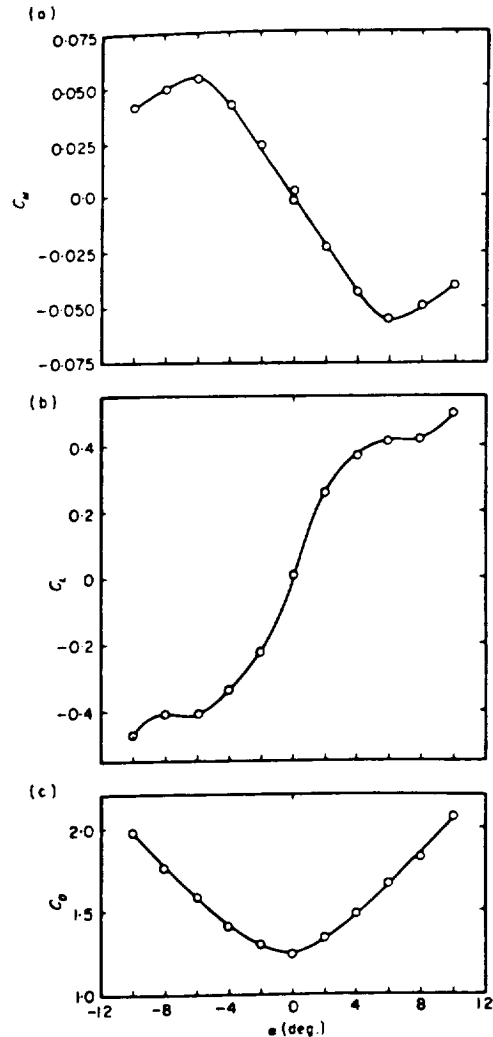


Figure 3-49. Steady moment and force coefficients depending on the angle of incidence ($Re = 8.1 \times 10^5$).

A value of 0.23 Hz was estimated for the frequency of the torsional oscillation which ultimately led to the collapse of the original Tacoma bridge. With this frequency the main resonance in torsion would occur at a critical flow speed of $u_c T = 5.2$ m/s, which was approximately one-fourth of the wind speed at which the catastrophic oscillations were observed. The condition was probably fulfilled for a subharmonic resonance of the one-fourth order. Due to the galloping instability of the H-section, it is believed that the torsional vibration caused the destructive oscillations of the old Tacoma bridge.

Strouhal Number for Several Bluff Bodies

Blevins (1986 and 1990) compiled Strouhal number data for several bluff body shapes in Figure 3-52. The length scale used in the Strouhal number is defined as the maximum width of the section normal to the freestream. In the table there are five Strouhal number data associated with H-sections. They are in the same range of the square section Strouhal numbers. Two of them have values of 0.12 which are comparable to those reported by Schewe (1989) and Nakamura and Nakashima (1986). When the angle-of-attack is 90° instead of 0° , the Strouhal number falls in the range of 0.137 to 0.145 as shown in the table. In the figure, Strouhal number versus Reynolds number for ten bluff body shapes are given. These shapes include a sharp-

OTHER BLUFF BODIES

edge plate, a tapered plate, a tail-flattened and a head-flattened circular cylinders, a round-edged plate, a forward and a backward triangular sections, a square section, a wavy wall and a sphere. The tail-flattened circular cylinder and the round-edged plate have Strouhal numbers close to that of a circular cylinder. The forward triangular section has a higher Strouhal number (~0.17) than that (~0.14) of the backward triangular section. Apparently, it is because the backward triangular section is bluffer to the flow than the forward one.

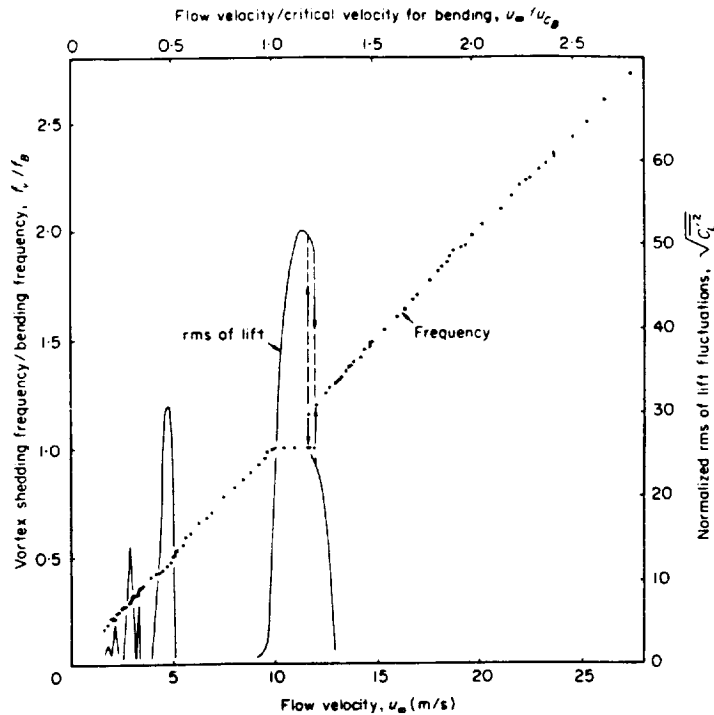


Figure 3-50. Measured vortex shedding frequency f_v (points) versus flow velocity

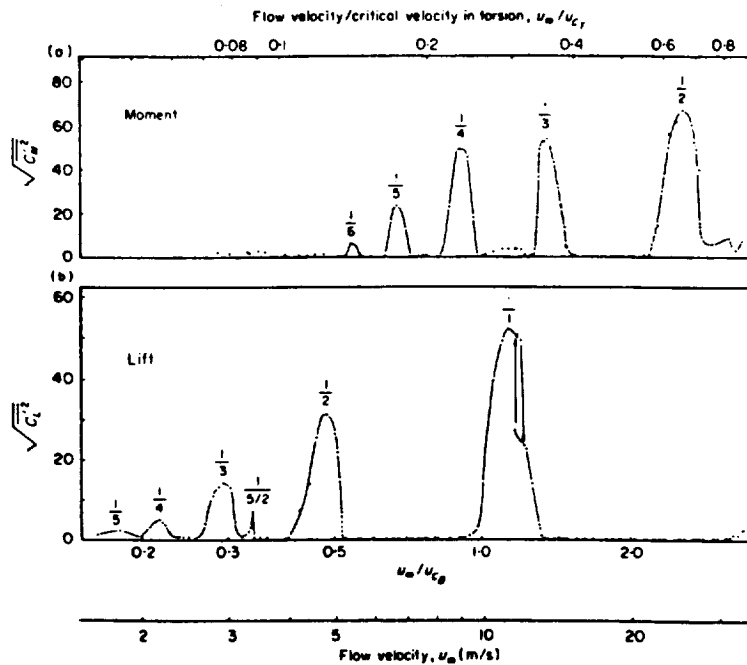


Figure 3-51. Moment (a) and lift (b) coefficients responses (The quotients n/m denote the order of the resonance)

OTHER BLUFF BODIES

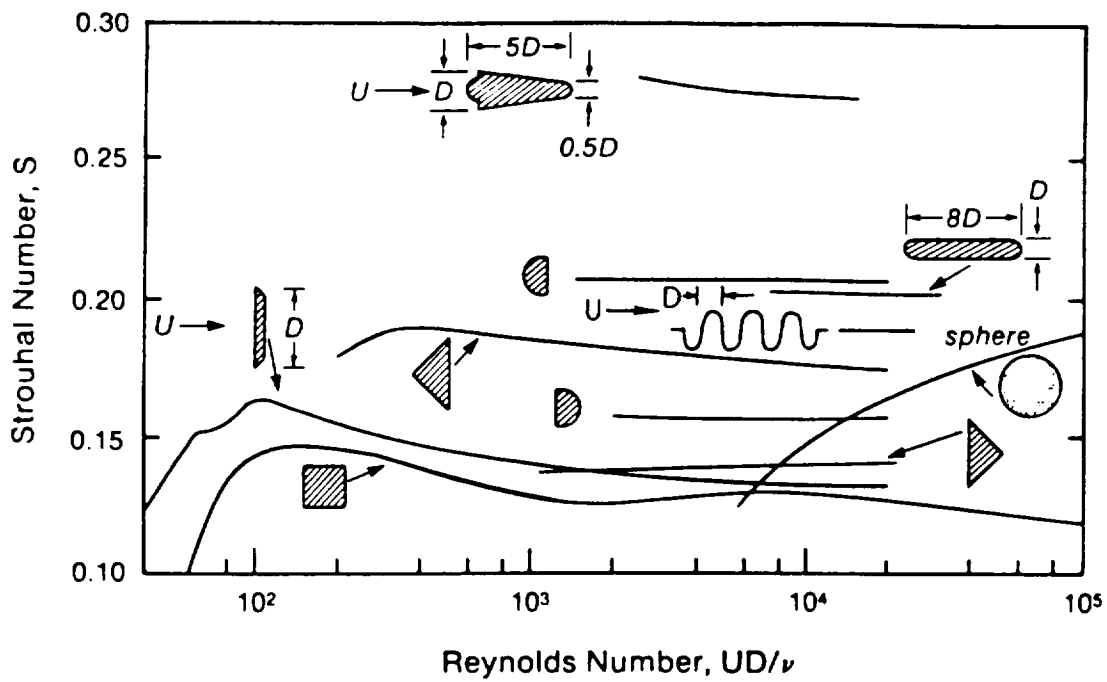


Figure 3-52. Strouhal Numbers for Noncircular Sections (Flow is Left to Right)
 [Roshko, 1954; Wardlaw, 1966; Mujumdar and Douglas, 1973; Vickery, 1966; Gerlach, 1972;
 Toebes and Eagleson, 1961; Okajima, 1982; Archenbach and Heinecke, 1981]

GEOMETRIC ANALYSIS

External Flow/Structural Elements (Streamlined Bodies)

PRECEDING PAGE BLANK NOT FILMED

PAGE 3.4.8 INTENTIONALLY BLANK

Airfoils and Turbomachinery Blades

3.5 Airfoils and Turbomachinery Blades

In comparison to bluff bodies, streamlined structural elements experience less flow-induced vibrations. However, flow induced vibrations often occur under off-design conditions. In the case of airfoil, it may develop unacceptable vibrations in the following cases: a) when the flow field is highly irregular or rotational, b) when the flow angle-of-attack is large enough for substantial flow separation or stall, or c) when icing takes place that the shape becomes blunt and bluff. On icing, Nark (1983) addressed the degraded lift and increased drag. Guffond et al (1989) included the blunt leading edges due to icing for several air velocities.

Airfoils

Brown and Stewartson (Brown, S. N. and Stewartson, K., "Trailing-Edge Stall," J. Fluid Mech. vol. 42, part 3, pp. 561-584, 1970) studied the trailing edge stall of an airfoil. The condition for separation was found to be

$$\alpha^* \sim \left(\frac{C}{Re}\right)^{\frac{1}{16}} \text{ for incompressible flow}$$

$$\alpha^* \sim \left(\frac{C}{Re}\right)^{\frac{1}{16}} \left(\frac{T_w}{T_\infty}\right)^{-\frac{3}{4}} (1 - M_\infty^2)^{\frac{7}{16}} \text{ for subsonic compressible flow}$$

$$\alpha^* \sim \left(\frac{C(M_\infty^2 - 1)}{Re}\right)^{\frac{1}{4}} \text{ for supersonic compressible flow}$$

where α^* is the critical angle of incidence, Re is the Reynolds number based on the chord length of the airfoil, C is the Chapman's constant for viscosity.

$$C = \frac{\mu_w T_\infty}{\mu_\infty T_w}$$

Blake (Blake, W. K., "Excitation of Plates and Hydrofoils by Trailing Edge Flows," J. Vibration, Acoustic, Stress, and Reliability in Design, vol. 106, pp. 351-363, July 1984) investigated vortex shedding and its induced vibration of lifting surfaces on which the boundary layers are turbulent. When the boundary layer becomes turbulent on an airfoil with sharp trailing edge on which flow separation cannot occur, no tones exist. On the other hand, blunt trailing edges generate additional excitation which overshadows the excitation provided by the boundary layer. Figure 3-53 shows an example of trailing edge sound radiated from a NACA 0012 airfoil. The airfoil with a sharp trailing edge has a completely broadband sound spectrum which is associated with the broadband surface pressures. When the edge is made blunt as shown, the spectrum of sound and surface pressures were enhanced considerably over a frequency band which extended over the 2500 Hz to 4000 Hz range.

Blake (1984) analyzed a beveled airfoil. Figure 3-54 shows the cross-section at its trailing edge and the distribution of the surface pressures and the local maxima of fluctuating velocity magnitude associated with the developing vortex street. Also shown are the loci of velocity maxima which are generated at various stations in the wake. These loci denote the paths y_U and y_l , the outer boundaries of the vortex curves as illustrated. The point where the separation $y_U - y_l$ is minimum coincides with the absolute maximum in velocity intensity and is taken to denote the formation length l_f of the first vortex behind the trailing edge. The pressure generated by the vortex street decay as $x^{-1/2}$, as shown in the upper part of the figure.

Airfoils and Turbomachinery Blades

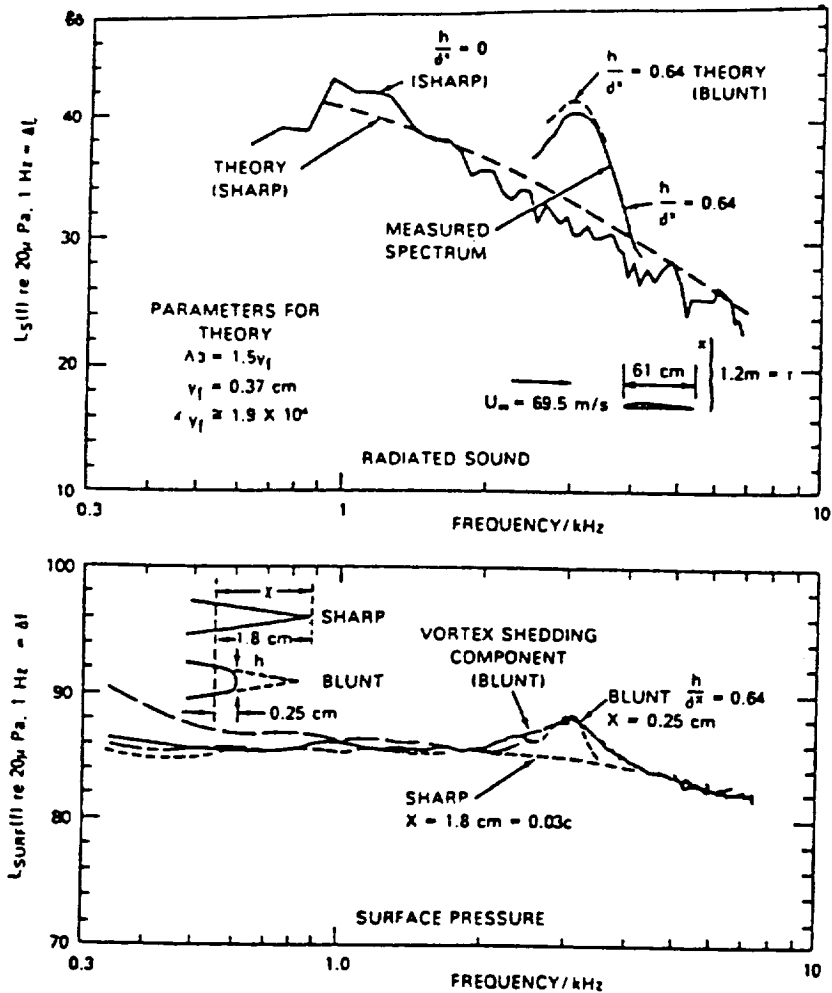


Figure 3-53. Radiated Sound and Surface Pressure for Sharp and Blunt Edges.

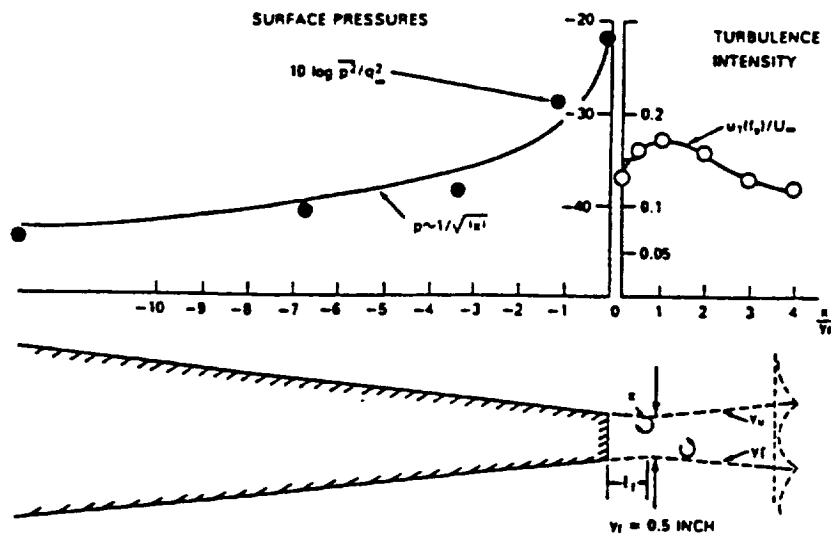


Figure 3-54. Profiles of Surface Pressure and Velocity Fluctuations at the Blunt Trailing Edge of a Tapered Airfoil. Measurements were Made at $U_\infty = 100$ ft/sec.

Airfoils and Turbomachinery Blades

Blake (1984) presented another example of increase of vibration levels with velocity and the behavior of lock-in as shown in reference Figure 3-55 for simple hydrofoils with two trailing edges. The maximum acceleration occurs at a reduced frequency, $\omega_S y_f / U_S = 1.1$ to 1.2 as shown in the figure. Apparently, the beveled trailing edge reduced the vibration level substantially.

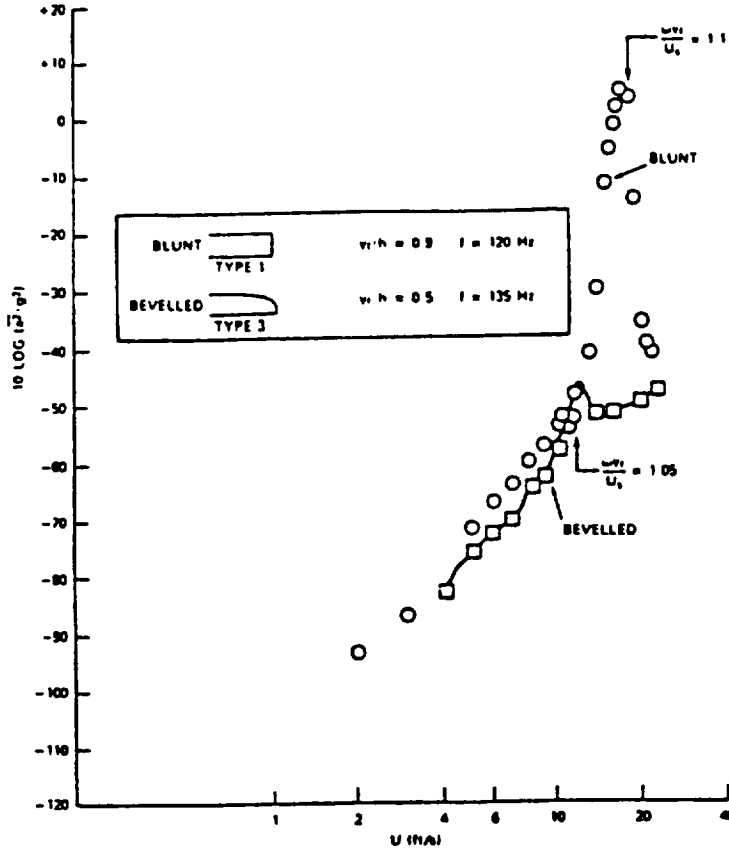


Figure 3-55. Flow-Induced Vibration of the 2,0 Mode of a Cantilever Hydrofoil with Blunt and Beveled Edges.

Turbomachinery

There are several types of flow-induced vibrations associated with turbomachines which utilize in most cases streamlined flow elements such as vanes, buckets and blades. Naudascher (Naudascher, E., *Hydrodynamic Forces*, A.A. Balkema/Rotterdam/Brookfield, 1991) presented a rather complete review in hydrodynamic forces. One of the sections discusses excitation forces in turbomachinery. Hartog (1985) addressed the 113.3 Hz penstock vibration of a hydraulic turbine, Figure 3-56 of the reference. The stream of water entering from the penstock splits into 18 partial streams due to the $n_1 = 18$ stationary guiding vanes. The water streams then flow through $n_2 = 17$ buckets of the runner into a vertical draft tube. Consequently, each partial stream is subjected to n_2 impulses during one revolution. Here the speed of rotation of the turbine, N_T , is 400/60 in revolutions per second. The frequency of the impulses is therefore

$$f_2 = N_T n_2 = 113.3 \text{ Hz}$$

As shown in the figure all the impulses are transmitted back to section AA of the penstock with the speed of sound. Two of the impulse paths are shown in the figure. Assuming that stream a experiences maximum impulse when vane 1 and bucket 1 line up, then the maximum impulse in stream b has happened $1/(17 \times 18)$ -th revolution earlier, i.e., when vane 2 and bucket

Airfoils and Turbomachinery Blades

2 line up. By coincidence, this time lead matches exactly to the longer path of transmission. Consequently, all impulses arrive at the penstock in phase with one another which add up and create a strong source of pressure pulsations. To eliminate the pulsations, the 17-bucket runner was replaced by a 16-bucket one. With the original design, the impulses due to buckets 1 and 9 arrived in section AA in phase. With the new design, the opposing buckets 1 and 9 yield out-of-phase impulses at section AA, thus canceling their contribution to the vibration source. It is noteworthy that in this case the number of runner bucket $n_2 = 16$ and the speed of turbine $N_T = 400/60$ rps are perfect matches. At off-design turbine speed, $n_2 = 16$ would no longer be optimal either.

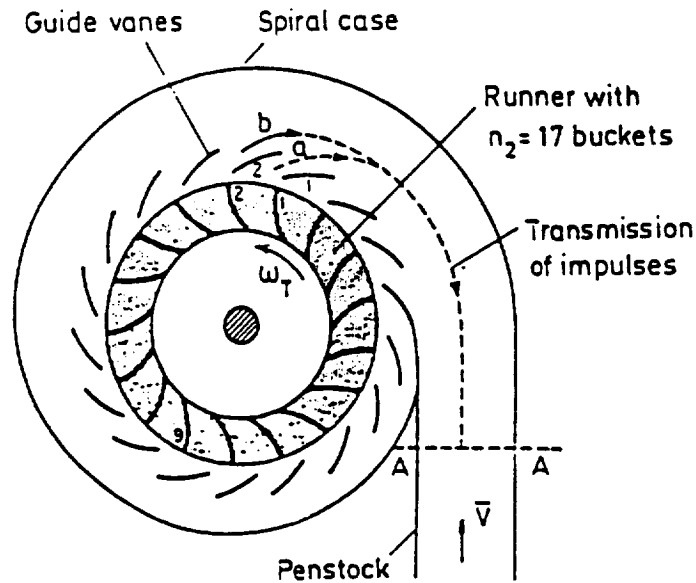


Figure 3-56. Horizontal Section of a Typical Francis Turbine (after Den Hartog, 1985)

Another source of turbine vibration is the forces on the runner blades due to the impinging wakes from the stationary vanes just ahead. The frequency of excitation is $f_1 = N_T n_1$ where n_1 is the number of stationary vanes. It is advisable to avoid resonance between f_1 and one of the natural frequencies of the runner blades and other turbine parts.

OTHER STREAMLINED BODIES

3.6 Other Streamlined Bodies

Struts and vanes are basically streamlined bodies that may be placed in the flow passages to obtain added strength for the structural assembly or guide the flow around turns or to straighten the flow ahead of or behind pumps and turbines. Struts and vanes may have elliptical shapes, may be straight or curved, or have effective camber like an airfoil. In general, they require at least two-degree-of-freedom analysis of coupled modes as does a turbine blade.

Instabilities and Onset Critical Flow Velocities of Vanes

Blevins (1990) included a detailed stability analysis example for airfoils and vanes. Formulations for critical onset flow velocities due to transverse and pitching moment vibrations were given. A FORTRAN program for a vane or turbine blade type of structure element is developed based on the reference theory and included in the handbook. The FORTRAN code is capable of calculating structural parameters for any typically given cross-sectional shapes. Flow onset velocities for plunge galloping and divergence are estimated. The inputs of the program include the geometrical shape of the vane profile and structure and fluid properties of the flow/structural system. Typical inputs are shown in Table 3-10. The data required are for vane length, chord, and aspect ratio; structural and fluid densities, Young's modulus and Poisson's ratio, bending and torsional mode frequency multipliers, and optional damping coefficients.

The corresponding outputs for the inputs of Table 3-10 are given in Table 3-11. As shown in the table, the code calculates polar area moment of inertia, torsional constant, effective mass including added mass, polar moment of inertia including added moment of inertia and relevant parameters with numerical integration over the cross-sectional area. Other parameters include effective bending and torsional spring constants, natural (circular) frequencies and four flow onset critical velocities for torsional divergence, torsional flutter, torsional galloping and plunge galloping. The bending mode plunge galloping is an instability for a damped structure when the rate of transverse force coefficient, $\partial C_Y/\partial \alpha$, is greater than zero and when the total damping becomes negative above a threshold flow velocity. For the vane shape in consideration, $\partial C_Y/\partial \alpha - \partial C_L/\partial \alpha < 0$, this bending mode galloping would not occur. The other three onset velocities which are related to torsional instabilities are greater than 76 ft/sec. The vane profile is shown in Figure 3-57. The effect of fluid density on a steel cantilevered vane is shown in Figure 3-58. The effect of fluid density on a fixed-fixed acrylic vane is shown in Figure 3-59 for torsional divergence.

Table 3-10. Inputs of the Vane Code

| | |
|--|-----------------|
| Length, in (m) | 12. (0.3048) |
| Chord, in (m) | 4. (0.1016) |
| Aspect ratio | 20 |
| ρ_s , lb/ft ³ (kg/m ³) | 482.76 (7733.) |
| ρ_f , lb/ft ³ (kg/m ³) | 75. (1201.) |
| E, psi (Pa) | 30.e6 (2.07e11) |
| Poisson ratio | 0.3 |
| Bending mode | 1st |
| Torsional mode | 1st |
| Bending structural damping | 0.02 |
| Torsional structural damping | 0.002 |
| Constraint | clamped-free |

OTHER STREAMLINED BODIES

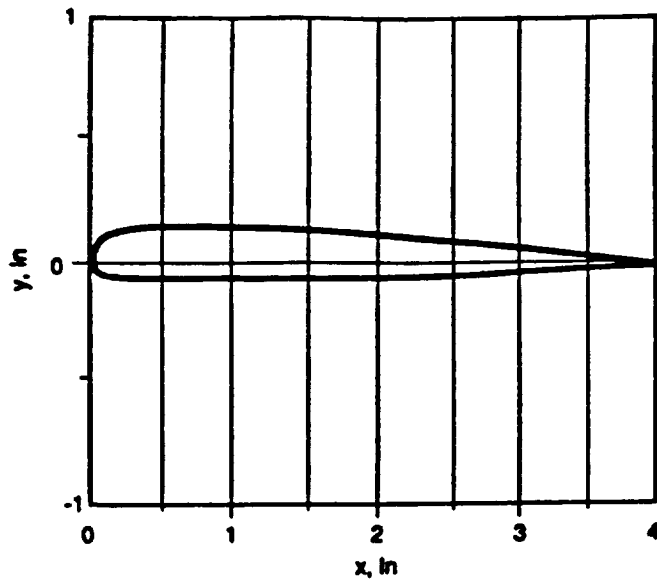


Figure 3-57. Sample Vane Profile

Table 3-11. Outputs of the Vane Code

| | |
|---|-------------------|
| I_p , ft ⁴ (m ⁴) | 2.49e-5 (2.15e-7) |
| T_c , ft ⁴ (m ⁴) | 2.57e-7 (2.22e-9) |
| m_t , slug/ft (kg/m) | 0.262 (12.5) |
| m_a , slug/ft (kg/m) | 0.203 (9.72) |
| J_t , slug-ft ² /ft (kg-m) | 1.08e-3 (4.80e-3) |
| J_a , slug-ft ² /ft (kg-m) | 7.06e-4 (3.14e-3) |
| k_y , lb/ft ² (Pa) | 1152. (55160.) |
| k_q , lb (N) | 3576. (15910.) |
| ω_y , 1/sec | 116.8 |
| ω_q , 1/sec | 1679. |
| U_d , ft/sec* (m/sec) | 97.4 (29.7) |
| U_p , ft/sec† (m/sec) | 76.8 (23.4) |
| U_{cr} , ft/sec** (m/sec) | 92.8 (28.3) |
| U_{pl} , ft/sec‡ (m/sec) | not applicable |

Note:

* Here torsional divergence is an instability when the lift-induced angular deformation and inertia exceed the torsional spring moment of the structure.

† Here the torsional plunge mode is also called flutter was dealt with by Pines (1958).

**For angle of attack up to 8° of an airfoil or vane, $\partial C_M / \partial \alpha > 0$, torsional galloping for damped structure would not occur. However, the positive value of $\partial C_M / \partial \alpha$ may induce a torsional divergence which is comparable to the lift-induced torsional divergence mentioned above.

‡ Bending mode plunge galloping is an instability for a damped structure when the rate of transverse force coefficient, $\partial C_Y / \partial \alpha$, is greater than zero and when the total damping becomes negative above a threshold flow velocity. Since $\partial C_Y / \partial \alpha \sim -\partial C_L / \partial \alpha < 0$, galloping would not occur in this case.

OTHER STREAMLINED BODIES

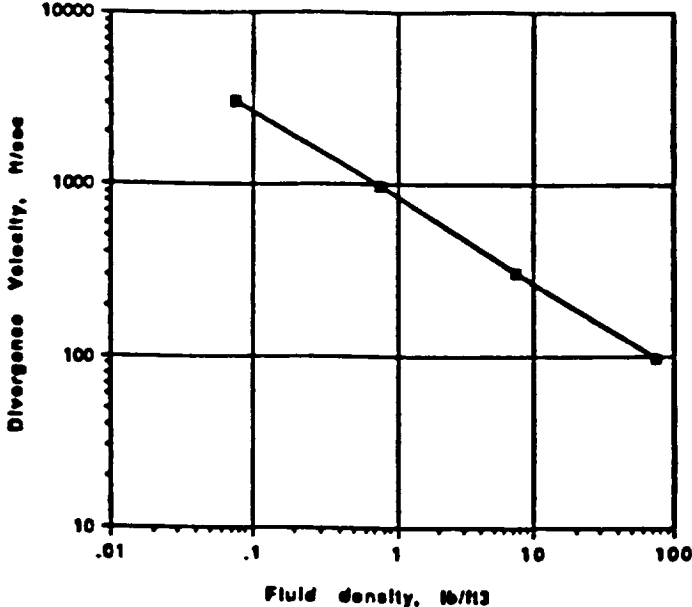


Figure 3-58. Estimated Torsional Divergence Velocity of a Cantilevered Steel Vane in a Flow Versus Fluid Density

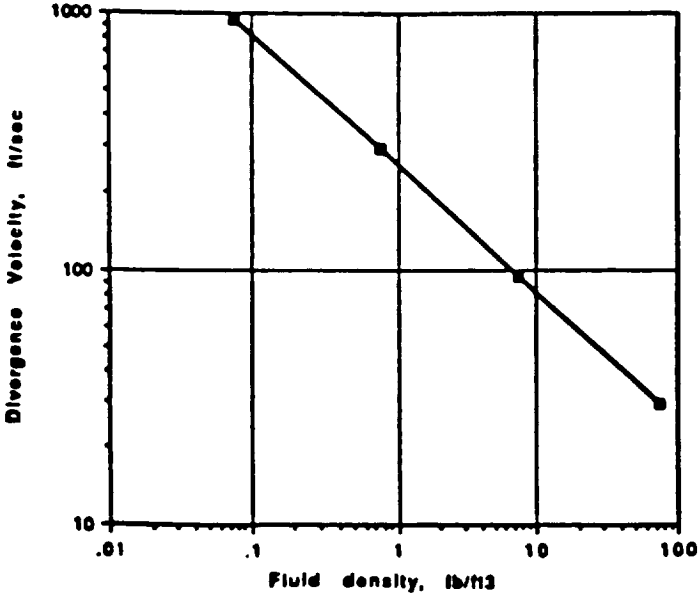


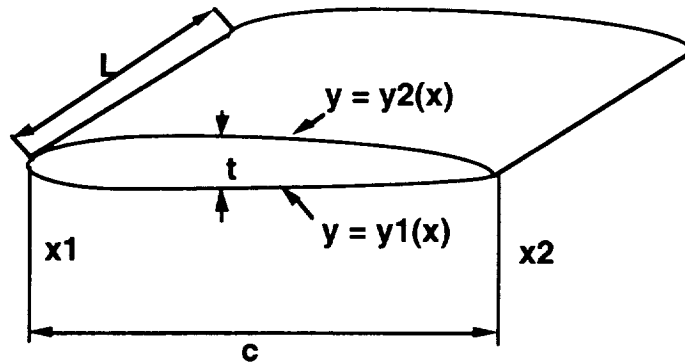
Figure 3-59. Torsional Divergence Velocity for a Fixed-Fixed Acrylic Vane in a Flow Versus Fluid Density

OTHER STREAMLINED BODIES

Vane Parameters Needed for Estimation of Onset Flow Velocities

Basic parameters needed for the estimation of the critical onset flow velocities are included in the following:

a) Structural geometric parameters include structural span length, L , chord length, $c = x_2 - x_1$ and chord thickness, t .



b) Structure material properties include Young's modulus, E , Poisson's ratio, ν , density, ρ_s , and Shear modulus, $G = \frac{E}{2(1+\nu)}$.

c) Flow properties include density, ρ_f , viscosity, μ , and flow velocity, U .

d) Additional relevant parameters include bending mode fluid added mass, $m_a = \frac{\pi}{4} \rho c^2$, area moment of inertia with respect to x - and y - axis:

$$I_x = \int_{x_1}^{x_2} \int_{y_1(x)}^{y_2(x)} y^2 dy dx, \quad I_y = \int_{x_1}^{x_2} \int_{y_1(x)}^{y_2(x)} x^2 dy dx,$$

$$\text{structure mass, } m_s = \rho_s \int_{x_1}^{x_2} \int_{y_1(x)}^{y_2(x)} dy dx = \rho_s A,$$

$$\text{effective mass, } m_e = m_s + m_a,$$

center of mass locations:

$$x_{cm} = \frac{\rho_s}{m_s} \int_{x_1}^{x_2} \int_{y_1(x)}^{y_2(x)} x dy dx, \quad y_{cm} = \frac{\rho_s}{m_s} \int_{x_1}^{x_2} \int_{y_1(x)}^{y_2(x)} y dy dx,$$

area moment of inertia with respect to center of mass:

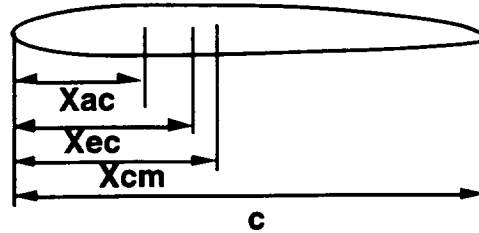
$$I_{xc} = I_x - A y_{cm}^2, \quad I_{yc} = I_y - A x_{cm}^2, \text{ and}$$

$$\text{aerodynamic force center location, } x_{ac} = \frac{c}{4}$$

Elastic center (x_{ec}, y_{ec}) is the axis where shear stress is zero and for homogeneous material, one has

OTHER STREAMLINED BODIES

$$\int_{x_1}^{x_2} \int_{y_1(x)}^{y_2(x)} \sqrt{(x - x_{ec})^2 + (y - y_{ec})^2} dy dx = 0$$



Polar moment of inertia is given: $J_s = \rho_s \int_{x_1}^{x_2} \int_{y_1(x)}^{y_2(x)} (x^2 + y^2) dy dx - m_s(x_{cm}^2 + y_{cm}^2)$.

Polar area moment of inertia, $I_p = \frac{J_s}{\rho_s}$, torsional constant, $T_c = \int_{x_1}^{x_2} (y_2(x) - y_1(x))^3 dx$,

fluid added polar moment of inertia, $J_a = \frac{\pi}{128} \rho_f c^4$, and effective polar moment of inertia,
 $J_e = J_s + J_a$

are also needed.

Continuing CFD efforts by Liu et al (1994) have produced new methods utilizing a moving grid that rotates as well as translates to deal with coupled flow/structural interactions of struts and vanes involving torsion or plunging as well as bending. Multidisciplinary interactions are utilized in these methods to iterate between the structural mass and stiffness effects, including the effects of end conditions, and the fluid flow effects. Both the transverse and the angular motions of a vane are derived from center section two-dimensional flow calculations to simulate the vane's response under negative system damping characteristics approximating lock-in.

Liu (1994) applied these methods to a case of LO₂ flow past a straight elliptical vane shape. The LO₂ flow case parameters are shown in Table 3-12. Computed flow streamlines are presented in Figure 3-60. Liu's computations show vortex shedding and exponential growth in vane oscillations as soon as the vane, initially fixed, is permitted to move. The computations indicate growth in oscillation amplitude to a maximum limit cycle value. The first few cycles of computed vane motion are detailed in Figure 3-61.

Table 3-12. Elliptical Cylinder LO₂ Flow Case Parameters

| | | |
|-------------------------|-------------------------|--------------------------|
| Strut size | 5.994 mm x 1.499 mm | 0.236" x 0.059" |
| Strut mass | 0.0881 kg/m | 0.00184 slug/ft |
| Strut moment of inertia | 1.617e-7 kg-m | 3.635e-8 slug-ft |
| Bending natural freq. | 2000. Hz | |
| Torsion natural freq. | 4000. Hz | |
| Structure damping ratio | 0.01 | |
| Total damping ratio | 0.04 | |
| Flow pressure | 22.06 MPa | 3200 psia |
| temperature | 102.8 K | 185.0 °R |
| velocity | 29.74 m/s | 97.56 ft/sec |
| density | 11301 kg/m ³ | 70.58 lb/ft ³ |
| viscosity | 1.856e-4 kg/m-s | 1.247e-5 lb/ft-s |
| Reynolds number based | | |
| on chord length | 1.086e6 | |
| Speed of sound | 914.7 m/s | 3001. ft/sec |
| Mach number | 0.03251 | |
| Specific heat ratio | 1.759 | |
| Dynamic pressure | 0.5 MPa | 72.49 psi |

OTHER STREAMLINED BODIES

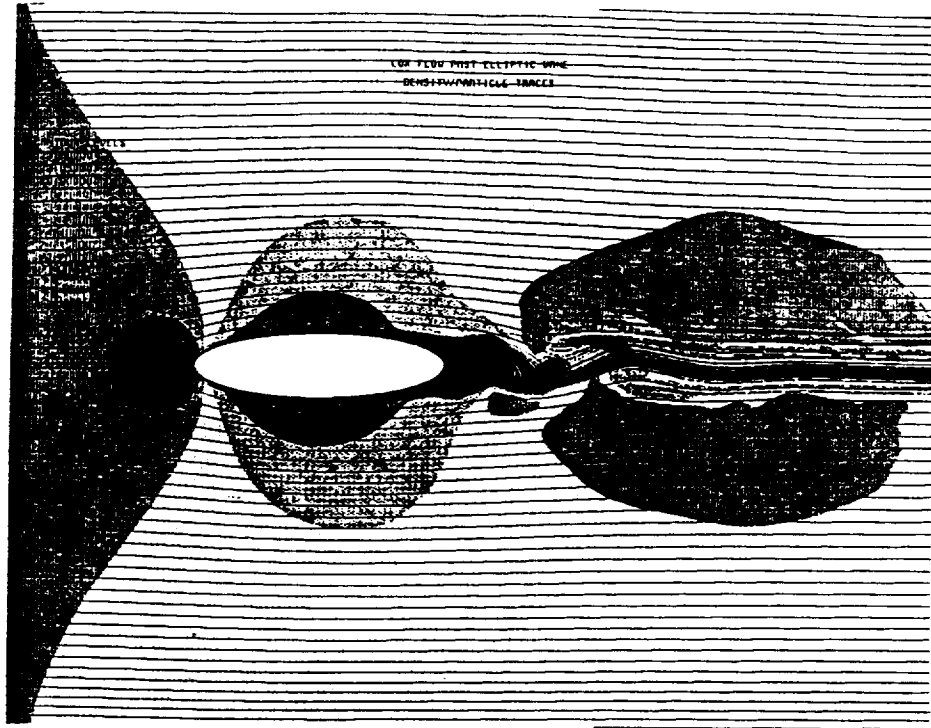


Figure 3-60. CFD Density and Particle Traces Past the Elliptic Vane

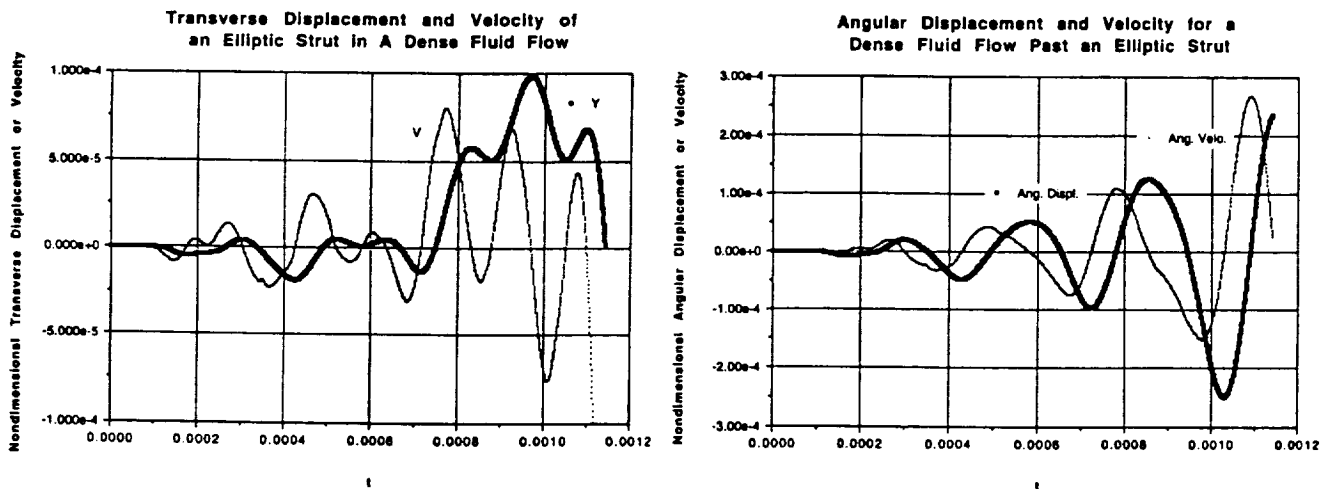


Figure 3-61. CFD Simulation of Coupled Bending and Torsional Responses of the Elliptic Vane

GEOMETRIC ANALYSIS

Internal Flow/Structural Elements

INTERNAL PIPE FLOW

3.7 Internal Flow in Pipes

Internal flow through a pipe decreases the pipe's natural frequency, with such a decrease generally associated with increasing fluid velocity. The pipe may become susceptible to resonance or fatigue failure if its natural frequency falls below certain limits. Indeed, if the fluid velocity is great enough, the pipe can become unstable. Even for pipes secured at both ends, sufficiently high, steady internal flow velocities can impose pressures on the pipe walls leading to the pipe being deflected or buckled, causing subsequent pipe rupture.

Equations of Motion

Note the span of pipe, illustrated in Figure 3-62. The pipe has a length L and an internal cross-sectional area A . Through the pipe flows a fluid of density ρ , pressure p , and constant velocity v . The internal fluid motion, promotes a transverse deflection Y of the pipe, the amount of deflection being a function of time t and location x along the pipe. The fluid is accelerated through the deflected section of the pipe because of the change in curvature and lateral vibration of the pipe. Fluid accelerations are opposed by the vertical component of fluid pressure on a given fluid element and the pressure force F per unit length applied on the element by the pipe walls. This is illustrated in Figure 3-63. A balance of forces on the element, shown in the y direction for small deformations, yields

$$F - \rho A \frac{\partial^2 Y}{\partial x^2} = \rho A \left(\frac{\partial}{\partial t} + v \frac{\partial}{\partial x} \right)^2 Y \quad (3.7.1)$$

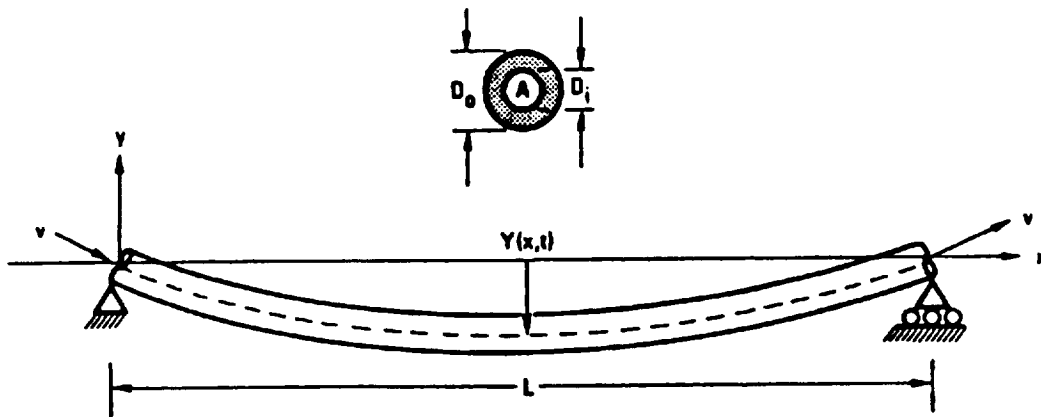


Figure 3-62. A Fluid-Conveying Pipe with Pinned Ends¹

The pressure gradient in the fluid along the pipe is opposed by the shear stress of fluid friction against the pipe internal walls. With a constant flow velocity,

$$A \frac{\partial p}{\partial x} + qS = 0 \quad (3.7.2)$$

¹ Blevins, R.D., "Flow-Induced Vibration," Kreiger Publishing Co., pp. 88-117, 1977.

INTERNAL PIPE FLOW

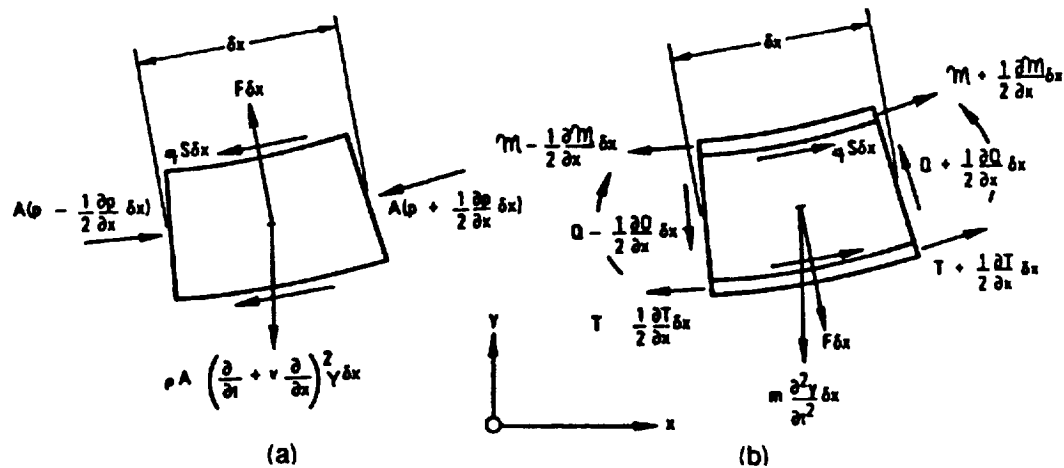


Figure 3-63. Forces and Moments Acting on Elements of (a) The Fluid and (b) The Pipe

where S is the pipe inner perimeter and q is the shear stress on the pipe internal surfaces. Using Figure 3-63, the derived equations of motion for the pipe element are

$$\frac{\partial T}{\partial x} + qS - \rho A \frac{\partial^2 Y}{\partial x^2} = 0 \quad (3.7.3)$$

and for small deformations,

$$\frac{\partial Q}{\partial x} + T \frac{\partial^2 Y}{\partial x^2} - F = m \frac{\partial^2 Y}{\partial t^2} \quad (3.7.4)$$

where Q and T are the transverse shear force and longitudinal tension in the pipe, respectively, and m is the mass per unit length of the empty pipe.

Noting that Q is related to the bending moment of the pipe M and the pipe deformation by

$$Q = \frac{-\partial M}{\partial x} = -EI \frac{\partial^3 Y}{\partial x^3} \quad (3.7.5)$$

One can therefore neglect the third term on the left-hand side of Equation 3.7.3 for small deformation analysis. Combining Equations 3.7.1, 3.7.4, and 3.7.5 yields

$$EI \frac{\partial^4 Y}{\partial x^4} + (\rho A - T) \frac{\partial^2 Y}{\partial x^2} + \rho A \left(\frac{\partial}{\partial t} + v \frac{\partial}{\partial x} \right)^2 Y + m \frac{\partial^2 Y}{\partial t^2} = 0 \quad (3.7.6)$$

where q is eliminated by combining Equations 3.7.2 and 3.7.3 to give

$$\frac{\partial(\rho A - T)}{\partial x} = 0 \quad (3.7.7)$$

The implication is that $(\rho A - T)$ is independent of position along the length of the pipe, where at $x=L$, $\rho = T=0$, leading to

INTERNAL PIPE FLOW

$$\rho A - T = 0 \quad (3.7.8)$$

for all x.

The substitution of Equation 3.7.8 into Equation 3.7.6 yields the equation of motion for free vibration of a fluid-conveying pipe, i.e.

$$EI \frac{\partial^4 Y}{\partial x^4} + \rho A v^2 \frac{\partial^2 Y}{\partial x^2} + 2\rho A v \frac{\partial^2 Y}{\partial x \partial t} + M \frac{\partial^2 Y}{\partial t^2} = 0 \quad (3.7.9)$$

where $M = m + \rho A$.

Boundary conditions associated with the pipe span fixed at both ends as shown in Figure 3-62 are

$$Y(0,t) = Y(L,t) = 0$$

$$\frac{\partial^2 Y}{\partial x^2}(0,t) = \frac{\partial^2 Y}{\partial x^2}(L,t) = 0 \quad (3.7.10)$$

and the boundary conditions for a cantilever pipe, secured at $x=0$ and free at $x=L$, are

$$Y(0,t) = \frac{\partial Y}{\partial x}(0,t) = 0$$

$$\frac{\partial^3 Y}{\partial x^3}(L,t) = \frac{\partial^2 Y}{\partial x^2}(L,t) = 0 \quad (3.7.11)$$

Pipe Fixed at Both Ends

The boundary conditions associated with the fixed-ended pipe span can be satisfied by a set of sinusoidal mode shapes

$$\psi_n(x) = \sin\left(\frac{n\pi x}{L}\right); \quad n = 1, 2, 3, \dots \quad (3.7.12)$$

The solution must contain spatially symmetric and antisymmetric terms, with the coefficients of these terms being interdependent, implying that the equation of motion can be expressed as

$$Y(x,t) = \sum_{n=1,3,5,\dots} a_n \sin\left(\frac{n\pi x}{L}\right) \sin(\omega_i t) + \sum_{n=2,4,6,\dots} a_n \sin\left(\frac{n\pi x}{L}\right) \cos(\omega_i t) \quad ; \quad i = 1, 2, 3, \dots \quad (3.7.13)$$

where ω_i is the natural frequency of the i vibration mode. Substitution into Equation 3.7.9 and term manipulation yields a set of equations that can be placed in the matrix form

$$[[K] - \omega^2 M] \{a\} = 0 \quad (3.7.14)$$

where

$$\{a\} = \begin{Bmatrix} a_1 \\ a_2 \\ \vdots \\ a_n \end{Bmatrix} \quad (3.7.15)$$

INTERNAL PIPE FLOW

and $[I]$ is the identity matrix. The stiffness matrix, $[K]$, has entries k_{rs} , where

$$k_{rs} = \begin{cases} EI r^4 \left(\frac{\pi}{L}\right)^4 - \rho A v^2 r^2 \left(\frac{\pi}{L}\right)^2 & r = s \\ \frac{8\rho A v \omega_j}{L} \left(\frac{s^2}{r^2 - s^2}\right) & r \neq s, r+s = \text{odd} \\ 0 & r \neq s, r+s = \text{even} \end{cases} \quad (3.7.16)$$

By setting the determinant of the coefficient matrix in Equation 3.7.14 equal to zero and considering only the first two natural modes in the system, one obtains

$$\left[1 - \left(\frac{v}{v_c}\right)^2 - \left(\frac{\omega_j}{\omega_N}\right)^2 \right] \left[16 - 4 \left(\frac{v}{v_c}\right)^2 - \left(\frac{\omega_j}{\omega_N}\right)^2 \right] + \frac{256}{9\pi^2} \left(\frac{v}{v_c}\right)^2 \left(\frac{\rho A}{M}\right) \left(\frac{\omega_j}{\omega_N}\right)^2 = 0 \quad (3.7.17)$$

where ω_N and v_c are the fundamental natural frequency of the pipe in the absence of fluid flow, and the critical velocity of flow for static buckling of the pipe, respectively, defined as

$$\omega_N = \frac{\pi^2}{L^2} \left(\frac{EI}{M}\right)^{0.5} \quad (3.7.18)$$

and

$$v_c = \frac{\pi}{L} \left(\frac{EI}{\rho A}\right)^{0.5} \quad (3.7.19)$$

Cantilever Pipe

The deflection of a cantilever pipe, as shown in Figure 3-64, is assumed to be of the form

$$Y(x,t) = R \left[\Psi(x/L) e^{i\omega t} \right] \quad (3.7.20)$$

where, R denotes the real part and i the imaginary part. If ω is real then,

$$e^{i\omega t} = \cos(\omega t) + i \sin(\omega t) \quad (3.7.21)$$

and, if ω is imaginary

$$e^{i\omega t} = e^{-\omega t} \quad (3.7.22)$$

Since ω has generally both constituents present, the vibrations are contained by an exponentially growing or decaying envelope.

The mode shapes of the cantilever pipe can be approximated by a series comprising of those mode shapes present in the absence of fluid flow, where

$$\Psi(x/L) = \sum_{r=1} a_r \psi_r(x/L) \quad (3.7.23)$$

where,

INTERNAL PIPE FLOW

$$\psi_r(x/L) = \cosh L\lambda_r x/L - \cos L\lambda_r x/L - \sigma_r (\sinh L\lambda_r x/L - \sin L\lambda_r x/L) \quad (3.7.24)$$

Substitution of Equation 3.7.23 into Equation 3.7.9 provides the equation of motion for the cantilever pipe, where

$$\sum_{r=1} \left[\psi_r'''' - \Omega^2 \psi_r + V^2 \psi_r'' + 2i\beta^{0.5} V \Omega \psi_r' \right] a_r = 0 \quad (3.7.25)$$

and

$$\begin{aligned} \beta &= \frac{\rho A}{M} \\ \Omega &= \omega L^2 \left(\frac{M}{EI} \right)^{0.5} \\ V &= v L \left(\frac{\rho A}{EI} \right)^{0.5} \\ M &= \rho A + m \end{aligned} \quad (3.7.26)$$

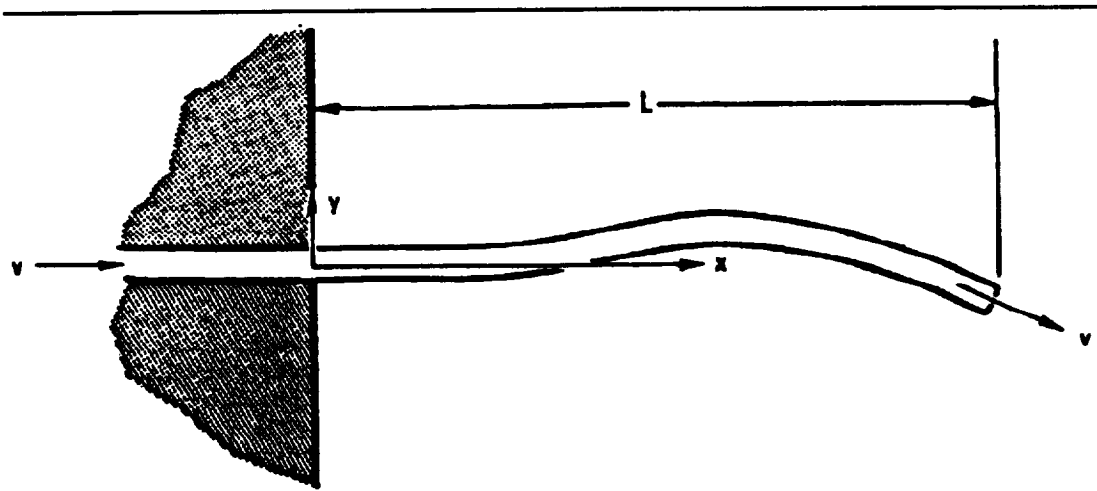


Figure 3-64. Schematic diagram of a cantilevered beam²

The derivatives of Y are with respect to x/L . This set of equations determines the natural frequencies and mode shapes of the pipe. Expressing the derivatives of the mode shapes as series in terms of the cantilever modes yields

$$\begin{aligned} \psi_r' &= \sum_{s=1} b_{rs} \psi_s \\ \psi_r'' &= \sum_{s=1} c_{rs} \psi_s \end{aligned} \quad (3.7.27)$$

$$\psi_r'''' = \lambda_r^4 \psi_r$$

where

² Blevins, R.D., op. cit.(1).

INTERNAL PIPE FLOW

$$b_{rs} = \frac{4}{\left(\frac{\lambda_s}{\lambda_r}\right)^2 + (-1)^{r+s}}$$

$$c_{rs} = \begin{cases} \frac{4(\lambda_r \sigma_r - \lambda_s \sigma_s)}{(-1)^{r+s} \left(\frac{\lambda_s}{\lambda_r}\right)^2} & r \neq s \\ \lambda_r \sigma_r (2 - \lambda_r \sigma_r) & r = s \end{cases} \quad (3.7.28)$$

and substitution into Equation 3.7.25 yields

$$\sum_{r=1}^n \left[(\lambda_r^4 - \Omega^2) \psi_r + V^2 \sum_{s=1}^n c_{rs} \psi_s + 2i\beta^{0.5} V \Omega \sum_{s=1}^n b_{rs} \psi_s \right] a_r = 0 \quad (3.7.29)$$

Multiplying through by y_s , integrating over the pipe span, and introducing the condition of orthogonality, yields in matrix form,

$$[[K] - \Omega^2 [I]] \{a\} = 0 \quad (3.7.30)$$

where the entries of the stiffness matrix [K] are

$$k_{rs} = \begin{cases} \lambda_r^4 + V^2 c_{rs} + 2\beta^{0.5} V \Omega b_{rs} ; & r = s \\ V^2 c_{rs} + 2\beta^{0.5} V \Omega b_{rs} ; & r \neq s \end{cases} \quad (3.7.31)$$

and nontrivial solutions exist only if the determinant of the coefficient matrix is zero, i.e.

$$| [K] - \Omega^2 [I] | = 0 \quad (3.7.32)$$

The dimensionless frequency ω can have real and imaginary parts,

$$\Omega = \Omega_R + i\Omega_I \quad (3.7.33)$$

and generally, the vibrations of the cantilever pipe are either amplified or reduced with time, depending on the sign of ω_I (a negative value promotes decay, a positive value promotes growth).

Curved Pipes

Vibration in curved pipes can take place in either symmetric or asymmetric modes, in the plane of the curved pipe or outside of the plane of curvature. The analysis of curved pipes is considerably more complicated than that of straight pipes due to the geometric coupling introduced by the pipe curvature. It is possible, however, to determine the appropriate equations of motion using variational calculus and applying matrix techniques to solve the linearized equations for the onset of instability.

INTERNAL PIPE FLOW

Pipe Whip

Consider the rupture of a pipe in a high pressure fluid system, with the contents spewing into surroundings. The potential impulsive reaction on the curved pipe can cause the pipe to violently whip about. This is the phenomenon of pipe whip.

The following analysis assumes:

- 1) the fluid forces primarily act normal to the pipe axis,
- 2) the pipe is uniform and possesses orthogonal modes, and
- 3) the deformations remain small, so that pipe response is linear.

Consider the fluid momentum equation, using the control volume in Figure 3-65,

$$\vec{F} = - \int_{S'} p \hat{n} ds - \frac{d}{dt} \int_V \rho \vec{\vartheta} d\vartheta - \int_{S'} \rho \vec{\vartheta} (\vec{\vartheta} \cdot \hat{n}) ds \quad (3.7.34)$$

where F is the vector fluid reaction force on the pipe, n is the outward normal unit vector from the control surface S , V is the enclosed volume, S' is the portion of S in contact with the fluid, p is the pressure of the fluid, and ϑ is the vector fluid velocity relative to S . Upon control volume depressurization to the atmosphere, Equation 3.7.34 reduces to

$$F_y = \rho A \left[v - \frac{\partial Y(l,t)}{\partial t} \right]^2 \quad (3.7.35)$$

where v is the fluid velocity component which is normal to the undeformed pipe axis and relative to the pipe which is bending away from the fluid jet at velocity $Y(l,t)/t$ at the point of rupture $x=l$, and A is the inner cross-sectional area of the pipe. Generally, the velocity of the fluid jet substantially exceeds the velocity of the pipe response, allowing the approximation

$$F_y = \rho A v^2 \quad (3.7.36)$$

Therefore, the equation of motion, Equation 3.7.9, for a uniform pipe responding to the instantaneous creation of a jet at $x=l$ is

$$EI \frac{\partial^4 Y(x,t)}{\partial x^4} + M \frac{\partial^2 Y(x,t)}{\partial t^2} = \begin{cases} 0 & t < 0 \text{ or } x \neq l \\ \rho A v^2 & x = l \text{ and } t \geq 0 \end{cases} \quad (3.7.37)$$

where the second and third terms of Equation 3.7.9 can be neglected.

Using modal expansion techniques, a solution

$$Y(x,t) = \sum_{j=1}^N y_j(t) \psi_j(x) \quad (3.7.38)$$

is assumed, where $Y_j(x)$ are mode shapes associated with the free vibrations of the pipe. With the mode shapes conforming with the geometric boundary conditions of the pipe, and assumed to be orthogonal over the pipe span, i.e.

INTERNAL PIPE FLOW

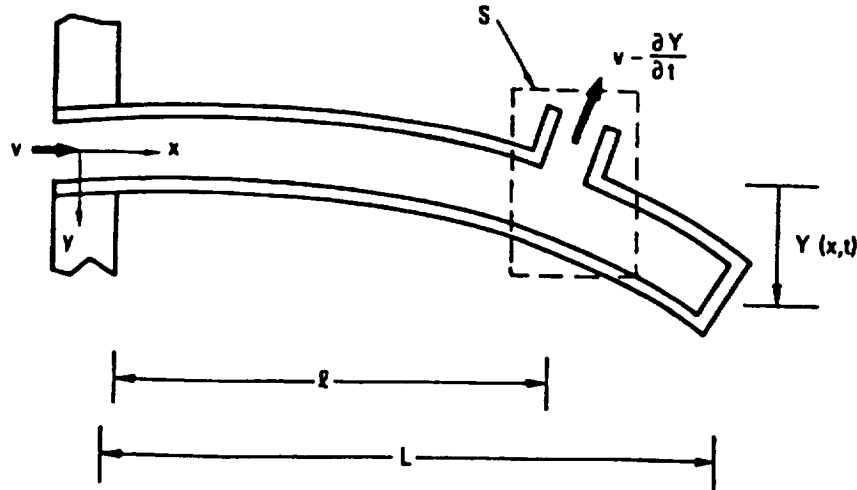


Figure 3-65. A Ruptured Cantilevered Pipe³

$$\int_0^L \psi_j(x/L) \psi_k(x/L) d(x/L) = 0, \quad \text{if } j \neq k \quad (3.7.39)$$

then Equation 3.7.38 can be substituted into Equation 3.7.37, and multiplying through by $\psi_k(x)$ (k being an arbitrary integer), yields a series of linear ordinary differential equations

$$\ddot{y}_j(t) + \omega_j^2 y_j(t) = \begin{cases} 0 & t < 0 \\ \frac{\rho A v^2 \psi_j(l)}{M L \int_0^L \psi_j^2(x/L) d(x/L)} & t \geq 0, \quad j = 1, 2, 3, \dots, N \end{cases} \quad (3.7.40)$$

These equations describe the response of the individual nodes, where ω_j is the natural frequency of vibration (rad/sec) associated with the free vibrations of the pipe in the j mode. If the pipe is motionless at the instant of rupture, the initial conditions are

$$y_j(0) = \dot{y}_j(0) = 0 \quad j = 1, 2, 3, \dots, N \quad (3.7.41)$$

Duhamel's integral provides a transient solution to Equation 3.7.40 and the initial conditions of Equation 3.7.41. The result is

$$y_j(t) = \left(\frac{\rho A v^2}{\omega_j^2 M L \int_0^L \psi_j^2(x/L) d(x/L)} \right) (1 - \cos(\omega_j t)) \quad j = 1, 2, 3, \dots, N \quad (3.7.42)$$

This solution oscillates about the steady displacement which would be obtained if the fluid force was statically applied and the dynamic response was neglected. The cycles persist with time because damping has been neglected. The amplitude of the modal responses, $y_j(t)$, are inversely proportional to the square of the modal natural frequencies ω_j . Since the modal natural

³ Blevins, R.D., op. cit.(1).

INTERNAL PIPE FLOW

frequencies increase with mode number, the response is generally dominated by the first few modes.

Structural damping can be incorporated in the analysis by adding the damping term, $2\zeta_j\omega_j y_j(t)$, where ζ_j is the damping factor of the j mode, to the left-hand side of Equation 3.7.40. The transient solution then becomes,

$$y_j(t) = \left(\frac{\rho A v^2}{\omega_j^2 M L \int_0^L \psi_j^2(x/L) dx} \right) \left(1 - \frac{e^{-\zeta_j \omega_j t}}{\sqrt{1-\zeta_j^2}} \cos(\sqrt{1-\zeta_j^2} \omega_j t - \phi) \right) \quad j = 1, 2, 3, \dots, N \quad (3.7.43)$$

where $\tan \phi = \zeta_j / (1 - \zeta_j^2)^{1/2}$. Solutions are shown in Figure 3-66.

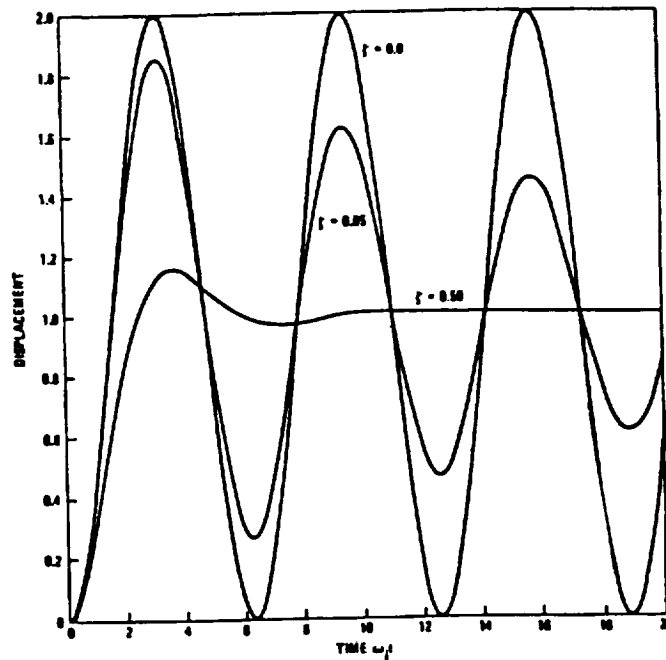


Figure 3-66. Displacement as a Function of Time and Damping⁴

The fluid velocity through a pipe rupture varies with time. The fluid is at operational velocity at the moment of rupture. Afterwards, the fluid responds to the pressure difference by quickly accelerating to a maximum velocity. Finally, the velocity gradually decays as the system blows down and the system pressure is relieved.

If the fluid velocity is approximately exponential in time, then

$$v = \begin{cases} 0 & t < 0 \\ v_0 e^{-Kt} & t \geq 0 \end{cases} \quad (3.7.44)$$

and, using Duhamel's integral, closed-form solutions can be found for the undamped response of the ruptured pipe. Substitution of Equation 3.7.44 into Equation 3.7.40 yields the solution,

⁴ Blevins, R.D., op. cit.(1).

INTERNAL PIPE FLOW

$$y_j(t) = \left(\frac{\rho A v_0^2}{ML\omega_j} \right) \left(\frac{\psi_j(\eta)}{4K^2 + \omega_j^2} \right) \left(\frac{1}{\int_0^L \psi_j^2(x/L) d(x/L)} \right) (\sin(\omega_j t) [2K(1 - e^{-2Kt} \cos(\omega_j t)) + \omega_j e^{-2Kt} \sin(\omega_j t)] - \cos(\omega_j t) [\omega_j(1 - e^{-2Kt} \cos(\omega_j t)) - 2K e^{-2Kt} \sin(\omega_j t)]) \quad (3.7.45)$$

With bending in the pipe, a moment is induced of

$$M = EI \frac{\partial^2 Y}{\partial x^2}(x,t) = EI \sum_{j=1}^N y_j(t) \frac{\partial^2 \psi_j(x)}{\partial x^2} \quad (3.7.46)$$

In many cases, the bending pipe exceeds the maximum moment which can be elastically borne by the pipe. The pipe yields plastically. The dynamic analysis of yielded pipes can be made by either using models of rigid pipe segments connected by plastic hinges, or using a finite element, elastic-plastic pipe model.

FITTINGS AND BENDS

3.8 Fittings and Bends

Disconnects, couplings, fittings, fixed joints, and seals are used in liquid-propellant rocket propulsion systems to contain and control the flow of the liquid propellants. NASA SP-8119 ("Liquid Rocket Discounts, Couplings, Fittings, Fixed Joints, and Seals," NASA Space Vehicle Design Criteria, Chemical Propulsion, NASA SP-8119, September 1976) is a monograph which treats the design of these components for use in booster and other space propulsion systems. Particular emphasis is placed on the high pressure (up to 10,000 psia), extreme temperatures (-423° to 2300° F), and considerable vibration levels. Some welding problems and corrective measures were discussed in the reference report and reviewed herein.

Fittings

Fixed joints are nonseparable connections of fluid system components. Since it is impractical to make line assemblies in one piece and the insertion of components such as valves and filters is required, fixed joints are necessary design elements. Welding is one of the common methods for joining tubular components in a propellant system. The types of welded joints currently being used are illustrated in Figure 3-67. Butt-welded joints were used on large lines (> 1 inch) on the Saturn V F-1 engine. The combination fillet/sleeve weld Figure 3-67 (d) was used for line sizes of 1-in diameter or less. The welding methods include inert-gas tungsten-arc, inert-gas metal arc, and electron-beam welding.

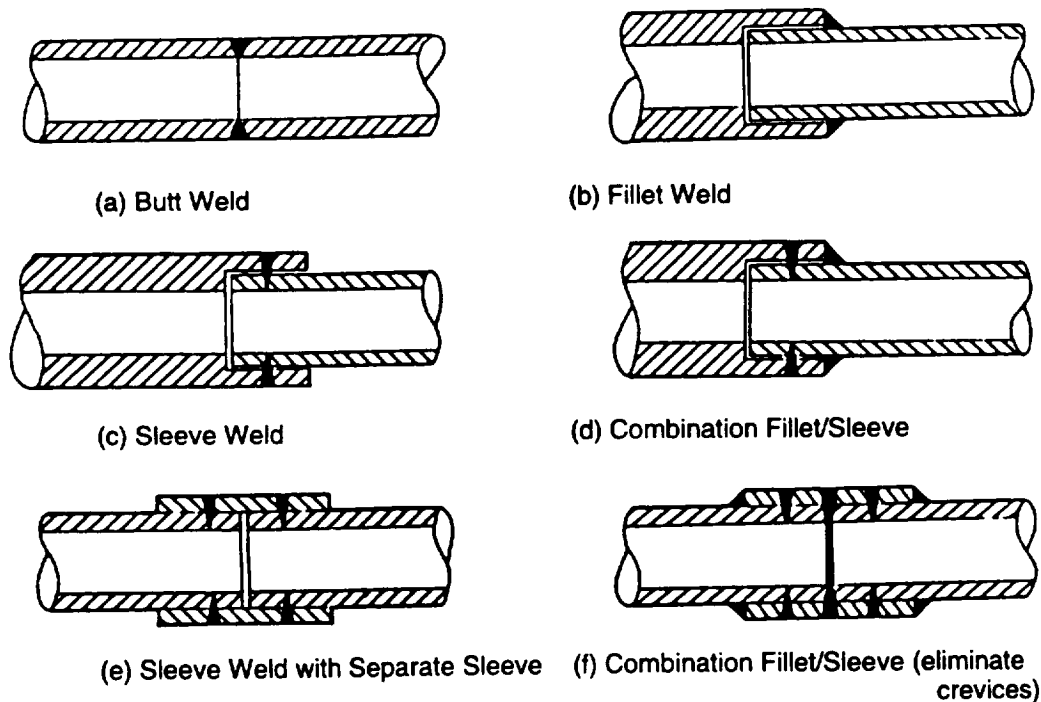


Figure 3-67. Types of Welded Joints Used in Fluid Systems

In-service failure with the F-1 tube sleeve-weld configuration developed in the form of fatigue cracks in the heat-affected zone of the weld. Cause was considered to be the high vibration environment. Fatigue failure has also been attributed to partial-penetration welds. Addition of fillet weld to the joint for increased fatigue strength and vibration damping clamps on the tubing to reduce amplitudes resolved this problem. While the use of good welding techniques in joining pipe sections makes for good joints without flow perturbations, abrupt flow contractions or expansions as in Figures 3-68 and 3-69 can cause flow separation and introduce pressure loss and flow unsteadiness. Loss coefficients are available in the standard pipe design references for abrupt contractions and expansions.

FITTINGS AND BENDS

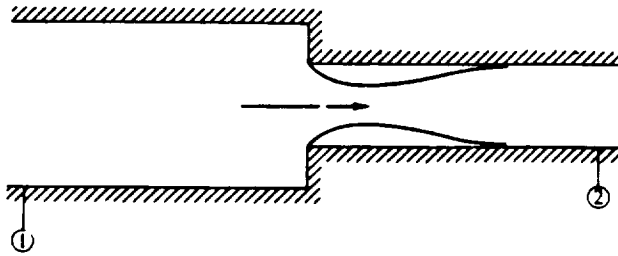


Figure 3-68. Abrupt Contraction

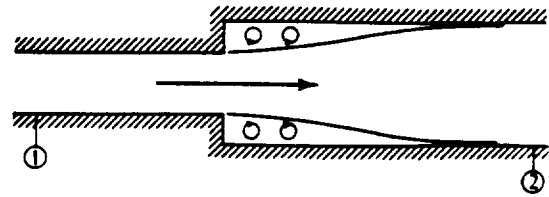


Figure 3-69. Abrupt Expansion

Bends

Frictional flow effects become important in pipe bends or elbows causing frictional pressure loss and adding turbulence to the overall flow. The scale of the turbulence is illustrated in the counter-rotating eddies indicated in Figure 3-70 and introduces high frequency oscillations to the flow.

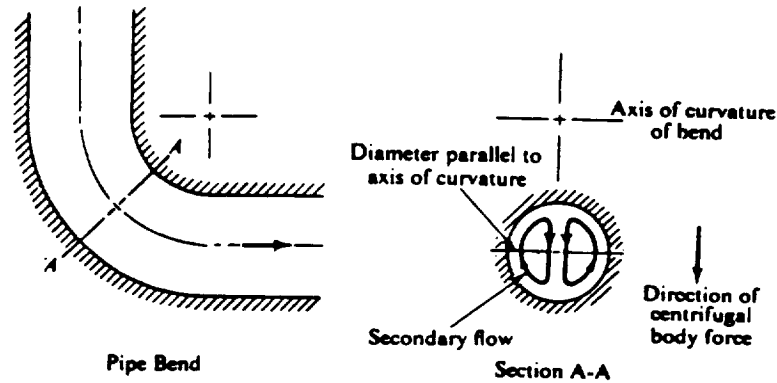


Figure 3-70. Secondary Flow in a Pipe Elbow

Straight elbows and tees, Figures 3-71, introduce losses and turbulence. Vaned elbows reduce the losses and the vibration due to turbulence. Loss coefficients for well-designed vaned elbows are on the order of 20 percent of those for standard elbows. Tees have either flow "through the run" where there is a side branch or "flow through the branch" parting left and right in opposite directions down the run.

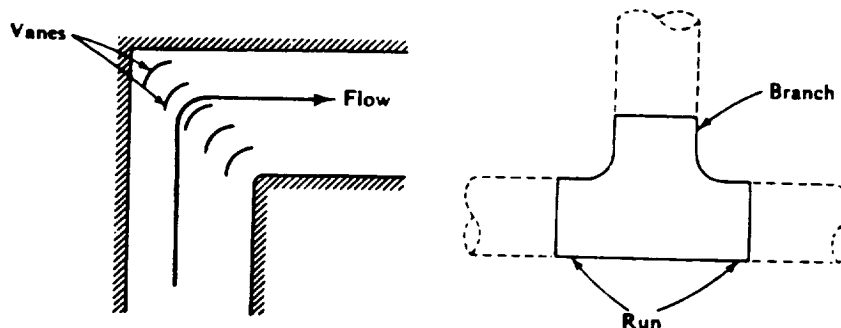


Figure 3-71. Vaned Elbows and Tees

Methods for dealing with dynamically coupled fluid-pipe or duct systems containing general pipe intersections, area or direction changes, long-radius bends, hydraulic losses, and hydraulic impedances are available.

Pipe Systems

Piping systems function under time-varying conditions, imposed by pump and valve operations, in the delivery of pressurized liquids. The analysis of the liquid's unsteady behavior was traditionally based upon solutions to the equations of motion and continuity, without considering any motion in the pipe. Transients propagate at the acoustic velocity, or wave speed, of the liquid. The diameter, wall thickness, and elastic modulus of the pipe are used in calculating the wave speed, after which the liquid is assumed to be flowing through a straight, rigid pipe. However, there is reason for concern that the transient behavior of liquids in piping systems that are neither rigid nor straight may differ from that predicted by a traditional rigid pipe analysis. Experimentation has shown that, in some systems, the elasticity of the pipes can amplify transient pressure in the liquid to a significant degree.

The dynamic forces exerted by the liquid on pipe fittings, where the flow direction or area changes (e.g., elbows, tees, valves), can set the pipe in motion and result in a feedback between the liquid and the pipe, causing alteration of the liquid transient. The amplitude and velocity of motion are functions of the restraint provided by the attached piping and supports. Therefore, a coupled liquid-pipe transient analysis must include these structural parameters.

There are two primary mechanisms which account for the dynamic interaction between the contained liquid and the piping. These are, 1) strain-related or Poisson coupling effects, which occur axially along pipe reaches; and 2) pressure-resultant effects, where coupling occurs only at fittings.

The strain-related, or Poisson coupling, results from the transformation of circumferential strain, ϵ_θ , (caused by internal pressure) into axial strain, ϵ_x , where

$$\epsilon_x = \nu \epsilon_\theta \quad (3.8.1)$$

and ν is the Poisson ratio. The pipe wall is treated as an elastic membrane to include the axial stresses and axial inertia of the pipe. During sudden valve closure, for instance, a tension wave is found to propagate in the pipe wall at a wave speed near that of the pipe material. Hence, a "precursor" wave travels ahead of the main pressure wave in the fluid. The axial tension is a Poisson effect in response to pipe dilation caused by the pressure transient. There is an increase in liquid pressure due to the tension wave, but the increase is small and a second-order Poisson effect.

At fittings where the pipe area or direction changes, the pressure resultant acts as a localized force on the pipe. Pipe motion can significantly alter pressure, and effects of support and piping stiffness contribute to the interaction.

One such set of methods applied to a liquid oxygen (LO₂) feed line in a rocket test stand was presented by Saxon¹ for NASA's testing of the Space Shuttle Main Engine. Structural analysis of piping systems, especially dynamic analysis, have typically considered the duct and fluid separately. Coupling the two, however, forms a new dynamic system with characteristics not necessarily described by superposition of the duct and fluid component characteristics.

Example Problem - POGO Pulsing

The coupled structural-fluid dynamic analysis of Saxon¹ was performed using finite line element methods in a study to determine the piston stroke requirements for POGO pulsing the

¹Saxon, J. B., "Modeling Dynamically Coupled Fluid Duct Systems with Finite Line Elements," NASA CR-193909, February 1993.

PIPING SYSTEMS

Space Shuttle Engine in a different test stand than the one normally used. This analysis was done for the Technology Test Bed (TTB) at MSFC. The problem was to predict the POGO pulsing effect on the facility feed line at 1 to 50 Hz and to identify all of the coupled system modes up to 200 Hz. Coupled modes at 14.3 and 34.9 Hz were found to be particularly sensitive in Saxon's analysis.

Structural analyses of piping systems are usually accomplished with finite line element models to which estimated fluid loads are applied. Under transient conditions, however, dynamic coupling occurs between the pipe and the contained fluid such that the two can no longer be considered separately. Saxon's (1993) methods allow simultaneous analysis of the structure and contained fluid column by representing both as overlaying strings of line elements. This requires the fluid to be treated as one dimensional; an assumption considered adequate from the structural analyst's perspective. The key is in maintaining the correct force transfer between the duct and fluid elements. The following exposition includes treatment of forces transferred at general intersections or direction/area changes, forces transferred at long radius bends, forces due to losses, and terminal hydraulic impedances. Secondary friction flow effects (at higher frequencies) are ignored here.

Dynamic Approach

In the presence of both steady-state and transient dynamics, it is desirable to consider the two separately and superimpose their results for a complete solution. In this method, the steady-state dynamics are analyzed with a quasi-static approach for which the Finite Element Analysis (FEA) representation of the fluid column assumes static equilibrium, but is understood to represent some steady-state dynamic condition. Forces transferred by the quasi-static model accurately mirror those of the true steady-state dynamic condition except that head losses are usually ignored. If a loss is considered significant, then the steady-state analysis should include forces applied by the analyst to the fluid-column and/or structure as a correction.

The underlying assumption of the transient analysis is that transient dynamic loads produce the same response whether applied to a quasi-static system or to a genuinely steady-state dynamic system. Under transient loads, velocities and loads experienced by the FEA representation of the fluid are understood to add vectorially to the corresponding steady-state values. Forces due to losses are generally a function of velocity squared, and therefore should have a transient component as well. Transient velocities are assumed to be small compared to steady-state velocity.

By analyzing steady-state and transients separately, a quantifiable error is introduced in the rate at which pressure perturbances are propagated up and downstream. Pressure wave propagation is a superposition of acoustic and steady-state velocities. Error due to the absence of a steady-state velocity is small, since acoustic velocities usually greatly exceed flow velocities.

Modeling a Fluid Column and Coupled Straight Pipe

Treatment of the contained fluid column is one dimensional and can be represented by structural rod elements (structural members that carry only tension/compression). Properties of the rod elements are based on properties of the fluid column they represent. Mass density of the rod equals density of the fluid, and cross-sectional area of the rod equals the cross-sectional area of fluid column. Young's Modulus of the rod corresponds to Effective Bulk Modulus, B_e , of the fluid, which is calculated from Bulk Modulus, B , corrected for radial stiffness of the pipe as shown below.

$$B_e = (BEt)/(2BR + Et) \quad (3.8.2)$$

PIPING SYSTEMS

where E = Young's Modulus of pipe
 t = pipe wall thickness
 R = nominal radius of pipe

For duct cross-sections more complex than cylindrical pipe, such as bellows, B_e may be calculated by methods given by Kiefling² Using these fluid/structural analogies, the axial stress in the rod is taken to equal the total pressure, static plus dynamic, in the fluid column.

The validity of this approach can be confirmed by a simple model of a fluid column constrained in all but the axial direction along its length and completely constrained at one end. FEA modal analysis should match hand calculated open-closed organ pipe frequencies.

For convenient coupling of the fluid to the pipe, it is beneficial to adopt certain conventions in defining the two coincident strings of line elements which represent the duct structure and the fluid column. Each node pair should be coupled such that they move independently in the direction corresponding to flow, but are otherwise rigidly joined. This is illustrated schematically in Figure 3-72, and may be accomplished with either Multi-Point-Constraint (MPC) equations or zero length springs.

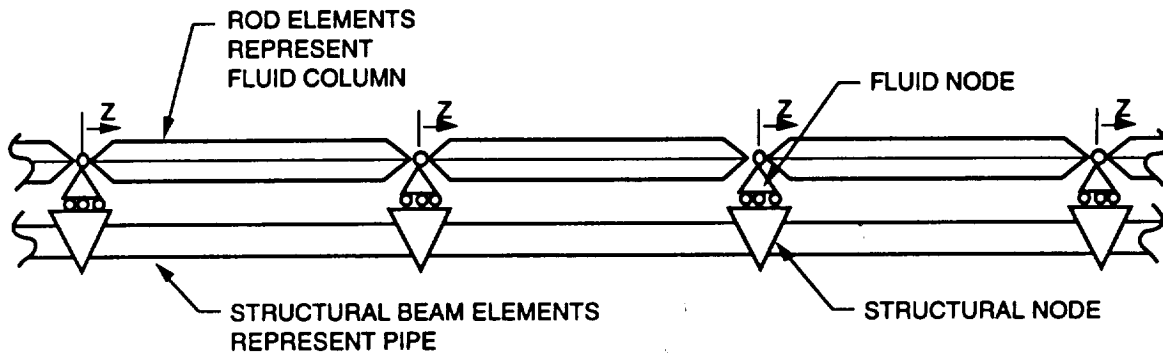


Figure 3-72. FEA of Straight Duct and Coupled Fluid Column

Coupling at Direction/Area Changes

At any point where the duct contains a bend, an intersection, or a change in flow area, additional considerations must be applied in order to correctly account for the transfer of forces between the fluid column and the duct structure at that location.

Figure 3-73 illustrates a pipe intersection involving all the features under consideration. (Planar geometry is not necessary, but is used here for clarity.) Mass continuity between the three fluid columns and force transfer between the fluid and the duct can be imposed with a single MPC equation involving the Z translations of each fluid node and the translational degrees of freedom of the intersection's structural node. The equation is derived by treating the intersection's structural node as if it were another incoming fluid branch oriented and sized such that all the Pressure•Area forces acting on the intersection added vectorially to zero.

A generalized approach, as applied to Figure 3-73, proceeds as follows. Each of the three branches entering the intersection should be modeled as described previously, and each branch should have its own fluid node at the point of intersection. For convenience, direct the Z axes of the intersection's three fluid nodes *into* the intersection. Let the vectors A_i equal the flow area of branch i times the unit Z vector of branch i 's fluid node at the intersection. Each A_i should be expressed in the reference frame defining the nodal displacements of the

²Kiefling, L., "Pressure-Volume Properties of Metallic Bellows," NASA TM-100365, Marshall Space Flight Center, ED-22, Huntsville, Alabama, May 1989.

PIPING SYSTEMS

intersection's structural node. Now define a vector A_S according to

$$A_S + \sum_{i=1}^3 (A_i) = 0 \quad (3.8.3)$$

Having defined A_S , the MPC equation enforcing mass continuity and force balance is

$$(A_{sx} \cdot X_S) + (A_{sy} \cdot Y_S) + (A_{sz} \cdot Z_S) + \sum_{i=1}^3 (A_i \cdot Z_i) = 0 \quad (3.8.4)$$

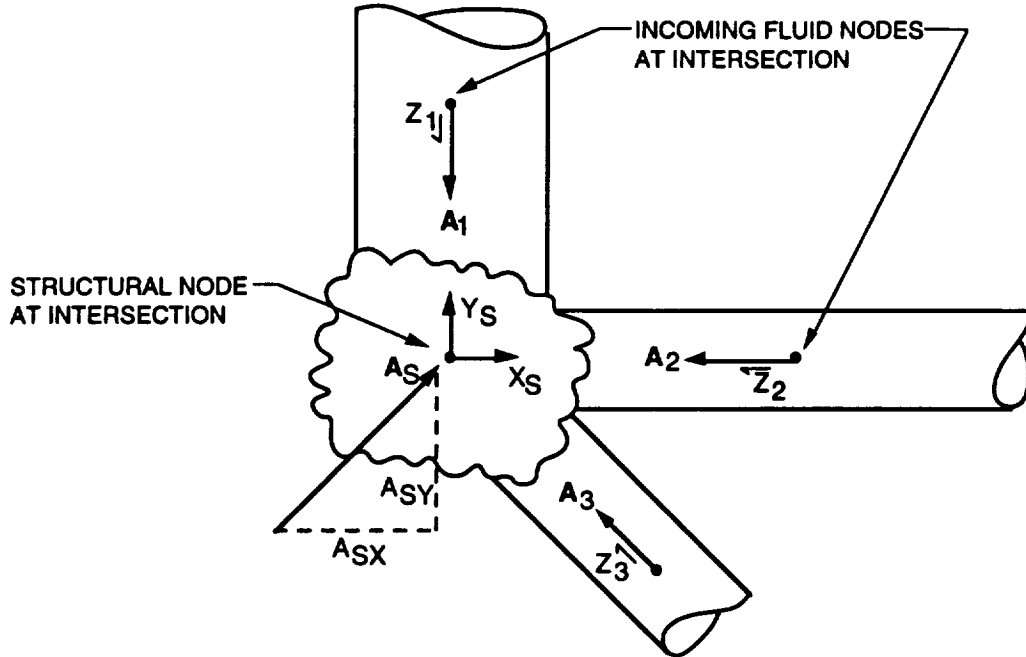


Figure 3-73. Duct Intersection and Area Change Example

Equations 3.8.3 and 3.8.4 are applicable to any number of incoming branches. If applied to one branch, a capped end is defined. If applied to two branches, an elbow is defined. For some analysis software, it may be necessary to enforce these constraints with large stiffness values rather than an MPC equation. In effect, the stiffness equations form the intersection element defined below for n branches intersecting at a point. Here, K_1 is an arbitrary multiplier large enough to make the fluid at the point of intersection relatively incompressible.

$$\begin{array}{l}
 F_{z1} \\
 F_{z2} \\
 F_{z3} \\
 F_{xs} \\
 F_{ys}
 \end{array}
 = K_1 \begin{array}{|c}
 A_1 \cdot A_1 \\
 A_1 \cdot A_2 \\
 A_2 \cdot A_2 \\
 A_1 \cdot A_3 \\
 A_2 \cdot A_3 \\
 A_3 \cdot A_3 \\
 \text{symm.} \\
 A_{sx} \cdot A_{sx} \\
 A_{sx} \cdot A_{sy} \\
 A_{sy} \cdot A_{sy}
 \end{array} \begin{array}{l}
 Z_1 \\
 Z_2 \\
 Z_3 \\
 X_s \\
 Y_s
 \end{array} \quad (3.8.5)$$

Long Radius Elbows

In some cases, the radius of a bend is not negligible compared to the total length of duct being modeled. Figure 3-74 shows such a bend, encompassing an angle θ , as modeled with n fluid/structural node pairs spaced evenly between the end points of the bend. As with straight pipe, the fluid and structural nodes should move independently in the direction tangent to the direction of flow, but be rigidly coupled perpendicular to flow as illustrated. This arrangement accurately models the forces transferred, however, the stresses in the rod elements will exceed the total pressure in the fluid. This can be corrected by adjusting the properties of the rods so as to maintain correct axial stiffness and achieve correct stresses. The basic properties of the rods in the bend, e.g. A , E , and ρ , should be adjusted to A' , E' , and ρ' according to

$$A' = A / \sin(\theta / (n+1)) \quad (3.8.6)$$

$$E' = E \cdot \sin(\theta / (n+1)) \quad (3.8.7)$$

$$\rho' = \rho \cdot \sin(\theta / (n+1)) \quad (3.8.8)$$

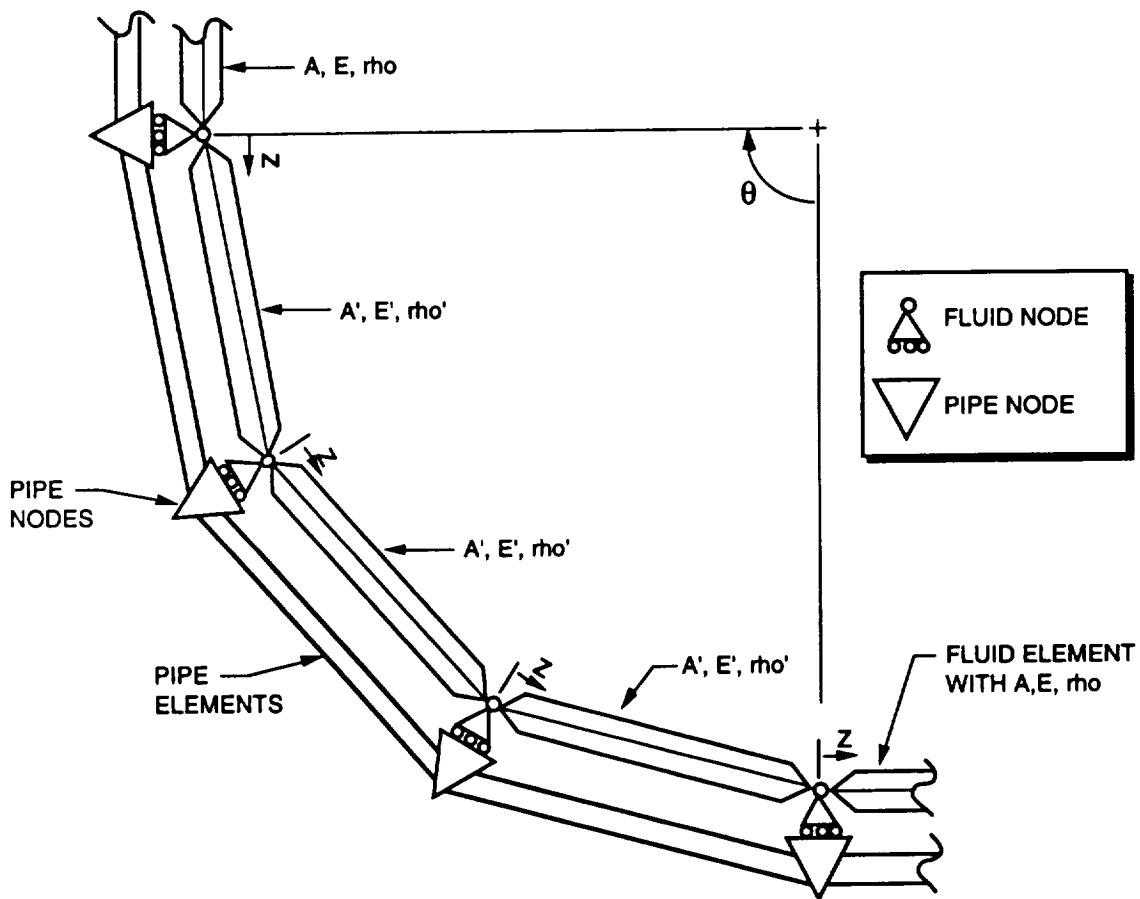


Figure 3-74. FEA of Curved Duct and Coupled Fluid Column

PIPING SYSTEMS

Losses

In addition to force transfer between fluid and duct at direction/area changes, head losses may play a significant role in how forces are distributed throughout the system. Steady-state losses must be accounted for. This is accomplished with equal and opposite forces applied to the fluid column in the upstream direction, and to the structure in the downstream direction. The magnitude of the loss, where steady-state velocity is a given quantity, must be determined as shown below, where C is obtained from reference data.

$$F_{Loss} = A \cdot C \cdot \rho \cdot (V_{SS})^2 \quad (3.8.9)$$

Figure 3-75 illustrates an elbow under steady-state conditions with an assumed loss. The mass and force balance equations would make pressure in the fluid column the same both up- and downstream of the elbow. The additionally applied forces for loss allow the fluid column downstream to see a reduced pressure while maintaining mass continuity.

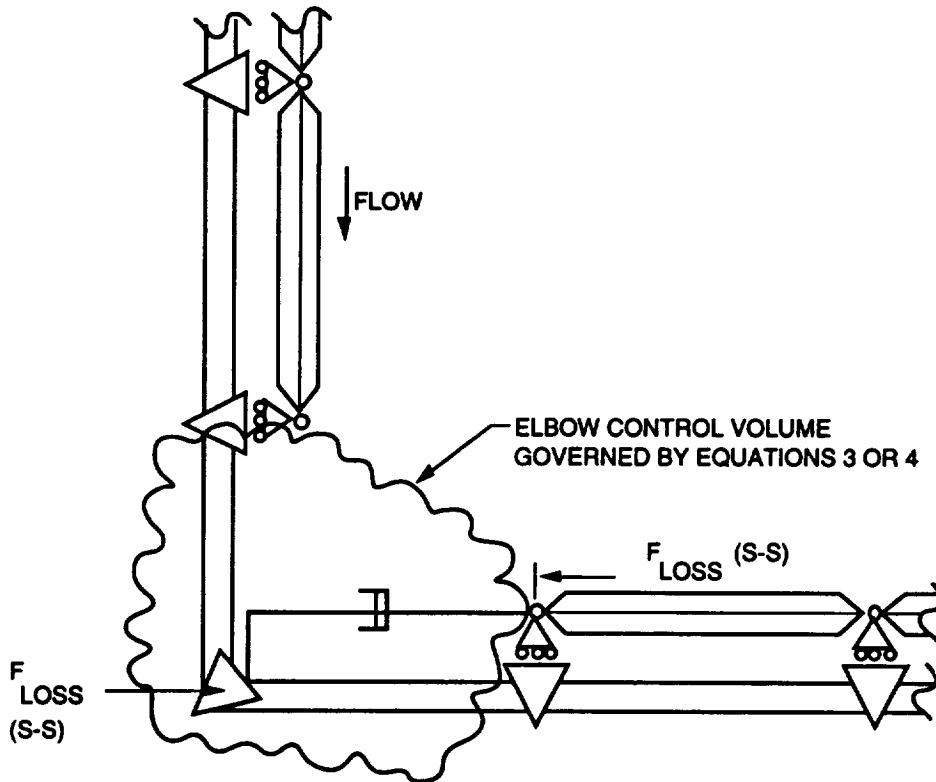


Figure 3-75. FEA of Elbow with Losses Considered

In the presence of transients, the total velocity, $V_{SS} + V_t$, should produce a force of loss equal to the sum of the steady-state loss, F_{SS} , and a transient component of loss, F_t , as shown below.

$$F_{Loss} = F_{SS} + F_t = A \cdot C \cdot \rho \cdot (V_{SS} + V_t)^2 \quad (3.8.10)$$

Assuming that the loss variable C does not appreciably change between velocities V_{SS} and $V_{SS} + V_t$, substituting equation 3.8.9 into 3.8.10 and solving for F_t gives

$$F_t = A \cdot C \cdot \rho \cdot (2 \cdot V_{SS} \cdot V_t + V_t^2) \quad (3.8.11)$$

PIPING SYSTEMS

If a further assumption is made that V_t^2 is insignificant compared with $2 \cdot V_{SS} \cdot V_t$, the transient force of loss can be estimated as

$$F_t = (2A \cdot C \cdot \rho \cdot V_{SS}) \cdot V_t \quad (3.8.12)$$

which is a linear damping term. As long as C is constant, the above estimation is 90% accurate for $V_t < (.2 \cdot V_{SS})$. The damper implied above should be affixed at the point of loss between the structural node and the downstream fluid node as seen in Figure 3-75. The damper increases the force of loss for a transient velocity that increases flow velocity magnitude and decreases the force of loss for a transient velocity that decreases flow velocity magnitude. The above treatment does not account for the fact that much of the loss represented by published values of C accounts for irreversible losses several diameters downstream of the elbow, thus reducing the static pressure in the fluid without causing an equal and opposite load on the duct. None-the-less, the above method does provide an estimate of force distribution due to transient losses.

Terminal Hydraulic Impedances

The duct terminates at the inlet to a rocket engine or an accumulator device which provided a quantifiable impedance to flow. The hydraulic impedance is expressed as compliance, resistance, and inertance, for which the mechanical equivalents are stiffness, resistance, and mass, respectively. For the steady state analysis, the terminal end of the fluid column can be fixed, thereby precluding the need to account for the impedance. In the transient analysis, however, the fluid column must terminate at a spring/mass/damper system, as shown in Figure 3-76, with K , M , and D defined in terms of compliance, mass, and resistance as follows:

$$K = \Gamma \cdot A / \text{Compliance} \quad (3.8.13)$$

$$M = \Gamma \cdot A^2 \cdot \text{Inertance} \quad (3.8.14)$$

$$D = \Gamma \cdot A^2 \cdot \text{Resistance} \quad (3.8.15)$$

where Γ is weight of density of fluid

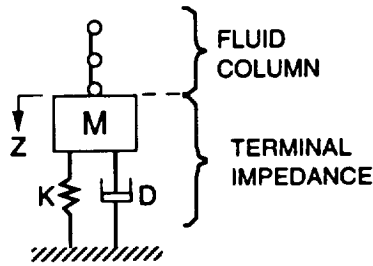
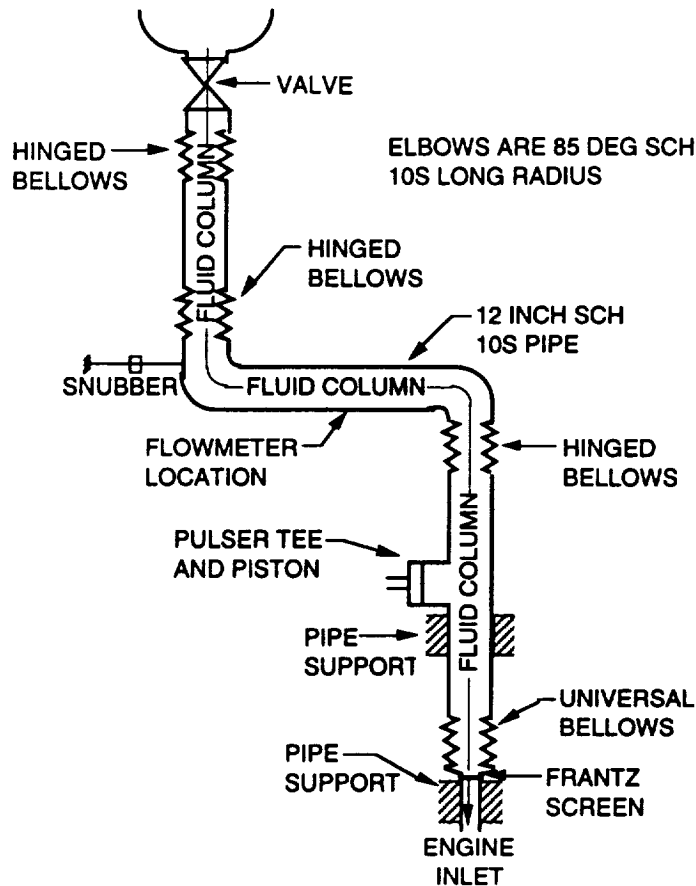


Figure 3-76. Mass-Spring-Damper System to Model Terminal Hydraulic Impedance

These impedance terms are frequency dependent. The example feedline is shown in Figure 3-77.



Figures 3-77. Schematic of TTB Liquid Oxygen Feedline

At both elbows and the pulser tee, stiffness matrices representing general area/direction changes were applied. Losses at valves, flowmeters, etc. were modeled with linear dampers, the damping values based partially on pressure data recorded during operation. The terminal hydraulic compliance of the engine was modeled with a spring, with no frequency dependence in the frequency range of interest. The applied loads, including those to account for losses, are shown in Figure 3-78.

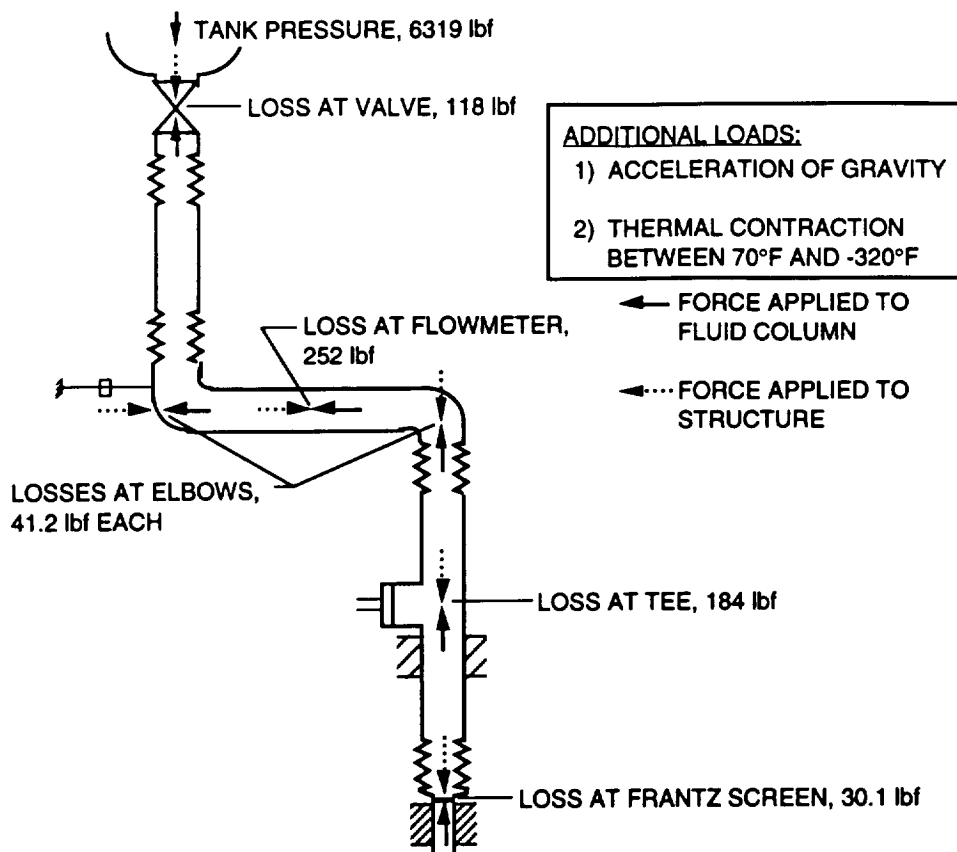


Figure 3-78. Loss Loads Applied to Feedline Model for Quasi-static Analysis of Steady-state Conditions

The results of three modal analyses, shown in Table 3-13, demonstrate the inadequacy of analyzing the fluid and structural system separately. The first set of modes considers the fluid acoustics only, as if the duct were perfectly rigid (except for radial expansion accounted for by equation 3.8.2). The second set of modes considers duct flexibility, but treats the fluid only as added mass. The last set of modes, which accounts for the fluid-duct coupling, is clearly more than the simple superposition of the first two cases.

Modes from the coupled system were used in two transient analyses simulating the start-up of POGO pulser operation at 15 Hz and 35 Hz. Both analyses were driven by enforcing sinusoidal displacement of the piston node. Figures 3-79 and 3-80 show response of the system presented as nodal displacement of a point in the fluid column near the engine inlet, and displacement of a node on the duct near the downstream elbow. In both cases, the larger motion is that of the structure. The transient response to 15 Hz POGO pulsing quickly settles to a steady-state containing higher frequency components. Response to 35 Hz POGO pulsing exhibits resonance with the coupled system mode at 34.9 Hz, amplifying the input signal.

The fact that 35 Hz was a critical system frequency would have remained unknown since it shows up in neither of the first two columns of Table 3-13.

PIPING SYSTEMS

Table 3-13. Comparison of Modal Results

| Fluid Acoustic Modes, Rigid Duct (Hz) | Duct Structural Modes, "Frozen" Fluid (Hz) | Coupled Fluid-Duct System Modes (Hz) |
|---------------------------------------|--|--------------------------------------|
| 1.8 | | 1.8 |
| | 6.9 | 6.1 |
| 29.6 | | 14.3 |
| | 32.4 | 22.1 |
| 59.1 | | 26.6 |
| | 66.1 | 32.2 |
| | 77.4 | 34.9 |
| 88.5 | | 62.5 |
| | 92.6 | 71.8 |
| | 97.6 | 84.8 |
| 118.0 | | 89.8 |
| | 124.2 | 93.6 |
| | 133.6 | 98.3 |
| | 142.2 | 118.6 |
| 147.6 | | 130.9 |
| 177.0 | | 143.8 |
| | 181.1 | 145.7 |
| | 192.9 | 162.7 |
| 205.2 | | 179.4 |
| | | 191.5 |

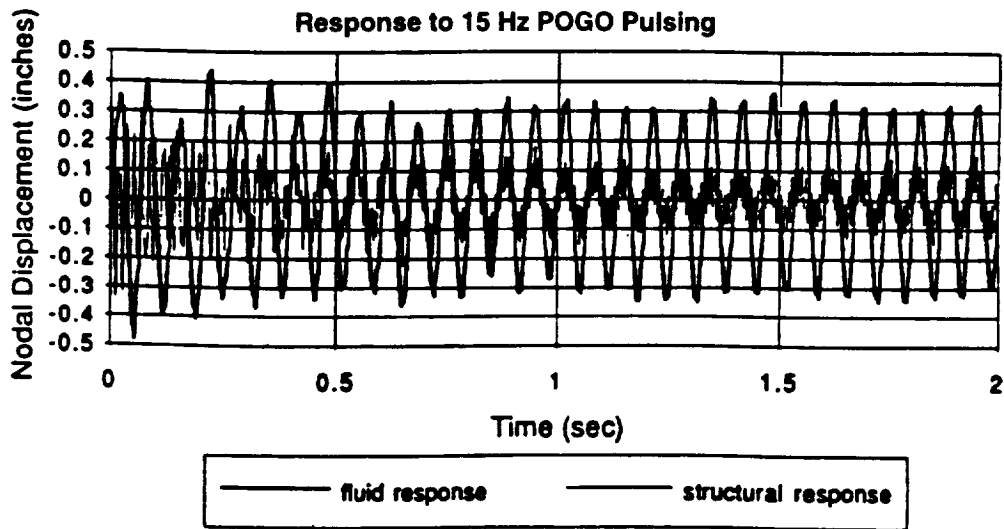


Figure 3-79. Transient Feedline Response to POGO Pulsing Start-up at 15 Hz

The undeformed and deformed mode shape 7 at 34.9 Hz depicted by the coupled fluid structure FEA of the feedline are shown in Figure 3-81.

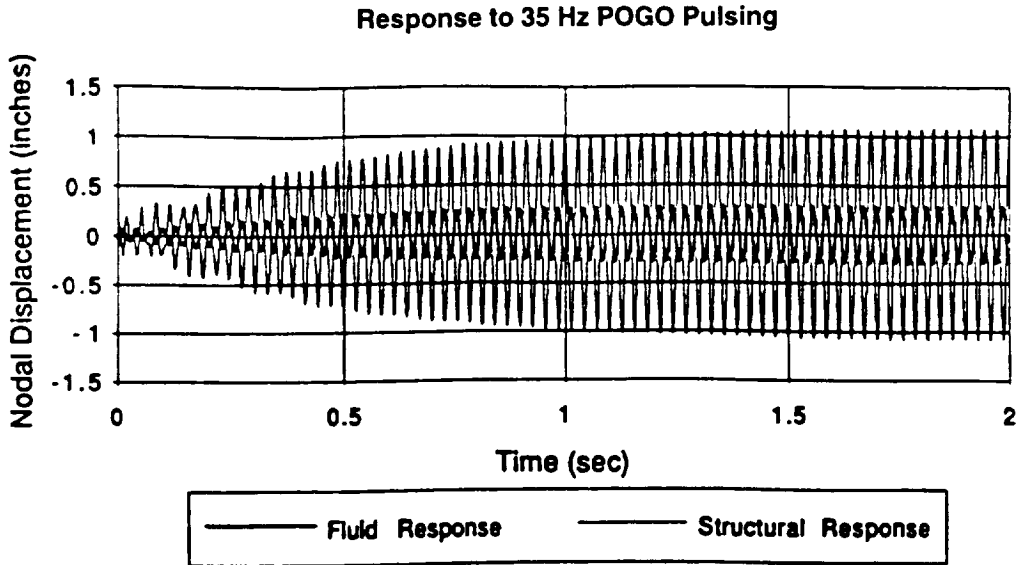


Figure 3-80. Transient Feedline Response to POGO Pulsing Start up at 35 Hz

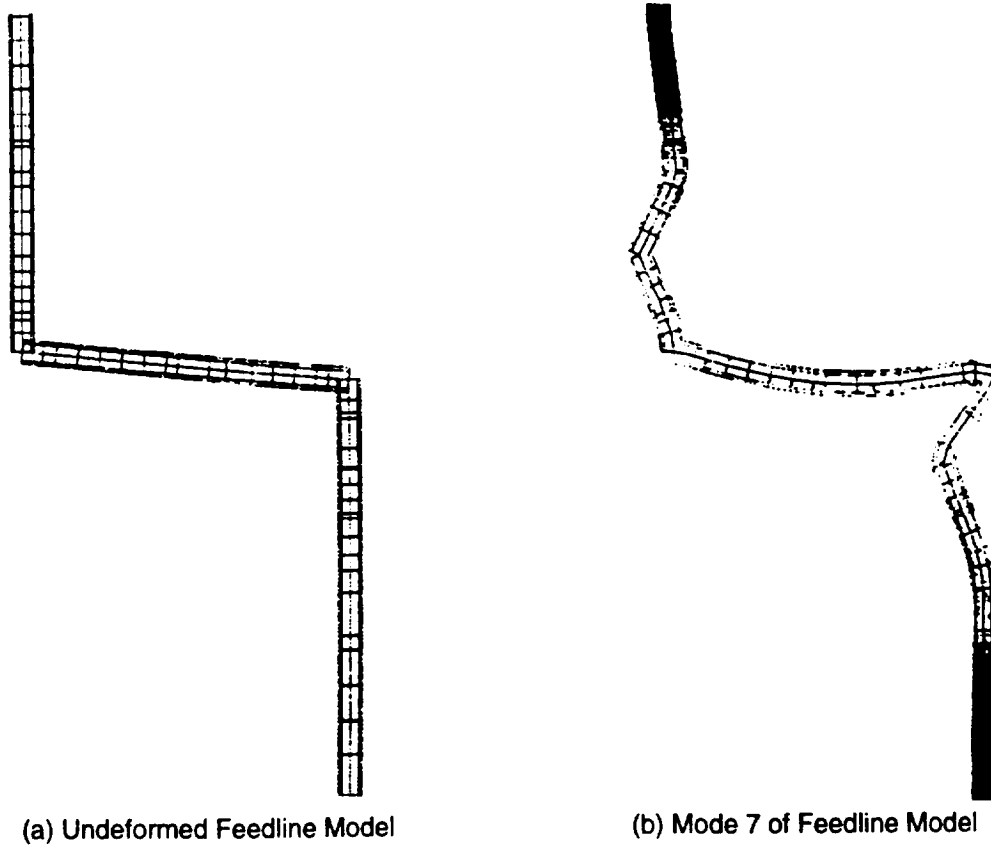


Figure 3-81. Undeformed and Deformed Feedline Mode Shape Depicted by the FEA at 34.9 Hz

BELLOWS AND LINERS

3.9 Bellows and Liners

Bellows and Flexible Hoses

The number of convolutes is a key parameter of a bellows. Certain flexible hoses resemble bellows in that they have convolutes. Relevant bellows nomenclature is given in Figure 3-82.

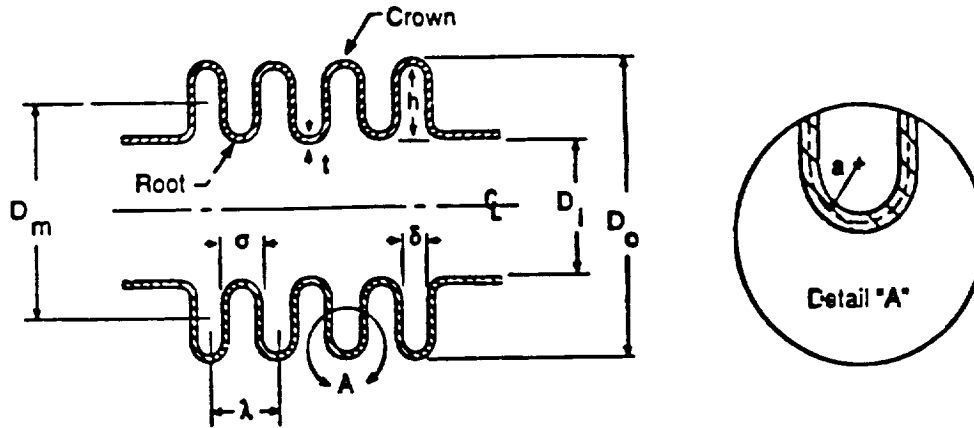


Figure 3-82. Bellows Parameters

- σ = convolute width
- ρ_m = material density
- δ = internal convolute gap
- D_i = inside diameter
- D_o = outside diameter
- h = mean disc height.
- N_p = number of plies
- t = convolute thickness per ply
- λ = convolute pitch
- ρ_f = fluid density
- a = mean forming radius
- D_m = mean bellows diameter
- E = Young's modulus
- N_c = number of convolutes
- L = bellows length

and mode parameters:

- $S_{\sigma U}$ = upper limit Strouhal number
- $S_{\sigma C}$ = critical Strouhal number
- $S_{\sigma L}$ = lower limit Strouhal number
- N = mode number
- k = elemental spring rate
- f_o = reference frequency
- $$= \frac{1}{2\pi} \left(\frac{k}{m} \right)^{1/2}$$

- f_N = modal frequency = $f_o B_N$
- K_a = overall bellow spring rate

BELLOWS AND LINERS

m = total mass including added mass
 B_N = dimensionless frequency number

$$= \sqrt{\left[2 + 2 \cos \left(\frac{\pi (2Nc - N)}{2 Nc} \right) \right]}$$

and lock-in range parameters:

$$\begin{aligned} V_{low} &= \text{excitation velocity lower limit} = f(n) \sigma / S_{\sigma u} \\ V^* &= \text{critical velocity} = f(n) \sigma / S_{\sigma c} \\ V_{up} &= \text{excitation velocity upper limit} = f(n) \sigma / S_{\sigma l} \end{aligned}$$

Empirical formulas for functional relationships among the key parameters were given in the reference report. It recommended a flow test to measure the overall bellows spring rate K_a for any new practical applications. It also suggested further analytic work to address multi-phase flows, overall static loads and conditions other than flow-induced vibrations.

The propellant feedlines in the Space Shuttle Main Engines contain bellows located throughout the feedline network. Basic geometry pertaining to bellows is shown in Figure 3-82. The figure shows that each convolute of the bellows presents a bluff shape to the flow, much like that of a cylinder. Vortex shedding from the individual convolute occurs at a Strouhal number of approximately 0.22. The resulting vibrations can be severe if the vortex shedding frequency locks in with a longitudinal natural frequency of the bellows. The problem is very similar to vortex shedding from a cylinder except that shed vortices from each convolute may be reinforced or canceled by vortices from adjacent, or nearby convolutes depending on convolute width and pitch.

The dynamics of bellows are characterized by the number of structural modes equaling the number of convolutes with individual convolutes moving in-phase or out-of-phase with one another. The frequency of these modes are strongly affected by the fluid trapped in the convolutions. The cited reference presents analysis procedures for avoiding flow-induced vibrations of flexible lines (bellows and flexhoses). These involve using the prescribed methods for calculating a frequency range that including all the longitudinal modes. A bellows bulging (i.e., convolute bending mode) frequency is also included. Using a Strouhal number of 0.1 (minimum) and 0.3 (maximum) provides limits of flow velocity where resonance may occur.

Premature failures were observed in flexible lines, namely, metal bellows and flexhoses due to the occurrence of flow-induced vibrations. This is attributed to a resonance caused by the coupling of vortex shedding from the convolutes with the natural frequencies of the flexible line. MSFC Design Reference Standards¹ present a comprehensive design analysis for these bellows and flexhoses either to prevent resonance from occurring or to predict the expected life of this flexible lines under flow-induced vibration loads.

The analytical methods include predicting the excitation flow range, frequency, and the corresponding stress resulting from flow-induced vibration loads. This then leads to prediction of the expected life of the bellows or flexhose, with a final objective of achieving a theoretically infinite life for flow-induced vibrations. The analytical method in this reference was developed for metal bellows and flexhoses manufactured with formed annular convolutes, as shown in Figure 3-82. These are the most commonly used type in propellant systems. The analytical model was developed by Tygielski, et al.² The equations in the reference were empirically derived from extensive testing and are the basis. The computer program of the analytical method for bellows is documented in the reference and is named as BELFIV (version 3.3).

¹ *Assessment of Flexible Lines for Flow Induced Vibration*, NASA/MSFC, Revision E, Dec. 19, 1991.

² Tygielski, P.J., Smyly, H.M. and Gerlach, C. R., "Bellows Flow-Induced Vibrations," NASA/MSFC Technical Memorandum, NASA TM-82556, October 1983.

BELLOWS AND LINERS

Sample problems are presented in the MSFC Design Reference Standards and summarized in the following:

- a) Bellows: a.1) Liquid Medium Example
 a.2) Gaseous Medium Example

b) Flexhose Example Problem

The input parameters needed in the bellows include

- a.3.1) title of the case
- a.3.2) flag to calculate the overall spring rate or to input its value instead
- a.3.3) flag to set for the liquid medium
- a.3.4) number of bellows
- a.3.5) number of convolutes counted from the outside
- a.3.6) number of plys
- a.3.7) inside convolute width
- a.3.8) inside convolute pitch
- a.3.9) mean inside convolute height
- a.3.10) ply thickness
- a.3.11) bellows inside diameter
- a.3.12) bellows outside diameter
- a.3.13) Young's modulus
- a.3.14) density of the material
- a.3.15) optional bellows overall spring rate
- a.3.16) length from the termination of the elbow to first convolute divided by the inside diameter of the pipe just before the bellows, zero if no elbow upstream

If the medium is a liquid, there are three more parameters needed

- a.3.17) liquid pressure
- a.3.18) liquid temperature
- a.3.19) liquid density

If the medium is a gas, there are eight more parameters needed

- a.3.17) gas pressure
- a.3.18) gas temperature
- a.3.19) gas pressure at reference state
- a.3.20) gas temperature at reference state
- a.3.21) gas density at reference state
- a.3.22) gas compressibility factor
- a.3.23) gas compressibility factor at reference state
- a.3.24) specific heat ratio for the gas

The outputs for the bellows include

- a.4.1) overall spring rate
- a.4.2) elbow factor
- a.4.3) flow-induced stress versus longitudinal mode number
- a.4.4) mode frequency versus longitudinal mode number
- a.4.5) lower, critical, and upper excitation flow velocities versus longitudinal mode number
- a.4.6) flow-induced stress for convolute bending mode
- a.4.7) mode frequency for convolute bending mode
- a.4.8) lower, critical, and upper excitation flow velocities for convolute bending mode

If the medium is a gas additional outputs include

- a.4.9) First radial acoustic mode frequency
- a.4.10) First radial acoustic mode velocity

BELLOWS AND LINERS

Bellows Numerical Example

A sample numerical example is included as follows:

Given: H₂O flowing through a 3 inch 321 stainless bellows at 68 °F and at 35 psig with an elbow 4 inches from the first convolute.

Find: Assess the fatigue life from flow-induced vibration loads for the first longitudinal mode $N = 1$ and the longitudinal mode of $N = N_C$.

The input parameters and step-by-step calculations are given in the following.

$$\begin{aligned}
 D_i &= \text{Inside diameter of the bellows} = 3 \text{ in} \\
 D_o &= \text{Outside diameter of the bellows} = 3.69 \text{ in} \\
 D_m &= \text{mean diameter of the bellows} = (D_i + D_o)/2 = 3.345 \text{ in} \\
 E &= \text{Young's modulus of the material} = 29.e6 \text{ psi} \\
 t &= \text{ply thickness} = 0.007 \text{ in} \\
 h &= \text{mean inside convolute height} = 0.325 \text{ in} \\
 N_p &= \text{Number of plies} = 3 \\
 \lambda &= \text{Inside convolute pitch} = 0.148 \text{ in} \\
 N_C &= \text{Number of convolute counted from the outside} = 16 \\
 K_a &= \text{overall bellows spring rate} = D_m E (N_p/N_C) (t/h)^3 = 181.735 \text{ lb}_f/\text{in} \\
 k &= \text{Elemental spring rate of one-half of a convolution} = 2 N_C K_a = 5815.52 (12) \text{ lb}_f/\text{ft} \\
 \sigma &= \text{inside convolute width} = 0.095 \text{ in} \\
 \rho_m &= \text{density of bellows material} = 0.286 \text{ lb}_f/\text{in}^3 \\
 a &= \text{Mean convolute radius} = (\sigma - t N_p)/2 = 0.037 \text{ in} \\
 m_m &= \text{Elemental metal mass} = \pi \rho_m t N_p D_m [\pi a + h - 2 a]/g = 7.2e-4 \text{ slug} \\
 \rho_f &= \text{fluid density} = 62.4/1728 \text{ lb}/\text{in}^3 \\
 m_{f1} &= \text{type 1 fluid added mass} = \pi \rho_f D_m h (2a - t N_p)/(2g) = 1.02e-4 \text{ slug} \\
 K_1 &= \text{type 1 added mass factor} = 1 \\
 K_2 &= \text{type 2 added mass factor} = 0.68 \\
 N &= \text{mode number} = 1, 2, \dots, 2N_C - 1 \\
 \delta &= \text{Inside convolute gap} = \lambda - \sigma = 0.053 \text{ in} \\
 m_{f2} &= \text{type 2 added mass} = \rho_f D_m h^3/(g \delta) = 2.43e-3 \text{ slug} \\
 m_f &= \text{total elemental fluid added mass} = K_1 m_{f1} + K_2 m_{f2} (N/N_C) = 2.05e-4 \text{ slug for } N = 1 \\
 m &= \text{total elemental mass} = m_m + m_f = 9.25 e-4 \text{ slug} \\
 B_N &= \text{frequency factor} = \{2[1 + \cos(\pi(2N_C - N)/(2N_C))]\}^{1/2} \\
 B_1 &= 0.0981 \\
 f_o &= \text{reference frequency} = \frac{1}{2\pi} \sqrt{\frac{k}{m}} = 1382.4 \text{ Hz} \\
 f(N) &= \text{modal frequency of mode } N = f_o B_N \\
 f(1) &= 135.61 \text{ Hz} \\
 S_{\sigma u} &= \text{upper Strouhal number} = 0.3 \\
 S_{\sigma c} &= \text{critical Strouhal number} = 0.2 \\
 S_{\sigma l} &= \text{lower Strouhal number} = 0.1 \\
 V_{low}(N) &= \text{lower limit velocity for mode } N = \frac{f(N) \sigma}{S_{\sigma u}} \\
 V^*(N) &= \text{critical velocity for mode } N = \frac{f(N) \sigma}{S_{\sigma c}} \\
 V_{up}(N) &= \text{upper limit velocity for mode } N = \frac{f(N) \sigma}{S_{\sigma l}}
 \end{aligned}$$

BELLOWS AND LINERS

$$V_{low}(1) = 3.58 \text{ fps}$$

$$V^*(1) = 5.37 \text{ fps}$$

$$V_{up}(1) = 10.74 \text{ fps}$$

Parameters for $N = N_c$:

$$m_f = K_1 m_{f1} + K_2 m_{f2} (N/N_c) = 1.75e-3 \text{ slug}$$

$$m = m_m + m_f = 2.47e-3 \text{ slug}$$

$$B_N = 1.414$$

$$f_o = 845.97 \text{ Hz}$$

$$f_c = \text{Critical frequency} = f_o B_N = 1196.4 \text{ Hz}$$

$$V_c = \text{Critical velocity at } N = N_c = \frac{f_c \sigma}{S_{\sigma c}} = 47.36 \text{ fps}$$

$$V' = \text{Normalized velocity parameter} = V^*/V_c = 0.113$$

$$\text{SSR} = \text{Specific spring rate} = \frac{K_a N_c}{D_m N_p} = 289.762 \text{ lb/in}^2$$

$$\text{Empirical coefficients: } C_1 = 0.13, C_2 = 0.462, C_3 = 1, C_4 = 10, C_5 = 0.06, C_6 = 1.25, C_7 = 5.5.$$

$$\text{CNP} = \text{Damping modifier coefficient} = 1 \text{ for } N_p = 1$$

$$= 1 - \frac{C_6 \frac{s}{h}}{1 + C_7 V'^2} \text{ for } N_p > 1$$

$$\text{CNP} = 0.659$$

$$C^* = \text{Force and damping coefficient} = 0.4 \text{ for the convolute bending mode}$$

$$= \frac{C_1}{C_2 + V'^2} + \frac{C_3 |\sin(\pi V')|}{C_4 + V'^2} + C_5 \text{ all else}$$

$$C^* = 0.369$$

$$P_D = \text{Free stream dynamic pressure} = \frac{\rho_f V'^2}{2g} = 0.194 \text{ psi}$$

$$DD = \text{Dynamic pressure factor} = \frac{C^* t P_D}{V' \text{SSR} \delta} = 2.89e-4$$

$$EE = \text{Spring rate factor} = 1 + 0.1 \left(\frac{400}{\text{SSR}} \right)^2 = 1.191$$

$$D = \text{Inside pipe diameter} = 3 \text{ in}$$

$$L = \text{Distance from elbow termination to the first bellows convolute} = 4 \text{ in}$$

$$C_E = \text{Elbow factor} = 1 \text{ for no elbow present}$$

$$= 1 + \frac{4.7}{2 + \frac{L}{D}}$$

$$C_E = 2.41$$

$$\text{FIS} = \text{Flow-induced stress} = EE DD E \text{CNP} C_E / N_p$$

$$= 5284 \text{ psi for longitudinal mode } N = 1$$

For longitudinal mode of $N = N_c$ the following can be calculated by noting that $V' = 1$ and $V_c = 47.36 \text{ fps}$:

BELLOWS AND LINERS

$$C_{NP} = 1 - \frac{1.25 (0.095/0.325)}{1 + 5.5} = 0.9438$$

$$C^* = \frac{0.13 (0.095/0.325)}{0.462 + 1} + 0 + 0.06 = 0.1489$$

$$P_D = \frac{(62.4/1728)47.36^2(12)}{2(32.174)} = 15.1$$

$$DD = \frac{C^* t P_D}{SSR \delta} = 1.025e-3$$

$$FIS = EE DD E C_{NP} C_E / N_p \\ = 26873 \text{ psi for longitudinal mode } N = N_c$$

UF = Uncertainty factor due to the estimation of overall spring rate = 2

FISC = Corrected (or conservative) flow-induced stress = UF FIS

FISC = 10568 psi for longitudinal mode N = 1
FISC = 53746 psi for longitudinal mode N = N_c

SEL = Endurance limit = 26500 psi for 321 stainless steel at 68 °F

Since SEL > FISC for longitudinal mode N = 1, the bellows has infinite life for that mode. However, since SEL < FISC for longitudinal mode N = N_c, the bellows should be redesigned if operated to a velocity capable of exciting the longitudinal mode of N = N_c.

Liners

Most of the liners can be approximated as a cylindrical shell. Guiggiani³ carried out experimental studies on the dynamics and stability of thin cylindrical shells fluid-coupled by means of a narrow water-filled annulus with a concentric outer rigid cylinder. Eleven aluminum shells, with radius 277.5 mm, thickness 0.8 mm and height 268 mm were tested. The axis of the shell and the cylinder is in the vertical direction. The shell-water system was excited by assigning to the outer cylinder a horizontal harmonic rigid-body motion with small amplitude. An unexpected dynamic instability, with nonstationary large vibrations of the shell and exponential amplification of the dynamic pressure in the liquid can occur. Such instability was observed whenever the frequency of excitation in the test range 10 to 45 Hz, provided that the amplitude of the excitation reaches a threshold value. This low-frequency example is illustrative of high-frequency liner responses that can occur in smaller or stiffer structures as well.

A heavy bottom was integrally machined with each of the thin shells. This arrangement resulted in shell models with a boundary condition at the lower edge that approximated the clamped-edge case. The standard deviation of the shell thickness is in the range of 0.014 to 0.054 mm. The Young's modulus and Poisson's ratio were E = 68 GPa, and n = 0.3, respectively.

³Guiggiani, M., "Dynamic Instability in Fluid-Coupled Coaxial Cylindrical Shells Under Harmonic Excitation", Journal of Fluids and Structures, (1989) 3, pp. 211-228.

BELLOWS AND LINERS

The proportional stress of the material was found to be 18 to 25 MPa, while the yield stress was 30 to 40 MPa. The annulus region between the shell and the cylinder has a nominal thickness of 7 mm. The scatter was in the range of -0.5 to +0.4 mm. The water level was generally set 15 mm below the shell upper edge. To avoid water leakage, a soft rubber seal was used. The seal is rather flexible and the boundary condition at the upper edge is deemed free boundary. The shaped seal, further, allowed the pressurization of the gap.

The vessel rigid body movement was monitored and recorded, having a frequency f and an amplitude x . The response of the shell - the wall radial vibration - was monitored by seven displacement transducers located 15 mm below the shell upper edge at 0° , 7.5° , 15° , 22.5° , 30° , 45° and 180° . With 0° defined to be opposite to the center of the hydraulic actuator. The dynamic pressure in the liquid was detected at the mid level at 0° , 30° , 60° , 90° and 180° .

The static buckling pressure was about 0.02 MPa, and was associated to a buckling mode with circumferential mode number $n = 9$. Static tests were performed to obtain reference values for the dynamic ones.

A clear superharmonic resonance of order three was detected when exciting the system in the range 10 to 20 Hz and low amplitude ($x_{rms} = 0.03$ to 0.07 mm). The response was mainly with a frequency of exactly three times that of the excitation. The amplitude of vibration reached its maximum value when f was about 15 Hz.

A kind of dynamic instability of the shell-liquid system was observed, whenever the frequency of excitation in the range 10 to 45 Hz. It was associated to a sudden (exponential in time) amplification of the shell vibration and of the dynamic pressure in the liquid annulus.

The onset of the instability was shown to be strictly related to certain combinations of the excitation amplitude x_{rms} and frequency f of. Plotting the critical values of the frequency and amplitude, a linear relationship was always obtained as a region of unstable dynamic vibration:

$$x_{rms} \geq 0.1514 - 0.00292 f$$

where x_{rms} in mm and f in Hz. Beyond this straight line, no stable dynamic behavior appeared to be possible. The amplification of the shell vibration induced by the instability was particularly violent in the low frequency range (<25 Hz). In these cases it often resulted in local permanent buckling of the shell.

The boundary between the stable and unstable regions in the f - x_{rms} plane was nearly unaffected by the superimposition of any static pressure (up to 0.015 MPa) in the annulus. The amplitude of the dynamic pressure (at mid-level and in the 0° direction) at the onset of the instability was always much lower than the static buckling pressure. This was an experimental study and an analytical model for this type of system is probably wanting.

Mode Shapes and Frequencies

Typical Shell modes of a cantilevered liner are shown in Figure 3-83. The vibration mode shapes and frequencies are cited by Blevins (1987) for several reference theories and sources. An estimation procedure is included in the following. Figure 3-84 (a) shows the coordinate

BELLOWS AND LINERS

system. The axial deformation is denoted by u in the axial direction, the circumferential deformation v in the shell tangential direction and the radial deformation w in the radial direction. The length of the shell is denoted by L , the radius by R and the thickness by h . The nodal patterns and indices i and j are shown in the reference Figure 3-84 (b).

Note: Frame numbers are sequenced in time.

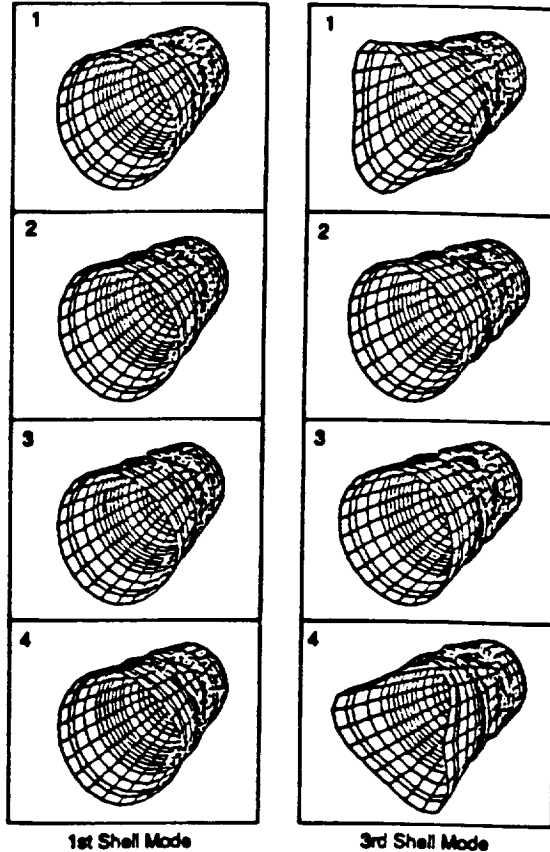


Figure 3-83. Typical Shell Modes of a Cantilevered Liner

The simplified general solution is given by

$$u = -\frac{A}{i^2} R \frac{d\tilde{\phi}_j}{dx} \cos i\theta \cos \omega t$$

$$v = -\frac{A}{i} \tilde{\phi}_j \sin i\theta \cos \omega t \quad \text{where } i = 2, 3, 4, \dots; j = 1, 2, 3, \dots$$

$$w = A \tilde{\phi}_j \cos i\theta \cos \omega t$$

The mode shape $\tilde{\phi}_j$ is the beam mode shape for appropriate boundary conditions. The mode shape factors, α_1 and α_2 are given in the reference Table 3-14. For instance, for the free-free boundary conditions the mode shape factors are

BELLOWS AND LINERS

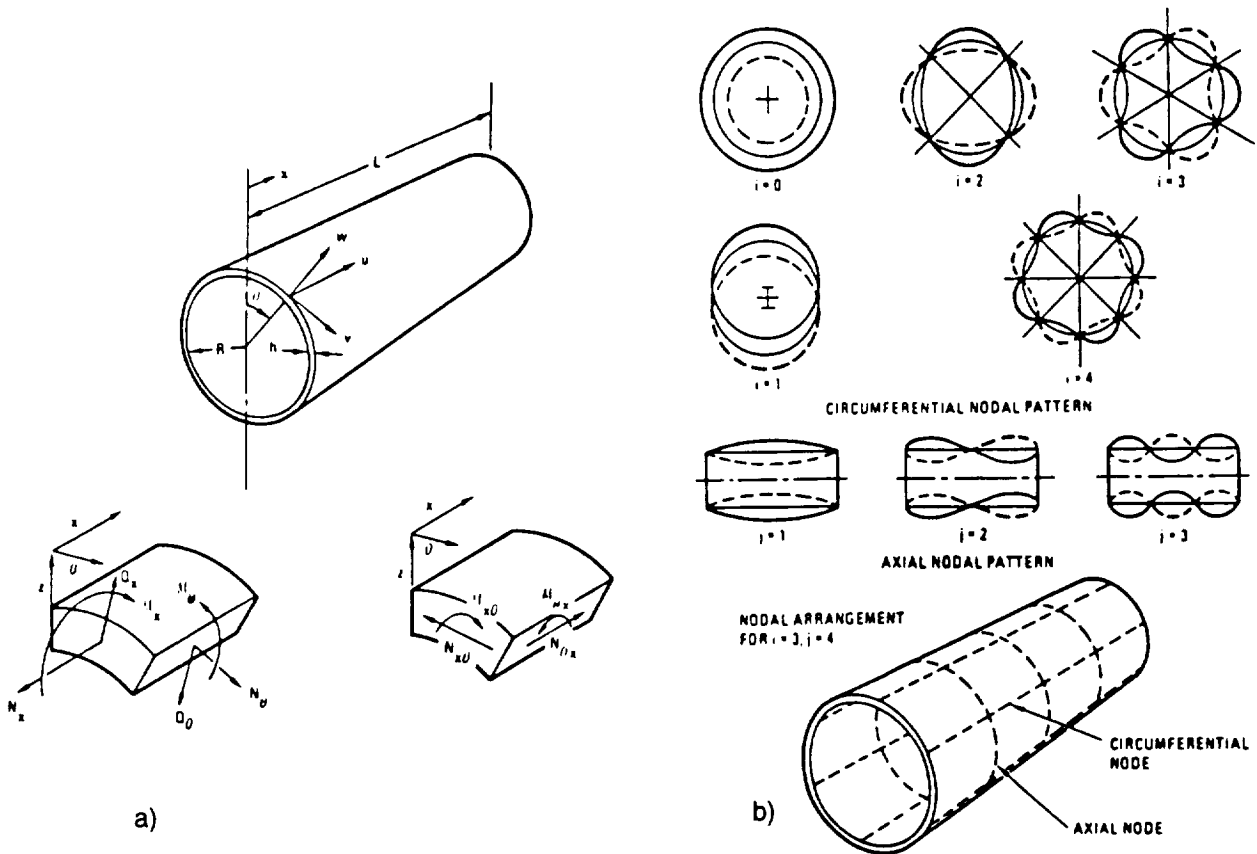


Figure 3-84. a) Coordinate System, Shell Element, Midsurface Deformations (u, v, w), and stress resultants (N, M, Q). The stresses σ_{xx} , $\sigma_{\theta\theta}$ and $\sigma_{x\theta}$ are parallel to N_x , N_θ , and $N_{x\theta}$, respectively; u is the axial deformation, v is the circumferential deformation, and w is the radial deformation. b) Nodal Patterns for a Simply Supported Cylinder Without Axial Constraints.

Table 3-14. Formulas for Parameters α_1 and α_2

| Boundary Conditions | Formula (a) for α_1 | Formula (a) for α_2 |
|---|---|---|
| 1. Free-free | $\frac{\sigma_j}{\lambda_j} (\sigma_j \lambda_j - 2)$ | $\frac{\sigma_j}{\lambda_j} (\sigma_j \lambda_j + 6)$ |
| 2. Free-pinned | $\frac{\sigma_j}{\lambda_j} (\sigma_j \lambda_j - 1)$ | $\frac{\sigma_j}{\lambda_j} (\sigma_j \lambda_j + 3)$ |
| 3. Clamped-free | $\frac{\sigma_j}{\lambda_j} (\sigma_j \lambda_j - 2)$ | $\frac{\sigma_j}{\lambda_j} (\sigma_j \lambda_j + 2)$ |
| 4. Clamped-pinned | $\frac{\sigma_j}{\lambda_j} (\sigma_j \lambda_j - 1)$ | $\frac{\sigma_j}{\lambda_j} (\sigma_j \lambda_j - 1)$ |
| 5. Clamped-clamped | $\frac{\sigma_j}{\lambda_j} (\sigma_j \lambda_j - 2)$ | $\frac{\sigma_j}{\lambda_j} (\sigma_j \lambda_j - 2)$ |
| 6. Pinned-pinned, sliding-sliding, sliding-pinned | 1/2 | 1/2 |

BELLOWS AND LINERS

$$\alpha_1 = \frac{\sigma_j}{\lambda_j}(\sigma_j \lambda_j - 2)$$

$$\alpha_2 = \frac{\sigma_j}{\lambda_j}(\sigma_j \lambda_j + 6)$$

and σ_j and λ_j are eigen-function parameter and eigenvalue of the beam. The natural frequencies are then obtained by

$$f_{ij} = \frac{\lambda_{ij}}{2 \pi R} \sqrt{\frac{E}{\mu(1-\nu^2)}}$$

where the frequency parameters are given by Sharma⁴ as

$$\lambda_{ij}^2 = \frac{(a_{11}a_{22}a_{33} + 2a_{12}a_{13}a_{23} - a_{11}a_{23}^2 - a_{22}a_{13}^2 - a_{33}a_{12}^2) i^4}{(a_{11}a_{22} - a_{12}^2)(\beta_j^2 \alpha_2 + i^2 + i^4)}$$

where $i = 2, 3, 4, \dots; j = 1, 2, 3, \dots$. The parameters are given by

$$a_{11} = \beta_j^2 + \frac{1}{2}(1+k)(1-\nu) i^2 \alpha_2$$

$$a_{12} = \nu i \beta_j \alpha_1 - \frac{1}{2}(1-\nu) i \beta_j \alpha_2$$

$$a_{13} = \nu \beta_j \alpha_1 + k \beta_j \left[-\beta_j^2 + \frac{1}{2}(1-\nu) i^2 \alpha_2 \right]$$

$$a_{22} = i^2 + \frac{1}{2}(1+3k)(1-\nu) \beta_j^2 \alpha_2$$

$$a_{23} = i + k \beta_j^2 \left[\nu \alpha_1 + \frac{3}{2}(1-\nu) \alpha_2 \right]$$

$$a_{33} = 1 + k \left[\beta_j^4 + (i^2 - 1)^2 + 2 \nu i^2 \beta_j^2 \alpha_1 + 2(1-\nu) i^2 \beta_j^2 \alpha_2 \right]$$

and

$$\beta_j = \frac{\lambda_j R}{L}, \quad k = \frac{h^2}{12 R^2}$$

Thus, an estimate of the liner shell frequencies can be made.

⁴(Sharma, C. B., "Simple Linear Formula for Critical Frequencies for Cantilevered Cylindrical Shells," J. Sound Vib. 55, 467-471, 1977.

3.10 Valves and Gates

Catastrophic failure of valves and gates are a relatively rare occurrence. Most common valve problems are associated with acoustics generated during valve oscillation and excessive wear of valve trim. Weaver¹, in a well written exposition on valve vibration, investigates valves operating at small openings and proposes three categories of mechanisms for valve motion due to fluid interaction. These categories are:

- 1) Jet flow - inertia mechanism,
- 2) Turbulence, and
- 3) Acoustic resonance.

Jet Flow - Inertia Induced Vibrations

The jet flow - inertia induced valve vibrations require a high velocity coherent flow through the valve orifice. Valve movement induces pulses in the fluid flow and subsequent force changes on the valve surface. The motion of the valve structural surface is perpetuated by the hysteresis in the fluid inertia. The motion is not simple harmonic. However, as Weaver states, when the inertia of the fluid is small, the oscillations are more nearly simple harmonic. The opening time for the oscillating valve is dominated by the elastic valve restraint and the closing time is dominated by the fluid forces acting on the valve. Increasing the valve restraint stiffness can result in a decrease in vibration frequency since the opening time will be reduced yet the closing time can be significantly increased because of the relative increase in the elastic restraining force as compared with the dynamic fluid closing force.

The static plug valve characteristics, Figure 3-85, where the flow tends to close the valve, illustrate valve oscillation at small openings. The static closing force for the valve is given by,

$$\rho \Delta H A_v \quad (3.10.1)$$

where ρ is the fluid density, A_v is the effective cross-sectional area of the valve, and ΔH is the hydrostatic head across the valve. For a given valve restraining stiffness, k , there is an initial zero load valve opening, x_0 , such that the restraining force balances the static fluid closing force, i.e.

$$k x_0 = \rho \Delta H A_v \quad (3.10.2)$$

For combinations of k and x_0 below this equilibrium position, the valve will be held closed against the seat and values above will not permit closure under static conditions. Under dynamic conditions in the region above the static characteristic, the fluid inertia along with the reduction of fluid flow creates sufficient dynamic head to close the valve. When the fluid comes to rest, the dynamic head reduces and the valve opens. In the region below the static characteristic, the static head is sufficient to hold the valve closed. However, the sudden valve closure causes pressure waves which tend to unseat the valve long enough to re-establish flow around the open valve.

¹Weaver, D.S. " *Flow Induced Vibrations in Valves Operating at Small Openings* ", Practical Experience with Flow-Induced Vibrations, Editors E. Naudascher and D. Rockwell, Springer-Verlag, 1980, p.305-316.

VALVES AND GATES

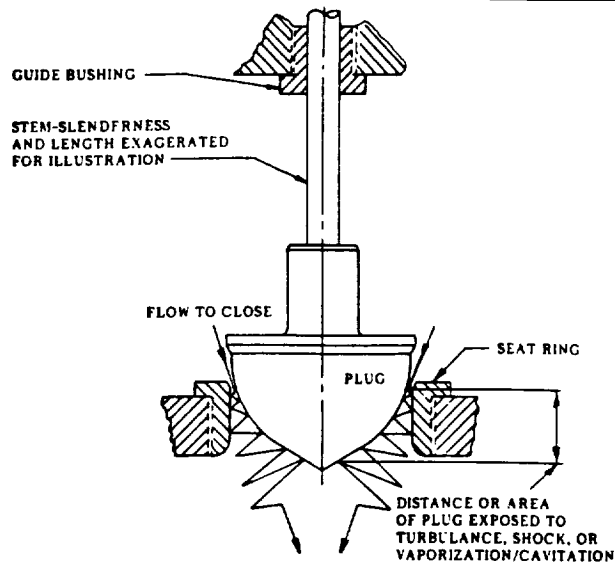


Figure 3-85. Static Plug Valve Characteristics

The effect of fluid inertia is to delay re-establishing the flow while the valve is opening and to maintain the flow while the valve is closing. Weaver and Ziada² have developed a theoretical model for vibrations in valves operating a small openings where the flow tends to close the valve. Kolkman³ has modeled vibration due to flow phenomena for gates and seals operating a small openings. Assuming the fluid discharge varies linearly with valve displacement, Kolkman's equations produce conservative estimates of the stability threshold for valves given that the mass of fluid in the pipe is large as compared to the effective mass of the valve.

Turbulence Induced Vibrations

Pressure fluctuations due to turbulence buffeting as well as direct flow impingement on internal valve components may cause damaging mechanical vibrations. These vibrations are induced by broadband random pressure or impinging velocity fluctuations. The greatest energy levels are in the lower frequency range. Lateral plug motion between the valve guide and the sealing surfaces is the most common result of turbulence buffeting. This motion has the effect of re-establishing the fluid flow to perpetuate the oscillatory behavior of the valve. Lateral motion can be excited at the plug first bending mode⁴ or higher frequencies, where the first bending mode can be approximated using

$$\omega_n = 0.159 \sqrt{\frac{k}{m}}$$

Flow instabilities, predominantly axial, involve pneumatical cylinder and controller hunting, also, usually in the adverse pressure gradient portion of plug travel (see Figure 3-86).

²Weaver, D.S. and S. Ziada, "A Theoretical Model for Self-Excited Vibrations in Hydraulic Valves and Seals", ASME PVP Conference, San Francisco, Ca. June, 1979.

³Kolkman, P.A., "Flow Induced Gate Vibrations", Ph.D. Dissertation, Delft University of Technology Publication 164, 1976.

⁴Illing, H., "Plug Vibrational Tendencies of Top Guided Throttling Control Valves," Second International Conference on Developments in Valves and Actuators for Fluid Control, Paper D1, Manchester, England, March 28-30, 1988.

VALVES AND GATES

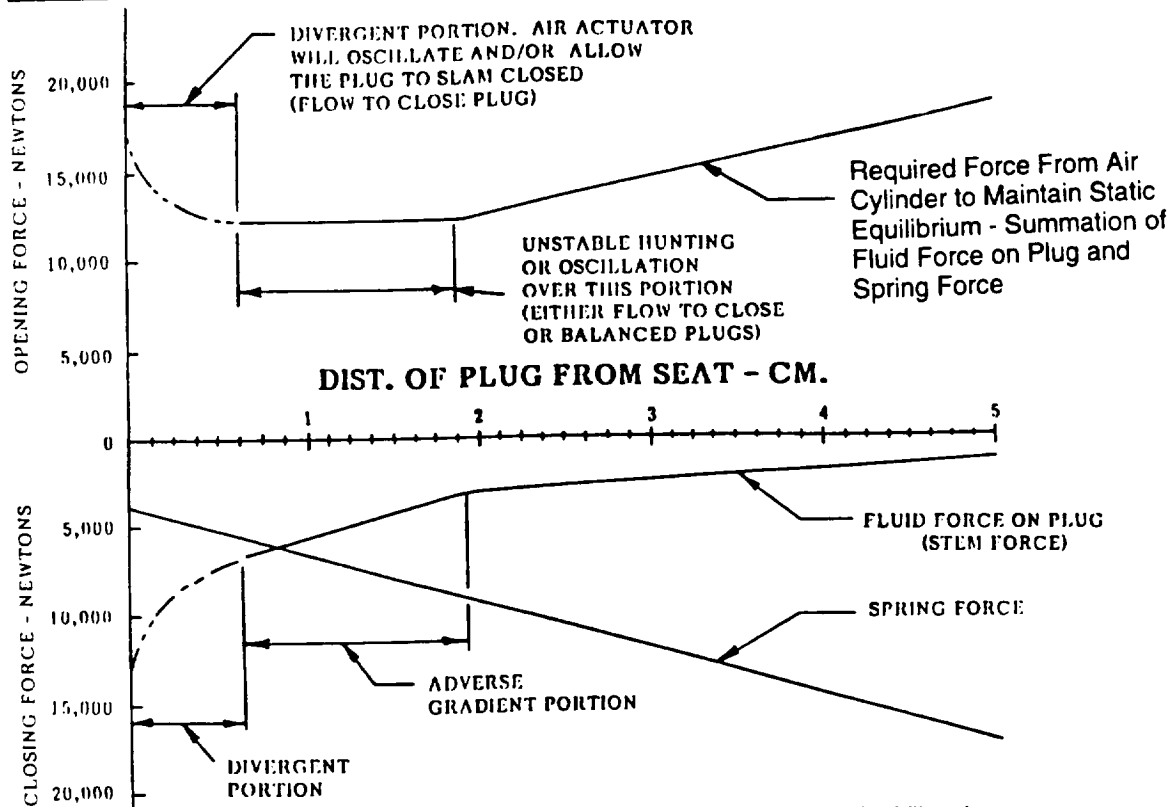


Figure 3-86. Forces That Can Create Axial Instability and/or Vibration in a Flow to Close Pneumatically Actuated Control Valve.

Acoustically-Induced Vibrations

The main problem with acoustically-induced vibrations involves coupling of flow induced oscillations with natural frequency of acoustic resonators in the system. Vortex shedding from the valve is a common generator of acoustic oscillations as is the oscillation produced by the flow over a cavity and flow impingement on a surface or edge. When fundamental pipe modes coincide with pipe bending modes a resonant condition occurs and the magnitude of frequency amplification can be dangerous. The section of the basic principles describing EFO oscillations details this type of acoustic generators and resonators (see p. 2.7.1).

Valve Whistling

Ziada⁵ investigated the whistling of a thermostatic radiator valve. Thermostatic radiator valves can produce unpleasant whistling sounds (1 to 6 kHz). While it was normally sufficient to change the setting of a valve in order to stop the whistling, this same adjustment in another building could result in re-initiation whistling. The damping in the hydraulic system was small and it was possible to vary the acoustic frequency in the water by changing the piping length. It was shown that the whistling sounds are caused by the excitation of an acoustic resonance in the hydraulic system, and its feedback to the vortex shedding in the valve.

An essential step to avoid the whistling is to decrease the coupling between the vortex shedding and the acoustic resonance oscillation. The loudness of the sounds can be decreased

⁵ Ziada, S., U. Bolleter, and E. Zahnd, "On the Whistling of Thermostatic Radiator Valves", Sulzer Technical Review 4/1983.

VALVES AND GATES

by rounding off the edges of the valve disk and valve body. Denticulation of the valve disk in the form of radial grooves brings about a further reduction of the whistling. The roundness of the seal also aids in curing oscillations at small valve strokes. Placing a plate immediately in front of the valve seat may also have a positive vibration reduction effect since the orifice then induces greater and coarser turbulence and coherent waves after the valve are precluded.

Gate Vibration

Gate valves, Figure 3-87, are usually used either fully open or fully closed but experience transient loading conditions during opening or closing. Martin and Naudascher⁶ investigated gate flow instability for a high gate with an extended lip. As the gate is lowered, the ratio between the opening and the gate width is changing as well as the ratio between the actual opening, and the extended lip of the gate. Fluctuations occur when the flow around the gate experiences intermittent separation. At certain combinations the gate displays pressure fluctuations resulting from intermittent separation that may be detrimental to the gate integrity.

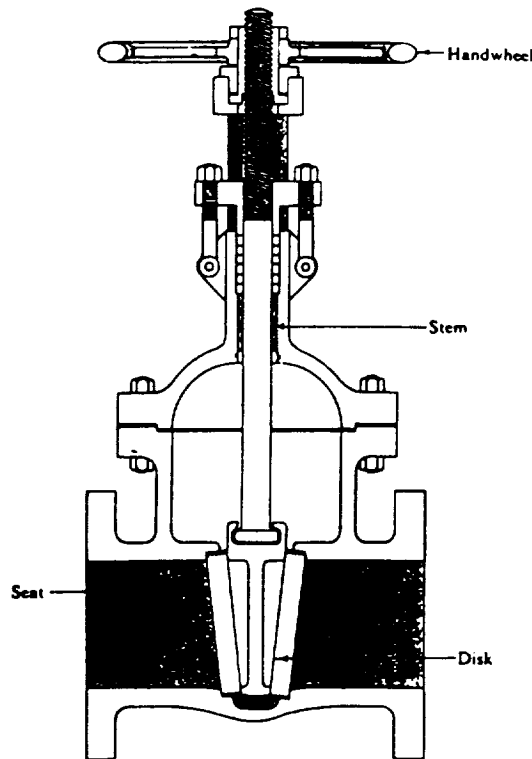


Figure 3-87. Typical Gate Valve.

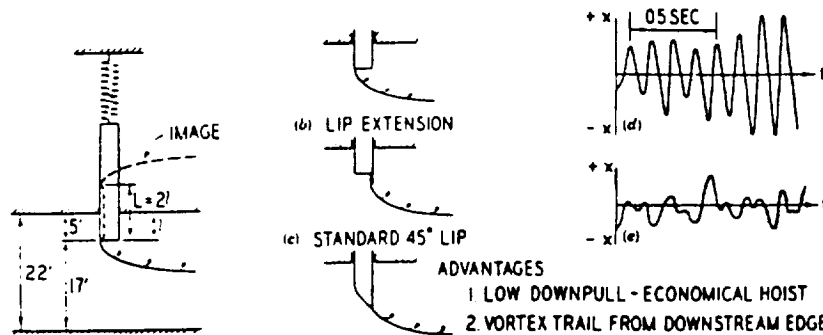
Campbell⁷ investigated exciting forces on hydraulic structures and gates. Hydraulic model studies of a mass on an elastic suspension, Figure 3-88, have been found useful in a study of exciting forces. Model tests displaying a vortex trail from a partially open flat bottom gate have produced vibrations and/or resonance when the forcing frequency is approximately 99% of the natural frequency of the plate. The Strouhal number for a flat plate normal to the flow was found to be approximately 1/7.

⁶ Martin and Naudascher

⁷ Campbell, F. B. et al "Vibration Problems in Hydraulic Structures," Vol. 127, Part I Paper No. 3282, ASCE Transactions, 1962

VALVES AND GATES

Various lip extensions from the downstream edge were tested. The flat bottom gate and the lip extension schemes are shown in Figure 3-88 (a) and (b). Typical oscillograms translated in terms of vertical displacement from the accelerometer records are shown in the reference Figure 3-88 (d) and (e). A fairly regular motion of 8 Hz may be seen in Figure 3-88 (d), whereas no such regularity is shown for the case of a lip extension. No tendency for vibration was found for the 45° gate lip and consequently, the 45°-lip gate became standard. In addition, the reservoir-gate conduit usually has an organ pipe mode of open-close ends. Let L be the distance between the intake from the reservoir and the gate, and a be the speed of sound, then the natural frequency of this mode is $a/(4L)$.



(a) Flat Bottom Gate Vortex Trail (b) Standard 45° Lip
Figure 3-88. Gate Valve Flow Modeling

Strouhal number data

Strouhal number data presented in the reference higher than the foregoing value of 1/7 may not be applicable to completely submerged flow paths. Strouhal number data in the range of 0.12 to 1/7 exist in the reference, but much higher values also documented in the reference. No detail description in the flow velocity used in the Strouhal number ($= f b / V_0$) was found. Here b is the gate opening and V_0 is the flow velocity. Flow velocity with or without flow blockage corrections at the gate can yield completely different data ranges.

Valve Struts

Figure 3-89 shows valves with 4 vanes (or struts) and with 6 vanes (or struts). The vibration mode of the 4-vane valve vibrates in a fundamental mode, while the 6-vane valve vibrates in a secondary mode of higher frequency, and the frequency ratio is 2.82. In the case of valve plates, the amplitude associated to the secondary mode is much smaller. Howell-Bunger recommended that the 5-vaned valve plate can produce even higher frequency modes and help in maintaining the intact welding seams on the valve plate.

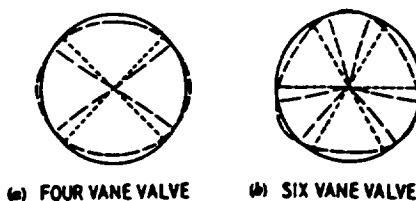


Figure 3-89. Howell-Bunger Valve Vibration.

SURGE TANKS AND SLOSHING

3.11 Surge Tanks and Sloshing

Surge Tanks

Surface wave effects may exist in a system where a surge tank is used. The surge tank is to suppress undesirable pressure wave fluctuations, however, the surface wave effects demand analysis. Ziada and Rockwell investigated subharmonic oscillations of a mixing layer-wedge system associated with free surface effects. An unstable mixing layer, in conjunction with free surface wave effects could give rise to well-defined subharmonic oscillations of the vortex shedding frequency provided certain streamwise phase conditions are satisfied. The investigation dealt with the interaction between a mixing layer impinging on a wedge and a traveling free surface wave. They first showed that there existed highly coherent oscillations in the absence of free surface effects. They then found that the simultaneous existence of a free surface wave and unstable oscillations of the mixing layer impinging on the wedge can lead to a five-fold increase in force induced at the impingement.

Their experimental test section consisting of a splitter plate producing streams having velocities U_1 and U_2 , a 30° wedge and a strain gage system for force measurement. The flow conditions were $U_1 = 18.35$ cm/s, $U_1/U_2 = 2.85$, momentum thickness, $\theta = \theta_1 + \theta_2$ ($\theta_1 = 0.62$ mm, $\theta_2 = 0.68$ mm), $Re = (U_1 - U_2) \theta/\nu = 157$, wedge submerged depth, $h_1/\theta_1 = 103$, tunnel depth, $h_2/\theta_1 = 365$, and $15 < L/\theta < 150$. In the experiments, all the parameters were held constant, except the impingement length L/θ , which was varied to allow transition between Case A (self-sustained oscillation) and Case B (with surface wave effects).

They found that the expression of Lamb (1932) for propagation speed of surface wave can be used to calculate the frequency of the surface wave,

$$C_{sw} = \sqrt{\frac{g \lambda_{sw} \tanh \frac{2\pi h}{\lambda_{sw}}}{2\pi}}$$
$$f = \frac{C_{sw}}{\lambda_{sw}}$$

Since $\lambda_{sw} = 2L$, $h = h_1 = 6.39$ cm, $L = 18.4$ cm, the calculated frequency is 1.84 Hz which is within 7% of the measured. By varying L , the measured frequency also agreed well to the calculated when surface wave effects dominate

In the self-sustained oscillation (Case A), the vortex-wedge interaction has the fundamental frequency of vortex formation (b). In the surface wave affected oscillation (Case B), there are pairs of vortices impinging on the wedge, the interaction is at the subharmonic (b/2) of vortex formation same as the surface wave frequency. Case B oscillations exist at larger impingement distance, belong to stage V and have higher instability and larger force amplitudes than the Case A oscillations which belong to stage III and IV.

Fluid Container Sloshing

Mclver (1989) investigated sloshing frequencies of fluid containers. In the paper the two-dimensional sloshing of a fluid in a horizontal circular cylindrical container and the three-dimensional sloshing of a fluid in a spherical container are considered. The linearized theory of water waves is used to determine the frequencies of free oscillations under gravity of an arbitrary amount of fluid in such tanks. Special coordinate systems are used and the problems are

SURGE TANKS AND SLOSHING

formulated in terms of integral equations which are solved numerically for the eigenvalues. The sloshing frequencies were presented for a range of fill-depths of the containers.

The natural frequencies of oscillation of fluid in a partially filled container are important design parameters. For instances, the sloshing of fuel in the tanks of an aircraft or space vehicle could seriously affect the performance of the control systems and so it is desirable to avoid external excitation at the natural oscillation frequencies of the fluid. Mathematically, the fluid system may be dealt with as follows. The velocity potential ϕ for the small time-harmonic irrotational motion of an inviscid, incompressible fluid must satisfy Laplace's equation in the fluid domain, having zero normal derivative at the solid walls of the container and satisfy the linearized free-surface condition

$$\frac{\partial \phi}{\partial z} + K\phi = 0$$

Here z is a coordinate measured vertically downwards with origin at the mean level of the free surface and the frequency parameter

$$K = \frac{\omega^2}{g}$$

where

ω = circular frequency of the oscillation
 g = gravitational acceleration

For a cylindrical container the Cartesian coordinates (x, z) can be replaced by bipolar coordinates (α, β) by the transformation

$$x + iz = a \tanh \frac{\alpha + i\beta}{2}, \quad -\infty < \alpha < \infty, \quad \pi < \beta \leq \pi$$

The transformed Laplace's equation within the fluid region is

$$\frac{\partial^2 \phi}{\partial \alpha^2} + \frac{\partial^2 \phi}{\partial \beta^2} = 0 \quad (-\infty < \alpha < \infty, \quad 0 < \beta < \beta_0)$$

and the zero flow condition at the solid wall is

$$\frac{\partial \phi}{\partial \beta} = 0 \quad (\beta = \beta_0)$$

Note that on the solid wall

$$\beta = \beta_0 = \cos^{-1} \left(1 - \frac{d}{c} \right)$$

where d = depth of the liquid level
 c = inner radius of the cylindrical tank

and the free surface condition yields

$$\frac{\partial \phi}{\partial \beta} + \frac{\lambda \phi}{1 + \cosh \alpha} = 0 \quad (\beta = 0)$$

SURGE TANKS AND SLOSHING

where $\lambda = K a =$ eigenvalue of the problem
 $a =$ half width of the free surface

The possible modes of oscillation are either symmetric or antisymmetric about $a = 0$. Solution of the above Laplace's equation can be written in integral form for both symmetric and antisymmetric modes. By applying Fourier cosine and sine transforms with respect to a , one may determine the eigenvalues K for the existence of nontrivial solutions. One should refer to the paper for further detail in the math manipulation. In the paper, numerical solution is then described and the results are given in a tabular form for the first four modes. For the first modes, values are included in the following:

Eigenvalues $K c$ for cylindrical container (given as $K a$ for $d/c = 2$)

| d/c | Antisymmetric | Symmetric |
|-----|-----------------|-----------|
| 0.2 | $K c = 1.04385$ | 2.92908 |
| 0.4 | 1.09698 | 2.89054 |
| 0.6 | 1.16268 | 2.88924 |
| 0.8 | 1.24606 | 2.93246 |
| 1.0 | 1.35573 | 3.03310 |
| 1.2 | 1.50751 | 3.21640 |
| 1.4 | 1.73463 | 3.53751 |
| 1.6 | 1.12372 | 4.14328 |
| 1.8 | 3.02140 | 5.62694 |
| 2.0 | $K a = 2.00612$ | 3.45333 |

Note that as d/c approaches 2, $K a$ is finite but K itself becomes unbound. Numerical examples are given here for a half-filled 1 ft radius tank. From above table, $d/c = 1$, $c = 1$ ft, and $K c = 1.35573$ for antisymmetric mode and $K c = 3.03310$ for symmetric mode. Since $K = \omega^2/g$, $f = \omega/(2 \pi) = 1.051$ Hz for antisymmetric mode and $f = 1.572$ Hz for symmetric mode.

Similar theoretical and numerical approaches were presented for the spherical tank in the paper. Numerical results are given in a tabular form for the first four modes and four azimuthal wave numbers. As an example, results for the fundamental mode are included here in the following table for the azimuthal wave number $m = 0$ and $m = 1$:

Eigenvalues $K c$ for spherical container (given as $K a$ for $d/c = 2$)

| d/c | $m = 0$ | $m = 1$ |
|-----|-----------------|---------|
| 0.2 | $K c = 3.82612$ | 1.07232 |
| 0.4 | 3.70804 | 1.15826 |
| 0.6 | 3.65014 | 1.26251 |
| 0.8 | 3.65836 | 1.39239 |
| 1.0 | 3.74517 | 1.56016 |
| 1.2 | 3.39812 | 1.78818 |
| 1.4 | 4.30102 | 2.12320 |
| 1.6 | 5.00753 | 2.68635 |
| 1.8 | 6.76418 | 3.95930 |
| 2.0 | $K a = 4.12130$ | 2.75475 |

Note that as d/c approaches 2, $K a$ is finite but K itself becomes unbounded. Numerical examples are given for a half-filled 1 ft radius tank. From above tables, $d/c = 1$, $c = 1$ ft, and $K c = 3.74517$ if $m = 0$, $K c = 1.56016$ if $m = 1$. Since $K = \omega^2/g$, $f = \omega/(2 \pi) = 1.747$ Hz for $m = 0$ mode, $f = 1.128$ Hz for $m = 1$ mode.

SURGE TANKS AND SLOSHING

Compressor Surge

Williams and Huang(1989) studied the stabilization of compressor surge. The paper describes the stabilization of compressor surge by an active method. It is known that surge follows when small disturbances grow in an unstable compression system, and that small growth can be modeled through a linear stability analysis. An active element was introduced to counter any tendency to instability and the control law governing the active stabilizer was determined from linear theory. The authors followed the suggestion put forward by Epstein et al. (1986). The theory was verified in an experiment on a compressor system whose plenum volume was controlled. Suppression of the flow instability was achieved by switching on the controller and the compressor was made to operate stably on a part of its characteristics beyond the nature stall line. Furthermore the controlled compressor was much more resilient to external disturbances than in the nature case. The controller was even effective on deep surge.

The paper showed a schematic illustration of the compressor system denoted inlet, rotor blades, plenum and outlet. There were equations of motion for the plenum pressure, the inlet and outlet ducts. These equations dealt with inertia terms, flow resistance in the compressor duct, pressure rise due to compressor, pressure drop across the outlet throttle, and the pressure difference between the plenum and the ambient. They found an empirical curve-fit for the mean pressure rise as a function of mass flow rate:

$$\text{mean pressure rise} = f_1(\bar{Q}_1) = \frac{1}{2} \rho U^2 \cdot \left\{ 0.045 \tan^{-1} [120 (\bar{\phi}_1 - 0.052)] + 1.18 + 0.85 \bar{\phi}_1 - 7.2 \bar{\phi}_1^2 + 4.7 \bar{\phi}_1^3 \right\}$$

where the nondimensional mass flow rate

$$\bar{\phi}_1 = \frac{\bar{Q}_1}{\rho A_c U}$$

and

\bar{Q}_1 = mean mass flow rate

ρ = mean air density

A_c = cross-sectional area of inlet duct

U = speed of the compressor blade tip

They found the Helmholtz resonance frequency for their system to be 37 Hz by measuring the system response to a pressure impulse. This frequency can also be calculated by

$$\omega_H = a (V \chi_c)^{\frac{1}{2}}$$

provided that the inertia of the flow in the throttle is negligible, where

$\omega_H = 2 \pi f_H$ = circular frequency of Helmholtz resonance

a = speed of sound = 340 m/s

V = plenum volume = $5.5 \times 10^{-3} \text{ m}^3$

χ_c = compressor parameter

\approx compressor length to diameter ratio = $3.9 \times 10^3 \text{ m}^{-1}$

SURGE TANKS AND SLOSHING

They showed that the equations of motion have solution of the form, $\exp(s t)$ with the characteristic equation

$$s^3 + a_2 s^2 + a_1 s + a_0 = 0$$

where

$$a_0 = (\lambda B \Gamma + \mu - B \Psi')$$

$$a_1 = 1 + \lambda + B \lambda \Gamma (\mu - B \Psi')$$

$$a_2 = B \lambda \Gamma + (\mu - B \Psi')$$

with

$$\lambda = \frac{\chi_c}{\chi_t}$$

χ_t = inertia parameter for the throttle duct

≈ length to diameter ratio of the outlet duct

$$B = \frac{U}{2 \omega_H A_c \chi_c}$$

$$T(\phi_2) = \frac{f_2(Q_2)}{\frac{1}{2} \rho U^2}$$

$$\Gamma = \frac{\partial T}{\partial \phi_2}$$

$$\phi_2 = \frac{Q_2}{\rho A_c U}$$

Q_2 = mass flow rate at outlet duct

$f_2(Q_2)$ = pressure drop at the outlet duct

$$\Psi = \frac{f_1(Q_1)}{\frac{1}{2} \rho U^2} = \text{pressure rise at compressor inlet}$$

$$\Psi' = \frac{\partial \Psi}{\partial \phi_1}$$

$$\mu = \frac{\sigma_c}{\omega_H \chi_c}$$

SURGE TANKS AND SLOSHING

$\sigma_c(Q_1 - \bar{Q}_1)$ = an experimentally determined term prescribing
the flow resistance in the compressor duct

The Routh-Hurwitz stability criterion gives necessary and sufficient conditions for the real parts of all roots to be negative as

$$a_0 > 0, a_2 > 0, a_1 a_2 > a_0$$

These constraints define the stable range of the compression system. By substituting the measured values and the functions into these criteria, the linear instability point at which these criteria will just be broken and the compression system will surge can be predicted. They also define the throttle characteristic corresponding to the instability point as the surge boundary. They then carried out experiments to measure the surge onset point and compared the measured result with the above predicted. Reasonable agreement was found. In a numerical simulation and some experimental measurement, they found that the surge frequencies are somewhat lower than the Helmholtz resonance frequency.

They introduced a controller consisting of an externally induced control force and a surface A3 which is part of a mass-spring system responding to the unsteady pressure fluctuation in the plenum: its displacement produces a volumetric change in the plenum. The mass in the plenum is thus changed accordingly. The displacement was found to be approximately proportional to the driving force. The control force was generated by a feedback system which processed the signal detected by a pressure sensor located in the plenum.

Results indicated that active stabilization of compressor surge has been achieved in their experiments; the controller was able to alter the system damping and the resonance frequency. The results showed that the compression system can be effectively stabilized by switching on the controller before or even after surge occurs. Their experiments indicated that the linear controller is effective even in this nonlinear aerodynamic case, and they believe that the stability and the performance of compression systems generally could be greatly improved through active control techniques of this type.

Greitzer (1981) made a rather complete review on the stall phenomena in turbomachines. Concerning axial compressors, large vibrating stresses in the compressor blades may be induced at lower-than-design flowrates by what is called rotating stall. When that occurs, one or more 'stall cells' (i.e., regions of separated flow) travel around the compressor annulus in the direction of the compressor with a speed close to one-half of the compressor speed, Figure 3-90. Causes of this off-design phenomenon is discussed by Naudascher (1991).

In centrifugal pumps and compressors, Jansen (1964) classifies the rotating stall into three types: a) rotating stall associated with large incidence angles in the impeller; b) rotating stall in radial-vaned diffusers; and c) rotating stall in vaneless pumps or diffusers associated with a decrease in radial velocity component that causes the angle between velocity vector and radius to exceed a limiting value. In summary, knowledge of flow-induced vibration can be very important for successful design of turbomachinery.

SURGE TANKS AND SLOSHING

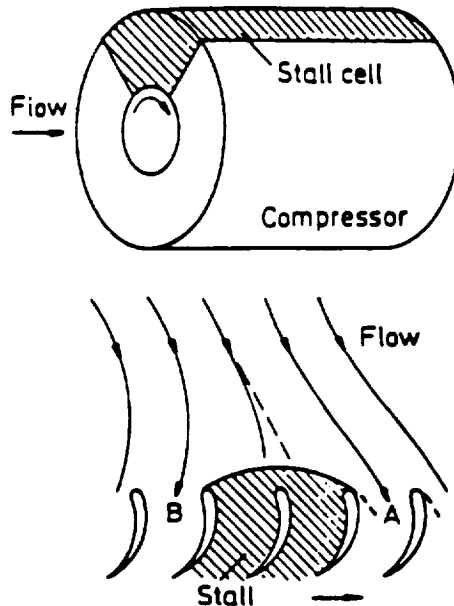


Figure 3-90. Illustration of Rotating Compressor Stall.

Piping systems containing compressors and surge tanks are generally designed with frequency response characteristics built into guard against fluid oscillations at particular critical frequencies. Anti-slosh baffles are used effectively to prevent sloshing in partially filled liquid containers. Compressor surge characteristics can be especially sensitive to the compressor inlet mean flow distribution and to the turbulence generated due to any inlet flow distortion present. For a more detailed treatment of compressor surge phenomena, the reader is referred to the literature on aircraft engine and engine-inlet compatibility.

AVOIDANCE AND CORRECTIVE MEASURES

4. Avoidance and Corrective Measures

This discussion is organized according to geometric and flow element modifications which alter the character of the flow/structural system.

Evidence of High Cycle Fatigue Cracking

Flow interaction with the structure under high operating pressures and performance margins have led to some cases of high cycle fatigue cracking. Specific examples are the 4 kHz SSME LO2 injector tee splitter vane "buzz" that was eliminated by scalloping the leading edge and beveling the trailing edge of the vane; shields added to some of the SSME LO2 injector posts; filling the SSME Main Oxidizer Valve (MOV) cavity eliminating a 7200 Hz anomaly, and the Apollo/Saturn AS-502 S-II engine augmented spark igniter LH2 fuel line rupture that resulted in the redesign to eliminate the bellow-type flexhoses in the original design.

4.1 Avoidance

Fatigue Reliability of Structures

Madsen¹ investigated fatigue reliability of structures. The use of lighter structures under dynamic loads increases the necessity of fatigue analysis. Prediction of fatigue life is encumbered with uncertainty in the loading process, uncertainty of the process parameters and uncertainty of the math models.

Madsen discussed the fatigue strength of tubular joints used in offshore structures. The number of stress cycles, N , under constant amplitude loading with stress range, S , necessary to cause failure is usually expressed by the S-N curve

$$\begin{aligned} N &= K S^{-3}, S > S_0 \\ &= K_1 S^{-5}, S \leq S_0 \end{aligned} \quad (4.1.1)$$

where S_0 is the stress level below which the fatigue takes place at a lower rate. The coefficients K and K_1 are empirical coefficients of the joints. Typical data of N and S are given in Figure 4-1. A conservative basic design would assume structure failure after 10^7 stress cycles for a stress level of 50 N/mm^2 and after 10^5 cycles for 240 N/mm^2 .

By assuming an exponential function for the stress range distribution, Madsen obtained an expression for a damage indicator, which has an initial value of 0 and monotonically increases to 1 at failure. A limit state function is then defined by incorporating a random variable to the damage indicator. The failure probability can be estimated based on this limit state function. Furthermore, a reliability index, β , is introduced as a measure to the failure probability, P .

$$\beta = -\Phi^{-1}(P) \quad (4.1.2)$$

An approximate curve-fit can be deduced to approximate the functional relationship

$$\log_{10}P = -0.301 - 0.338\beta - 0.152\beta^2 - 0.007\beta^3, \quad 0 < \beta < 5 \quad (4.1.3)$$

¹Madsen, H. O., "Fatigue Reliability of Marine Structures," in Sobczyk, K. (Editor), Stochastic Approach to Fatigue: Experiments, Modeling & Reliability Estimation, CISM Courses and Lectures No. 334, International Center for Mechanical Sciences, Springer-Verlag, 1993

AVOIDANCE

By knowing the time rate of stress cycle for a given stress level, one may estimate the failure probability and reliability index, β , versus time and then the expected life time of the structure.

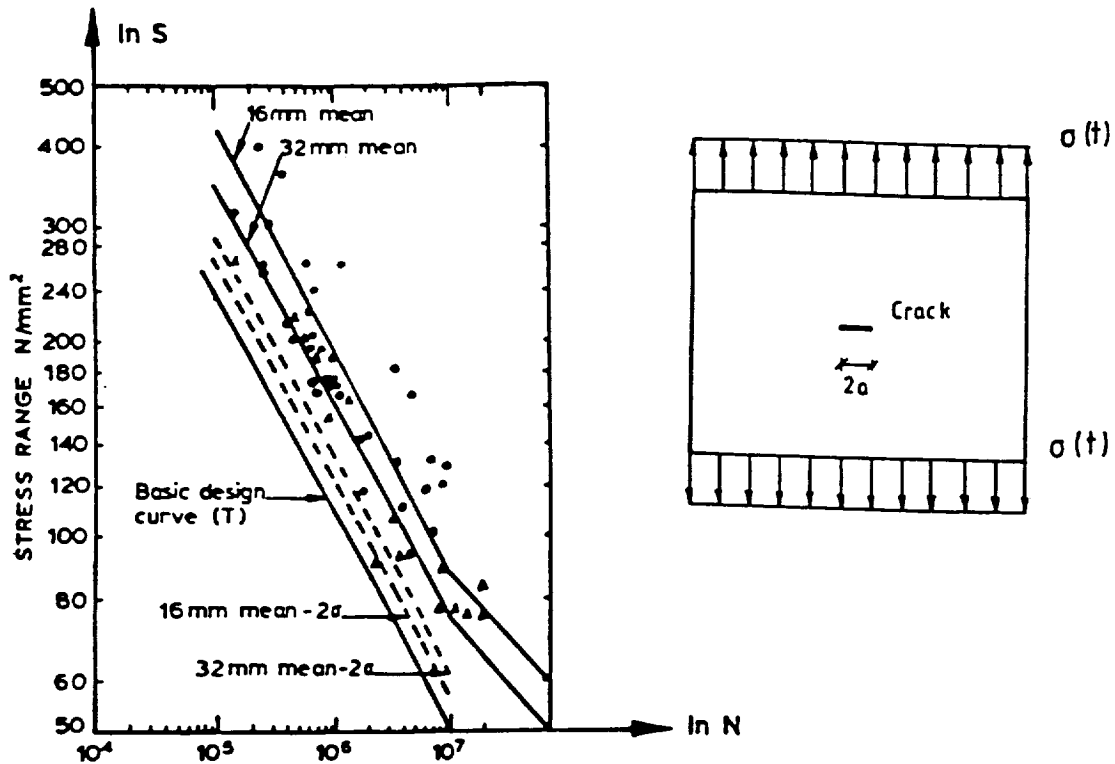


Figure 4-1. T-Curve and Fatigue Test Results

According to the reference, in a linear elastic fracture mechanics approach the increase in crack size, a , with respect to number of stress cycles, N , is related to the range of the stress intensity factor, ΔK ,

$$\frac{da}{dN} = C (\Delta K)^m \quad (4.1.4)$$

where C and m are material constants of the structure. The stress intensity factor is usually taken in the form as

$$K = \sigma Y(a) \sqrt{\pi a} \quad (4.1.5)$$

where σ is the far-field stress from the crack site and $Y(a)$ is the geometry function. In case of a through-thickness crack, the crack size is a scalar and the differential equation is written as

$$\frac{da}{Y(a) \sqrt{\pi a}} = C (\Delta \sigma)^m dN, \quad a(0) = a_0 \quad (4.1.6)$$

where a_0 is the initial crack size. Experimental data exist for crack growth under constant amplitude loading on the edges of the specimen. Figure 4-2 shows experimental results for 64 center cracked specimens made of 2024-T3 aluminum. The initial half crack length of each specimen was $a_0 = 9$ mm and the width of the panel was $2b = 152.4$ mm. The geometry function can be approximated by

$$Y(a) = \frac{1}{\sqrt{\cos(\pi a/b)}}, \quad \text{if } a/b < 0.7 \quad (4.1.7)$$

AVOIDANCE

Figure 4-3 shows the crack length as a function of N obtained by solving Equation (4.1.6) with fixed values of C , m and a_0 . Although the experimental curves resemble the model curve, they are all different, irregular and intermingling. In the experiments the only non-deterministic factor in Equation (4.1.6) is the material constant, C . An attempt was made to randomize C to better simulate the experimental data by writing

$$C = C_1/C_2(a) \quad (4.1.8)$$

where C_1 is a random variable describing random variations between mean values in different specimens, while $C_2(a)$ is a positive random process describing variations from the mean value along the crack path within each specimen. The mean value of $C_2(a)$ is one and the process was assumed to be homogeneous. The type of the process is suggested as log normal. The equation can then be numerically integrated and the results resemble the experimental data in that a) sample curves of a versus N are irregular and not very smooth but tend to cluster in a statistical trend, b) sample curves of a versus N become more smooth for larger values of a , and c) sample curves of a versus N intermingle in particular for smaller values of a . For additional details one should refer to Madsen (1993).

When crack size versus number of stress cycles under a given stress level is known, one may further estimate reliability index β versus number of stress cycles and the life time of the structure as outlined in the reference.

Fracture detection, monitoring, and control are highly developed specialties in rocket engines and propellant feed systems as well as nuclear, marine, and chemical industrial applications. Beyond the above example of probability based methods in marine structures, the reader is referred to detailed practices in the particular discipline area of interest and emphasis is placed here on avoidance of these conditions that lead to the various modes of flow/structural interaction described in this handbook.

Avoidance is taken into account in the design process in selecting geometric shapes, materials, and strength achieved through component thickness and manufacturing hardening processes. Avoidance is also taken into account in staying outside critical Reynolds number - reduced frequency ranges.

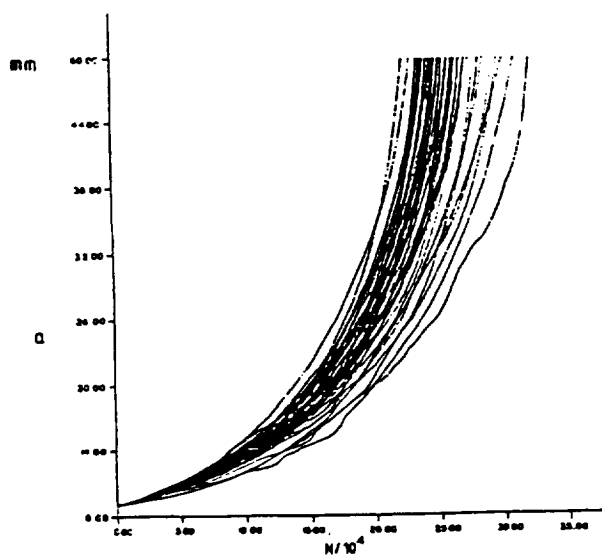


Figure 4-2. Experimental Results

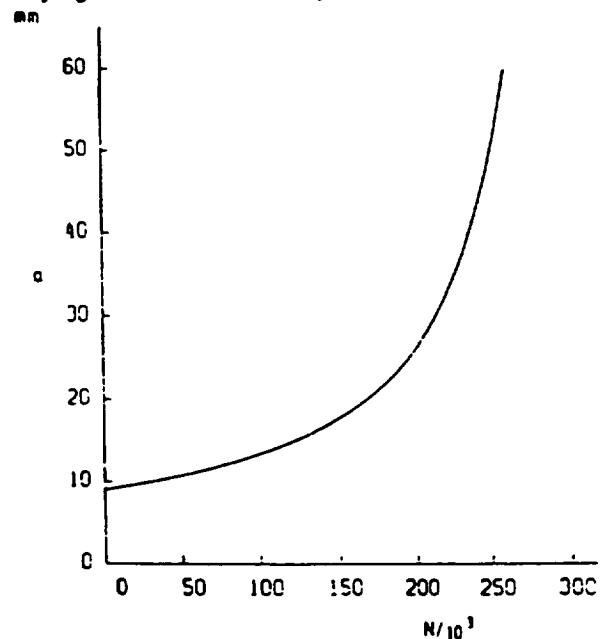


Figure 4-3. C Deterministic

4.2 Corrective Measures

The propellant feedlines in the Space Shuttle Main Propulsion System and Engines contain bellows located throughout the feedline network. Each convolute of the bellows presents a bluff shape to the flow, much like that of a cylinder. Vortex shedding from the individual convolute occurs at a Strouhal number of approximately 0.22. All Shuttle bellows have been checked and cleared for flow-induced vibrations. Resulting vibrations can be severe if the vortex shedding frequency locks in with a longitudinal natural frequency of the bellows and has occurred in the past on other vehicle systems, notably the Saturn V. The problem is very similar to vortex shedding from a cylinder except that shed vortices from each convolute may be reinforced or canceled by vortices from adjacent, or nearby convolutes depending on convolute width and pitch.

The dynamics of bellows are characterized by the number of structural modes equaling the number of convolutes with individual convolutes moving in-phase or out-of-phase with one another. The frequency of these modes are strongly affected by the fluid trapped in the convolutions. The cited reference presents analysis procedures for avoiding flow-induced vibrations of flexible lines (bellows and flexhoses). These involve using the prescribed methods for calculating a frequency range that including all the longitudinal modes. A bellows bulging, or convolute bending mode frequency is also included. Use of a Strouhal number of 0.1 (minimum) and 0.3 (maximum) provides limits of flow velocity where bellows resonance may occur.

Bellows Elimination- the Apollo/Saturn S-II Stage Engine Shutdown Occurrence

A flow-induced flow problem in the augmented spark igniter (ASI) fuel line of one engine in the AS-502 S-II Stage resulted in a premature shutdown early in the Apollo/Saturn program, April 4, 1968². It was caused by flow-induced bellows resonance in the upper flex hose. Post-flight evaluation of the telemetered data led to the conclusion that the ASI LH2 line in S-II engine number 2 failed and ultimately caused shutdown of the engine³. The LH2 flow rate through the 1.27 cm original ASI fuel line flexible hose produced flow-induced vibrations of the bellows when flow rate was as high as 0.5 kg/s and the flow velocity was 61 m/s or higher.

Flow-induced high cycle, low amplitude vibration fatigue failures of the upper NAS-260035 flexible bellows sections, Figure 4-4, were observed in a number of ground tests that followed only when the flexible link was placed in a dry-vacuum environmental test chamber. Ground tests in open air found that liquefaction of air on the outside of the bellows (caused by the cold condition of LH2 flowing through the bellows) had resulted in both fluid damping of the oscillations and changing of the flow/structural, the coupling of the assembly for engine sea level static firing. This was a significant event in the accumulation of knowledge about conditions for bellows fatigue to learn that external environment factors - liquid air and the frost trapped between the outer braid of the hose and between bellows convolutes - drastically changed the flexhose operating environment.

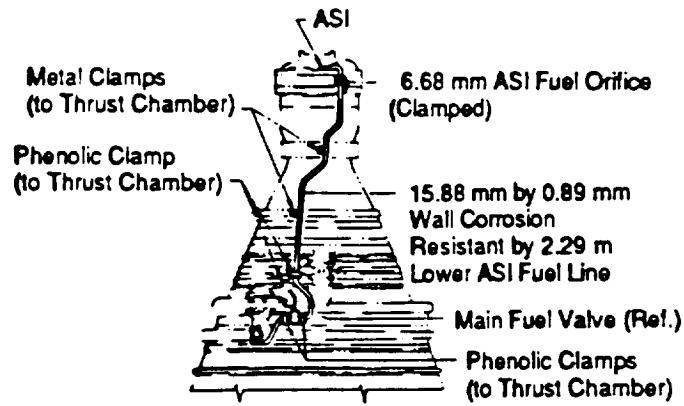
This was an important discovery for earth-to-orbit propulsion technology which fortunately did not compromise the mission, as the AS-502 orbit was successfully achieved. Numerous tests to verify a "fix" for the ASI fuel line to operate in the space environment. Options tested in this important case are shown in Figure 4-4. They were: 1) an upper ASI fuel line with a single bellows, single-braid overlap flexhose, 2) an upper ASI fuel line with a triple bellows, double-braid overlap flexhose, and the two lower flexhoses eliminated, and 3) an all "hard-line" ASI fuel line with all three flexhoses eliminated. The measurements made were ASI fuel line temperatures,

² "Saturn V Launch Vehicle Flight Evaluation Report - AS-502 Apollo 6 Mission," MPR-SAT-FE-68-3, June 25, 1968.

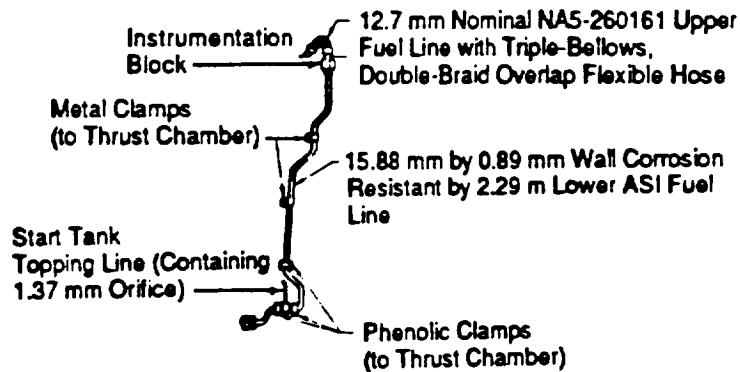
³ "J-2 Engine AS-502 (Apollo 6) Flight Report S-II and S-IVB Stages," R-7450-2, Volumes 2 and 3, June 17, 1968, Volume 4, September 13, 1968.

CORRECTIVE MEASURES

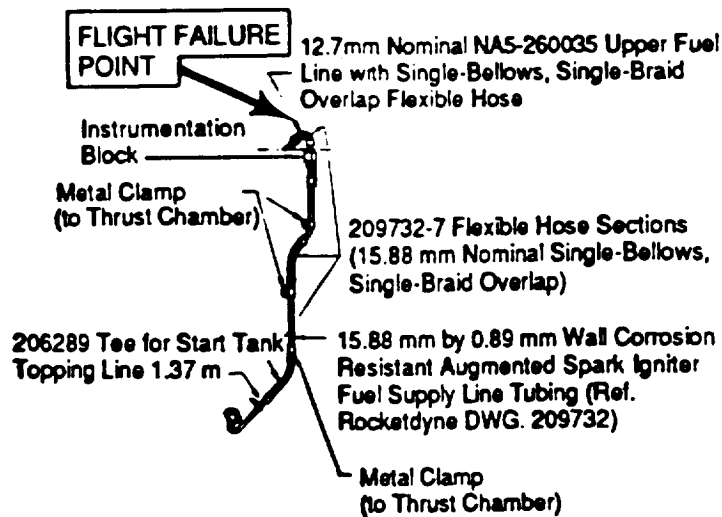
pressures, strains and accelerations. In this case the final fix was that no flexhose was needed, and all three flexhoses were eliminated from the design.



(a) Final "Fix" (No Flexhoses)



(b) Trial "Fix"



(c) Original Design

Figure 4-4. The ASI Fuel Line Bellows Were Removed From the J-2 Engine After Apollo 6

CORRECTIVE MEASURES

Addition of Flow Shields-Stiffeners to Injector LO₂ Posts

An example of successful prevention was the fix of the LO₂ posts in the SSME injector, Figure 4-5. An addition of a test-verified shield stopped the vortex-induced vibrations of the LO₂ posts. The shield apparently increased the stiffness of the posts as well as changed the flow field so that vortex shedding no longer exceeds the structure natural frequencies. This is a hot turbine exhaust gas flow mixture which is hydrogen - rich and is mixed in the fuel injector coaxial elements with pure GH₂ from the fuel feed system.

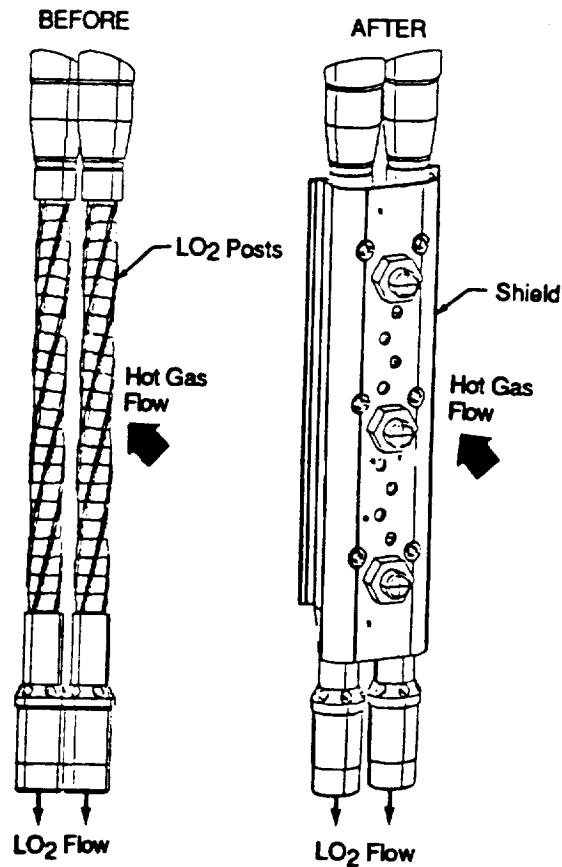


Figure 4-5. The LO₂ Post Fix in the SSME Injector

Reduce Vortex Shedding Effects - the LO₂ Inlet Tee Vanes 4 kHz Phenomenon

G. M. O'Conner and J. H. Jones⁴ reported on the SSME flow-induced vibration problem with the LO₂ inlet tee zones in the main combustion chamber inlet splitter tee/diffuser. Jones et al⁵

⁴O'Conner, G. M. and Jones, J. H., "Flow-Induced Vibrations of the SSME LOX Inlet Tee Vanes," AIAA-88-3132, AIAA/ASME/SAE/SAEE 24th Joint Propulsion Conference, Boston, Mass., July 11-13, 1988.

⁵Jones, J. H., Guest, S. H., Nesman, T. E., Matienzo, J. J. and Reed, D. K., "Acoustic, Overpressure and Unsteady Flow Phenomena Associated with the Saturn/Space Shuttle Systems: A Review of Selected Issues," presented at the Symposium on Acoustic and Dynamic Environment of Space Transportation Systems, Chatillon, France, February 1994.

CORRECTIVE MEASURES

presented a fix certification history in concise form from which a case history is exerted here. This problem was known as the "4KHz phenomenon".

In October of 1985, on SSME test 750-262, a routine hot fire test, a very high amplitude vibration response was observed on engine 2025 (P/H 4003) on several of the gimbal bearing accelerometer measurements. This was an anomalous frequency and not associated with any synchronous components of the SSME turbopumps. A power spectral density plot (PSD) as measured during 109-percent operation of the engine, is shown in Figure 4-6. This represents a very severe response at this location on the SSME. During subsequent testing, the source of this excitation was quickly located to the LO₂ inlet/tee section and main injector region of the SSME (see Figures 4-7 and 4-8). The LO₂ flow conditions at the inlet to this LO₂ tee are shown in Table 4-1. This region is an integral part of a larger section referred to as the powerhead (P/H), which consists of the LO₂ and fuel preburner chamber as well as the main combustion chamber which houses the main injector.

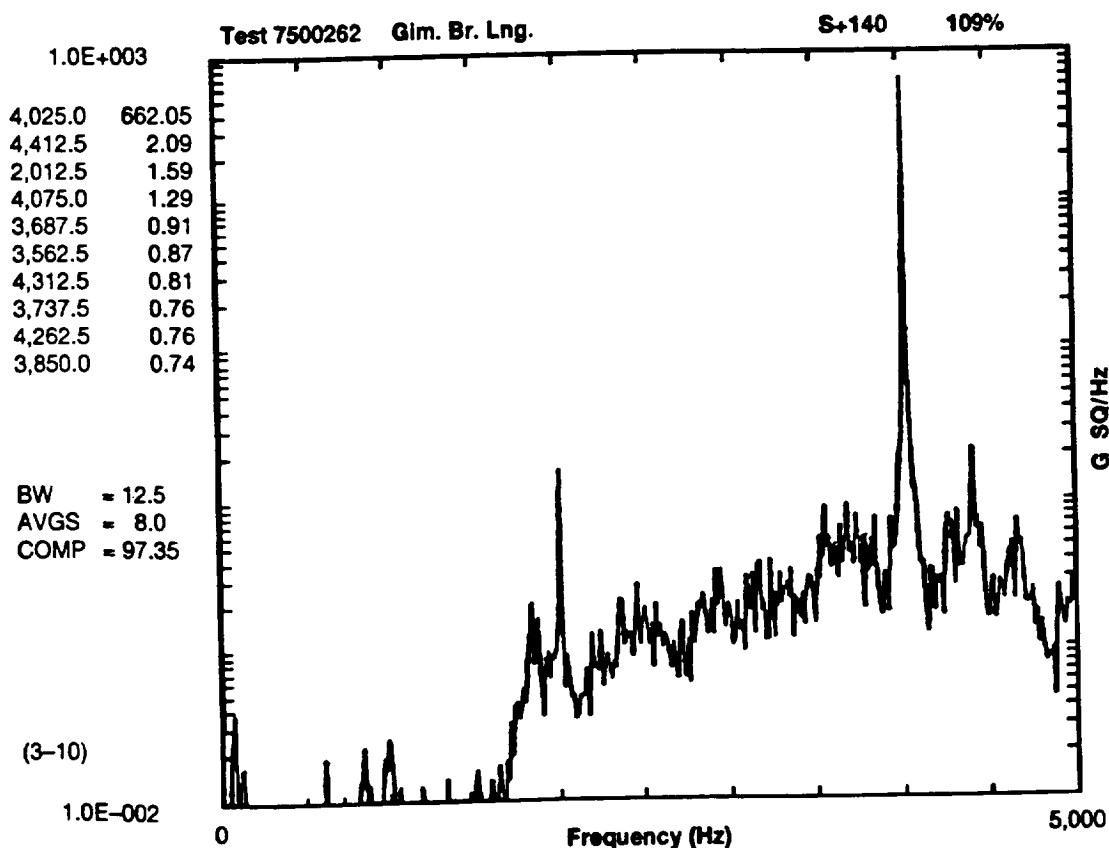


Figure 4-6. SSME 4,000 Hz Phenomenon Gimbal Bearing Accelerometer - Engine No. 2025

CORRECTIVE MEASURES

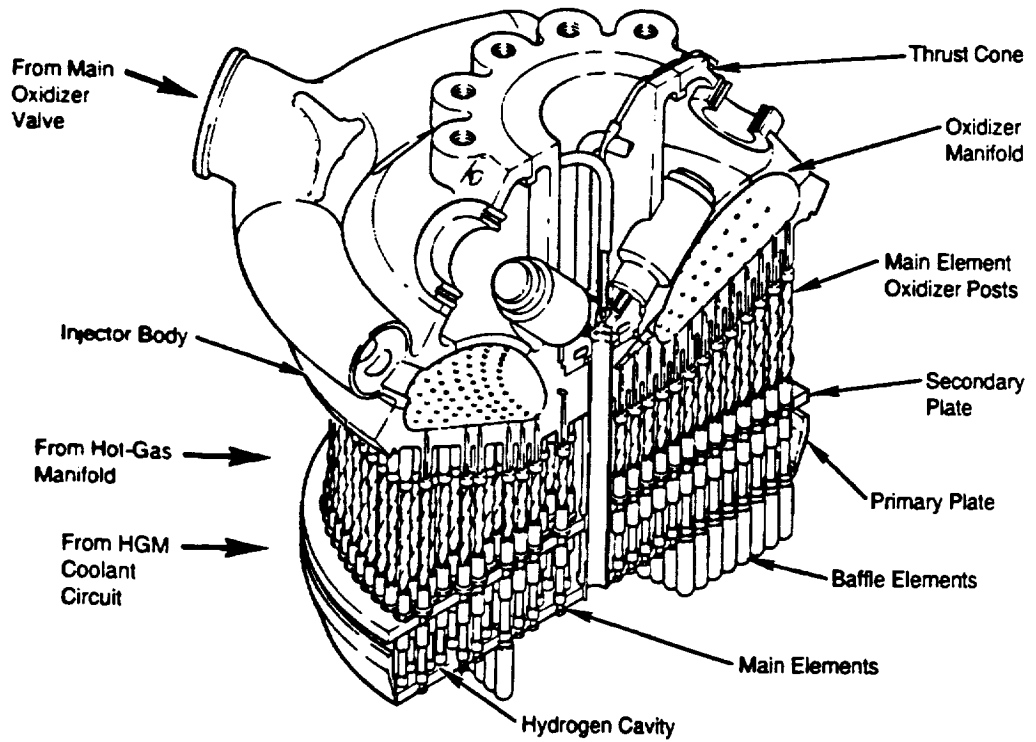


Figure 4-7. SSME Main Injector Assembly

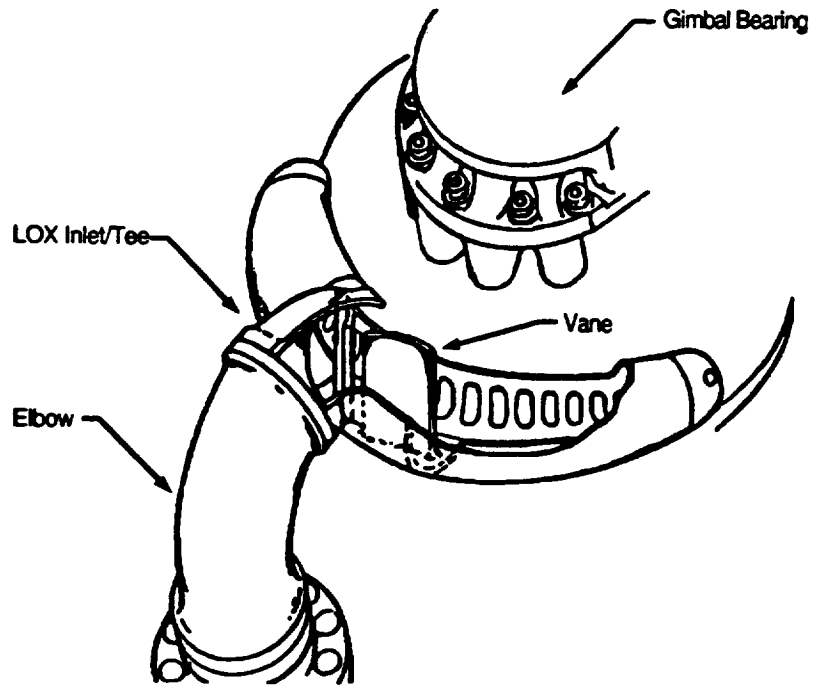


Figure 4-8. SSME 4,000 Hz Phenomenon Orientation of LOX Inlet/Tee - Splitter Vanes and Gimbal Bearing

CORRECTIVE MEASURES

Table 4-1. SSME 4,000 Hz Phenomenon Flow Conditions at LO2 Inlet Tee

| Parameter | 109% PWL |
|--|------------------|
| ρ , density (lbs/in ³) \Rightarrow | 0.0405 |
| P, pressure (lbs/in ²) \Rightarrow | 4400 |
| V, velocity (ft/sec) \Rightarrow | 181.0 |
| q, dynamic pressure (lbs/in ²) \Rightarrow | 247.0 |
| C, speed of sound (ft/sec) \Rightarrow | 3100 |
| R, Reynolds No., Based on Vane Chord (-) | 22×10^6 |
| W, mass flow rate (lbs/sec) | 850 |
| M, mach number (-) | 0.0584 |

A 4,000 Hz investigation team consisting of members from Rocketdyne and MSFC was formed to resolve this issue. Extensive efforts were required on the part of all members of both groups to reach a solution to this problem.

A review of all previous test data from all engine tests was made to determine if evidence of this phenomenon occurred previously. This was an extensive survey, revealing that additional engines (powerheads) had exhibited similar effects. The engine hardware was also reviewed and no evidence of any damage could be found. Only the engines which had been tested at power levels (PWL's) of 100 percent or greater, and not all of those, had the 4,000 Hz. There was a large variability in the amplitude of the response from engine to engine, with engine 2025 having by far the largest response. The 4,000 Hz characteristics were generally very repeatable within a given set of engine hardware. Although the frequency varied slightly from engine to engine, it was always in the range of 4,000 Hz.

Also in support of this problem study, a wide variety of different activities was initiated at both Rocketdyne and MSFC to investigate this phenomena. This included structural modeling of the tee/vane (Figure 4-9), evaluation of the added mass effect, and the effect of vane cracking, vibration tests in ambient and cryogenic conditions, CFD modeling of the internal flow (Figure 4-10), water flow testing and LN2 flow testing of actual hardware, two dimensional water table testing, water flow tests with plastic vanes and additional dynamic measurements on hot firing tests (acceleration and strain). CFD modeling was done for fully separated flow at 23 deg α , and attached flow at 0 deg α . The attached flow case was the dangerous condition producing vortex shedding lock-in. This was simplified modeling of fixed (not moving) vane geometry. The view that began to emerge from this activity was that this phenomenon was related to vortex shedding from the LOX inlet tee's splitter vanes' bluff trailing edge, interacting with the vane's structural mode. A key piece of information, uncovered during the review of past data, was that on one unit, engine (2116), the frequency began to decrease with increasing test time. This decrease was progressive over the course of 15 tests. This frequency change would track and be consistent from test to test. From the finite element structural modeling studies of the LOX tee splitter vane, it was known that the vane's first torsional mode was at 4,000 Hz. The most plausible cause of the frequency shift was that the vane had begun to crack and the crack began to propagate during these series of tests, causing a gradual decrease in frequency of this vane mode. This was predicted by analysis.

CORRECTIVE MEASURES

In order to inspect for cracking of the vane, the elbow at the inlet had to be removed (see Figure 4-8). This was done and a crack was found in one vane near the outer shell of the tee. This was the first direct evidence that the LOX splitter tee vane was a part of, or participating in, this phenomena. Only one other engine showed any frequency decrease similar to this, i.e., on Engine 0005B, both vanes were cracked and two slightly different frequencies changes (decreases) were observed in the data. This was the only hardware damage associated with the phenomenon.

These results clearly indicate that the phenomenon is characteristic of fluid/structural interaction, and that at the onset-velocity, significant increases in the response can be expected. As the lock-in occurred the response became periodic.

The 4,000 Hz fix that was developed consisted of two hardware changes. One change was to asymmetrically bevel the trailing edge of the vanes and the other was to cut back (scallop) the leading edge of the vanes. The bevel was designed to eliminate the vortex shedding from the trailing edge and thereby eliminate the source of excitation. The scalloping of the leading edge of the vane shifted the frequency of the torsional mode to a higher frequency, totally out of the operation flow/PWL range of the SSME. Both of these changes were implemented and constitute the 4,000 Hz fix (see Figure 4-11).

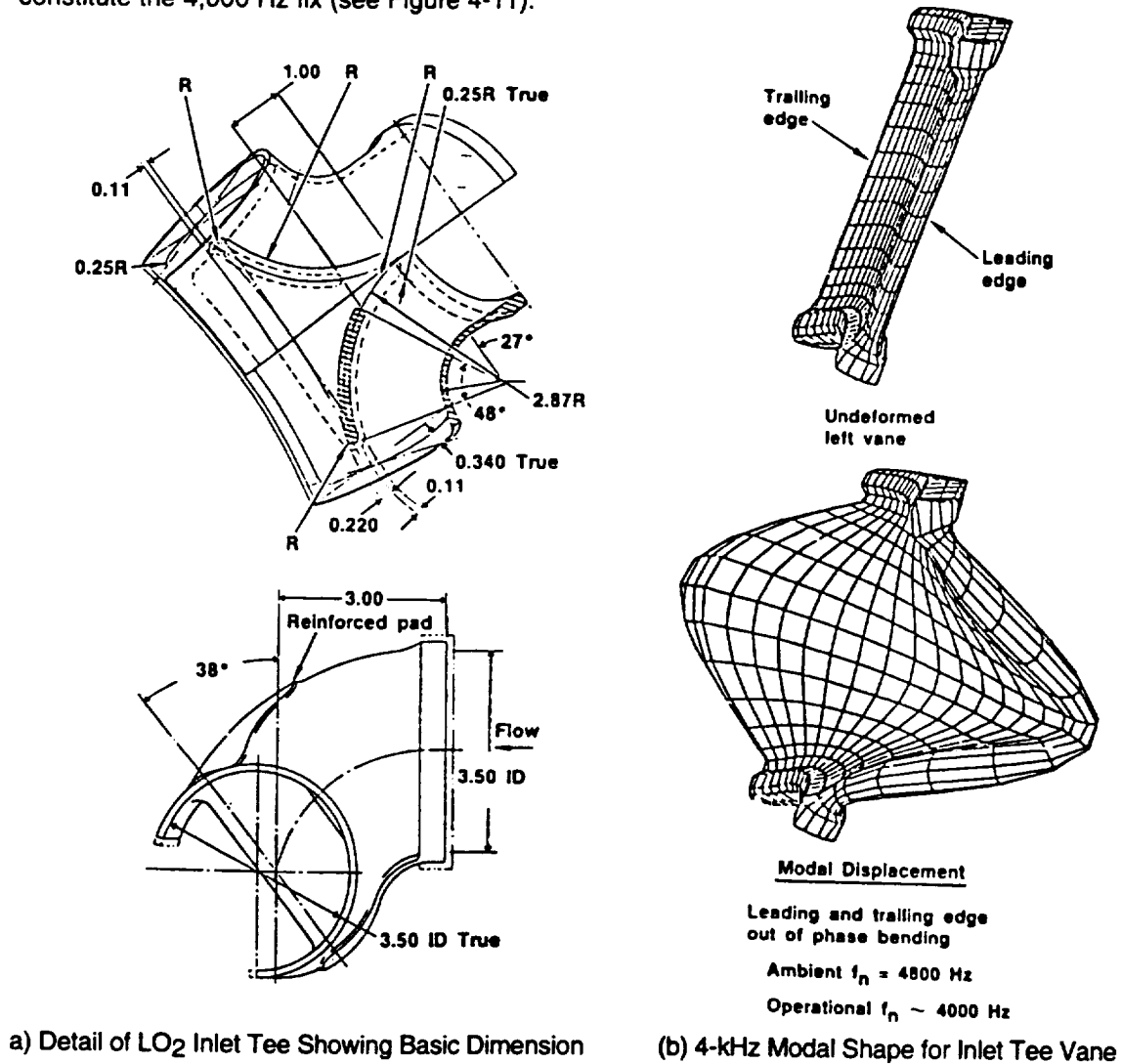


Figure 4-9. Structural Modeling of the LO₂ Inlet Tee Vane

CORRECTIVE MEASURES

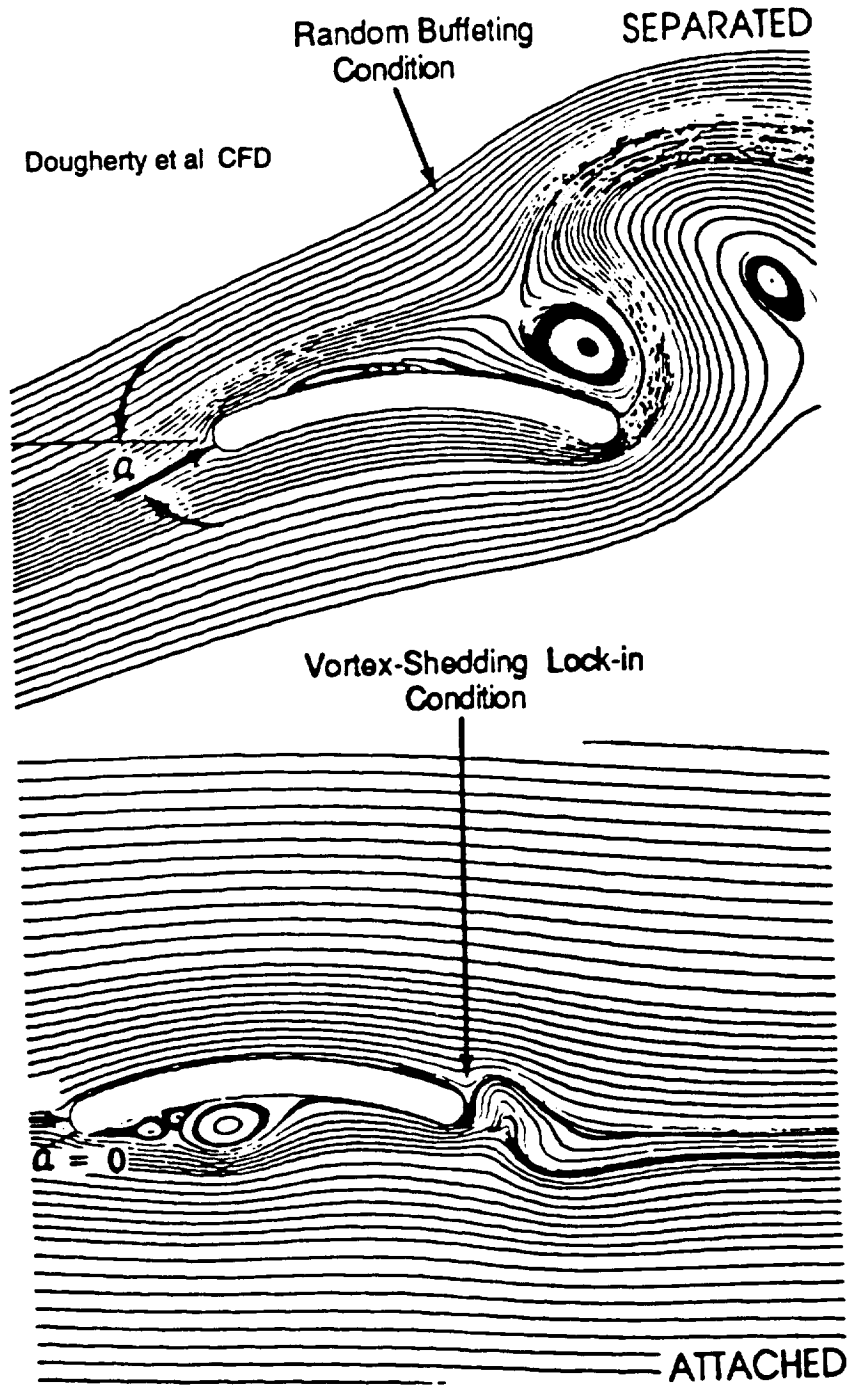


Figure 4-10. CFD Modeling of the LO₂ Inlet Tee Vane

CORRECTIVE MEASURES

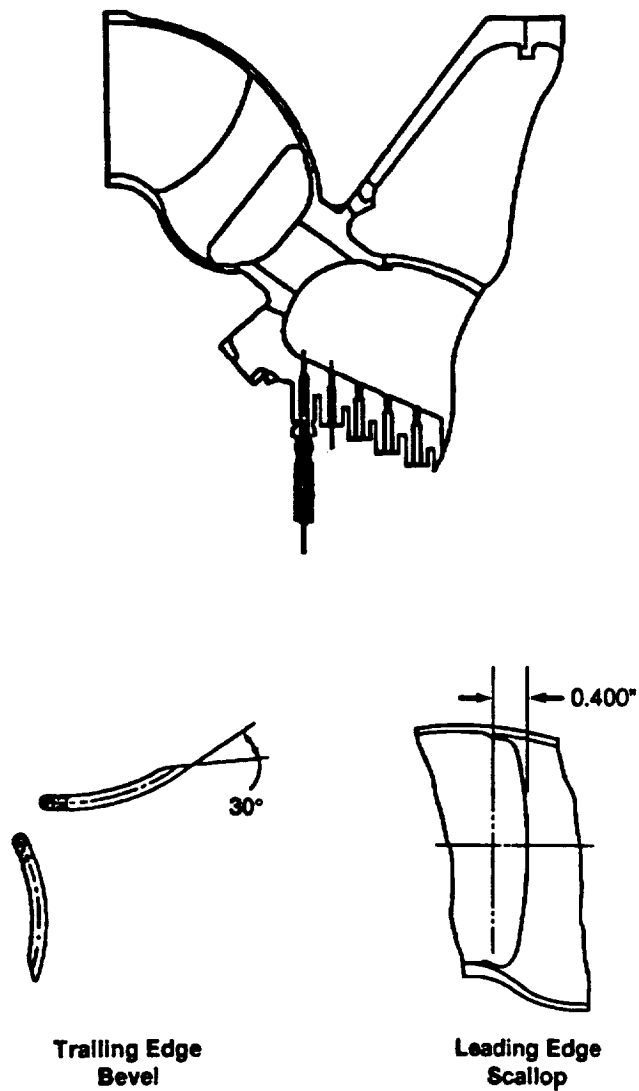


Figure 4-11. SSME 4,000 Hz Vane Modification Geometry

Probability density analysis of the raw data was also performed. These results indicated that the 4,000 Hz signal was discrete or periodic in nature. This is indicative of conditions at "lock-in". The amplitude of response at 4,000 Hz is plotted for the hot-fire units as well as the water-flow unit that exhibited this phenomenon (see Figure 4-12). These results are shown as a function of reduce velocity, i.e.,

$$\text{Reduced velocity} = \frac{U}{fD}$$

CORRECTIVE MEASURES

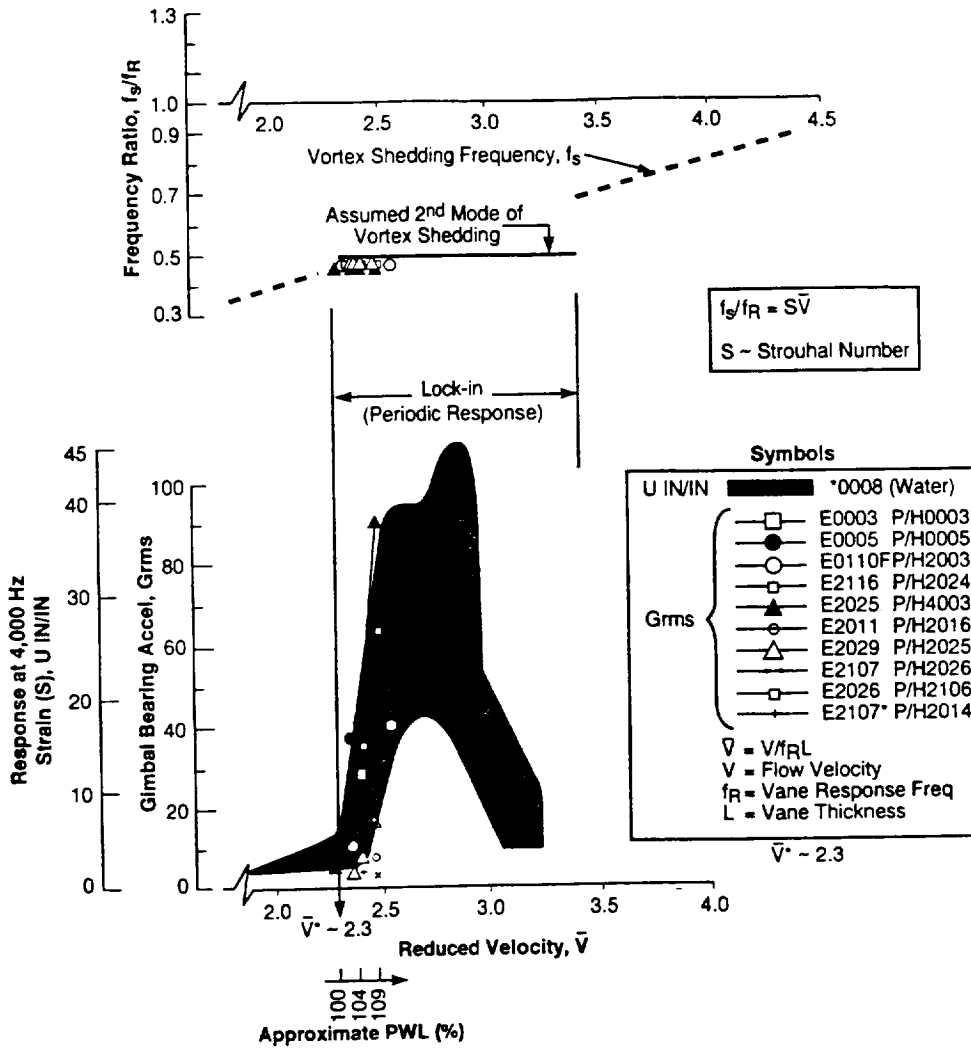


Figure 4-12. SSME 4,000 Hz Phenomenon

All of this work, including the fix certification, was performed during the downtime after Challenger. A 4,000 Hz flight monitoring system was also incorporated and flown on STS-26 in September 1988. This flight monitoring system consists of two accelerometers mounted on the gimbal bearing which is still on flight systems today. In addition to monitoring for 4,000 Hz, these measurements are also being used to monitor for "pop" in the LO₂ and fuel preburners and in the main combustion chamber of the SSME.

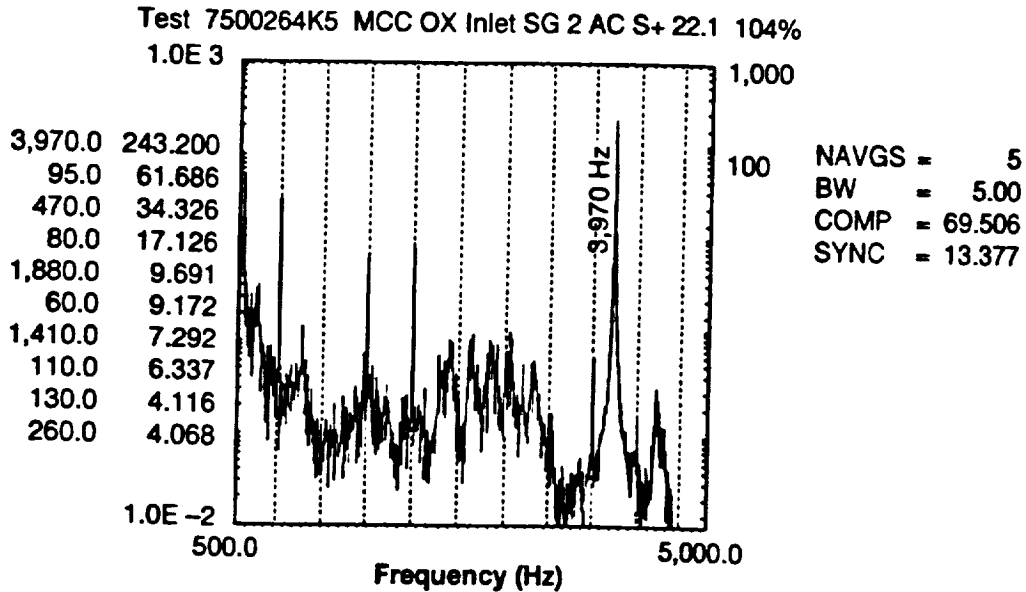
It was desired to test these fixes on non-flight or non-development hardware before it was actually tried on existing hot fire units (engines). The SSME program wanted to preserve as many flight/ development powerheads as possible.

During the LN₂ tests that were conducted at MSFC, the full-scale hardware did not show any evidence of the 4,000 Hz phenomena. This was due in part to the fact that the LN₂ flow velocity could not be increased enough to initiate the excitation. However, on the water flow tests at MSFC, the hardware exhibited the 4,000 Hz response; consequently, the fix was implemented first and then the leading edge scallop was implemented on this test series. The trailing edge

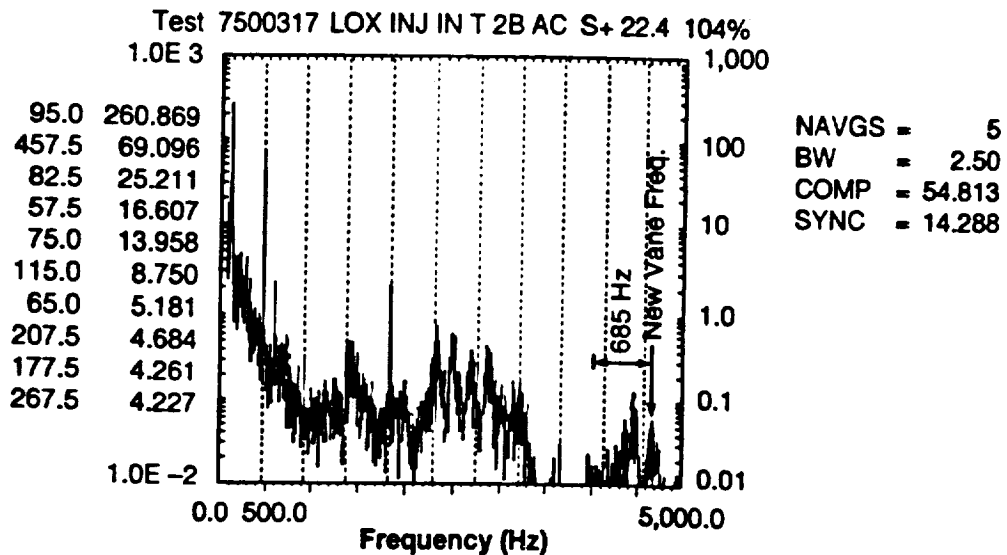
CORRECTIVE MEASURES

bevel was implemented first and then the leading edge scallop was implemented on the following test.

The 4,000 Hz fix was then implemented on engine 2025. This is the unit that first raised the issue of 4,000 Hz and it had the highest vibration response. The result of the fix is seen in Figure 4-13, which shows data from a strain gauge measurement at the base of the tee. Strain measurements were added during the course of this investigation. Figure 4-13a (upper portion) shows the strong vane response and Figure 4-13b shows the effect of the fix; no response is seen at 3970 Hz. The new vane frequency has been shifted approximately 685 Hz higher by analysis.



(a) Without Vane Modification: Engine No. 2025



(b) With Vane Modification: Engine No. 0212

Figure 4-13. SSME 4,000 Hz Phenomenon Hot Firing with and without Fix

CORRECTIVE MEASURES

This engine modification had to go through a flight certification test series (two test cycles of 5,000 seconds each). This certification was performed on engine 2025 (renumbered Engine 0212) and was successful. All new powerheads that are built will have this modification and all units that did not exhibit this phenomenon will have this modification implemented when they are recycled for rework. These vane modifications have been implemented by Rocketdyne.

Eliminate Cavity Noise - the Main Oxidizer Valve (MOV) Buzz Phenomenon

The phenomenon discussed next is acoustical in nature and has resulted in high vibration levels of the MOV and eventually led to failure of the MOV. The main oxidizer valve is located about 1 foot upstream of the LOX inlet tee and main injector. The MOV (Figure 4-14) is a ball-valve type of construction and it operates in the fully open position at main stage conditions.

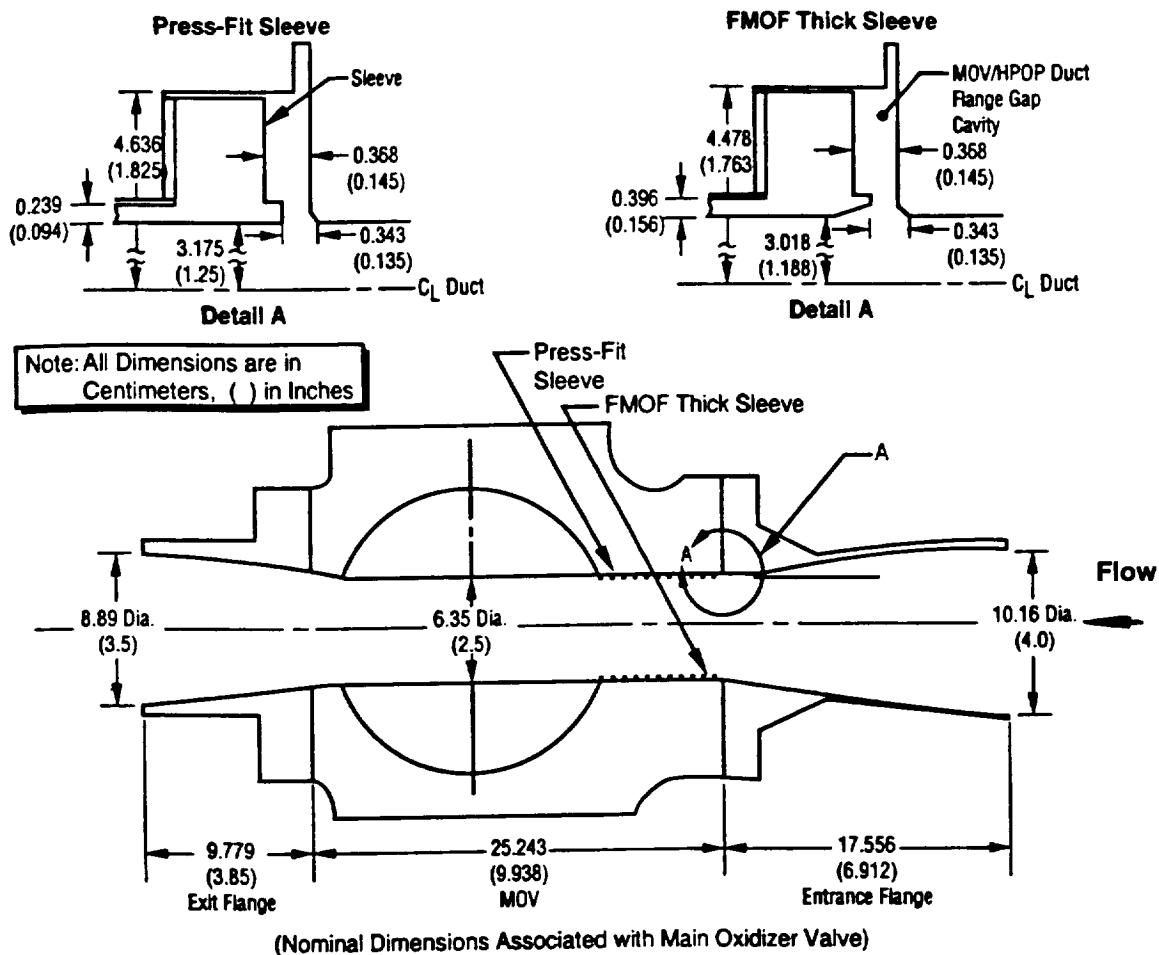


Figure 4-14. Geometry of SSME Main Oxidizer Valve Showing Gap at Inlet Flange

This phenomena was first observed during hot fire testing in February 1979. The source of these vibrations was then isolated to the MOV on subsequent testing. The frequency of these vibrations/oscillation was 7,200 Hz, as measured in the LOX environment. At the inlet to the MOV, a discrete pressure oscillation of 130 psi was measured on SSME test 750-013. This resulted in severe vibrations of the valve that caused fretting of the mating surfaces in the LOX environment and resulted in degradation of the seals and subsequent LOX leakage and hardware damage. A number of different types of fixes were investigated. The final fix was completely successful as seen in Figure 4-15.

CORRECTIVE MEASURES

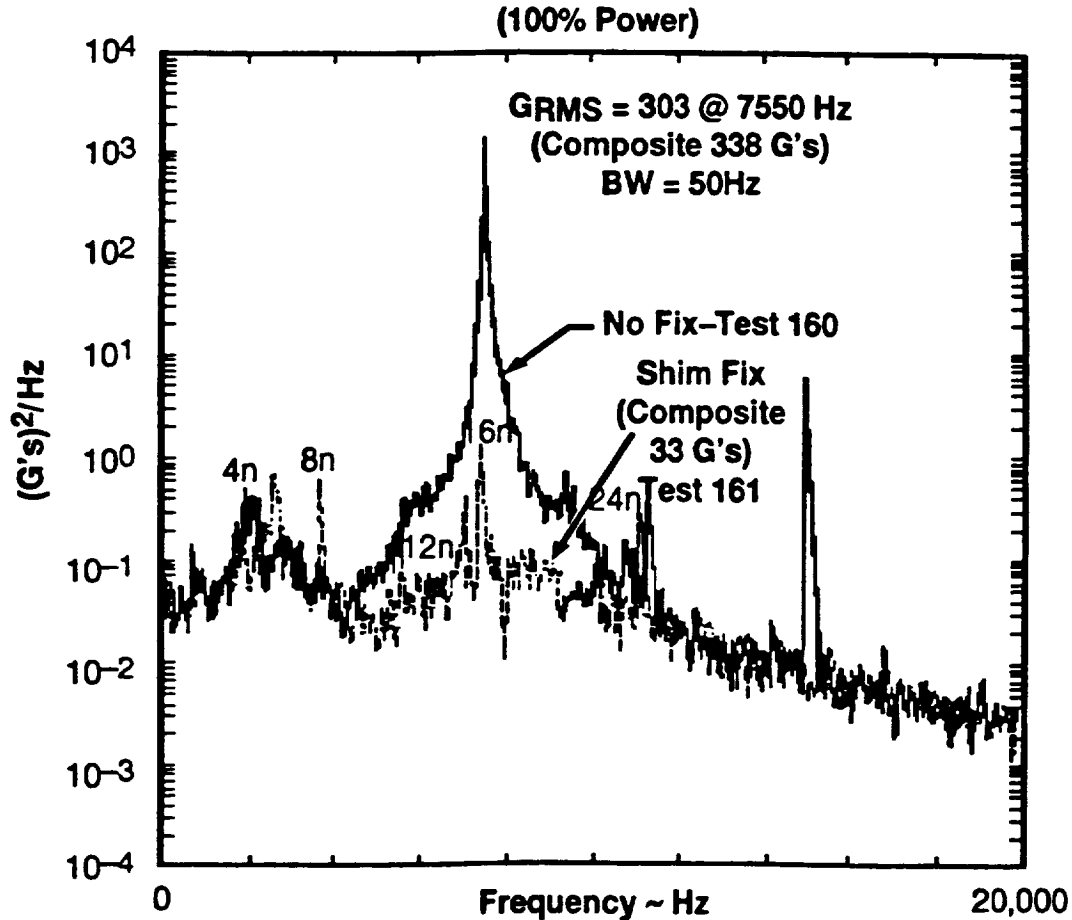


Figure 4-15. Comparison of SSME Hot Firing - MOV AX ACC with/without Shim Fix

To develop a better understanding of this phenomenon, it was decided to perform laboratory type tests in LN₂ with the MOV and its associated high pressure LOX discharge ducting. These tests were conducted in a flowdown-type test mode at MSFC. During the course of this testing, it became obvious that the characteristics of the phenomena closely resembled that of an edge tone/organ pipe mechanism. This mechanism was then exciting the acoustic modes of the valve. This characteristic was discovered during slow ramp-testing. The LN₂ flow was swept from zero to full-scale flow velocities (100-percent PWL at that time). During this ramp-up, lower frequency acoustic modes of the valve were observed to initiate and then drop out until the velocity reached the 100 percent PWL condition where the mode of interest was initiated. This is illustrated in Figure 4-16 by the "solid" horizontal bars. The frequency of this mode was 6,800 Hz in LN₂. This is consistent with the speed of sound difference between LN₂ and LO₂.

Early fix attempts involved improving the structural integrity of the valve by using various types of damped-sleeve, thick-sleeve and/or press-fit-sleeve configurations. These fixes, however, did not address the source of the excitation. Once the edge tone mechanism layer instability was identified. It became evident what was required was to remove the excitation mechanism. Eventually the gap was located as shown in Figure 4-14. The MOV is a convergent/divergent valve configuration. A gap was present between the duct-flange at the entrance to the valve and the MOV sleeve itself. This was discovered during review of the fit-up drawings of the valve/duct flange and this gap is shown in Detail A" of Figure 4-14.

CORRECTIVE MEASURES

The Rossiter model, similar to the model discussed earlier, was used to describe this phenomenon. The vortex shedding frequencies from this model were computed and are plotted as the shaded region of Figure 4-16. When this excitation frequency is near one of the valve's longitudinal acoustic modes, then discrete acoustic tones are generated. This is indicated by the "dashed" horizontal lines indicated in Figure 4-16. Acoustic modes higher than the 6,800 Hz, (7,200 Hz in LOX), were evident in these LN₂ tests and were also observed in LOX during hot-fire testing. The frequency matchings at about 6,800 Hz for 158 ft/sec velocity occurs at N 75 and J22 with $\gamma = 0.25$.

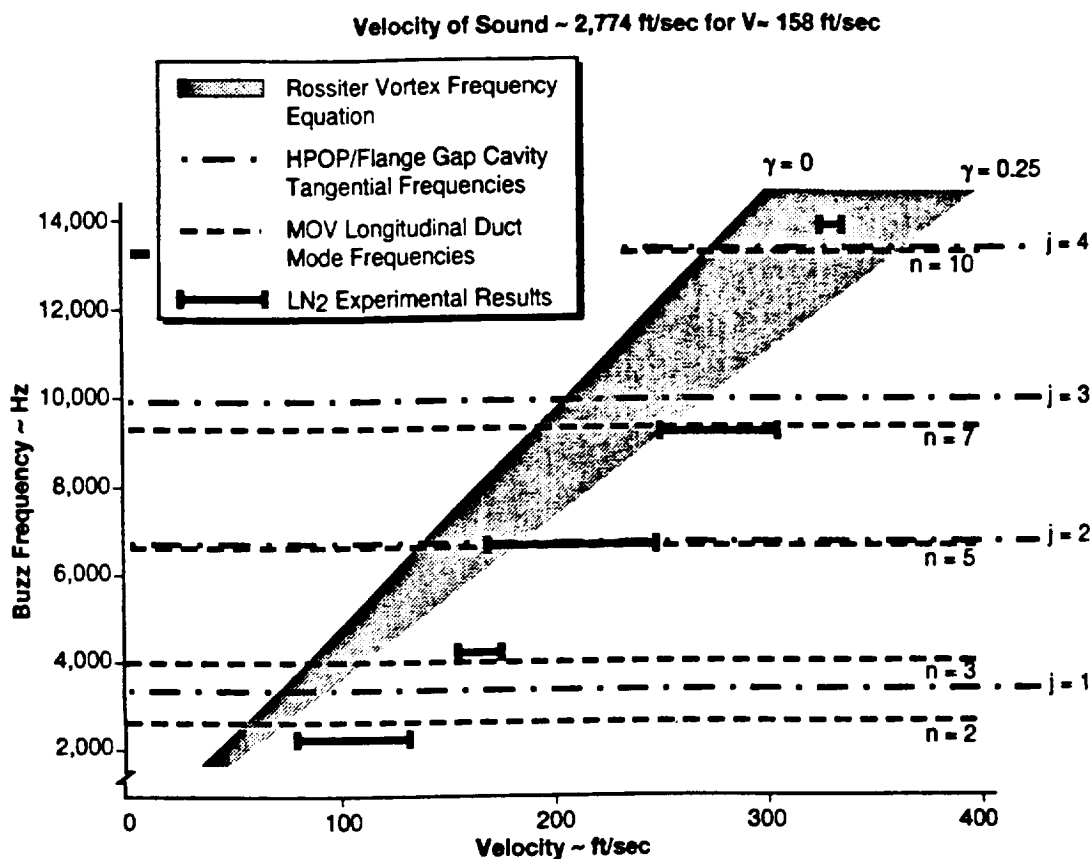


Figure 4-16. SSME Main Oxidizer Valve "Buzz" Phenomenon
- Comparison of Predicted Excitation with MOV Acoustic Modes

A shim (washer) was designed to fill or plug the gap, i.e., fill the opening. Addition of the shim constituted the fix. The shim used in the LN₂ tests was successful. This shim configuration was next tested on actual hot-fire engine MOV configuration in June, 1979. SSME Test 902-160 was conducted without the shim, and Test 902-161 was with the shim. As can be seen on Test 160 (no fix), the tone was eliminated. This mechanism was a shear layer instability, interacting with a downstream edge causing acoustic excitation, which in turn excited the second tangential mode of the gap and the fifth longitudinal acoustic mode of the valve. This fix (or configuration change) has been incorporated into MOV duct flange fit-up geometry for all engines. This example shows that acoustics inherent to internal flow geometries with wave propagations and reflections in all directions characteristic of low subsonic flows can cause very strong structural excitations and can be eliminated altogether by an appropriate fix.

CORRECTIVE MEASURES

Reduce the Turbulence Intensity

Internal turbulence intensities can be as high as 40 percent of the mean characteristic flow velocity inside ducts containing rotating turbomachinery elements (pump or turbine blades), valves, bends, struts, and vanes. The above-cited Earth-to-orbit rocket system component case histories are well-documented cases of motion-induced flow/structural interaction that required specific, critical actions to guarantee successful system operation. Each had its own peculiar structural lock-in or acoustic resonance amplification to discrete high-frequency responses of the structural components at specific frequencies. Each had its own associated destructive potential for structural fatigue. Each involved a structural change as it was not possible to adjust the flow and avoid the interaction flow regime. Without specific example, turbulence intensities approaching 40 percent carry potentials for very strong random buffeting of structural elements such as duct liners and struts or vanes that might be immersed in the flow. As a rule of thumb, the magnitude of the random buffeting forces caused by the turbulence scales directly with the local mean characteristic dynamic pressure, q , in the flow (proportional to density and to the mean velocity squared). These are the motion-independent random forces that can occur on structural elements in the flow.

Dense fluids at high subsonic velocities, e.g. LO₂ or gases at high pressure, are capable of driving large structural dynamic responses due to turbulent buffeting. Internal flow systems always have an inherent velocity profile across the duct. The location of the local maximum in the velocity profile is a likely location for highest turbulent buffeting of an object should 1) it be placed at that location in the flow and 2) there be a source of turbulence sufficiently close upstream. This turbulence can be introduced by bends, struts, vanes, sudden enlargements or sudden contractions upstream that introduce velocity shear profiles and wakes behind them. Convection of that turbulence downstream provides the mechanism for buffeting a structural component downstream. Generally, the spectrum of the turbulence downstream will be found to be broadband random with a frequency range dependent upon the shape and dimensions of the source of the turbulence.

Structural dynamics analysts treat turbulent buffeting response predictions with a random pressure-area loading across the frequency range of interest. Narrow-band random structural responses occur at the natural frequencies and mode shapes characteristic of the structural component being buffeted. While the amplitudes involved may not be nearly so large as in cases of motion-induced discrete-frequency lock-in, destructive fatigue potentials can exist. All sides of an immersed object may be exposed to the buffeting. An extreme case might be a turning vane and a turbulence scale on the order of the vane's chord length where the flow completely separates and alternately reattaches from the lee side of the vane as in Figure 4-10a. Here, the analyst may apply the unsteady loading as a differential force acting across the complete planform of the vane. Whether or not fatigue will occur depends upon the S-N curve for the particular structure and the existence of turbulence in the flow sufficient to cause the fatigue stresses.

Reducing the turbulence levels in the design is possible taking into account knowledge of the types of shear flows and wakes that can be introduced, allowing sufficient distance downstream for placing objects where possible after any turbulence generated will have dissipated, and reducing the local q in the flow by smoothing out, or at least somehow altering, the local mean velocity profile. If the local velocity can be reduced a factor of 2, for example, then the dynamic loading might be reduced a factor of 4, which might be sufficient to preclude fatigue. The fluid dynamics analyst therefore using knowledge of the flow physics often has the opportunity to reduce the turbulence intensity and preclude the potential for fatigue.

Units

Consistency for a set of units is essential for correct expression of formulas. A consistent set of units is one in which Newton's Second Law, force equals mass times acceleration, is identically satisfied without introduction of scaling factors.

$$1 \text{ unit force} = 1 \text{ unit mass} \times 1 \text{ unit acceleration.}$$

The SI system of units is used exclusively throughout this handbook. The resulting Second Law is, in terms of the SI units:

$$1 \text{ newton} = 1 \text{ kilogram} \times 1 \text{ meter/second/second.}$$

The following abbreviations for the SI system of units are used throughout the handbook. The preferred unit is in bold with the symbol (SI).

Basic Units

Length

| | | |
|--------------|----------|------|
| centimeter | cm | |
| meter | m | (SI) |
| kilometer | km | |

Temperature

| | | |
|-----------------------|-----------|------|
| degrees Kelvin | °K | (SI) |
| degrees Celsius | °C | |

| | | |
|----------------|------------|------|
| degree | deg | |
| *radian | rad | (SI) |

Mass

| | | |
|-----------------|-----------|------|
| kilogram | kg | (SI) |
| gram | g | |

Time

| | | |
|---------------|------------|------|
| second | sec | (SI) |
|---------------|------------|------|

Derived Units

Force

| | | |
|---------|-----|-----------------------|
| newton | N | kg·m/sec ² |
| pascal | Pa | N/m ² |
| decibel | db | |
| dyne | dyn | g·cm/sec ² |

Frequency

| | | |
|-------|----|------------|
| hertz | Hz | cycles/sec |
|-------|----|------------|

* Radian measure is defined as a ratio of two lengths and is a dimensionless quantity.

GLOSSARY

The following format order is used for definitions in this glossary:

Defined Quantity { symbol } < units > (1) primary definition (Optional information), (2) secondary definition (Optional information). Then, related material and formulas if any.

Acceleration < m/sec²> (1) The vector quantity specifying the time rate of change of the velocity.

Added mass { m_a } < kg > (1) The mass of fluid that is accelerated due to motion of a body in a fluid, (2) The mass of fluid added to that of the structure in calculating the total kinetic energy of the structure, (3) The mass of fluid displaced or entrained by movement of a body in the fluid.

Angular momentum { ω } < kg-m/sec > Product of the moment of inertia and the angular velocity of a body.

Anti-node A point, line, or surface in a standing wave or on a structure where amplitude or deflection is at a maximum during vibration in a given mode.

Beam A structure whose cross-sectional properties and deflection vary only along its axis.

Buffeting (1) The structural response to the aerodynamic excitation produced by separated flows¹, (2) Transient vibrations of structures due to aerodynamic impulses produced by wakes of structures in the flow², (3) Forces felt by a structure due to fluctuations in the flow impinging on that structure.

Bulk modulus of elasticity { B } The ratio of the tensile or compressive stress to the relative change in volume.

Cable A uniform, massive one-dimensional structure which can bear only tensile loads parallel to its own axis. Cables will stretch in response to tensile loading.

Cable modulus The rate of change in the longitudinal stress in a cable for a small unit longitudinal strain.

Cavitation A phenomenon of a submerged solid surface in a fluid, in which vapor bubbles emerge and subsequently collapse at a high rate due to large fluctuations in flow velocity and pressure. It usually occurs where the fluid pressure decreases significantly due to locally high flow velocity.

Center of gravity The mid point of a body which satisfies: the sum of gravitational force multiplied by distance from this point over each element of a body is zero. (for uniform gravitational acceleration it is the center of mass).

Centroid The geometric center of a plane area.

Chain A uniform, massive one-dimensional structure which can bear only tensile loads parallel to its own axis. Chains do not stretch in response to tensile loading.

Circular frequency { ω } < rad/sec > The frequency of periodic phenomena times 2π .

Clamped boundary A geometric boundary condition allowing neither displacement nor rotation along a given boundary.

Compressibility A measure of the change of volume of a liquid or gas under the action of external forces.

Damping The ability of a medium/structure to absorb vibrational energy. Damping can be generated within the material of the structure (material damping), by the fluid surrounding the structure (fluid damping), or by the impact and scraping at joints (structural damping).

Deformation The displacement of a structure from its equilibrium position.

Density { ρ } < kg/m³ > The mass per unit volume of a material.

Displacement < m > A change either in translational distance or rotational angle.

Drag { D } < N > Fluid force component on a body in the direction of the incident flow.

Drift (1) A motion of a body or a fluid element in a fluid medium. (2) { ξ } < m > The drift of a particle in the fluid is defined as the total displacement of the fluid particle in the direction of movement of the body.

Drift volume { D } < m³ > (1) Volume traveled or traced by a drift motion. (2) Drift volume is defined as the volume enclosed between the initial and final position of an infinitely thin plane which has been perturbed by passage of a body through that plane.

Elastic deformation Deformations which change linearly with the change of applied load.

Effective mass { m } < kg > The sum of structural mass and fluid added mass.

Flutter Structural fluctuation or vibration due to fluctuational aerodynamic forces.

Free boundary A boundary of a structure along which no restraints are applied.

Galloping Structural fluctuation or vibration due to fluctuational aerodynamic forces which generate negative fluid damping.

Incompressible For fluid in which compressibility is low, usually for low Mach number (< 0.3) flows.

Inertia (1) Ability or property of matter/body which resists change in motion of the body. (2) For linear motion, it is mass of the body.

Inviscid An adjective same as nonviscous which describes idealized fluid with no viscosity.

Isotropic A term applied to a material whose properties are unchanged by rotation of the axis of measurement. Only two elastic constants, the modulus of elasticity, E , and Poisson's ratio, ν , are required to completely specify the elastic behavior of an isotropic material.

Joint acceptance { J } < dimensionless > A weighting factor which is a function of or equals to the ratio of the vortex correlation length to cylinder length.

Kinematic viscosity { ν } < m²/sec > Dynamic (or absolute) viscosity divided by fluid density.

Lift { D } < N > Fluid force component on a body transverse to the direction of the incident flow.

Mass < kg > An inherent property of matter which is reluctant to the acceleration of the body.

GLOSSARY

Membrane A thin elastic sheet which can support only tensile loads along its surface.

Mode shape A function defined over a structure which describes the relative displacement of any point on the structure as the structure vibrates in a single mode. A mode shape is associated with each natural frequency of a structure.

Modulus of elasticity { E } The rate of change of normal stress for a unit normal strain of a given material. Some materials have a directional modulus of elasticity. (Young's Modulus).

Moment of inertia < kg-m² > The sum of the products obtained by multiplying each element of mass within a body by the square of its distance from a given point.

Momentum < kg-m/sec > Product of mass and velocity of the mass.

Natural frequency The frequency at which a linear elastic structure will tend to vibrate once it has been set in motion. The lowest natural frequency is called the fundamental natural frequency.

Neutral axis The axis of zero (shear) stress in the cross section of a structure.

Newton { N } < kg-m/sec² > Basic unit of force in SI system. The force required to accelerate one kilogram to one meter per second in one second.

Node Point on a structure which does not deflect during vibration in a given mode.

Orthotropic A term applied to a thin lamina if the material properties of the lamina possess two mutually perpendicular planes of symmetry. Four material constants are required to specify the elastic behavior of an orthotropic lamina.

Pinned boundary A boundary condition such that the structure is free to rotate but not displace at that boundary.

Plate A thin flat two-dimensional elastic structure. A plate without bending rigidity is a membrane.

Point mass A relatively concentrated mass in space which is assumed to have zero moment of inertia for rotation about its center of mass.

Poisson's ratio The ratio of the lateral shrinkage (expansion) to the longitudinal expansion (shrinkage) of a bar of a given material which has been placed under a uniform longitudinal tensile (compressive) load. Some materials have a directional Poisson's ratio.

Reduced frequency A nondimensional frequency is also usually called Strouhal number (q.v., Strouhal number).

Rotating stall A condition occurring in a turbines where one or more regions of separated flow, stall cells, travel around the compressor annulus in the direction of the compressor with a speed usually close to half of the compressor rotation speed. There is little flow through the stall cell and the periodicity of the passage of the cell over a turbine blade produces oscillations which may coincide with natural frequencies of the turbine blade.

Shear A force or stress acts on a surface tangentially.

Shear coefficient <dimensionless> A quantity, defined as the ratio of the average shear strain over

a beam cross section to the shear strain at the centroid.

Shear layer A fluid flow generated by two or more streams at different velocities and/or other properties.

Shear modulus The rate of change in the shear stress of a material with a unit shear strain. Some materials have a directional shear modulus.

Shell A thin elastic structure whose geometry is approximates a curved surface. A shell without rigidity in bending is a membrane.

Sliding boundary A boundary condition such that a structure is free to displace in a given direction along a boundary but rotation is prevented.

Spring constant:

Linear The change in load on a linear elastic structure required to produce a unit increment of deflection.

Torsional The change in moment (torque) on a linear elastic structure required to produce a unit increment of rotation.

Stall A status of a lift-generating structure in which sudden drop of lift occurs due to flow separation at large angle-of-attack or other flow instability.

Stiffness The material strength or ability which resists translational or rotational strain under loads.

String A thin (long) structure which can only bear tension along its axis.

Strut A supporting structure to a (main) structure to enhance stiffness or to increase damping for reduction of vibration.

Strouhal number { S } <dimensionless> The nondimensional frequency of vibration, frequently of vortex shedding from a bluff body in a flow. Strouhal number is the frequency of vibration times the characteristic length divided by the freestream velocity.

$$S = \frac{fL}{U}$$

Supercavitation A cavitation due to increase of flow velocity in a duct flow such as in a liquid flow in a nozzle due to acceleration of the flow near or behind the throat.

Velocity { $\frac{dX}{dt}$, \dot{X} } < m/sec > The rate of change of position with respect to time.

Vibrational Reynolds number { S } < dimensionless > The Vibrational Reynolds number is defined as the product of the angular velocity and the square of the radius of the body divided by the kinematic viscosity.

$$S = \frac{\omega R^2}{\nu}$$

Virtual mass { m } < kg > The sum of the structural mass, m_s , and the fluid added mass, m_a . (same as effective mass)

Viscosity The ability of a fluid to resist shearing deformation. The viscosity of a Newtonian fluid is defined as the ratio between the shear stress applied to a fluid and the shearing strain that results.

Vortex correlation length A length which measures the two-dimensionality of the vortex sheet over a (long) structure which has a

characteristic diameter, D . It is usually in the range of 3 to 10 times of D . The larger this length, the less the spanwise variation.

Wake The flow separation region in the lee side of a structure which is a measure of the bluntness of the structure.

¹Mabey, D.G., "Some Remarks on Buffeting of Wings, Wind Tunnel Models", Royal Aircraft Est., Report RAE-TM-STRUCT-980 BR78530.

²Bisplinghoff, R.L., H. Ashley and R.L. Halfman "Aeroelasticity", Addison-Weseley, 1955.

Index

A

Acoustic resonance 2.7.5,3.10.3
Added mass
 added mass 2.2.3,3.2.7
 pipe arrays 3.3.2
 single circular cylinder 3.2.6
 two parallel cylinders 3.2.9

B

Beam
 boundary conditions 3.2.13

C

CFD 2.7.2,3.2.5,3.6.6,4.1.11
Cavitation 3.5.1
Cantilever Pipe 3.7.1
Cylinder
 area moment of inertia 3.2.12
 displacement 3.2.16
 lateral force auto spectral density 3.2.24
 vibrating cylinder 3.2.12
 rigid cylinder 3.2.19
Correlation model 3.2.17
Correlation length 3.2.12
Crossflow velocity 3.2.11
Curved pipes 3.7.6

D

Damping
 free decay 3.2.14
 fluid damping 3.2.15
 fluid damping ratio 3.2.15
 logarithmic decrement 3.2.14
 structural damping 3.2.14
Denticulation (valve disk) 3.10.4
Drag
 drag 3.3.3
 drag coefficient 3.2.20, 3.3.5
Duhamel's integral 3.7.9
Dynamic head 3.10.1

E

Effective mass 3.2.7
EFO oscillations 2.7.1,3.10.3
Equation of motion
 external pipe motion 3.3.3
 fluid-conveying pipe 3.7.3, 3.7.5

G

Gates 3.10.1
Griffin and Ramberg model 3.2.16

H

Harmonic oscillator model 3.2.16
Hydrodynamic mass coefficient 3.2.7

I

In-line structural bending frequencies 3.2.20
Inertial coupling 3.3.2

J

Jet flow - inertia mechanism 3.10.1
Jet switching 3.3.1, 3.3.6
Joint acceptance 3.2.12, 3.2.23, 3.2.26

K

Karman vortex street 3.2.4
Kolkman's equations (valves) 3.10.2

L

Lift
 tube arrays 3.3.4
 coefficient 3.1.7,3.2.18, 3.3.5
Lock-in 2.1.5,3.1.13,3.4.4
 amplitudes 3.2.17

M

Mass
 mass ratio 3.2.15
 reduced mass 3.2.15
 structural mass 3.2.7
Mode shape
 mode shape factor 3.2.13,3.2.26
 mode shape factor for displacement 3.2.26
 mode shape function 3.2.13
 cantilever pipe 3.7.4

O

Orifice 3.10.1

P

Pipes 3.3.1, 3.7.1
Pipe whip 3.7.7
Pipe fixed at both ends 3.7.3
Power
 non-dimensional cycle power 3.2.18

R

Reduced mass 3.2.15
Reduced velocity 3.2.17, 3.2.21
Resonant frequency 2.7.5,3.2.15
Restraining force (valves) 3.10.1
Reynolds number 3.2.10
Ruptured pipe 3.7.9
 cantilevered pipe 3.7.8

S

Sarpkaya model, 3.2.16
Separation point 3.2.4
Spring constant 2.1.6
Static closing force (valve) 3.10.1
Stagnation point 3.2.4
Strouhal number 3.2.10,3.9.1
Structure
 bending frequencies 3.2.11
 damping 3.2.14

T

Thermostatic radiator valve 3.10.3
Transverse
 bending frequencies 3.2.17

- displacement amplitude 3.2.16
- Tube array 3.3.1
 - staggered tube arrays 3.3.6,3.3.7
- Turbulence
 - Induced Vibrations 3.2.22, 3.2.24, 3.10.1, 3.10.2
 - spectra 3.2.23

V

- Valves 3.10.1
 - static closing force 3.10.1
- Vibrational Reynolds number 3.2.7
- Viscous damping factor 3.2.14
- Vortex
 - convection speed 3.2.4
 - correlation length 3.2.12
 - filaments 3.2.12
 - shedding 3.2.3
 - tilt angle of a filament 3.2.12
 - transport velocity 3.2.12

W

- Wake 3.2.5,3.3.6
 - wake oscillator model 3.2.16
 - wake response parameter 3.2.21
- Wall effect 3.2.7,3.2.22,3.2.27
- Whirling 3.3.1
- Whistling 3.10.3
 - avoidance of 3.10.3

Y

- Yielded pipes 3.7.10
- Young's modulus 3.2.12

REFERENCES

References

- Andjelic, M, H. Bardowicks and K. Popp, "Non-Linearities in Fluidelastic Vibrations of Tube Bundles", In "Proceedings of International Conference on Flow Induced Vibrations", paper number K5, pp. 477-485, delivered at conference at Bowness-on-Windermere, England: 12-14 May, 1987, sponsored by the British Nuclear Energy Society, The Fluid Engineering Centre, BHRA.
- Andjelic, M. and K. Popp, "Stability Effects in a Normal Triangular Cylinder Array", *Journal of Fluids and Structures* (1989) 3, pp. 165-185.
- Andjelic, M., Austermann, R. and Popp, K., "Multiple Stability Boundaries of Tubes in a Normal Triangular Cylinder Array," Institute of Mechanics, University of Hannover, Germany, 1988.
- Arai, Norio and Tani, Takashi, "Active Control of Vortex Shedding Frequency by a Splitter Plate," Proceeding of International Congress on Recent Developments in Air- and Structure-Borne Sound and Vibration, pp. 501-508, Auburn University, March 6-8, 1990.
- Au-Yang, M.K., "Flow-Induced Vibration: Guidelines for Design, Diagnosis, and Troubleshooting of Common Power Plant Components",
- Au-Yang, M.K., "Free Vibration of Fluid-Coupled Coaxial Cylindrical Shells of Different Lengths", *Transactions of the ASME: Journal of Applied Mechanics*, September 1976, pp. 480-484.
- Au-Yang, M.K., "Generalized Hydrodynamic Mass for Beam Mode Vibration of Cylinders Coupled by Fluid Gap", *Transactions of the ASME*, March 1977, pp. 172-173.
- Badr, H. M., Coutanceau, M., Dennis, S. C. R. and Menard, C., "Unsteady Flow Past a Rotating Circular Cylinder at Reynolds numbers 10^3 and 10^4 ," *J. Fluid Mech.*, vol. 220, pp. 459-484, 1990.
- Bailey, F.R., "Numerical Calculation of Transonic Flow About Slender Bodies of Revolution", NASA Technical Note, NASA TN D-6582, December 1971.
- Ballou, C.L., "Investigation of the Wake Behind a Cylinder at Coincidence of a Natural Frequency of Vibration of the Cylinder and the Vortex Shedding Frequency", Department of Mechanical Engineering, Massachusetts Institute of Technology, Cambridge, Massachusetts, May 19, 1967, Technical Report No. 76028-2.
- Bauer, H. F. and Eidel, W., "Hydroelastic Vibrations in a Circular Cylindrical Container with a Flexible Bottom in Zero Gravity," *J. Fluids and Structures*, Vol. 7, pp. 783-802, 1993
- Bearman, P. W. and Luo, S. C., "Investigation of the Aerodynamic Instability of a Square-Section Cylinder By Forced Oscillation", *J. Fluids and Structures*, 2, 161-176, 1988.
- Bearman, P. W. and Trueman, D. M., "An Investigation of the Flow Around Rectangular Cylinders," *Aeronautic Quarterly*, Vol. 23, 229-237, 1972.
- Bearman, P. W., Gartshore, I. S., Maull, D. J., and Parkinson, G. V., "Experiments on Flow-Induced Vibration of a Square-Section Cylinder," *J. of Fluids and Structures*, 1, 19-34, 1987.
- Beavers, G. S. and Wilson, T. A., "Vortex Growth in Jets," *J. of Fluid Mechanics*, vol. 44, part 1, pp. 97-112, 1970.
- Bechert, D. and Pfizenmaier, E., "Optical Compensation Measurements on the Unsteady Exit Condition at a Nozzle Discharge Edge," *J. Fluid Mech.*, vol. 71, Part 1, pp. 123-144, 1975
- Becker, H. A. and Massaro, T. A., "Vortex evolution in a Round Jet," *J. of Fluid Mechanics*, vol. 31, part 3, pp. 435-448, 1968.
- Bellows, W. J., "An Experimental Study in Leading Edge Separating-Reattaching Boundary Layer Flows," Rensselaer Polytechnic Institute, Ph.D. Thesis, 1985

REFERENCES

- Bennett, M.D. and G.E. Barr, "Average Surface Pressure Around Inclined Bodies of Revolution at Hypersonic Speed", Sandia Laboratories, June 1971, Report No. SC-RR-71 0287.
- Beranek, L.L., "Noise and Vibration Control," McGraw-Hill, 1974, pp. 373-374.
- Berger, E. and Plaschko, P., "Hopf Bifurcations and Hysteresis in Flow-Induced Vibrations of Cylinders," J. Fluids and Structures, 7, 849-866, 1993.
- Berger, E., D. Scholz and M. Schumm, "Coherent Vortex Structures in the Wake of a Sphere and a Circular Disk At Rest and Under Forced Vibrations", Journal of Fluids and Structures (1990) 4, pp. 231-257.
- Biermann, D. and Herrnstein, W. H., "The Interference Between Struts in Various Combinations," National Advisory Committee for Aeronautics, Tech. Rep. 468, pp. 515-524, 1933
- Birkhoff, G., "Formation of Vortex Streets", Journal of Applied Physics, Vol. 24 (1), January 1953.
- Bisplinghoff, R.L., H. Ashley and R.L. Halfman "Aeroelasticity", Addison-Weseley, 1955.
- Blake, W. K., "Excitation of Plates and Hydrofoils by Trailing Edge Flows," J. Vibration, Acoustic, Stress, and Reliability in Design, vol. 106, pp. 351-363, July 1984
- Blevins, R. D. and Burton, T. E., "Fluid Forces Induced by Vortex Shedding," J. of Fluid Engineering, 95, 19-24, 1976.
- Blevins, R.D., Flow Induced Vibration, Van Nostrand Reinhold Company NewYork 1977.
- Blevins, R. D., Flow-Induced Vibration, second edition, Van Nostrand Reinhold, 1990.
- Blevins, R. D., Formulas for Natural Frequency and Mode Shape, Van Nostrand Reinhold, New York, 1979.
- Blevins, R.D., Formulas for Natural Frequency and Mode Shape, 2nd ed., R. Kreiger Pub. Co., 1987.
- Blevins, R.D. "A Rational Algorithm for Predicting Vibration-Induced Damage to Tube and Shell Heat Exchangers" Proceedings of Symposium on Flow-Induced Vibrations, Vol. 3, Vibrations in Heat Exchangers, 1984, pp. 87-102, New York: ASME.
- Bokaian, A. R. and Geoola, F., "Hydroelastic Instabilities of Square Cylinders,"J. Sound and Vibration, 92(1), 117-141, 1984.
- Bokaian, A., "Interference Galloping of Upstream Member of a Pair of Circular Cylinders", Journal of Sound and Vibration (1987) 117(3), pp. 433-446.
- Borland, C. J., "Numerical Prediction on the Unsteady Flow Field in an Open Cavity, AIAA 10th Fluid & Plasmadynamics Conference, AIAA 77-673, Albuquerque, N. Mex., June 27-29, 1977
- Borthwick, A.G.L. and Herbert, D. M., "Resonant and Non-Resonant Behaviour of a Flexibly Mounted Cylinder in Waves", Journal of Fluids and Structures (1990) 4, pp. 495-518.
- Borthwick, A.G.L. and Herbert, D. M., "Loading and Response of a small diameter Flexibly mounted Cylinder in Waves," J. of Fluid and Structure, 2, 479-501, 1988.
- Brown, G.B., "The Vortex Motion Causing Edge Tones", Proc. Physical Society(London), vol.49,pp.493-507, 1937.
- Brown, S. N. and Stewartson, K., "Trailing-Edge Stall," J. Fluid Mech. vol. 42, part 3, pp. 561-584, 1970
- Brown, S.J., "A Survey of Studies Into the Hydrodynamic Response of Fluid-Coupled Circular Cylinders", Journal of Pressure Vessel Technology, vol. 104, pp. 2-19, February 1982.
- Brune, G. W., Sikavi, D. A. et al "Confluent Boundary Layer Measurements, Boeing Report No. D6-51453TN, 1982

REFERENCES

- Burton, T.E., "Sound Speed in a Heat Exchanger Tube Bank", *Journal of Sound and Vibration*, (1980) 71(1), pp. 157-160.
- Campbell, F. B. et al "Vibration Problems in Hydraulic Structures," Vol. 127, Part I Paper No. 3282, ASCE Transactions, 1962
- Carlucci, L.N., "Damping and Hydrodynamic Mass of a Cylinder in Simulated Two-Phase Flow", *Journal of Mechanical Design*, July 1980, vol. 102, pp. 597-602.
- Castrejon, A. and D. B. Spalding, "An Experimental and Theoretical Study of Transient Free-Convection Flow Between Horizontal Concentric Cylinders", *Journal of Heat and Mass Transfer*, Great Britain, vol. 31, No. 2, pp. 273-284, 1988.
- Chan, Y. Y., "Wavelike Eddies in a Turbulent Jet," *AIAA Journal*, vol. 15, No. 7, pp. 992-1001, 1977
- Chanaud, R. C., "Aerodynamic Whistles," *Scientific American*, pp. 40-46, June 1970.
- Chanaud, R.C., and A. Powell, "Some Experiments Concerning the Hole and Ring Tone," *Journal of the Acoustical Society of America*, Volume 37, number 5, May 1965.
- Chang, T. C. and Craig, R. R., "Normal Modes of Uniform Beams," *J. Eng. Mech. Div, ASCE*, 95, 1027-1031(1969).
- Chen, S.S. and Chung, H. "Design Guide for Calculating Hydrodynamic Mass Part I: Circular Cylindrical Structures", Components Technology Division, Argonne National Laboratory, Argonne, Illinois, June 1976, Document No. ANL-CT-76-45.
- Chen, S.S. and G.S. Rosenberg, "Dynamics of a Coupled Shell-Fluid System", *Nuclear Engineering and Design* (1975), vol. 32, pp. 302-310.
- Chen, S.S. and G.S. Rosenberg, "Free Vibrations of Fluid-Conveying Cylindrical Shells", *Transactions of the ASME: Journal of Engineering for Industry*, May 1974, pp. 420-426.
- Chen, S.S. and H. Chung "Design Guide for Calculating Hydrodynamic Mass Part I: Circular Cylindrical Structures", Components Technology Division, Argonne National Laboratory, Argonne, Illinois, June 1976, Document No. ANL-CT-76-45.
- Chen, S.S. and J.A. Jendrzejczyk, "Dynamic Response of a Circular Cylinder Subjected to Liquid Cross Flow", *Transactions of the ASME: Journal of Pressure Vessel Technology*, May 1979, vol. 101, pp. 108-112.
- Chen, S.S. and M.W. Wambsganss, "Parallel-Flow-Induced Vibration of Fuel Rods", *Nuclear Engineering and Design*, 18 (1972), pp. 253-278.
- Chen, S.S., "A General Theory for Dynamic Instability of Tube Arrays in Crossflow", *Journal of Fluids and Structures*, vol. 1, pp. 35-53, 1987.
- Chen, S.S., "Dynamic Responses of Two Parallel Circular Cylinders in a Liquid", *Transactions of the ASME: Journal of Pressure Vessel Technology*, May 1975, pp.78-83.
- Chen, S.S., "Flow-Induced Vibration of Circular Cylindrical Structures -- Part 1: Stationary Fluids and Parallel Flow", Source unknown.
- Chen, S.S., "Instability Mechanisms and Stability Criteria of a Group of Circular Cylinders Subjected to Cross-Flow", *Journal of Vibration, Acoustics, Stress, and Reliability in Design*, January 1983, Vol. 105, pp. 51-58.
- Chen, S.S., M.W. Wambsganss and J.A. Jendrzejczyk, "Added Mass and Damping of a Vibrating Rod in Confined Viscous Fluids", *Transactions of the ASME: Journal of Applied Mechanics*, June 1976, pp. 325-329.

REFERENCES

- Chen, Y.N. and W.C. Young "The Orbital Movement and the Damping of Fluidelastic Vibration of Tube Banks Due to Vortex Formation Part III: Damping Capability of the Tube Bank Against Vortex-Excited Sonic Vibration in the Fluid Column", Transactions of the ASME, August 1974, pp.1072-1075.
- Chen, Y.N., "Flow-Induced Vibration and Noise in Tube-Bank Heat Exchangers Due to von Karman Streets", Transactions of the ASME, February 1968 pp. 134-146
- Chen, Y.N., "The Orbital Movement and the Damping of Fluidelastic Vibration of Tube Banks Due to Vortex Formation Part I: The Interplay Between the Self-Excited Vibration of the Single Circular Cylinder and the Karman Vortex", Transactions of the ASME, pp.1060-1064, August 1974.
- Cherdron, W., Durst, F. and Whitelaw, J. H., "Asymmetric flows and instabilities in symmetric ducts with sudden expansions," J. Fluid Mech., vol. 84, part 1, pp. 13-31, 1978
- Chung, H. and Chen, S. S., "Hydrodynamic Mass," Argonne National Laboratory.
- Clements, R. R. and Maull, D. J., "The Representation of Sheets of Vorticity By Discrete Vortices," Aerospace Science, Vol. 16, No. 2, pp. 129-146, Pergamon Press, 1975
- Clever, W.K., "Transmittal of an Interim Test Report from the Cylinder Vortex Shedding Wind Tunnel Test TWT662", Internal NASA Communication, George C. Marshall Space Flight Center, Structures and Dynamics Laboratory, Document No. ED23-81-65, May 28, 1981.
- Coles, D. E., "The law of the Wall in Turbulent Shear Flow," 50 Jahre Grenzschichtforschung, Vieweg und Dohn, Braunschweig, pp. 153-163, 1955
- Connors, H.J., "Flow-Induced Vibration and Wear of Steam Generator Tubes", Nuclear Technology (1981), vol. 55, pp. 311-331.
- Connors, H.J., "Fluidelastic Vibration of Tube Arrays Excited by Cross Flow, in Proceedings of the Symposium "Flow Induced Vibration in Heat Exchangers", 1970, pp. 42-56, New York: ASME.
- Corless, R. M. and Parkinson, G. V., "Mathematical Modeling of the Combined Effects of Vortex-Induced Vibration and Galloping. Part II", J. Fluids and Structures, 7, 825-848, 1993.
- Courchesne, J. and Laneville, A., "An Experimental Evaluation of Drag Coefficient for Rectangular Cylinders Exposed to Grid Turbulence," J. Fluids Engineering, Vol. 104, 523-528, 1982.
- Coyle, D.J., C.W. Macosko and L.E. Scriven, "Stability of Symmetric Film-Splitting Between Counter-Rotating Cylinders", Journal of Fluid Mechanics (1990), vol. 216, pp. 437-458.
- Crawley, E. F. and Van Schoor, M. C., "Material Damping in Aluminum and Metal Matrix Composites," MIT Industry Liason Program Report, June 5, 1987.
- Dahm, W.K., "Composite Model of a Random Forcing Function for the Excitation of Long Pipes by a Crossflow", Internal NASA Communication, George C. Marshall Space Flight Center, Structures and Dynamics Laboratory, Document No. ED31-79-15, August 13, 1979.
- Darwin, C., Proc. Camb. Phil. Soc., 49, (1953), p.342-354.
- Davenport.A.G., and M. Novak, "Vibration of Structures Induced by Wind" in Harris, C. M., Shock and Vibration Handbook, McGraw-Hill, 1988
- Dickinson, S. M., "The Buckling and Frequency of Flexural Vibration of Rectangular, Isotropic and Orthotropic Plates Using Rayleigh's Method," J. Sound Vibration, 61, 1-8, 1978.
- Donaldson, R. M., "Hydraulic Turbine Runner Vibration," ASME Journal of Engineering for Power, Vol. 78, 1141-1147, 1956.
- Dougherty, N. S., Holt, J. B., Liu, B. L. and O'Farrell, J. M., "Time-Accurate Navier-Stokes Computations of Unsteady Flows: The Karman Vortex Street," AIAA 89-0144, 27th Aerospace Sciences Meeting, Reno, Nevada, Jan. 9-12, 1989.

REFERENCES

- Dougherty, N. S., Liu, B. L. and O'Farrell, J. M., "Numerical Simulation of the Edge Tone Phenomenon," NASA Contract Report 4581, February 1994.
- Dowell, E.H., A.V. Srinivasan, J.D. McLean and J. Ambrose, "Aeroelastic Stability of Cylindrical Shells Subjected to a Rotating Flow", AIAA 12th Aerospace Sciences Meeting, Washington, D.C. January 30-February 1, 1974, Paper No. AIAA-74-142.
- Dowell, E.H., "Interior Noise Studies for Single- and Double- Walled Cylindrical Shells", AIAA 5th Aeroacoustics Conference, Seattle, Washington, March 12-14, 1979, Paper No. 79-0647.
- Ericsson, L.E. and J.P. Reding, "Steady and Unsteady Vortex-Induced Asymmetric Loads on Slender Vehicles", Journal of Spacecraft, vol.18 No.2, 1980, pp. 97-109.
- Ericsson, L.E., "Karman Vortex Shedding and the Effect of Body Motion", AIAA 12th Fluid and Plasma Dynamics Conference, Williamsburg, Va., July 23-25, 1979, Paper No. AIAA-79-1531.
- Ericsson, L.E., "Vortex Unsteadiness on Slender Bodies at High Incidence", Journal of Spacecraft, vol.24 No.4, 1987, pp. 319-326; also, AIAA 24th Aerospace Sciences Meeting, January 1986, Reno, Nevada, Paper No. AIAA-86-0486.
- Every, M. J., King, R. and Griffin, O. M., "Hydrodynamic Loads on Flexible Marine Structures due to Vortex Shedding," Trans. ASME, J. Energy Resources Tech., vol. 104, pp. 330-336, 1982.
- Farivar, Dj, "Turbulent Uniform Flow Around Cylinders of Finite Length", AIAA Journal, Vol. 19(3) March 1981, pp. 275-277.
- Fitzpatrick, J.A., I.S. Donaldson and W. McKnight, "Strouhal Numbers for Flows in Deep Tube Array Models", Journal of Fluids and Structures (1988), 2, pp. 145-160.
- Freythuth, P., "Vortex Patterns of Dynamic Separation," Chapter 11 in Turbulence Phenomenon and Modeling
- Friehe, C. A., "Vortex Shedding from Cylinders at Low Reynolds Number," J. Fluid Mechanics, 100, 237-241, 1980.
- Fritz, R.J., "The Effect of Liquids on the Dynamic Motions of Immersed Solids", ASME Vibrations Conference, Toronto, Canada, September 8-10, 1971, Paper No. 71-Vibr-100.
- Fujino, Y. and Sun, L. M., "Vibration Control by Multiple Tuned Liquid Dampers (MTLDs)," ASCE, J. Structural Engineering, Vol. 119, No. 12, Dec. 1993.
- Fujita, K., Ito, T. and Kohno, N., "Experimental study on the vibration of circular cylinders subjected to cross-flow jetted from a narrow gap," Journal of Fluids and Structures (1990) 4, 99-124.
- Gaster, M., "Some Observations on Vortex Shedding and Acoustic Resonances", Ministry of Aviation Supply, Aeronautical Research Council, Aerodynamics Department NPL, London, A.R.C. C. P. No. 1141, January 1970.
- Goodyer, M.J., "Some Experimental Investigations into the Drag Effects of Modifications to the Blunt Base of a Body of Revolution", University of Southampton, Institute of Sound and Vibration Research, Report Number 150, July 1966.
- Granger, S., "A New Signal Processing Method for Investigating Fluidelastic Phenomena", Journal of Fluids and Structures, Volume 4, pp. 73-97, 1990.
- Greenspon, J. E., "Vibrations of Cross-stiffened and Sandwich Plates with Application to Underwater Sound Radiators," J. Acoustic Soc. Am., 33,1485-1497, 1961.
- Greenway, M. E. and Wood, C. J., "The Effect of a Beveled Trailing Edge on Vortex Shedding and Vibration," J. Fluid Mechanics, vol. 61, part 2, pp. 323-335, 1973

REFERENCES

- Griffin, O. M. and Ramberg, S. E., "Some Recent Studies of Vortex Shedding with Application to Marine Tubulars and Risers," *J. Energy Resources Technology*, 104, 2-13, 1982.
- Griffin, O. M., "Vortex Shedding From Bluff Bodies in a Shear Flow: A Review," *Trans. ASME*, vol. 107 pp. 298-306, Sept. 1985.
- Griffin, O.M., "Vibrations and Flow-Induced Forces Caused By Vortex Shedding", Pre-publication correspondence, Naval Research Laboratory.
- Grinsted, B., "Nodal Pattern Analysis," *Proc. Inst. Mech. Eng.*, ser. A, vol. 166, pp. 309-326, 1952.
- Guiggiani, M., "Dynamic instability in fluid-coupled coaxial cylindrical shells under harmonic excitation," *J. Fluids and Structures* pp.211-228, vol. 3, 1989.
- Gupta, R.N. and K.P. Lee, "Hypersonic Viscous Shock-Layer Solutions over Long Slender Bodies-Part I: High Reynolds Number Flows", *Journal of Spacecraft*, Volume 27, No.2, pp. 175-184, 1990.
- Hamill, G. A. and Johnston, H. T., "The decay of Maximum Velocity Within the Initial Stages of a Propeller Wash," *J. Hydraulic Research*, vol. 31, No. 5, pp. 605-613, 1993
- Hannoyer, M.J. and M.P. Paidoussis, "Dynamics of Slender Tapered Beams With Internal or External Axial Flow - Part 1: Theory", *Journal of Applied Mechanics*, Vol. 46, March 1979, pp. 45-51.
- Hannoyer, M.J. and M.P. Paidoussis, "Dynamics of Slender Tapered Beams With Internal or External Axial Flow - Part 2: Experiments", *Journal of Applied Mechanics*, Vol. 46, March 1979, pp. 52-57.
- Hannoyer, M.J. and M.P. Paidoussis, "Instabilities of Tubular Beams Simultaneously Subjected to Internal and External Axial Flows", *Transaction of the ASME: Journal of Mechanical Design*, April 1978, vol. 100, pp. 328-336.
- Hara, F. and T. Iijima, "Vibrations of Two Circular Cylinders in Tandem Subjected to Two-Phase Bubble Cross Flows", *Journal of Fluids and Structures* (1989), 3, pp. 389-404.
- Hara, F., "Unsteady Fluid Dynamic Forces Acting on a Single Row of Cylinders Vibrating in a Cross Flow", *Journal of Fluids and Structures* (1989), 3, pp. 97-113.
- Harris, C.M., Handbook of Shock and Vibration, McGraw-Hill, 1988.
- Hartog, J.P.D., "Transmission Line Vibration Due to Sleet", Summer Convention of the AIEE, Cleveland, Ohio, June 20-24, 1932.
- Heilker, W.J. and R.Q. Vincent, "Vibration in Nuclear Heat Exchangers Due to Liquid and Two-Phase Flow", *Transactions of the ASME: Journal of Engineering for Power*, April 1981, vol. 103, pp. 358-366.
- Heller, H. H. and Bliss, D. B., "Flow-Induced Pressure Fluctuations in Cavities and Concepts for Their Suppression," *Progress in Astronautics and Aeronautics*, edited by Schwartz, I. R. et al., vol. 45, AIAA, 1976.
- Heskestad, F. and Olberts, D. R., "Influence of Trailing Edge Geometry on Hydraulic Turbine Blade Vibration," *ASME Journal of Engineering for Power*, vol. 82, 103-110, 1960.
- Hoerner, S. F., "Fluid Dynamic Drag," *Hoerner Fluid Dynamics*, Bricktown, New Jersey, 1965
- Horton, H. P., "A Semi-Empirical Theory for the Growth and Bursting of Laminar Separation Bubbles," *ARC CP#1073*, 1969
- Humphreys, J. S., "On a Circular Cylinder in a Steady Wind at Transition Reynolds Number," *J. Fluid Mechanics*, 9, 603-612, 1960.
- Illing, H., "Plug Vibrational Tendencies of Top Guided Throttling Control Valves," *Second International Conference on Developments in Valves and Actuators for Fluid Control*, Paper D1, Manchester, England, March 28-30, 1988.

REFERENCES

- Ippen, A. T., et al., "The Hydroelastic Behavior of of Flat Plate as Influenced by Trailing Edge Geometry," MIT Hydromechanics Lab., Dept. of Civil Eng., Report 36, 1960.
- "J-2 Engine AS-502 (Apollo 6) Flight Report S-II and S-IVB Stages," R-7450-2, Volumes 2 and 3, June 17, 1968, Volume 4, September 13, 1968.
- Jacobsen, L. S., "Steady Forced Vibration as Influenced by Damping," Trans. ASME 52 (Applied. Mech. Section), 169-178(1930).
- Jones, E. W., Cincotta, J. C. and Walker, R. W., "Aerodynamic Forces on a Stationary and Oscillating Circular Cylinder at High Reynolds Numbers," NASA TR R-300, 1969.
- Jones, J. H, Guest, S. H., Nesman, T. E., Matienzo, J. J. and Reed, D. K., "Acoustic, Overpressure and Unsteady Flow Phenomena Associated with the Saturn/Space Shuttle Systems: A Review of Selected Issues," presented at the Symposium on Acoustic and Dynamic Environment of Space Transportation Systems, Chatillon, France, February 1994.
- Karadimas, Georges, "The Position of the Unsteady Flow Computation in the Compressor and Turbine Design and Analysis Process," AIAA 92-0015, 30th Aerospace Sciences Meeting & Exhibit, Reno, NV, January 6-9, 1992
- Karadogan, H. and Rockwell, D., "Toward Attenuation of Self-Sustained Oscillations of a Turbulent Jet Through a Cavity," J. of Fluids Engineering, vol. 105, pp 335-340, September 1983.
- Kays, W. M. and Crawford, M. E., Convective Heat and Mass Transfer, Second Edition, McGraw-Hill, New York, 1980
- Kiefling, L., "Pressure-Volume Properties of Metallic Bellows," NASA TM-100365, Marshall Space Flight Center, ED-22, Huntsville, Alabama, May 1989.
- Kim, C.M. and A.T. Conlisk, "Flow Induced Vibration and Noise by a Pair of Tandem Cylinders Due To Buffeting", Journal of Fluids Structures (1990), 4, pp. 471-493.
- King, R., "Vortex Excited Oscillations of Yawed Circular Cylinders," J. Fluid Engineering, 99, 495-502, 1977.
- Kinsler, L. E. and Frey, A. R., Fundamentals of Acoustics, Wiley and Sons, Inc., New York, 2nd Edition, 1962.
- Klebanoff, P. S., "Characteristics of Turbulence in a Boundary Layer with Zero Pressure Gradient," NACA Report 1247, 1954.
- Knisely, C. and D. Rockwell, " Self-Sustained Low-Frequency Components in an Impinging Shear Layer," Journal of Fluid Mechanics 116, pp. 157-186, 1982.
- Knisely, C. W., "Strouhal Numbers of Rectangular Cylinders at Incidence: A Review and New Data," J. Fluids and Structures, 4, 371-393, 1990.
- Knisely, C.W., M. Matsumoto and F. Menacher, "Rectangular Cylinders in Flows with Harmonic Perturbations", Journal of Hydraulic Engineering, August 1986, vol. 112, no. 8.
- Koenig, K. and Roshko, A., "An Experimental Study of Geometrical Effects on the Drag and Flow of Two Bluff Bodies Separated by a Gap," J. Fluid Mech., vol. 156, pp. 167-204, 1985.
- Kolkman, P.A., "Flow Induced Gate Vibrations ", Ph.D. Dissertation, Delft University of Technology Publication 164, 1976.
- Koopmann, G. H. "The Vortex Wakes of Vibrating Cylinders at Low Reynolds Numbers," J. Fluid Mechanics, 28, part 3, 501-512, 1967.
- Kotter, G., Daines, J. V., Webster, R., Lai, T., Caskey, R. M. and Sperry, K., "Reuse Certification," Thiokol Corporation, Space Operation. Technical Interface Meeting at NASA/MSFC, January 28, 1992.

REFERENCES

- Kuhn, G.D., S.B. Spangler and J.N. Nielsen, "Theoretical Study of Vortex Shedding From Bodies of Revolution Undergoing Coning Motion", NASA Technical Note, NASA CR-1448, October 1969.
- Lai, J.L., E.H. Dowell and T.R. Tauchert, "Propagation of Harmonic Waves in a Composite Elastic Cylinder", *Journal of the Acoustical Society of America*, vol. 49 1(2), 1979, pp. 220-228.
- Lecoq, Y and J. Piquet, "Unsteady Viscous Flow Round Moving Circular Cylinders and Airfoils", AIAA 7th Computational Fluid Dynamics Conference, Cincinnati, July 15-17, 1985, Paper No. AIAA-85-1490.
- Leissa, A. W., "The Free Vibration of Rectangular Plates," *J. Sound Vibration*, 31, 257-293, 1973.
- Lever, J.H. and D.S. Weaver, "A Theoretical Model for Fluidelastic Instability in Heat Exchanger Tube Bundles", presented at The Pressure Vessel and Piping Conference, Orlando, Florida, June 27-July 2, 1982, PVP - Vol 63, sponsored by ASME.
- Lever, J.H. and D.S. Weaver, "On the Stability of Heat Exchanger Tube Bundles, Part I: Modified Theoretical Model", *Journal of Sound and Vibration* (1986) 107(3), pp. 375-392.
- Lever, J.H. and D.S. Weaver, "On the Stability of Heat Exchanger Tube Bundles, Part II: Numerical Results and Comparison with Experiments", *Journal of Sound and Vibration* (1986) 107(3), pp. 393-410.
- Lever, J.H. and G. Rzentkowski, "Determination of the Fluid-Elastic Stability Threshold in the Presence of Turbulence: A Theoretical Study", *Transactions of the ASME: Journal of Pressure Vessel Technology*, November 1989, vol.111, pp.407-419.
- Levinsky, E.S. and M.H.Y. Wei, "Nonlinear Lift and Pressure Distribution of Slender Conical Bodies with Strakes at Low Speeds", NASA Technical Note, NASA CR-1202, October 1968.
- Lienhard, J. H., "Synopsis of Lift, Drag and Vortex Frequency Data for Rigid Circular Cylinders," Washington State University, College of Engineering, Research Division Bulletin 300, 1966.
- Lin, T.C. and G.W. Morgan, "Wave Propagation through Fluid Contained in a Cylindrical, Elastic Shell", *Journal of the Acoustical Society of America* (November 1956), vol. 28(6), pp. 1165-1176.
- Lin, W.H. and S.S. Chen, "On the Added Mass and Radiation Damping of Rod Bundles Oscillating in Compressible Fluids", *Journal of Sound and Vibration* (1981) 74(3), pp. 441-453.
- Lindholm, U. S., Kana, D. D. and Abramson, H. N., "Elastic Vibration of Cantilever Plate in Water," *J. Ship Res.*, 9, 11-22 (1965).
- Lindner, H., "Influence of Turbulence on Galloping Oscillations of a Rectangular Cylinder," *ZAMM - Z. angew. Math. Mech.* 70 (1990) 4, pp. 74-77, 1990.
- Liu, B. L., O'Farrell, J. M., Farris, T., Nesman, T. E. and Reed, D. K., "An Interactive Fluid/Structure Interaction Analysis Computer Program," Paper presented in the 1992 Conference on Advanced Earth-To-Orbit Propulsion Technology, NASA/MSFC, May, 1992.
- Liu, B. L., O'Farrell, J. M., Holt, J. B. and Dougherty, N. S., "Time-Dependent Navier-Stokes Computations for Flow-Induced Vibrations of Vanes," *Proceedings of the Seventh International Conference on Finite Element Methods in Flow Problems*, UAH Press, April 3-7, 1989.
- Lou, Y.K., and T.C. Su, "Free Oscillations of Submerged Spherical Shells", *Journal of the Acoustical Society of America*, 49(5), May 1979, pp. 1402-1407.
- Mabey, D.G., "Some Remarks on Buffeting of Wings, Wind Tunnel Models", Royal Aircraft Est., Report RAE-TM-STRUCT-980 BR78530.
- Madsen, H. O., "Fatigue Reliability of Marine Structures," in Sobczyk, K. (Editor), *Stochastic Approach to Fatigue: Experiments, Modeling & Reliability Estimation*, CISM Courses and Lectures No. 334, International Center for Mechanical Sciences, Springer-Verlag, 1993.

REFERENCES

- Maheri, M.R. and R.T. Severn "Experimental Added-Mass in Modal Vibration of Cylindrical Structures", Accepted for publication in Engineering Studies (1991).
- Maheri, M.R. and R.T. Severn "Impulsive Hydrodynamic Pressures in Ground-Based Cylindrical Structures", Journal of Fluids and Structures, vol. 3, pp. 555-577, 1989.
- Mahrenholtz, O., "Fluidelastische Schwingungen", Applied Mathematics and Mechanics (1986), vol. 66(1), pp. 1-21.
- Martin, W. W. and Naudascher, E., "FLUID-DYNAMIC EXCITATION INVOLVING FLOW INSTABILITY,"
- Martin, W.W. E. Naudascher and M. Padmanabhan, "Fluid-Dynamic Excitation Involving Flow Instability", Journal of the Hydraulics Division, Proceedings of the ASCE vol. 101, No. HY6, June 1975, pp. 681-698.
- Mateescu, D., M.P. Paidoussis and F. Belanger, "Unsteady Pressure Measurements on an Oscillating Cylinder in Narrow Annular Flow", Journal of Fluids and Structures (1988) 2, pp. 615-628.
- McCroskey, W. J., "Some Current Research in Unsteady Fluid Dynamics - The 1976 Freeman Scholar Lecture," ASME Journal of Fluids Engineering, vol. 99, series 1, No. 1, pp.8-44, 1977.
- McDevitt, J.B. and R.A. Taylor, "Pressure Distributions at Transonic Speeds for Slender Bodies Having Various Axial Locations of Maximum Diameter", NACA Technical Note 4280, July 1958.
- McIver, P., "Sloshing Frequencies for Cylindrical and Spherical Containers filled to an Arbitrary Depth", Journal of Fluid Mechanics, (1989), vol. 201, pp. 243-257.
- Mei, V.C. and I.G. Currie, "Flow Separation on a Vibrating Circular Cylinder", The Physics of Fluids, vol. 12, No. 11, November 1969, pp. 2248-2254.
- Meyerhoff, W. K., "Added Mass of Thin Rectangular Plates Calculated from Potential Theory," J. Ship Res. 14, 100-111 (1970).
- MIL-HDBK-5E. AISI Low-Alloy Steels, pp. 2-16 to 2-19, 1 June 1987.
- Milne-Thompson, L.M., "Theoretical Hydrodynamics (5th Edition)", Macmillan Co., 1968, p.545-554.
- Moorty, S. and M.D. Olson, "A Numerical Study of Low Reynolds Number Fluid-Structure Interaction", Journal of Fluids and Structures (1989) 3, pp. 37-60.
- Morkovin, M. V., "Flow Around a Circular Cylinder - A Kaleidoscope of Challenging Fluid Phenomena," Symposium on Fully Separated Flows, (ed. A. G. Hansen), ASME, New York, pp.102-118, 1964.
- Mulcahy, T. M., "One-Dimensional Leakage-Flow Vibration Instabilities," J. of Fluids and Structures, 2, 383-403, 1988.
- Mulcahy, T.M., "Fluid Forces on Rods Vibration in Finite Length Annular Regions", Journal of Applied Mechanics, vol. 102, 234-240.
- Nakamura, J. and Nakashima, M., "Vortex Excitation of Prisms with Elongated Rectangular, H and T Cross-Sections," J. of Fluid Mechanics, 163, 149-169, 1986
- Naudascher, E. and Wang, Y., "Flow-Induced Vibrations of Prismatic Bodies and Grids of Prisms," Journal of Fluids and Structures, Vol. 7, 341-373, 1993
- Naudascher, E., "Flow-Induced Streamwise Vibrations of Structures", Journal of Fluids and Structures (1987) 1, pp. 265-298.
- Naudascher, E., "Hydrodynamic Forces", IAHR Monograph, Balkema/Rotterdam/Brookfield/ 1991.
- Newman, J.N., "Marine Hydrodynamics", MIT Press, England, 1977, 103-155.
- O'Connor, G. M. and Jones, J. H., "Flow-Induced Vibrations of the SSME LOX Inlet Tee Vanes," AIAA-88-3132, AIAA/ASME/SAE/ASEE 24th Joint Propulsion Conference, Boston, Mass., July 11-13, 1988.

REFERENCES

- Obasaju, E. D., "An Investigation of the Effects of Incidence on the Flow Around a Square Section Cylinder," Dept. of Aeronautics, Imperial College, London.
- Obasaju, E. D., "Forced Vibration Study of the Aeroelastic Instability of a Square-Section Cylinder Near Vortex Resonance," *Journal of Wind Engineering and Industrial Aerodynamics*, vol. 12, 313-327, 1983.
- Ohta, K., K. Kagawa, H. Tanaka and S. Takahara, "Study on the Fluidelastic Vibratin of Tube Arrays Using Modal Analysis Technique", *Journal of Pressure Vessel Technology*, February 1984, Vol. 106, pp. 17-24.
- Okajima, A., Mizota, T. and Tanida, Y., "Observation of Flow Around Rectangular Cylinders," pp. 381-386 in Yang, W. J. (editor), *Proceedings of the Third International Symposium on Flow Visualization*, September 6-9, 1983, Hemisphere Publishing Corporation.
- Paidoussis, M.P. and S. Suss, "Stability of a Cluster of Flexible Cylinders in Bounded Axial Flow", *Journal of Applied Mechanics*, September 1977, pp. 401-408.
- Paidoussis, M.P., "Dynamics of flexible slender cylinders in axial flow Part 1: Theory ", *Journal of Fluid Mechanics*, (1966), vol. 26, part 4, pp. 717-736.
- Paidoussis, M.P., "Flow Induced Vibrations in Nuclear Reactors and Heat Exchangers", In "Proceedings of the Symposium on Practical Experiences with Flow Induced Vibrations", Karlsruhe, Germany, 1979, pp. 1-80, Berlin: Springer-Verlag.
- Paidoussis, M.P., "Fluidelastic Vibration of Cylinder Arrays in Axial and Cross Flow - State of the Art - ", *Flow-Induced Vibration Design Guidelines*, ed. P.Y. Chen, ASME Special Publication, PVP, Vol. 52, 1981.
- Paidoussis, M.P., N.T. Issid and M. Tsui, "Parametric Resonance Oscillations of Flexible Slender Cylinders in Harmonically Perturbed Axial Flow - Part I: Theory", *Journal of Applied Mechanics* Vol. 47, December 1980, pp. 709-714.
- Paidoussis, M.P., N.T. Issid and M. Tsui, "Parametric Resonance Oscillations of Flexible Slender Cylinders in Harmonically Perturbed Axial Flow - Part II: Experiments", *Journal of Applied Mechanics* Vol. 47, December 1980, pp. 715-719.
- Paidoussis, M.P., "Stability of Flexible Slender Cylinders in Pulsatile Axial Flow", *Journal of Sound and Vibration*, (1975) 42(1), pp. 1-11.
- Pattani, P.G. and M.D. Olson, "Periodic Solutions of Rigid Body-Viscous Flow Interaction", *International Journal for Numerical Methods in Fluids*, Vol 7 (1987), pp. 653-695.
- Perroni, A., "Vortex Shedding Induced Loads on the RSRM", Aerojet , ASRM Division, George C. Marshall Space Flight Center Presentation, 1991.
- Pettigrew, M.J., Y. Sylvestre and A.O. Campagna, "Vibration Analysis of Heat Exchanger and Steam Generator Designs", *Nuclear Engineering and Design*, 48 (1978), pp. 97-115.
- Pines, S., "An Elementary Explanation of the Flutter Mechanism," *Proceedings National Specialists Meeting on Dynamics and Aeroelasticity*, Institute on the Aeronautical Sciences, Ft. Worth, Tex. , 1958.
- Price, S. J. and Abdallah, R., "On the efficiency of mechanical damping and frequency detuning in alleviating wake-induced flutter of overhead power conductors," *Journal of fluids and structures* (1990) 4, 1-34.
- Price, S.J. and M.P. Paidoussis, "A Single-Flexible-Cylinder Analysis for the Fluidelastic Instability of an Array of Flexible Cylinders in Cross-Flow", *Journal of Fluids Engineering*, June 1986, Vol. 108, pp. 193-199.

REFERENCES

- Price, S.J. and M.P. Paidoussis, "Fluidelastic Instability of an Infinite Double Row of Circular Cylinders Subject to a Uniform Cross-Flow", *Journal of Vibration, Acoustics, Stress, and Reliability in Design*, January 1983, Vol 105, pp. 59-66.
- Price, S.J. and R. Abdallah, "On the Efficacy of Mechanical Damping and Frequency Detuning in Alleviating Wake-Induced Flutter of Overhead Power Conductors", *Journal of Fluids and Structures*, (1990) 4, pp. 1-34.
- Price, S.J., M.P. Paidoussis, R. MacDonald, and B. Mark, "The Flow-Induced Vibration of a Single Flexible Cylinder in a Rotated Square Array of Rigid Cylinders with a Pitch-To-Diameter Ratio of 2-12", *Journal of Fluids and Structures*, (1987) 1, pp. 359-378.
- Ramberg, S. E., "The Effects of Yaw and Finite Length upon the Vortex Wakes of Stationary and Vibrating Cylinders," *J. Fluid Mechanics*, **128**, 81-107, 1983.
- Reed, D., Nesman, T. and Howard, P., "Vortex Shedding Experiment with Flat and Curved Bluff Plates in Water," ASME Symposium, Chicago, Illinois, December 1989.
- Reed, D., "Solid Rocket Booster (SRB) Vortex Shedding During Reentry", Internal NASA Communication, George C. Marshall Space Flight Center, Structures and Dynamics Laboratory, Document No. ED33(135-91), November 1991.
- Roark, R. J. and Young, W. C., Formulas for Stress and Strain (5th ed.), p. 290, McGraw-Hill, New York, 1975.
- Roberts, B.W., "Low Frequency, Aeroelastic Vibrations in a Cascade of Circular Cylinders," *Mechanical Engineering Science Monograph No. 4*, September 1966.
- Rockwell International, Space Systems Division, "Structure Manual: Stability of Shells," Number 9.22.10, 1970.
- Rockwell, D. and Knisely, C., "Vortex-Edge Interaction: Mechanisms for Generating Low Frequency Components," *Phys. Fluids* 23(2), pp 239-240, Feb. 1980.
- Rockwell, D. and Naudascher, E., "Review - Self-Sustaining Oscillations of Flow Past Cavity," *J. Fluid Engineering, Transactions of ASME*, vol. 100, pp. 152-165, June 1978.
- Rockwell, D. O. and Niccolls, W. O., "Natural Breakdown of Planar Jets," *J. of Basic Engineering, Transactions of ASME*, pp. 720-730, December 1972.
- Rockwell, D. O. and Toda, K., "Effects of Applied Acoustic Fields on Attached Jet Flows," *J. of Basic Engineering, Transactions of ASME*, vol. 93, Series D, No. 1, pp. 63-73, March 1971.
- Rockwell, D. O., "External Excitation of Planar Jets," *J. of Applied Mechanics, Transactions of the ASME*, pp. 883-890, December 1972
- Rodrigues, O., "The Circular Cylinder in Subsonic and Transonic Flows," *AIAA J.*, Vol. 22, No. 12, pp. 1713-1718, Dec., 1984.
- Rodriguez, O., "The Circular Cylinder in Subsonic and Transonic Flow", *AIAA Journal*, Vol. 22 (12), December 1984, pp. 1713-1718.
- Rooney, D. M. and Peltzer, R. D., "Pressure and Vortex Shedding Patterns Around a Low Aspect Ratio Cylinder in a Sheared Flow at Transitional Reynolds Numbers," *J. Fluids Engineering*, **103**, 88-96, 1981.
- Roseau, M., Vibrations in Mechanical Systems, translated by Orde, H. L. S., pp. 135-136, Springer Verlag, New York, 1980.
- Rossiter, J. E., "Wind Tunnel Experiments on the Flow over Rectangular Cavities at Subsonic and Transonic Speeds", Royal Aircraft Establishment Technical Report No. 64037, October 1964.
- Ruzicka, J. E., Derby, T. F., *Influence of Damping in Vibration Isolation, the Shock and Vibration Information Center*, Naval Research Laboratory, 1971.

REFERENCES

- Ruzicka, Jerome E., and Derby, Thomas F., Influence of Damping in Vibration Isolation, the Shock and Vibration Information Center, Naval Research Laboratory, 1971.
- Sarpkaya, T., "Vortex-Induced Oscillations", Journal of Applied Mechanics, vol. 46, pp. 241-258, June 1979.
- Sato, H., "The Stability and Transition of a Two-Dimensional Jet," J. of Fluid Mechanics, vol. 7, pp. 53-80, 1959.
- "Saturn V Launch Vehicle Flight Evaluation Report - AS-502 Apollo 6 Mission," MPR-SAT-FE-68-3, June 25, 1968.
- Savkar, S.D., "A Note on the Phase Relationships Involved in the Whirling Instability in Tube Arrays", Transactions of the ASME, December 1977, pp. 241-258.
- Saxon, J. B., "Modeling Dynamically Coupled Fluid Duct Systems with Finite Line Elements," NASA CR-193909, February 1993.
- Schewe, G., "Die auf Stumpfe Profile bei Grotsen Reynolds-Zahlen Wirken," DFVLR-Mitt. 84-19, Untersuchung der Aerodynamischen Krafte, Gottingen, 1984
- Schewe, G., "Experimental Observation of the 'Golden Section' in Flow Round a Circular Cylinder," Physics Letters, vol. 109A, No. 1,2, pp. 47-50, North-Holland Physics Publishing Division, May 1985.
- Schewe, G., "Force Measurements in Aerodynamics Using Piezo-Electric Multicomponent Force Transducers," In Proceedings of 11th International Congress on Instrumentation in Aerospace Simulation Facilities, Stanford University, pp.263-268, Aug. 26-28, 1985.
- Schewe, G., "Investigation of the Aerodynamic Forces on Bluff Bodies at High Reynolds Numbers", European Space Agency Technical Translation ESA-TT-914, June 1985, Translation of DFVLR-Mitt-84-19, Institute for Aeroelasticity, Goettingen, West Germany.
- Schewe, G., "On the Force Fluctuations Acting on a Circular Cylinder in a Crossflow from Subcritical up to Transcritical Reynolds Numbers", Journal of Fluid Mechanics, Great Britain, (1983), vol. 133, pp. 265-285.
- Schewe, G., "Sensitivity of Transition Phenomena to Small Perturbations in Flow Round a Circular Cylinder", Journal of Fluid Mechanics, Great Britain, (1986), vol. 172, pp. 33-46.
- Schewe, G., "Nonlinear Flow-Induced Resonances of an H-Shaped Section," J. of Fluids and Structure, 3, 327-348, 1989
- Schutzenhofer, L. A., Howard, P. W., Clever, W. W. and Guest, S. H., "Space Shuttle Solid Rocket Aft Skirt Reentry Noise Induced by an Aerodynamic cavity-Flow Interaction," The Shock and Vibration Bulletin Part 1, The Shock and Vibration Information Center, Naval Research Laboratory, Washington, D.C., September 1979.
- Simmons, J. M. and Cleary, P. M. G., "Measurement of Aerodynamic Power Associated with Vortex-Induced Vibration of Electrical Transmission Lines," IEEE Power Engineering Society Paper F79 713-9, 1979.
- Simpson, A. and J.W. Flower, "An Improved Mathematical Model for the Aerodynamic Forces on Tandem Cylinders in Motion With Aeroacoustic Applications", Journal of Sound and Vibration (1977) 51(2), pp. 183-217.
- Simpson, A., " Determination of the Natural Frequencies of Multi-Conductor Overhead Transmission Lines," J. Sound and Vibration 20, pp. 417-449, 1972.
- Simpson, A., " On the Flutter of a Smooth Cylinder in a Wake," Aeronautical Quarterly 22, pp. 25-41, 1971.
- Skop, R. A., Griffin, O. M. and Ramberg, S. E., "Strumming Predictions for the SEACON II Experimental Mooring," Offshore Technology Conference Paper OTC 2884, May 1977.

REFERENCES

- Slaouti, A. and J.H. Gerrard, "An Experimental Investigation of the End Effects on the Wake of a Circular Cylinder Towed through Water at Low Reynolds Numbers", *Journal of Fluid Mechanics*, Great Britain, (1981), vol. 112, pp. 297-314.
- Southworth, P.J. and M.M. Zdravkovich, "Effect of Grid-Turbulence on the Fluid-Elastic Vibrations of In-Line Tube Banks in Cross Flow", *Journal of Sound and Vibration*, (1986), 39(4), pp. 461-469.
- Szechenyi, E., "Supercritical Reynolds number Simulation for Two-Dimensional Flow Over Circular Cylinders," *J. Fluid Mech.*, Vol. 70, Pt. 3, pp. 529-543, 1975.
- Tanaka, H., S. Takahara and K. Ohta, "Flow-Induced Vibration of Tube Arrays With Various Pitch-to-Diameter Ratios", *Transactions of the ASME: Journal of Pressure Vessel Technology*, August 1982, vol. 104, pp. 168-174.
- Theisen, J.G., "Vortex Periodicity in Wakes", *AIAA 5th Aerospace Meeting*, Nyny, Jan 23-26 1967, Paper number AIAA-67-0034.
- Thompson K.D., "The Estimation of the Drag of Circular Cylinders at Subcritical Reynolds Numbers and Subsonic Speeds", *Technical Notes, Weapons Research Establishment, Department of Supply, Salisbury, Australia* May 1969.
- Thomson, W. T., *Theory of Vibration*, Prentice-Hall, 1973.
- Timoshenko, S., and D.H. Young, "Vibration Problems in Engineering," D. Van Nostrand, New York, pp. 425, 1954.
- Tokumar, P. T. and Dimotakis, P. E., "The Lift of a Cylinder Executing Rotary Motions in a Uniform Flow," *J. Fluid Mech.*, vol. 255, pp. 1-10, 1993.
- Tsuboi, K., T. Tamura, K. Kuwahara, "Numerical Study for Vortex Induced Vibration of a Circular Cylinder in High-Reynolds-Number Flow", *27th Aerospace Sciences Meeting*, Reno, Nevada, January 9-12, 1989, Paper No. AIAA-89-0294.
- Vandiver, J. K., "Drag Coefficients of Long Flexible Cylinders," *Paper OTC 4490, Offshore Technology Conference*, Houston, Tex., May 2-5, 1983.
- Vickery, B. J. and Watkins, R. D., "Flow-Induced Vibrations of Cylindrical Structures," in *Proceedings of the First Australian Conference held at the University of Western Australia*, 1962.
- Wardlaw, A. and W.J. Yanta, "The Flow Field About, and Forces on Slender Bodies at High Angles of Attack", *AIAA 18th Aerospace Sciences Meeting*, January 14-16, 1980, Pasadena, Ca., Paper No. AIAA-80-0184.
- Washizu, K. et al., "Aeroelastic Instability of Rectangular Cylinders in a Heaving Mode," *J. Sound and Vibration*, 59, 195-210, 1978.
- Weaver, D.S. "Flow Induced Vibrations in Valves Operating at Small Openings", Practical Experience with Flow-Induced Vibrations, Editors E. Naudascher and D. Rockwell, Springer-Verlag, 1980, p.305-316.
- Weaver, D.S. and H.G.D. Goodyer, "An Experimental Study of Fluidelastic Instability in a Three-Span Tube Array", *Journal of Fluids and Structures* (1990) 4, pp. 429-442.
- Weaver, D.S. and J.A. Fitzpatrick, "A Review of Flow Induced Vibrations in Heat Exchangers", In "Proceedings of International Conference on Flow Induced Vibrations", paper number A1, pp. 1 - 17, delivered at conference at Bowness-on-Windermere, England: 12-14 May, 1987, sponsored by the British Nuclear Energy Society, The Fluid Engineering Centre, BHRA.
- Weaver, D.S. and L.K. Grover, "Cross-Flow Induced Vibrations in a Tube Bank - Turbulent Buffeting and Fluid Elastic Instability", *Journal of Sound and Vibration* (1978) 59(2), pp. 277-294.
- Weaver, D.S. and S. Ziada, "A Theoretical Model for Self-Excited Vibrations in Hydraulic Valves and Seals", *ASME PVP Conference*, San Francisco, Ca. June, 1979.

REFERENCES

- Widnall, S.E. and E.H. Dowell, "Aerodynamic Forces on an Oscillating Cylindrical Duct with an Internal Flow", *Journal of Sound and Vibration* (1967) 6(1), pp. 71-85.
- Williams, J. E. F. and Huang, X. Y., "Active stabilization of compressor surge," *J. Fluid Mech.*, pp. 245-262, vol. 204, 1989.
- Williams, J.E.F. and B.C. Zhao, "The Active Control of Vortex Shedding", *Journal of Fluids and Structures* (1989) 3, pp. 115-122.
- Williamson, C.H.K. and A. Roshko, "Vortex Formation in the Wake of an Oscillating Cylinder", *Journal of Fluids and Structures* (1988) 2, pp. 355-381.
- Yauta, W and A. Wardlaw, "Multi-Stable Vortex Patterns on Slender, Circular Bodies at High Incidence", *AIAA 19th Aerospace Sciences Meeting*, January 12-15, 1981, St. Louis, Mo., Paper No. AIAA-81-0006.
- Yeh, T.T. and S.S. Chen, "Dynamics of a Cylindrical Shell System Coupled by Viscous Fluid", *Journal of the Acoustic Society of America*, Vol. 62, No. 2, August 1977, pp. 262-270.
- Younger, J. E., "Structure Design of Metal Airplanes," McGraw-Hill Book Company, 1935
- Zdravkovich, M.M. and J.R. Volk, "Effect of Shroud Geometry on the Pressure Distributed Around a Circular Cylinder", *Journal of Sound and Vibration* (1972), 20(4), pp. 451-455.
- Zdravkovich, M.M., "Flow Induced Oscillations of Two Interfering Circular Cylinders", *Journal of Sound and Vibration*, (1985) 101(4), pp. 511-521.
- Zdravkovich, M.M., "Interference Between Two Circular Cylinders Forming a Cross", *Journal of Fluid Mechanics*, (1983) Vol. 128, pp. 231-246.
- Zdravkovich, M.M., "Modification of Vortex Shedding in the Synchronization Range", *Journal of Fluids Engineering*, December 1982, Vol. 104, pp. 513-517.
- Zdravkovich, M.M., "Observation of Vortex Shedding Behind A Towed Circular Cylinder Near a Wall",
- Zdravkovich, M.M., "Review and Classification of Various Aerodynamic and Hydrodynamic Means for Suppressing Vortex Shedding", *Journal of Wind Engineering and Industrial Aerodynamics*, 7 (1981), pp. 145-189.
- Zdravkovich, M.M., "Review of Flow Interference Between Two Circular Cylinders in Various Arrangements", *Transactions of the ASME*, December 1977, pp. 618-633.
- Zdravkovich, M.M., "Review of Interference-Induced Oscillations in Flow Past Two Parallel Circular Cylinders in Various Arrangements", *Journal of Wind Engineering and Industrial Aerodynamics*, 28 (1988), pp.183-200.
- Zdravkovich, M.M., "The Effects of Interference Between Circular Cylinders in a Cross Flow", *Journal of Fluids and Structures* (1987) 1, pp. 239-261.
- Ziada, S. , Bolleter, U. and Zahnd, E., "On the whistling of Thermostatic Radiator Valves," a reprint from the *Sulzer Technical Review*, pp.28-30, 4/1983.
- Ziada, S. and A. Oengoren, "Flow-Induced Acoustical Resonances of In-Line Tube Bundles", *Sulzer Technical Review* 1/1990, pp. 45-47.
- Ziada, S. and A. Oengoren, "Vorticity Shedding and Acoustic Resonance in an In-Line Tube Bundle - Part I: Vorticity Shedding", *International Conference on Flow-Induced Vibrations*, (Brighton,U.K.), May 1991 .
- Ziada, S. and Rockwell, D., "Subharmonic Oscillations of a Mixing Layer-Wedge System Associated with Free Surface Effects," *Journal of Sound and Vibration*, 3, 483-491, 1983.

REFERENCES

Ziada, S., A. Oengoren and E.T. Buhlmann, "On Acoustical Resonance In Tube Arrays - Part I: Experiments", *Journal of Fluids and Structures* (1989) 3, pp. 293-314.

Ziada, S., A. Oengoren and E.T. Buhlmann, "On Acoustical Resonance In Tube Arrays - Part II: Damping Criteria", *Journal of Fluids and Structures* (1989) 3, pp. 315-324.

Ziada, S., and A. Oengoren, "Vorticity Shedding and Acoustic Resonance in an In-Line Tube Bundle - Part II: Acoustic Resonance", *Symposium on Flow-Induced Vibrations, PVP - Conference, (San Diego, CA), June 1991* .

Ziada, S., and E.T. Buhlmann, " Flow Impingement as an Excitation Source in Control Valves," *Journal of Fluids and Structures* 3, pp. 529-549, 1989.

Ziada, S., and E.T. Buhlmann, " Multiple Side-Branches as Tone Generators," *International Conference on Flow-Induce Vibrations, Brighton, U.K. May 1991. (Submitted: J. Fluids and Structures)*

Ziada, S., U. Bolleter and Y.N. Chen, "Vortex Shedding and Acoustic Resonance in a Staggered-Yawed Array of Tubes", *ASME Symposium on Flow-Induced Vibrations* (1984).

Ziada, S., U. Bolleter, and E. Zahnd, "On the Whistling of Thermostatic Radiator Valves", *Sulzer Technical Review* 4/1983.

REPORT DOCUMENTATION PAGE

Form Approved
OMB No. 0704-0188

Public reporting burden for this collection of information is estimated to average 1 hour per response, including the time for reviewing instructions, searching existing data sources, gathering and maintaining the data needed, and completing and reviewing the collection of information. Send comments regarding this burden estimate or any other aspect of this collection of information, including suggestions for reducing this burden, to Washington Headquarters Services, Directorate for Information Operations and Reports, 1215 Jefferson Davis Highway, Suite 1204, Arlington, VA 22202-4302, and to the Office of Management and Budget, Paperwork Reduction Project (0704-0188), Washington, DC 20503.

| | | | | |
|--|---|--|---|--|
| 1. AGENCY USE ONLY (Leave blank) | | 2. REPORT DATE March 1995 | 3. REPORT TYPE AND DATES COVERED Contractor Report | |
| 4. TITLE AND SUBTITLE High Frequency Flow / Structural Interaction in Dense Subsonic Fluids | | | 5. FUNDING NUMBERS NAS8-38187 | |
| 6. AUTHOR(S) Baw-Lin Liu and J.M. O'Farrell | | | | |
| 7. PERFORMING ORGANIZATION NAME(S) AND ADDRESS(ES) Rockwell International Space Systems Division, Huntsville Operations 555 Discovery Drive Huntsville, Alabama 35806 | | | 8. PERFORMING ORGANIZATION REPORT NUMBER M-773 | |
| 9. SPONSORING / MONITORING AGENCY NAME(S) AND ADDRESS(ES) National Aeronautics and Space Administration George C. Marshall Space Flight Center Marshall Space Flight Center, Alabama 35812 | | | 10. SPONSORING / MONITORING AGENCY REPORT NUMBER NASA CR-4652 | |
| 11. SUPPLEMENTARY NOTES Prepared for Structures and Dynamics Laboratory, Science and Engineering Directorate Contract Monitor: Tom E. Nesman | | | | |
| 12a. DISTRIBUTION / AVAILABILITY STATEMENT Subject Category: 02 Unclassified-Unlimited | | | 12b. DISTRIBUTION CODE | |
| 13. ABSTRACT (Maximum 200 words) Prediction of the detailed dynamic behavior in rocket propellant feed systems and engines and other such high-energy fluid systems requires precise analysis to assure structural performance. Designs sometimes require placement of bluff bodies in a flow passage. Additionally, there are flexibilities in ducts, liners, and piping systems. A design handbook and interactive data base have been developed for assessing flow/structural interactions to be used as a tool in design and development, to evaluate applicable geometries before problems develop, or to eliminate or minimize problems with existing hardware. This is a compilation of analytical/empirical data and techniques to evaluate detailed dynamic characteristics of both the fluid and structures. These techniques have direct applicability to rocket engine internal flow passages, hot gas drive systems, and vehicle propellant feed systems. Organization of the handbook is by basic geometries for estimating Strouhal numbers, added mass effects, mode shapes for various end constraints, critical onset flow conditions, and possible structural response amplitudes. Emphasis is on dense fluids and high structural loading potential for fatigue at low subsonic flow speeds where high-frequency excitations are possible. Avoidance and corrective measure illustrations are presented together with analytical curve fits for predictions compiled from a comprehensive data base. | | | | |
| 14. SUBJECT TERMS Vortex shedding, Edgetone, Unsteady flow, Galloping, Lock-in, Flow/structural interaction, Flow instability, Oscillation | | | 15. NUMBER OF PAGES 227 | |
| | | | 16. PRICE CODE A11 | |
| 17. SECURITY CLASSIFICATION OF REPORT Unclassified | 18. SECURITY CLASSIFICATION OF THIS PAGE Unclassified | 19. SECURITY CLASSIFICATION OF ABSTRACT Unclassified | 20. LIMITATION OF ABSTRACT Unlimited | |



National Aeronautics and
Space Administration
Code JTT
Washington, DC
20546-0001

*Official Business
Penalty for Private Use, \$300*

Postmaster: If Undeliverable (Section 158 Postal Manual), Do Not Return
